

AD-A048 275

LOCKHEED MISSILES AND SPACE CO INC HUNTSVILLE ALA HU--ETC F/G 1/1
LASER DOPPLER VELOCIMETER MEASUREMENTS OF B-747 WAKE VORTEX CHA--ETC(U)
SEP 77 M R BRASHEARS, A D ZALAY DOT-TSC-1145
LMSC-HREC-TR-D496975 FAA-RD-77-85 NL

UNCLASSIFIED

1 of 3
AD
A048275



OK

12

REPORT NO. FAA-RD-77-85

AD A048275

LASER DOPPLER VELOCIMETER
MEASUREMENTS OF B-747 WAKE
VORTEX CHARACTERISTICS

M. R. Brashears
A. D. Zalay

LOCKHEED MISSILES & SPACE COMPANY, INC.
HUNTSVILLE RESEARCH & ENGINEERING CENTER
4800 Bradford Drive
Huntsville AL 35807



SEPTEMBER 1977
FINAL REPORT



DOCUMENT IS AVAILABLE TO THE U.S. PUBLIC
THROUGH THE NATIONAL TECHNICAL
INFORMATION SERVICE, SPRINGFIELD,
VIRGINIA 22161

AD No.
DDC FILE COPY

Prepared for
U.S. DEPARTMENT OF TRANSPORTATION
FEDERAL AVIATION ADMINISTRATION
Systems Research and Development Service
Washington DC 20591

NOTICE

This document is disseminated under the sponsorship of the Department of Transportation in the interest of information exchange. The United States Government assumes no liability for its contents or use thereof.

NOTICE

The United States Government does not endorse products or manufacturers. Trade or manufacturers' names appear herein solely because they are considered essential to the object of this report.

18
FAA-RD, TSC

Technical Report Documentation Page

1. Report No. 77-85 FAA-77-23	2. Government Accession No.	3. Recipient's Catalog No. 11
4. Title and Subtitle LASER DOPPLER VELOCIMETER MEASUREMENTS OF B-747 WAKE VORTEX CHARACTERISTICS	5. Report Date September 1977	6. Performing Organization Code
7. Author(s) M. R. Brashears and A. D. Zalay	8. Performing Organization Report No. DOT-TSC-FAA-77-13 LMSC-HREC-TR-D496975	9. Work Unit No. (TRATS) FA705/R7126
10. Performing Organization Name and Address Lockheed Missiles & Space Company, Inc.* Huntsville Research & Engineering Center 4800 Bradford Drive Huntsville AL 35807	11. Contract or Grant No. DOT-TSC-1145	12. Type of Report and Period Covered Final Report Nov 1975 - Jan 1977
12. Sponsoring Agency Name and Address U. S. Department of Transportation Federal Aviation Administration Systems Research and Development Service Washington DC 20590	13. Sponsoring Agency Code	
15. Supplementary Notes *Under Contract to: U. S. Department of Transportation Transportation Systems Center Kendall Square Cambridge MA 02142		
16. Abstract To determine the behavior of the wake vortices of a B-747 at low altitudes and to measure the vortex-decay process behind the B-747 as a function of altitude above ground, flap and spoiler settings, and different flight configurations, a B-747 aircraft flew 54 passes at low level over a ground-based laser Doppler velocimeter (LDV) system. From the LDV measurements, the location and flow field of the wake vortices and the general vortex roll-up, transport, and decay trends were obtained. Results of the study indicated that the deployment of spoilers and flaps enhanced the decay of the vortex peak tangential velocity in the near wake while aircraft altitude, glide slope, and landing gear deployment had little effect. The report discusses the LDV wake vortex measurements including the instrumentation used, the experimental test sequence, the results of the wake measurements in terms of the vortex roll-up, transport, and decay trends, and a comparison of the wake vortex characteristics for different configurations.		
17. Key Words Aircraft Wakes, Trailing Vortex, Wake Vortices, Laser Doppler Velocimetry	18. Distribution Statement DOCUMENT IS AVAILABLE TO THE U.S. PUBLIC THROUGH THE NATIONAL TECHNICAL INFORMATION SERVICE, SPRINGFIELD, VIRGINIA 22161	
19. Security Classif. (of this report) Unclassified	20. Security Classif. (of this page) Unclassified	21. No. of Pages 224
22. Price		

Form DOT F 1700.7 (8-72)

Reproduction of completed page authorized

ii 220105

1/P

ACCESSION for	
NTIS	White Section <input checked="" type="checkbox"/>
DDC	Buff Section <input type="checkbox"/>
UNANNOUNCED	<input type="checkbox"/>
JUSTIFICATION	
BY	
DISTRIBUTION/AVAILABILITY CODES	
SPECIAL	
A	

PREFACE

The laser Doppler velocimeter measurements of wake vortex characteristics described in this report were carried out by Lockheed Missiles & Space Company, Inc., Huntsville Research & Engineering Center working in conjunction with AeroVironment, Inc., under the "Wake Decay near the Ground" program sponsored by the U.S. Department of Transportation. Lockheed-Huntsville's role in the program consisted of operating the Lockheed Mobile laser Doppler velocimeter system and collecting measurements of vortex characteristics with the system and processing and analyzing the measurements to determine the dominant vortex decay characteristics.

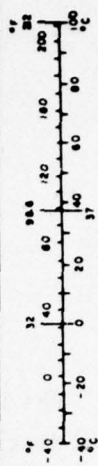
The following Lockheed-Huntsville personnel made significant contributions to this effort: C. E. Craven, B. B. Edwards, J. L. Jetton, A. J. Jordan, M. C. Krause, T. R. Lawrence, and K. R. Shrider. The authors are grateful to the Optics Branch at NASA-Marshall Space Flight Center for making their filter bank and signal processor available for this study and to J. W. Bilbro and H. B. Jeffreys at NASA-MSFC and to Bill Keenum, Earl Lucas, and Rick Bynum at Computer Sciences Corporation for processing the measurements obtained with the NASA-MSFC filter bank and signal processor. The authors are grateful to Dr. J. N. Hallock, TSC Contracting Officer's Technical Monitor, and to Dr. D. C. Burnham, staff scientist at TSC, for their technical contributions and able assistance during the performance of this contract.

DDC
RECEIVED
NOV 4 1977
F.

METRIC CONVERSION FACTORS

Approximate Conversions to Metric Measures			
Symbol	When You Know	Multiply by	To Find
LENGTH			
in	inches	2.5	centimeters
ft	feet	30	centimeters
yd	yards	0.9	meters
mi	miles	1.6	kilometers
AREA			
in ²	square inches	6.5	square centimeters
ft ²	square feet	0.09	square meters
yd ²	square yards	0.8	square meters
mi ²	square miles	2.6	square kilometers
acres	acres	0.4	hectares
MASS (weight)			
oz	ounces	28	grams
lb	pounds	0.45	kilograms
	short tons (2000 lb)	0.5	tonnes
VOLUME			
teaspoon	teaspoons	5	milliliters
tablespoon	tablespoons	15	milliliters
fluid ounce	fluid ounces	30	milliliters
cup	cups	0.24	liters
pint	pints	0.47	liters
quart	quarts	0.95	liters
gallon	gallons	3.8	liters
cu ft	cubic feet	0.03	cubic meters
yd ³	cubic yards	0.76	cubic meters
TEMPERATURE (degrees)			
F	Fahrenheit temperature	5/9 (after subtracting 32)	Celsius temperature

Approximate Conversions from Metric Measures			
Symbol	When You Know	Multiply by	To Find
LENGTH			
cm	centimeters	0.04	inches
m	meters	0.4	feet
km	kilometers	0.6	miles
AREA			
cm ²	square centimeters	0.16	square inches
m ²	square meters	1.2	square yards
ha	hectares (10,000 m ²)	0.4	square miles
	hectares (10,000 m ²)	2.5	acres
MASS (weight)			
g	grams	0.035	ounces
kg	kilograms	2.2	pounds
t	tonnes (1000 kg)	1.1	short tons
VOLUME			
ml	milliliters	0.03	fluid ounces
l	liters	2.1	pints
m ³	cubic meters	1.06	quarts
	cubic meters	0.26	gallons
	cubic meters	35	cubic feet
	cubic meters	1.3	cubic yards
TEMPERATURE (degrees)			
C	Celsius temperature	9/5 (then add 32)	Fahrenheit temperature



CONTENTS

<u>Section</u>		<u>Page</u>
	PREFACE	
1	INTRODUCTION	1
2	INSTRUMENTATION	3
	2.1 Laser Doppler Velocimeter System	3
	2.1.1 Arc-Scan Mode of Operation	12
	2.1.2 Finger Scan Mode of Operation	14
	2.2 Data Processing	17
3	DESCRIPTION OF EXPERIMENTAL TESTS	21
	3.1 Flight Test Program	21
	3.2 Operation of Laser Doppler Velocimeter Remote Sensor	23
	3.2.1 Calibration	23
	3.2.2 Wake Surveys	23
4	RESULTS OF WAKE VORTEX MEASUREMENTS	28
	4.1 Vortex Roll-Up	28
	4.1.1 Initial Spanwise Downwash Distribution	28
	4.1.2 Vortex Pair Characteristics	60
	4.1.3 Multiple Vortex Characteristics	64
	4.2 Vortex Transport	68
	4.2.1 Near Wake Vortex Tracks	68
	4.2.2 Far Wake Vortex Tracks	68
	4.2.2.1 Low-Speed Data	71
	4.2.2.2 High-Speed Data	71
	4.3 Vortex Decay	76
	4.3.1 Decay of Vortex Rotational Velocity	81
	4.3.2 Core Radius Time History	83
	4.3.3 Circulation Decay	83
	4.3.4 Comparison of Vortex Decay Trends for Different Flight Configurations	89

<u>Section</u>		<u>Page</u>
5	CONCLUSIONS	94
	REFERENCES	95
<u>Appendix</u>		
A	External Logs for Rosamond Tests	A-1
B	Sample Output from Vortex Azimuth Display and Vortex Tracker Program for Rosamond Flyby 25	B-1
C	Sample Output from NASA-MSFC LDV Data Processing Routines for Rosamond Flyby 47	C-1
D	Wake Vortex Tracks Computed from Low-Speed Measurements	D-1
E	Wake Vortex Tracks Computer from High-Speed Measurements	E-1
F	Time History of Vortex Rotational Velocity	F-1
G	Time History of Vortex Circulation	G-1
H	Report of Investigations	H-1

LIST OF TABLE

<u>Table</u>		<u>Page</u>
1	Summary of B-747 Flight Parameters	24

LIST OF ILLUSTRATIONS

1	Lockheed LDV System Monitoring Wake Vortex Generated by a B-747 Aircraft at the Rosamond California, Test Site	4
2	Component Configuration of the Lockheed Laser Doppler Velocimeter	6
3	View Through Side Window of Laser Doppler Velocimeter Depicting Scanning Optics (Note relection of telescope primary mirror in elevation scanning mirror)	7
4	Interior View of Laser Doppler Velocimeter Van Looking Forward (Depicted in foreground is elevation scanning mirror on left and laser on right. Teleprinter in right rear.)	8

LIST OF ILLUSTRATIONS (Continued)

<u>Figure</u>		<u>Page</u>
5	Interior View of Laser Doppler Velocimeter Van (Display and scanner controls in first rack, computer in second rack, digital tape unit aft, and optics package on right.)	9
6	Definition of Laser Doppler Velocimeter Output Signature	11
7	Geometry for Arc Scanning for Rosamond Wake Vortex Tests	13
8	Magnitude of Characteristic LDV Velocity Component Observed During One Finger - Scan Sweep	16
9	Data Processing Sequence Carried Out for the Rosamond Wake Decay Measurements	18
10	Spoiler and Flap Arrangement on B-747 Aircraft	22
11	Location of Lockheed LDV During the Rosamond Wake Vortex Measurements	26
12	Overhead Arc Scan Configuration Illustrated for Rosamond Flyby 11	27
13	$ V_{pk} $ as a Function of Lateral Distance for Rosamond B-747 Flyby 8	29
14	$ V_{pk} $ as a Function of Lateral Distance for Rosamond B-747 Flyby 11	36
15	$ V_{pk} $ as a Function of Lateral Distance for Rosamond B-747 Flyby 12	45
16	$ V_{pk} $ as a Function of Lateral Distance for Rosamond B-747 Flyby 13	52
17	Magnitude of Line-of-Sight Velocity Component for Rosamond B-747 Flyby 11 at $t \sim 2$ sec, Assuming a Fully Rolled-Up Vortex Pair	61
18	Magnitude of Wake Vortex Velocity Distribution with 0 Spoilers	63
19	Circulation as a Function of Radius for 0 Spoiler Flight Configuration	65
20	Magnitude of Line-of-Sight Velocity Component for Rosamond B-747 Flyby 11 at $t \sim 2$ sec, Assuming Multiple Wake Vortices	67

LIST OF ILLUSTRATIONS (Concluded)

<u>Figure</u>		<u>Page</u>
21	Vortex Descent as a Function of Downstream Distance for Flybys with 30/30 Flaps, 0 Spoilers	69
22	Vortex Spacing as a Function of Downstream Distance for Flybys with 30/30 Flaps, 0 Spoilers	70
23	Comparison of Photographic and LDV Measurements for Rosamond B-747 Flyby 27	72
24	Comparison of Photographic and LDV Measurements for Rosamond B-747 Flyby 28	77
25	Decay of Magnitude of Wake Vortex Rotational Velocity Component for Flyby 44	82
26	$ V_{pk} $ as a Function of Time for Flyby 27 Using Photographic Tracks to Locate the Vortex Center	84
27	$ V_{pk} $ as a Function of Time for Flyby 28 Using Photographic Tracks to Locate the Vortex Center	85
28	Vortex Core Radius as a Function of Time for Flyby 27	86
29	Vortex Core Radius as a Function of Time for Flyby 28	87
30	Vortex Core Radius as a Function of Time for Flyby 44	88
31	Comparison of Magnitude of Wake Vortex Rotational Velocity for B-747 Flybys With and Without Spoilers	90
32	Comparison of Magnitude of Wake Vortex Rotational Velocity Component for B-747 With and Without Flaps	91
33	Comparison of Magnitude of Wake Vortex Rotational Velocity Component for B-747 With and Without Gear Down	92
34	Comparison of Magnitude of Wake Vortex Rotational Velocity Component for B-747 in Level Flight and in Descending Flight	93

1. INTRODUCTION

Wake vortex transport and decay parameters near the ground are important factors in determining safe aircraft separation distances for terminal areas. For an operational Wake Vortex Avoidance System (WVAS), a knowledge of the location and intensity of wake vortices near the terminal area is necessary to determine the minimum-delay safe spacings. Under light cross-wind conditions, a wake vortex can remain in the approach corridor, and the minimum aircraft separation distance is dictated primarily by the wake decay process near the ground. Therefore, an important consideration in determining safe aircraft separations is the decay of the wake vortex near the ground. While numerous vortex decay theories have been proposed, there are little full-scale experimental data available for comparison. Experimental vortex decay data near the ground are also lacking for aerodynamic wake minimization concepts where variations in aircraft geometry are used to tailor the wake vortex flow. Flight tests by NASA have shown that certain flap and spoiler settings can reduce the imposed rolling moments on following aircraft (in the near wake); however, wake vortex measurements near the ground for full-scale aircraft with different wake minimization concepts are needed. Thus, for both wake vortex avoidance and wake vortex minimization techniques, a knowledge of the vortex-rollup, transport, and decay characteristics near the ground is important.

To determine the behavior of aircraft wake vortices at low altitudes, a flight test program was conducted by DOT/NASA. The primary goal of the test program was to measure the wake vortex decay process behind a conventional jumbo jet as a function of altitude above ground, flap and spoiler settings, and different flight configurations. To isolate the influence of aircraft and flight parameters on the wake decay process, the flight tests were conducted at the Rosamond Dry Lake test area in California during the

early morning hours when calm atmospheric conditions prevailed. The Rosamond wake decay measurements were sought to quantify the effect of burst, link and viscous decay parameters on the wake vortex dissipation process. The wake decay measurements were also sought to demonstrate the effectiveness of recently developed vortex minimization concepts. In addition to the wake decay measurements, the flight tests were also focused on measuring the wake vortex rollup and transport phenomena in ground plane proximity.

The Rosamond flight tests involved airborne and ground-based meteorological sensors, an acoustic Doppler system, a mobile laser Doppler velocimeter, a flow visualization using smoke and balloons. In this report the measurements obtained with the laser Doppler velocimeter system (LDV) are discussed including: (1) the initial downwash field; (2) the lateral and horizontal transport of the coherent wake vortex; and (3) the decay of the vortex flow in terms of the time history of the circulation, peak tangential velocity, and the diffusion of the viscous core radius. While the application of LDV techniques for the study of wake vortex flows is not novel, this is the first time, to our knowledge, that the details of the vortex formation and decay process have been extracted for a full-scale aircraft using an LDV system. In addition to providing detailed wake measurements for comparison with available theoretical and empirical models, the results show the influence of changes in flap, spoiler, and landing gear settings on the wake characteristics.

The report discusses the LDV wake vortex measurements including the instrumentation used, the experimental test sequence, and the results of the wake measurements in terms of the vortex-rollup, transport, and decay trends, and a comparison of the wake vortex decay characteristics for different configurations. A brief discussion of the LDV wind measurements is given followed by the overall conclusions and recommendations.

2. INSTRUMENTATION

The wake vortex and atmospheric wind measurements were carried out by means of a scanning LDV system contained in a mobile van. Preliminary processing of the data was carried out with a SEL computer aboard the van. Reduction and analysis of the vortex and wind signatures were carried out by off-line processing software using a Univac 1108 and a PDP11 computer. A description of the instrumentation and the data processing methods for the Rosamond tests is given in terms of the LDV system configuration and the data processing techniques used.

2.1 Laser Doppler Velocimeter System

The Lockheed-Huntsville LDV was used to obtain wake vortex measurements during the Rosamond flight tests. A photograph of the van-mounted LDV system is given in Fig. 1. The wake measurements were accomplished as follows: (1) the wake generated by the aircraft was scanned by the CO₂ laser; (2) the radiation backscattered from the aerosol in the wake was collected; (3) the radiation was photomixed with a portion of the transmitted beam on a photodetector; and (4) the intensity and Doppler shift frequency of the signal were displayed.

The difference in frequency between the transmitted and backscattered signal generated at the photodetector, the Doppler shift frequency, is a measure of the aerosol's absolute line-of-sight velocity within the laser focal volume

$$|\bar{V}| = \frac{\lambda \Delta f}{2 \cos \gamma}, \quad (1)$$

where $|\bar{V}|$ is the magnitude of the velocity component in the region being sensed, λ is the laser radiation wavelength (10.6 μm), Δf is the Doppler shift,

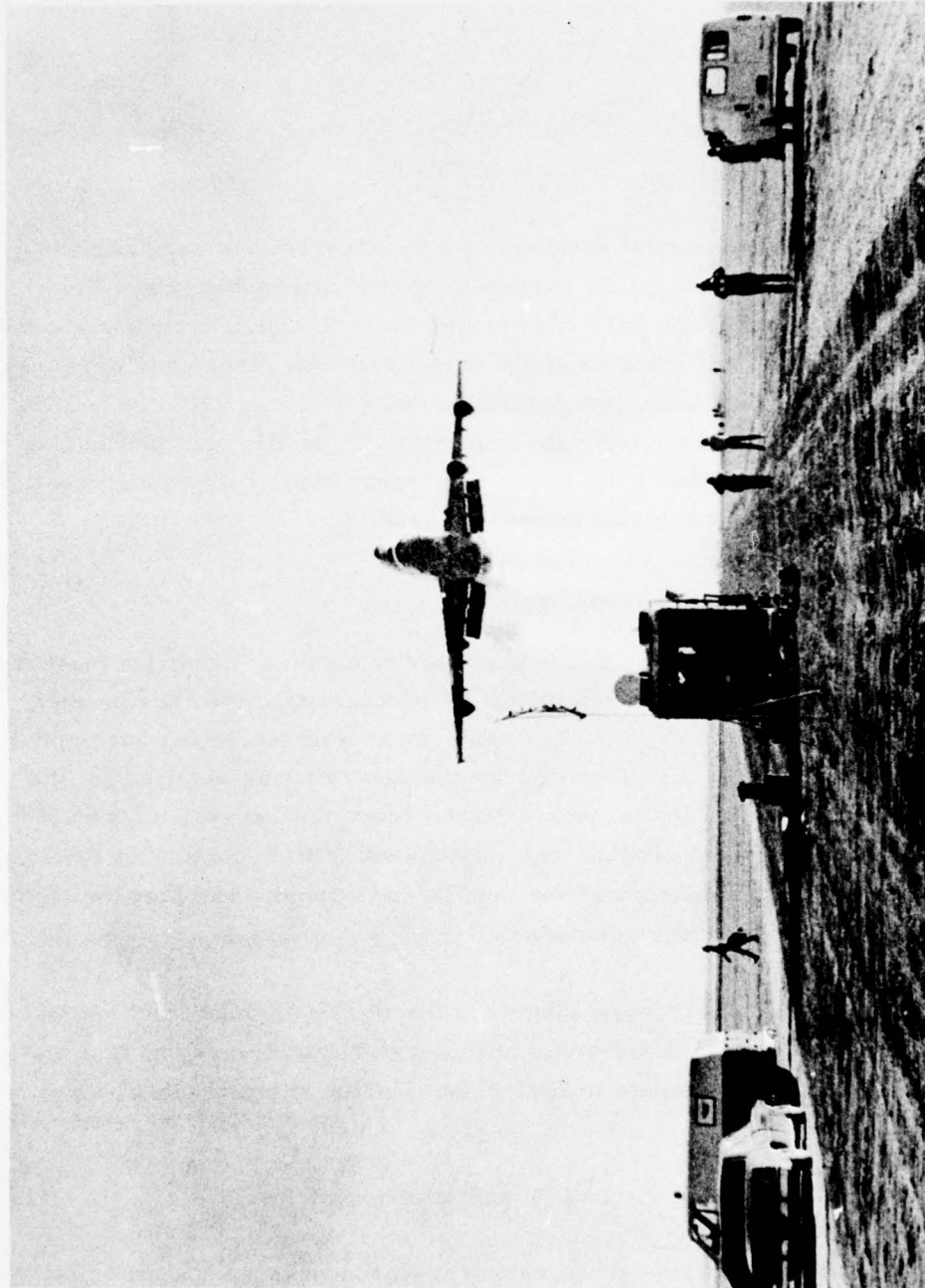


Fig. 1 - Lockheed LDV System Monitoring Wake Vortex Generated by a B-747 Aircraft
at the Rosamond, California, Test Site

and γ is the angle subtended by the velocity vector and the optic system line of sight. From Eq.(1), it is noted that the Doppler shift is a direct and absolute measure of aerosol velocity component and a frequency shift of 188 kHz corresponds to a 1 m/sec magnitude line-of-sight velocity.

A sketch of the optical and electronic equipment for measuring the intensity and frequency spectrum of the coherent backscatter from the focal volume is shown in Fig. 2, and described in more detail in Refs. 1, 2, and 3. Photographs of the optical and electronic equipment for measuring the aerosol backscatter are shown in Figs. 3, 4, and 5.

The Lockheed LDV system used in the Rosamond wake vortex tests monitors the magnitude of the velocity component of ambient atmospheric particulate matter within its instantaneous sensing volume. The pertinent operating characteristics of the LDV are summarized as follows:

Performance

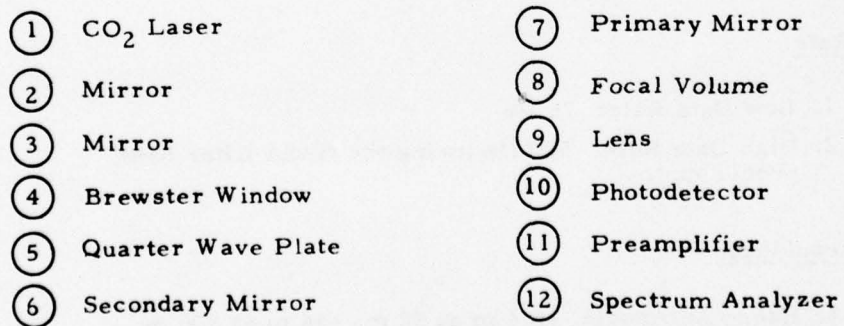
1. Threshold of Magnitude of Velocity Component: 0.5 m/sec
2. Range of Magnitude of Velocity Component: 0.5 to 28 m/sec

Sample Rate

1. Low Data Rate: 70 Hz
2. High Data Rate: 500 Hz (using the NASA filter bank processor).

Spatial Resolution

1. Range Accuracy: ± 0.4 m at 30 m, ± 44 m at 300 m
2. Elevation Angle Accuracy: ± 0.25 deg.



6

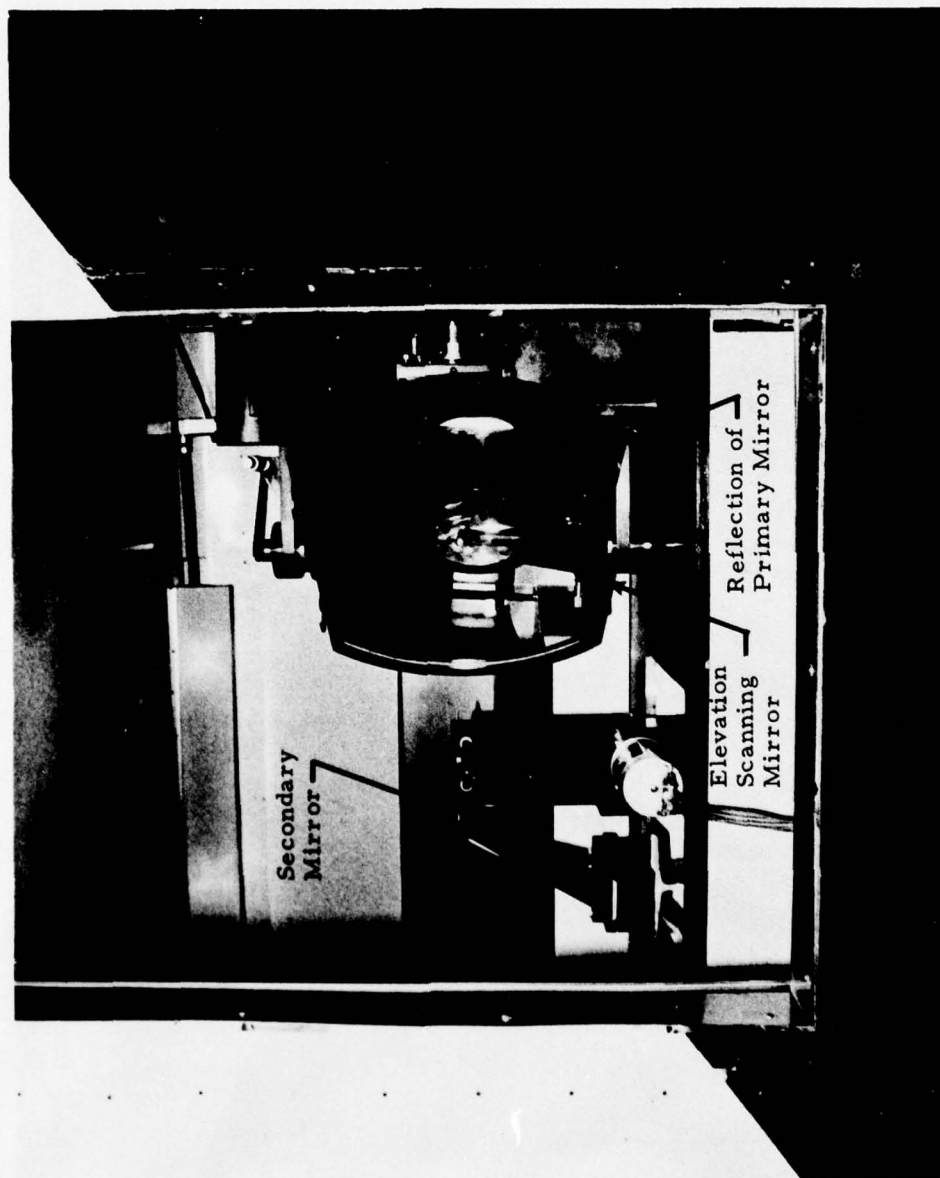


Fig. 3 - View Through Side Window of Laser Doppler Velocimeter Depicting Scanning Optics (Note reflection of telescope primary mirror in elevation scanning mirror)

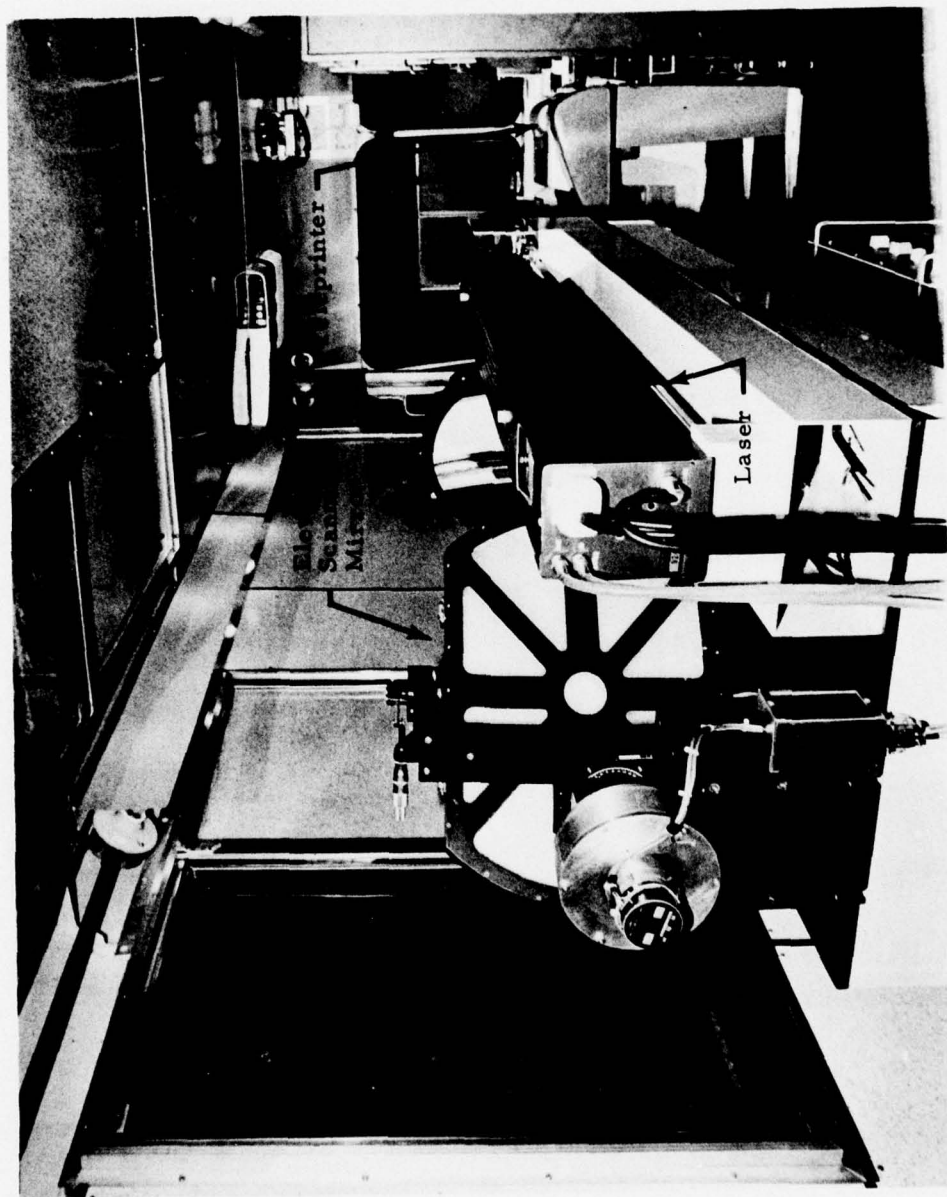


Fig. 4 - Interior View of Laser Doppler Velocimeter Van Looking Forward (Depicted in foreground is elevation scanning mirror on left and laser on right. Teleprinter in right rear.)

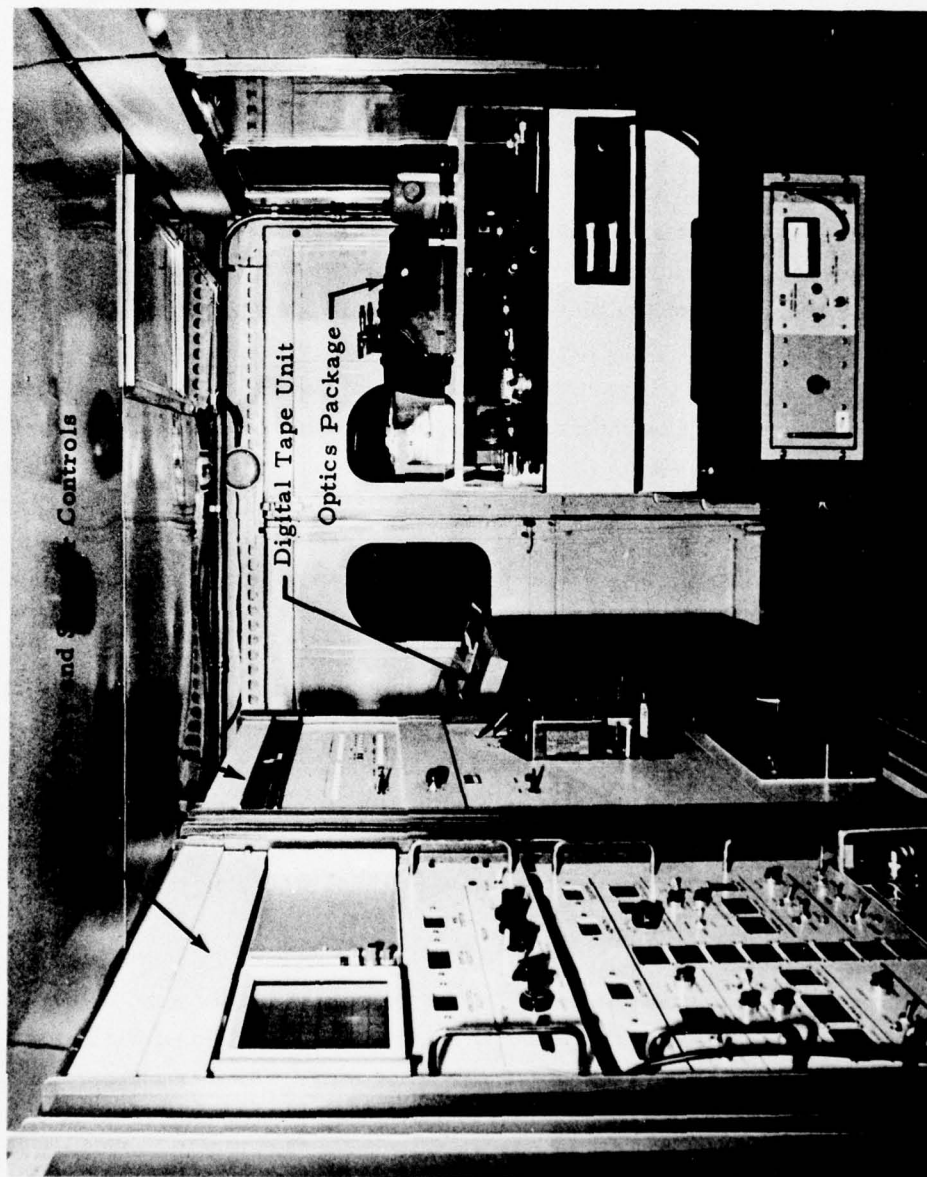


Fig. 5 - Interior View of Laser Doppler Velocimeter Van (Display and scanner controls in first rack, computer in second rack, digital tape unit aft, and optics package on right.)

Scan Modes

- | | |
|-----------------------|-------------------------------------|
| 1. Range or Line Scan | 5. Horizontal Wind |
| 2. Elevation | 6. Vertical Wind |
| 3. Altitude | 7. Wind Direction |
| 4. Azimuth | 8. Line-of-Sight Velocity Component |

The characteristic output signal from the LDV system is an intensity versus frequency spectrum illustrated in Fig. 6. The output parameters V_{pk} and V_{ms} are indicative of the magnitude of the velocity component in the LDV focal volume corresponding to the fastest particle (or particles) above the amplitude threshold and the particle (or particles) having the highest backscatter, respectively. The bandwidth, N , is a measure of the range of particle velocities in the focal volume. Intensity and frequency thresholds are applied to the signal, as shown, to eliminate noise and to improve the resolution of the system. For example, in the vortex tracking mode the frequency threshold of the LDV is set relatively high to filter out the low-frequency signal associated with the ambient wind.

The velocity resolution of the LDV is determined by the signal-to-noise ratio characteristics of the system as well as the atmospheric aerosol particle-size distribution. During the Rosamond tests, no difficulty was encountered detecting the high velocity regions, as high as 28 m/sec, associated with the wake vortex phenomena. The very low ambient winds, on the order of 1 to 2 m/sec, were also detected by the LDV at Rosamond which were above the system's threshold of 0.5 m/sec.

The spatial resolution of the LDV is determined by the size of the laser beam sensing volume where the beam is focused. The extent of the laser Doppler system sensing volume is a function of range which is shown in the following table ($\Delta r = 9.84 \times 10^{-4} (m^{-1}) R^2$) obtained from calibration measurements (Ref. 4).

- V_{pk} = Magnitude of velocity component of highest channel above amplitude threshold
- V_{ms} = Magnitude of velocity component of the channel having the peak signal

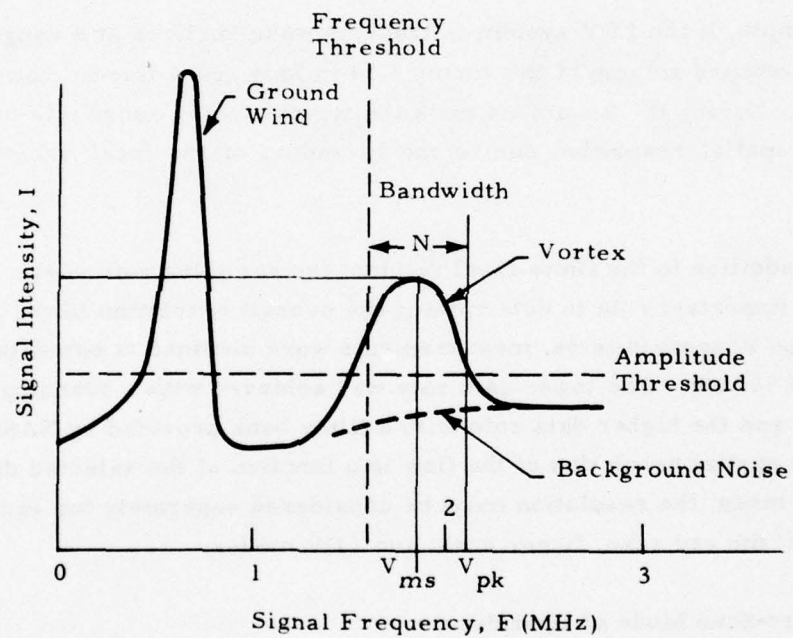


Fig.6 - Definition of Laser Doppler Velocimeter Output Signature

Range to Focus, R(m)	Sensing Volume Length (Half Power Value) Δr (m)
76	5.68
100	9.84
152	22.73

For example, if the LDV system is tracking wake vortices at a range of 60 m, a needle-shaped volume of the vortex 3.54 m long and 4 mm in diameter is sampled. During the Rosamond tests, the typical vortex range was 60 m so that the spatial resolution due to the spreading of the focal volume was 3.54 m.

In addition to the finite focal volume, the sampling rate of the LDV plays an important role in determining the overall resolution of the system. During the Rosamond tests, measurements were obtained at two data rates, at 70 and 500 Hz. The lower data rate was achieved with a scanning spectrum analyzer and the higher data rate with a filter bank provided by NASA-MSFC. Since the spatial resolution of the flow is a function of the selected data rate and scan mode, the resolution must be considered separately for each type of operation; the arc scan, finger scan, and LDV modes.

2.1.1 Arc-Scan Mode of Operation

In the arc-scan mode, the LDV interrogates the vortex wake at a fixed range along an arc normal to the aircraft flight path. As shown in Fig. 7, the sensing volume is moved between two elevation limits (the typical cone angle is $2\alpha = 30$ deg) at a fixed rate (the typical scan rate is 0.5 Hz) while the vortex drifts past the scanned arc. Thus, the arc scan measurements indicate the spanwise downwash distribution in the wake of the aircraft, provided that vortex range is sufficiently close to the selected scan range.

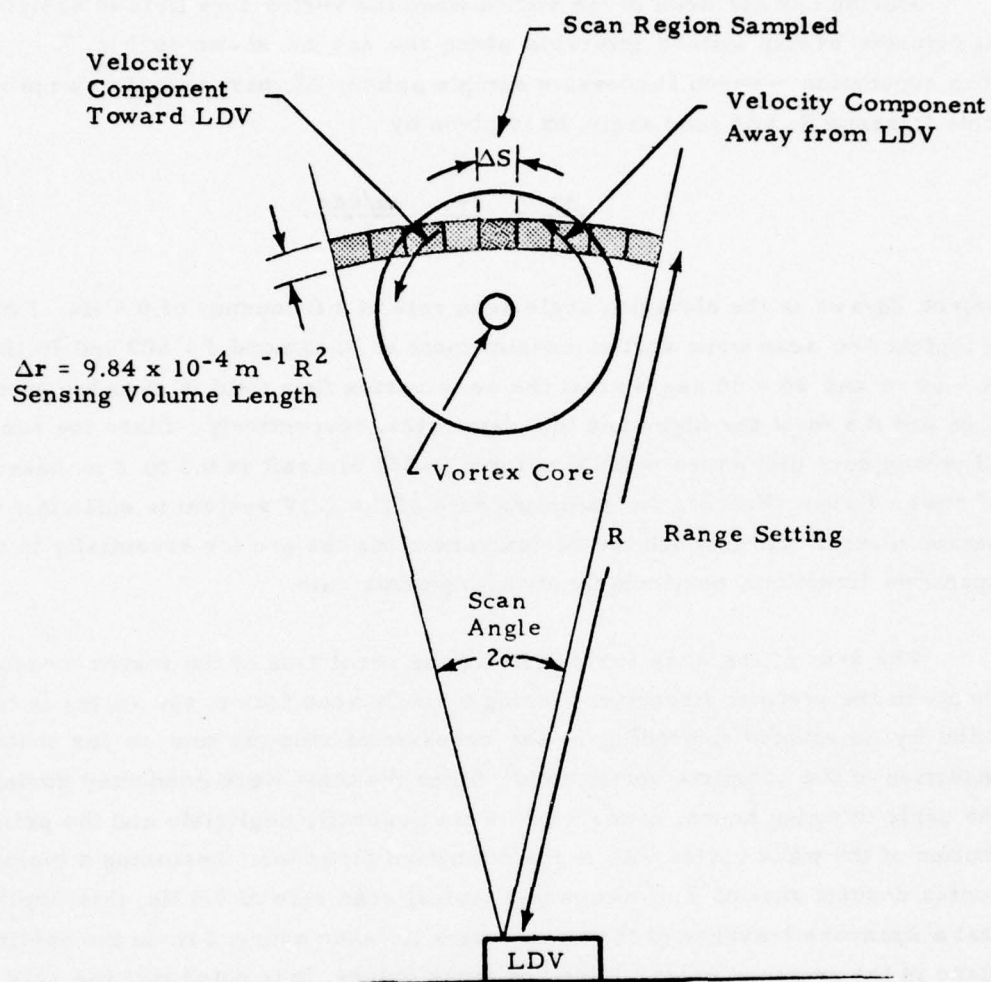


Fig. 7 - Geometry for Arc Scanning for Rosamond Wake Vortex Tests

During one arc scan of the vortex wake, the vortex flow field is sampled at discrete evenly spaced intervals along the arc as shown in Fig. 7.

The separation between successive sample points, ΔS , based on the sampling rate f , range R , and cone angle 2α is given by

$$\frac{\Delta S}{R} = \frac{2\pi}{360^\circ} \frac{2\alpha/\text{sec}}{f}, \quad (2)$$

where $2\alpha/\text{sec}$ is the elevation angle scan rate at a frequency of 0.5 Hz. For a typical arc scan wake vortex measurement at Rosamond, $f = 500$ and 70 Hz, $R = 60$ m and $2\alpha = 30$ deg, so that the wake vortex flow field is sampled every 0.06 and 0.4 m at the high- and low-data rates, respectively. Since the range of vortex core diameters measured for a B-747 aircraft is 0.3 to 2 m based on tower flybys (Ref. 5), the sampling rate of the LDV system is sufficient to obtain several cuts through the vortex core along the arc (or essentially in the spanwise direction), particularly at the high data rate.

The drift of the wake vortex affects the resolution of the vortex measurements in the vertical direction. During a single scan frame, the vortex is translated by an amount depending on the cross-wind velocity and on the mutual induction of the complete vortex field. Since the tests were conducted during the early morning hours, cross winds were generally negligible and the primary motion of the wake vortex was in the downward direction. Assuming a typical vortex descent rate of 2 m/sec, and a typical scan rate of 0.5 Hz, this implies that a spanwise traverse of the wake vortex is taken every 2 m in the vertical plane in the arc-scan mode. Based on these values, it is noted that the LDV arc-scan technique can observe the detailed characteristics of the wake vortex phenomena which are larger in extent than 0.06 and 2 m in the horizontal and vertical directions, respectively.

2.1.2 Finger-Scan Mode of Operation

During the Rosamond flight tests, 56% of the LDV wake vortex measurements were conducted using the finger-scan mode. In the finger-scan mode, both the range and elevation of the laser beam were varied simultaneously and

linearly with time, producing a multiple lobe scan pattern with the laser beam as shown in Fig. 8. The settings and sampling rates for the finger-scan mode are given in Appendix A.

The distance between sample points for the finger-scan mode is higher than for the previous arc-scan mode. From Appendix A, it is noted that the typical range scan excursion for the finger scan mode is 105 m, and the normal range rate is 3.5 Hz. It follows that the beam-scan velocity is 735 m/sec. Because the LDV measurements were sampled every 2 and 14.3 msec at the low and high data rates, the wake vortex flow field is measured at every 1.5 and 10.5 m increment in range, respectively. Thus, the finger scan mode can interrogate a large cross-sectional area rapidly, and this is ideal for vortex tracking. In addition, the LDV finger scan measurements contain essential information regarding the wake vortex phenomena.

The characteristic line-of-sight component as a function of range and elevation angle during one finger-scan sweep is shown in Fig. 8. A pair of double-peak patterns is noted in the line-of-sight velocity profile as a function of elevation angle. The maximum values occur at the elevation angles where the line of sight is tangent to the viscous core radius of the vortex. Thus, the mean elevation angle of the local maxima in the V_{pk} vs θ curve yields the elevation angle of the wake vortex, $\theta_{vortex} = (\theta_1 + \theta_2)/2$. Similarly, the difference between the two elevation angles is a measure of the vortex viscous core radius, $r_{vortex\ 1} = R_1 \left| \tan \frac{\theta_1 - \theta_2}{2} \right|$. The peak tangential velocity and core circulation of the vortex is given by $V_{pk\ vortex\ 1} = (V_{pk\ \theta_1} + V_{pk\ \theta_2})/2$ and $\Gamma_{vortex\ 1} = 2\pi R_{vortex\ 1} V_{pk\ vortex\ 1}$, assuming circular symmetry. The peak line-of-sight component at the two edges of the vortex, $V_{pk\ \theta_1}$ and $V_{pk\ \theta_2}$ are not necessarily equal due to a contribution by the other vortex and the ambient winds. The range of the vortex, R_1 , is given by the local maximum in the line-of-sight component at the two edges of the in the bottom of Fig. 8, and is not affected by the ambient winds. Based on the characteristic LDV signature observed for one scan, it is noted

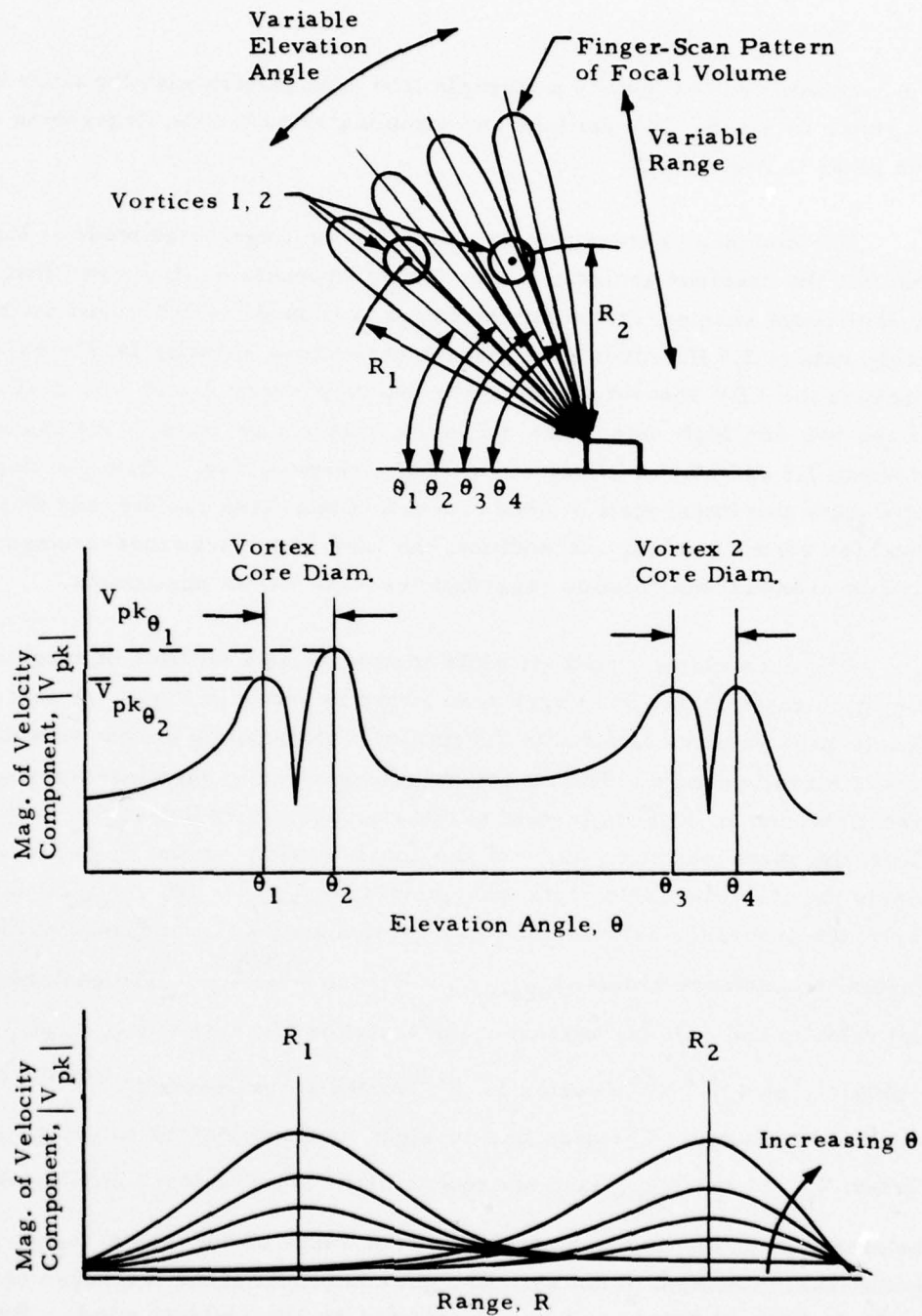


Fig. 8 - Magnitude of Characteristic LDV Velocity Component Observed During One Finger-Scan Sweep

that several successive finger scans contain the essential decay history of the wake vortices, provided that at least two sample points are obtained for each vortex, one upwash and one downwash measurement, where the line of sight is tangent to the viscous core and the mean vortex range is within the LDV focal volume.

2.2 DATA PROCESSING

The output from the LDV system consisting of the coherent backscatter intensity versus frequency from the focal volume as well as the location of the focal volume in space was processed to yield the aircraft downwash field and the wake vortex characteristics. Reduction and analysis of the LDV measurements were carried out as follows: (1) the low-speed signal was digitized and stored on magnetic tape by the onboard SEL computer and subsequently processed off-line on a Univac 1108 computer, and (2) the high-speed data were both digitized and processed off-line on a Univac 1108 computer and the vortex tracks computed on a PDP 11 computer. A flow chart of the data processing sequence used for the Rosamond wake decay study is shown in Fig. 9. The software system for processing the low-speed and high-speed LDV data is described in more detail in Refs. 4 and 6, respectively.

The high-speed processor utilized the raw range and elevation signal, while the low-speed processor used the raw range and commanded elevation signal to determine the location of the LDV focal volume. As a result, the magnitude of the velocity component versus elevation angle measured with the high-speed processor showed scatter due to the ± 0.25 deg elevation angle resolution. In addition, noise was present in the elevation angle versus time distribution from the high-speed data characterized by a square wave with a frequency of 14 Hz and an amplitude of 0.7 deg. This was believed to be a symptom of a processing or decode problem. The normal scatter in the elevation angle was not noticeable at the low data rate, but the low-speed data did show a finite lag in the scan pattern. A time lag of approximately 0.3 sec, and a corresponding lag in the position of the LDV focal volume depending on the selected scan rate was observed. The lag in the system resulted from the difference between commanded versus actual angular position of the scanning mirror.

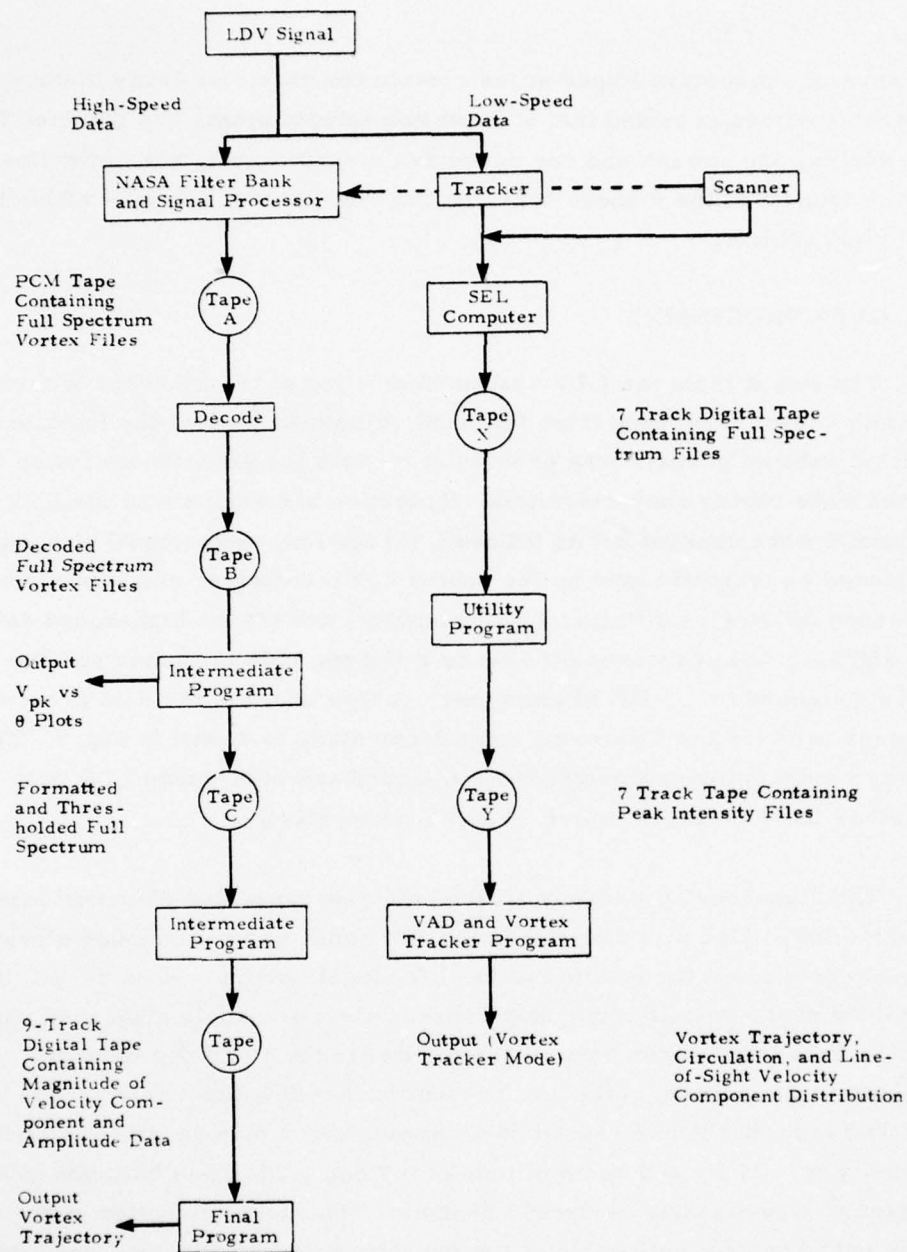


Fig. 9 - Data Processing Sequence Carried Out for the Rosamond Wake Decay Measurements

The manner in which the wake vortex measurements were processed from both the high-speed and low-speed data is summarized as follows. The frequencies and amplitudes associated with the laser Doppler signal were sampled at fixed intervals. The spectrum was recorded if it was above the frequency and amplitude threshold settings (Fig.6). The amplitude and frequency threshold settings for the Rosamond tests are given in the log sheets in Appendix A. From the array of recorded frequency and intensity points, the magnitude of the line-of-sight velocity component was computed, and the vortex parameters including location and velocity distribution were determined.

To compute the wake vortex transport and decay characteristics from the low-speed line-of-sight velocity component magnitude, the Rosamond measurements were analyzed using the "Velocity Azimuth Display and Vortex Track Program" (Ref.5). Based on previous experience with the program, the following parameters were selected for the analysis of the Rosamond data:

INTVEL = 2	Flag INTVEL = 1, Velocity oriented vortex determination INTVEL = 2, Intensity oriented vortex determination
NPSUF = 4	Sufficient number of points to determine vortex position
APERCT = 0.1	Fraction of points below the maximum velocity or intensity points
BPERCT = 0.1	Fraction of points within the correlation circle where Q is at least APERCT fraction of the maximum Q (Q is velocity or intensity as determined by INTVEL)
RPERCT = 0.3	Fraction of number of points in correlation circle used for determining vortex 1 (required for determination of vortex 2)
RPERCT = 0.3	Fraction of aircraft wing span used for correlation radius
EPERCT = 2.0	Fraction of correlation radius from vortex 1 for excluding initial point of vortex 2
NOISEF = 0	Noise floor
ADJI = 0.0	Intensity adjustment (fraction of noise floor added to total intensity).

A sample output from the VAD and Vortex Track Program is presented in Appendix B. The intermediate sorting parameters used in determining the location of the vortex core region are also given in the printouts along with "scatter plots" indicating the line-of-sight velocity magnitudes. From the typical line-of-sight velocity magnitude illustrated in Appendix B, the time history of the vortex wake was determined for many of the flybys.

In parallel with the low-speed data acquisition and processing, the LDV signal was also fed into the high-speed NASA-MSFC data processing system as illustrated in Fig. 9. The high-speed data processing technique is similar to the low-speed technique described earlier, and is described in detail in Ref. 6. A sample output from the NASA-MSFC LDV data processing routines is shown in Appendix C, including the listing of the magnitude of the raw line-of-sight velocity component, the plot of $|V_{pk}|$ versus elevation angle, and plots of the vortex trajectory.

3. DESCRIPTION OF EXPERIMENTAL TESTS

A two-day test sequence was carried out to determine the wake vortex characteristics of a B-747 aircraft as a function of spoiler, flap, and landing gear settings, altitude above ground, and glideslope. The test consisted of 54 low level passes during the early morning hours over the LDV system deployed at Rosamond Dry Lake near Edwards AFB, California, on 2 and 3 December 1975.

3.1 FLIGHT TEST PROGRAM

The aircraft used for the tests was a Boeing 747-123 aircraft. A plan view of the aircraft showing the details of the flap and spoiler configurations is presented in Fig. 10.

Aircraft configuration varied from run to run, with dominant emphasis on as close to a normal landing configuration as operating conditions would allow. The clean configuration was also studied, and special flap and spoiler configurations were investigated for vortex alleviation effectiveness. The Boeing 747 flew at 30 to 250 m above the ground level of 700 m MSL. Runs were made in level flight as well as in descending and climbing flight. Descents were at about 250 m/min. A lift coefficient of approximately 1.4 was used for all flaps-down runs.

Of the 54 runs, 35 (or about 65%) were made with the inboard flaps lowered 30 deg and the outboard flaps lowered 30 deg (denoted 30/30); eight (approximately 15%) with 10/10 flaps; and five (approximately 9%) with flaps retracted. The remaining six runs had the inboard flaps lowered 30 deg and the outboard flaps lowered 1 deg, to test the effects of this configuration

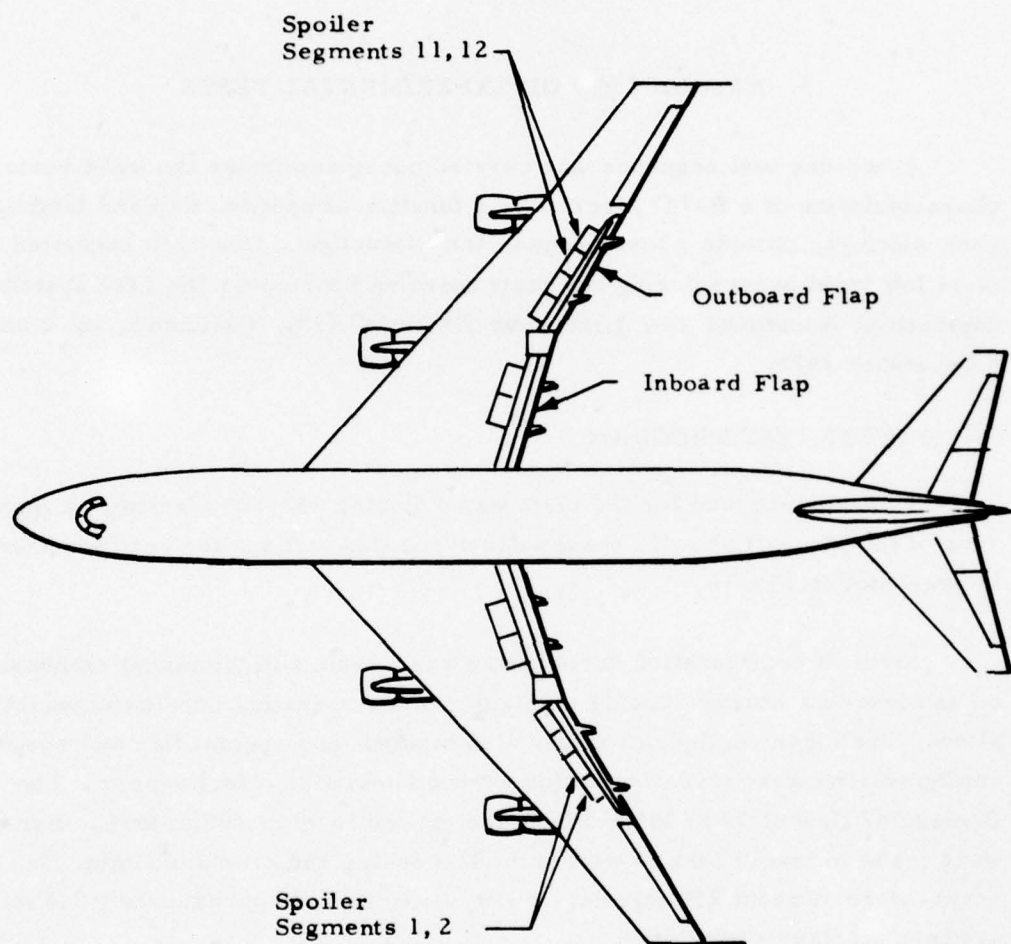


Fig. 10 - Spoiler and Flap Arrangement on B-747 Aircraft

on vortex alleviation. For each flap setting, runs were conducted with the gear down or retracted, and some had spoilers deployed (the extension angle was always 41 deg) in addition to the flap. A summary of the aircraft altitude, speed, weight, and flap, landing gear, and spoiler settings for each of the flybys is given in Table 1.

3.2 OPERATION OF LASER DOPPLER VELOCIMETER REMOTE SENSOR

The LDV system was set up and calibrated at the Rosamond test site prior to conducting the actual wake surveys. A discussion of the calibration procedure and the conduct of the wake vortex surveys is summarized below.

3.2.1 Calibration

During the set-up process, the optical bench was leveled with the external van jacks using a bubble level for reference (estimated accuracy of ± 0.5 deg). For the second day of the tests, the scanner was offset 45 deg using a tri-square for reference (estimated accuracy of ± 0.5 deg). Prior to the actual wake surveys, the elevation and azimuth angle readouts from the LDV were calibrated. The calibration involved pointing the optical system at the sun and comparing the observed elevation and azimuth angle readouts with those given in the ephemeris. The results indicated that a -3 deg and ± 139 deg correction should be applied to the raw elevation and azimuth readouts from the LDV, respectively.

During the Rosamond tests, the range resolution and signal-to-noise ratio characteristics of the LDV were not recalibrated. The range and signal-to-noise ratio calibrations taken a few months earlier and documented in Ref. 4 were assumed to be representative of the systems overall performance.

3.2.2 Wake Surveys

During the Rosamond wake decay tests, 53 aircraft flybys were recorded with the LDV system (flyby 36 was lost due to a loss in electrical power). The test conditions and the LDV scan, range, and elevation settings for the

Table 1
SUMMARY OF B-747 FLIGHT PARAMETERS

<u>Flyby No.</u>	<u>Altitude (m AGL)</u>	<u>IAS (knots)</u>	<u>Weight (kg/1000)</u>	<u>Flap (deg)</u>	<u>Spoilers Deployed</u>	<u>Thrust (EPR)</u>	<u>Gear</u>
1	56	146	255	30/30	0	1.25	Down
2	52	146	252	30/30	0	1.21	Down
3	68	145	250	30/30	0	1.25	Down
4	65	145	249	30/30	0	1.22	Down
5	122	144	248	30/30	0	1.22	Down
6	122	144	247	30/30	0	1.23	Down
7	244	143	245	30/30	0	1.23	Down
8	244	143	244	30/30	0	1.20	Down
9	61	143	236	30/30	1, 2, 11, 12	1.26	Down
10	122	143	235	30/30	1, 2, 11, 12	1.26	Down
11	183	142	234	30/30	1, 2, 11, 12	1.25	Down
12	244	142	232	30/30	1, 2, 11, 12	1.25	Down
13	64	142	230	30/30	1, 2, 11, 12	1.24	Down
14	65	138	228	30/30	1, 2, 11, 12	1.20	Down
15	61	138	227	30/30	1, 2, 11, 12	1.20	Down
16	61	138	226	30/30	1, 2, 11, 12	1.18	Down
17	30	141	222	30/1	0	1.19	Down
18	37	141	218	30/1	0	1.18	Down
19	38	141	216	30/1	0	1.18	Up
20	57	139	215	30/1	0	1.18	Down
21	54	139	213	30/1	0	1.16	Up
22	91	139	212	30/1	0	1.23	Down
23	122	148	250	30/30	0	1.24	Down
24	122	220	259	0/0	0	1.03	Up
25	122	147	258	30/30	0	1.24	Down
26	122	215	256	0/0	0	1.06	Up
27	67 (LDG)	146	255	30/30	0	1.20	Down
28	66	146	254	30/30	0	1.20	Down
29	72 (LDG)	146	252	30/30	0	1.14	Down
30	66	145	251	30/30	0	1.24	Down
31	107 (TO)	156	243	10/10	0	1.38	Up
32	65	156	242	10/10	0	1.11	Up
33	57 (TO)	156	241	10/10	0	1.36	Up
34	59	143	240	10/10	0	1.15	Up
35	63	142	239	30/30	0	1.20	Down
36	68	142	238	30/30	0	1.20	Up
37	67	141	237	30/30	0	1.21	Down
38	61	141	236	30/30	0	1.22	Up
39	47 (TO)	151	230	10/10	1, 2, 11, 12	1.36	Up
40	46 (TO)	151	228	10/10	0	1.36	Up
41	48 (TO)	150	227	10/10	1, 2, 11, 12	1.36	Up
42	54 (TO)	150	226	10/10	0	1.40	Up
43	61	138	225	30/30	0	1.24	Down
44	63 (LDG)	138	224	30/30	0	1.12	Down
45	50 (LDG)	138	223	30/30	0	1.16	Down
46	37	137	222	30/30	0	1.24	Down
47	91	135	215	30/30	0	1.15	Down
48	91	135	214	30/30	1, 2, 11, 12	1.20	Down
49	37	134	213	30/30	1, 2, 11, 12	1.20	Down
50	91 (LDG)	134	210	30/30	0	1.11	Down
51	122	200	209	0/0	0	1.11	Down
52	122	200	208	0/0	0	1.03	Up
53	122	133	207	30/30	0	1.22	Down
54	122	200	206	30/30	0	1.05	Up

LDG: Aircraft descending along imaginary glideslope.

TO: Aircraft ascending as in actual takeoff.

Rosamond tests are summarized in the log sheets given in Appendix A, while a list of the flight parameters is given in Table 1. Primarily, those flybys have been processed from the wake measurements where flow visualization and photographic data (photographs were taken of vortices at 1 sec increments) were available for comparison with the LDV measurements.

To maximize the amount of data collected regarding wake vortex trajectories, velocity profiles, and decay rates, the LDV was operated in different scan modes including: arc-scan and, finger-scan configurations. The wake vortex surveys were conducted in the following manner.

On the first test day, the LDV was located directly under the flight path (Fig. 11) and scanned arcs in a plane perpendicular to the flight path (Fig. 12) with a complete scan every 2 sec. Scans were at a fixed range until the vortex passed through the scan arc, at which time the sensor range was lowered and remained fixed again until the vortex descended through the new range. The objective of the overhead arc scan measurements was the measurement of the initial downwash field and the wake vortex roll-up process.

On the second test day, the LDV was moved 60 m north of the flight path (Fig. 11) and scanned simultaneously in elevation and range (finger-scan mode) at a frequency of 0.2 Hz, and 2 to 2.5 Hz, respectively. The objective of the finger scan measurements was to track the location of the vortex pair and to observe the vortex decay rates. The coordinated variations in range and elevation settings for the finger scan mode were selected on the basis of the aircraft wake vortex parameters. In addition, during the last sorties, the azimuth angle was changed during the run to 90- and 180-deg angles to scan both down the vortex (axially) and to follow the vortex drift away from the LDV.

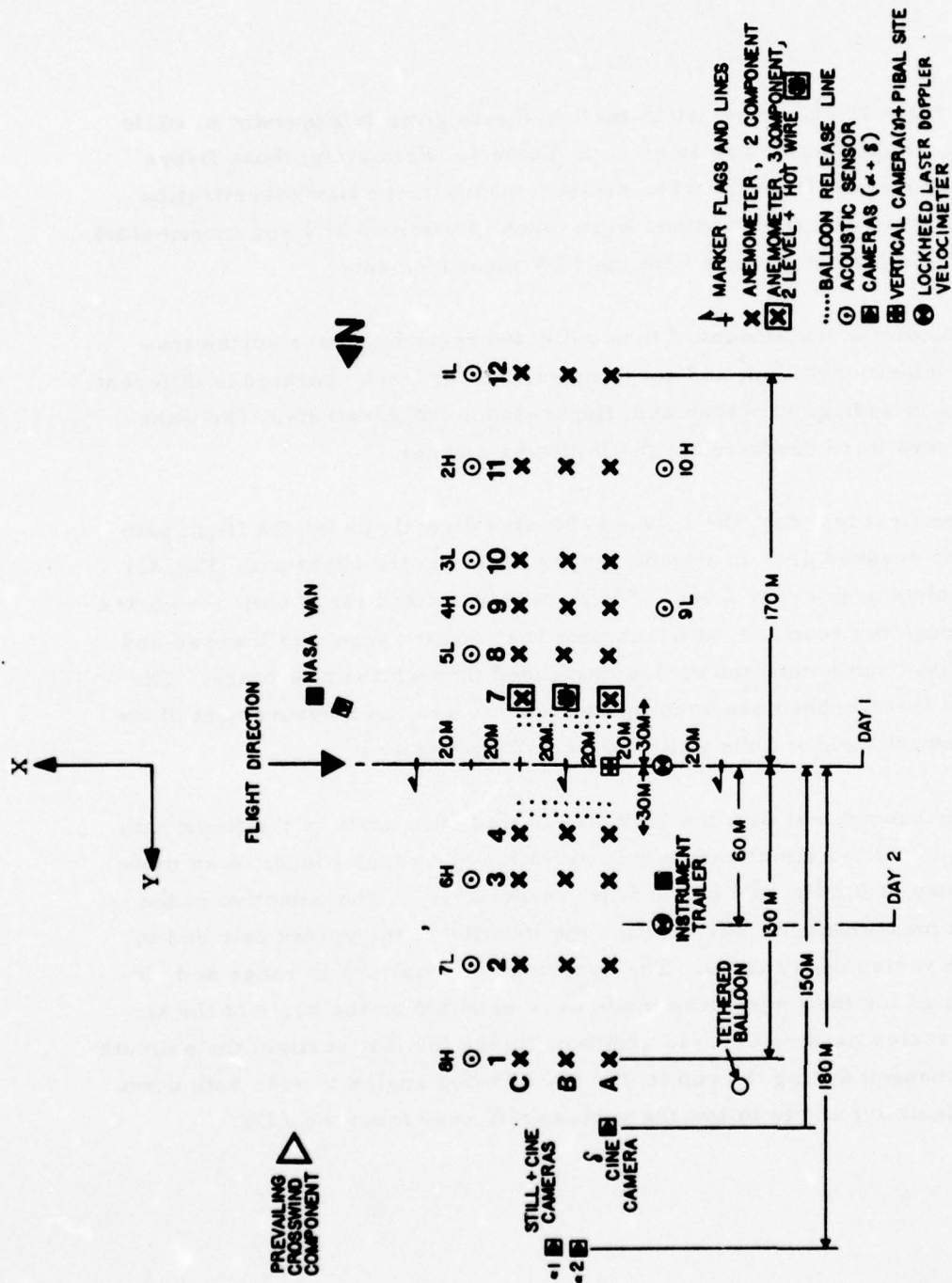


Fig. 11 - Location of Lockheed LDV During the Rosamond Wake Vortex Measurements

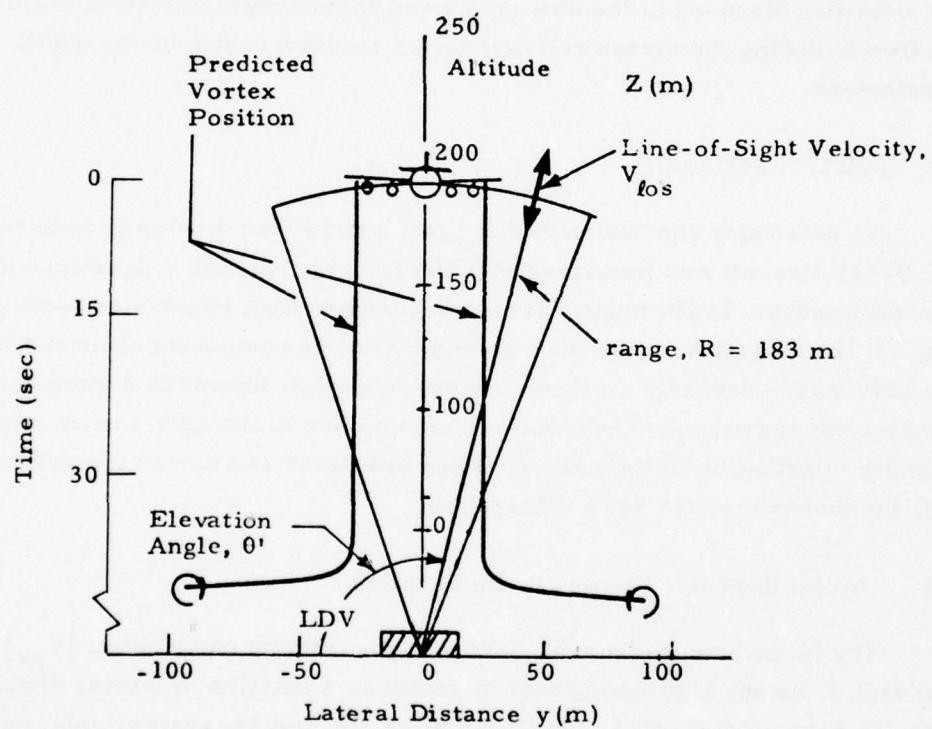


Fig. 12 - Overhead Arc Scan Configuration Illustrated for Rosamond Flyby 11

4. RESULTS OF WAKE VORTEX MEASUREMENTS

The LDV measurements obtained during the Rosamond tests have been analyzed to determine the dominant characteristics of the B-747 wake. In the following discussion, the observed wake vortex characteristics are described including the vortex roll-up, vortex transport, and vortex decay parameters.

4.1 VORTEX ROLL-UP

To determine the vortex roll-up parameters, the downwash field behind the B-747 aircraft was measured with the LDV operated in a constant-range arc-scan mode. In the typical arc-scan configuration, illustrated earlier in Fig. 13, the magnitude of the line-of-sight velocity component observed by the LDV was essentially a measure of the spanwise downwash distribution in the aircraft nearwake. Thus, from the magnitude of the LDV line-of-sight velocity distribution in the near wake the downwash and vortex formation and roll-up characteristics were determined.

4.1.1 Initial Spanwise Downwash Distribution

The magnitude of the peak line-of-sight velocity component, $|V_{pk}|$ (m/sec), from the high-speed data is shown as a function of lateral distance, y (m), in Figs. 13 through 16 for flybys 8, 11, 12, and 13, respectively, over the time interval $t = 0$ to 8 sec. Each scan is defined as the period between two successive elevation angle reversals and is approximately 1 sec in duration. Occasionally, some overlapping occurs between successive scans due to limitations in the processing software. Therefore, successive scans shown in Figs. 13 through 16 do not always have the same starting and ending limits, and, as a result, the lateral scales can be different. The direction and mid-time of each scan is indicated in the figures. The lateral distance, y , was computed directly from the raw range, R , and raw elevation angle

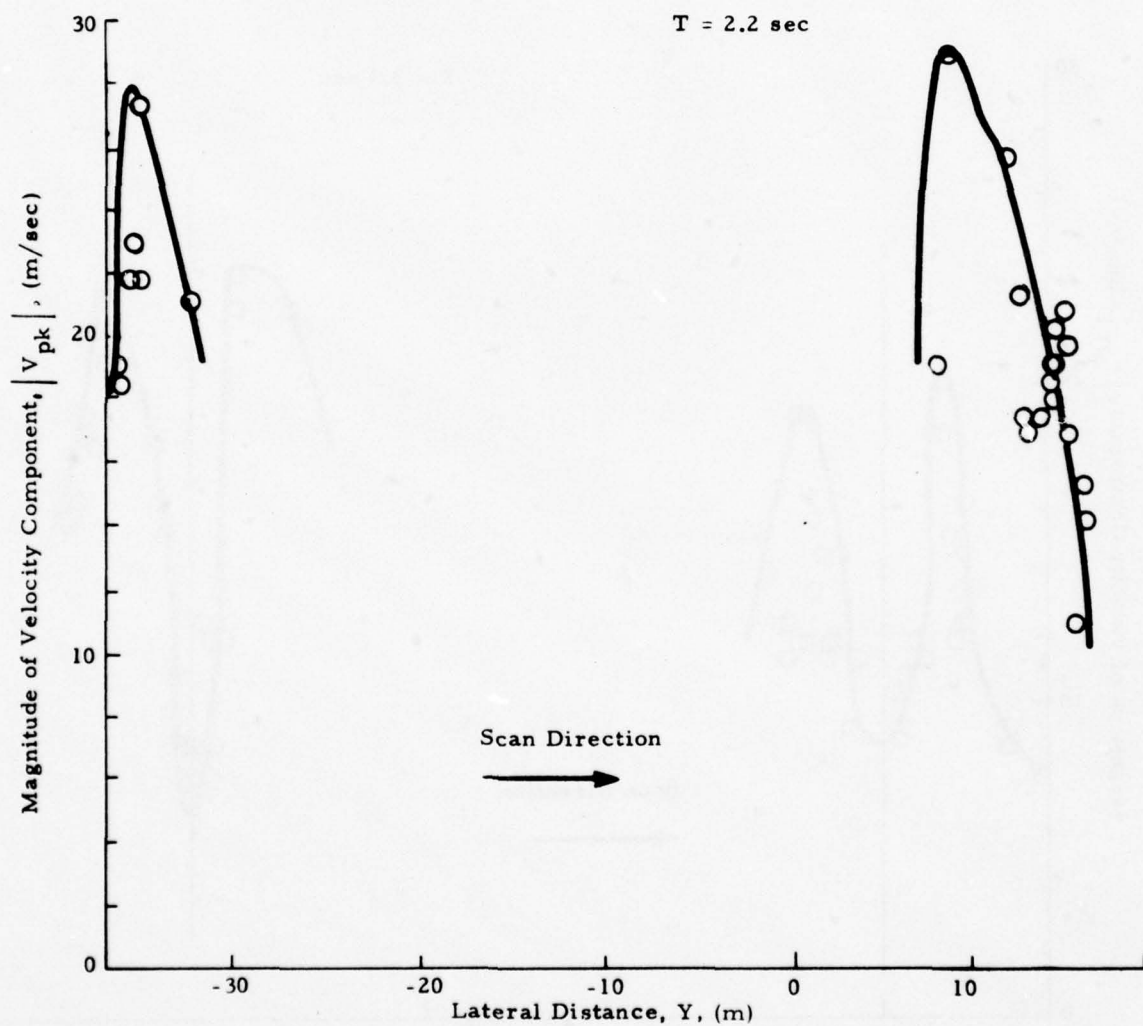


Fig. 13 - $|V_{pk}|$ as a Function of Lateral Distance for Rosamond B-747 Flyby 8

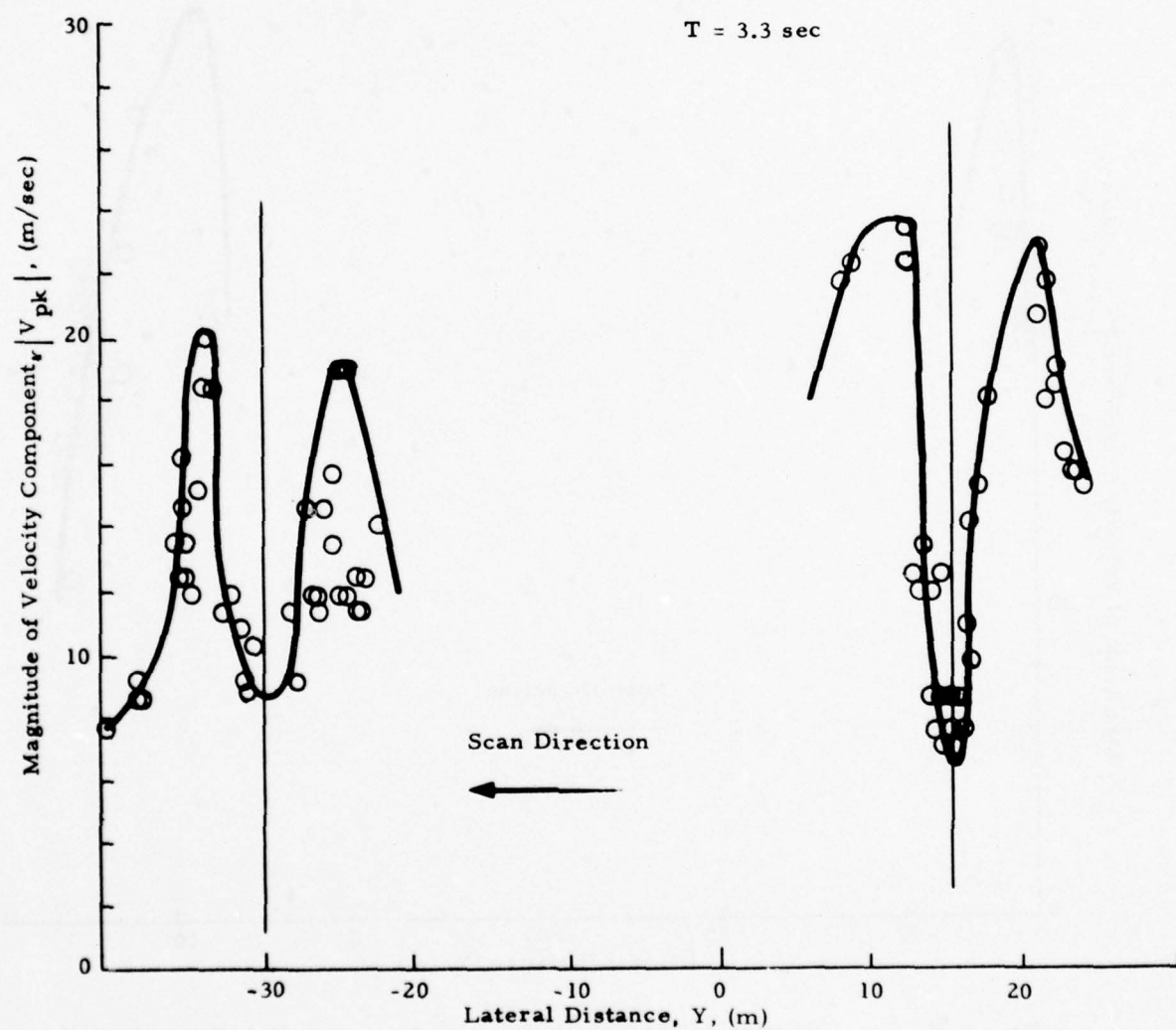


Fig.13 (Continued)

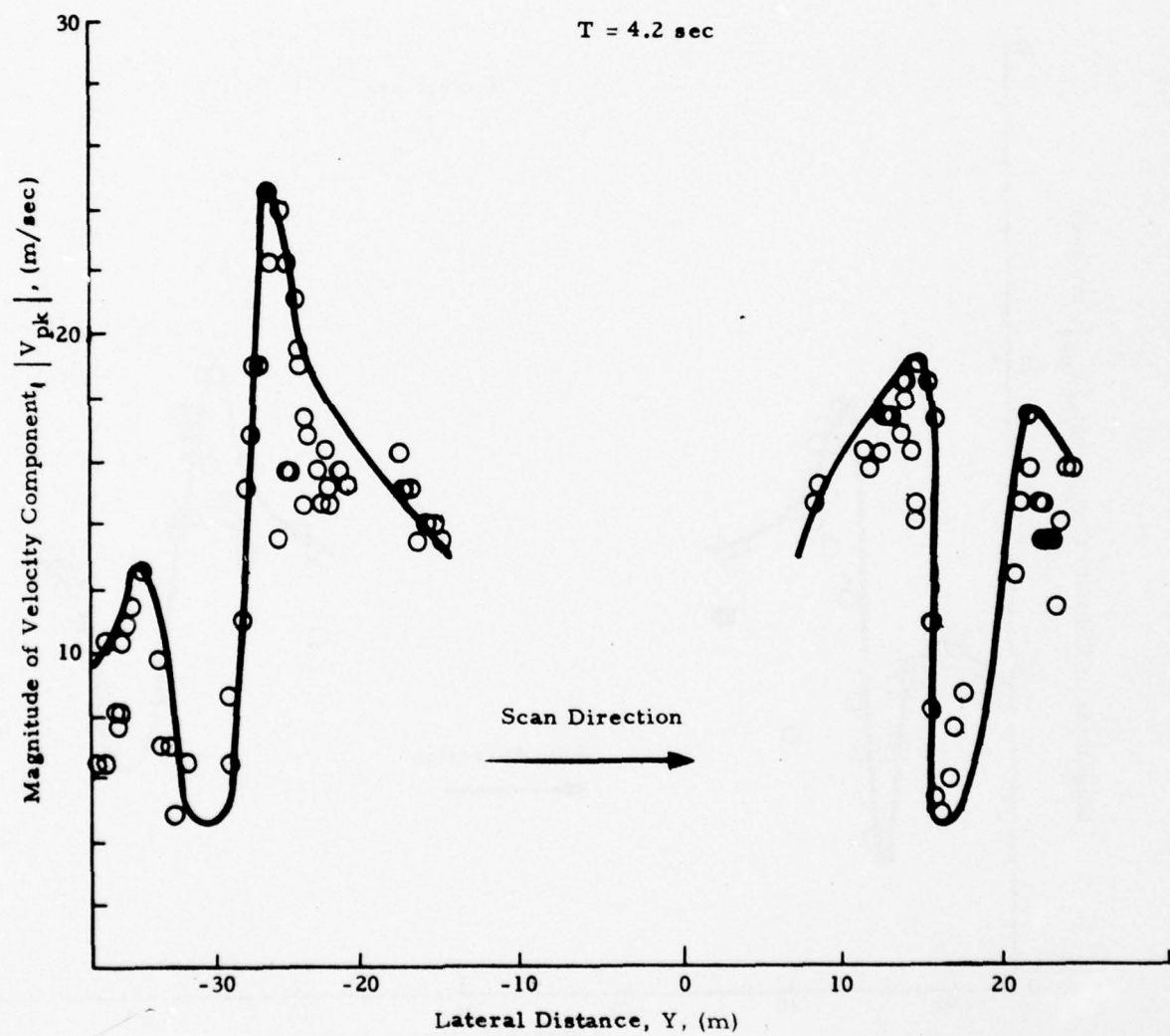


Fig. 13 (Continued)

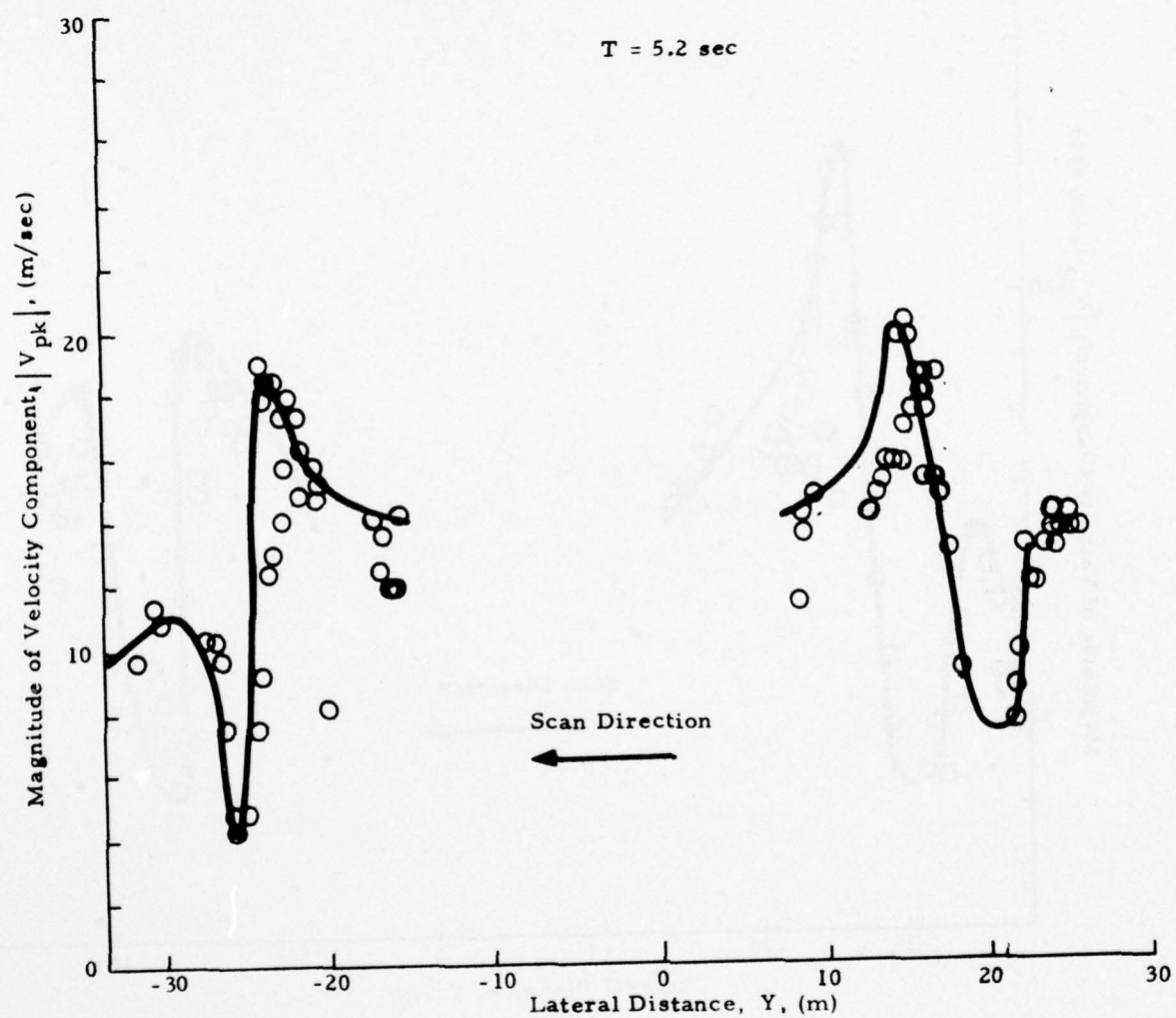


Fig. 13 (Continued)

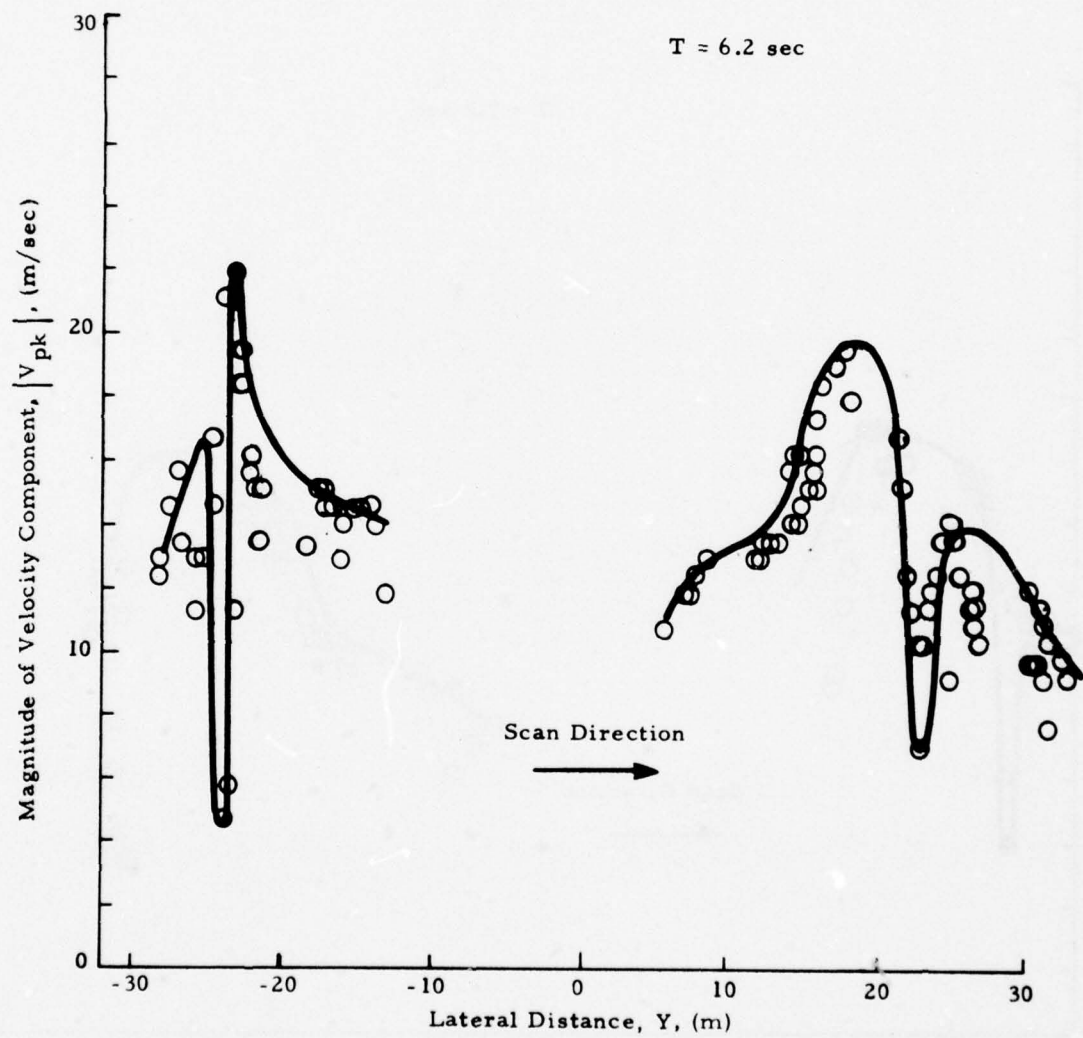


Fig. 13 (Continued)

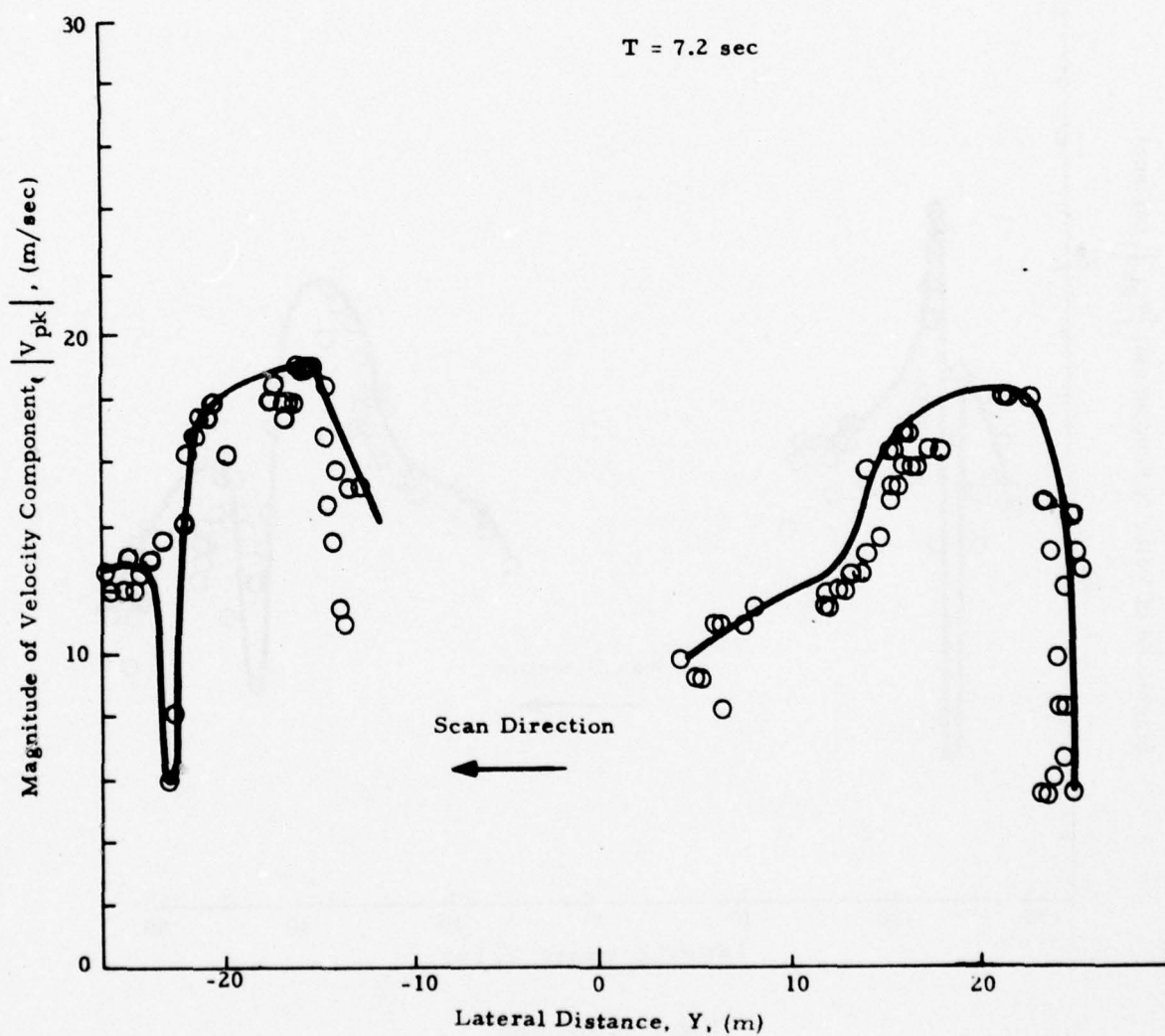


Fig. 13 (Continued)

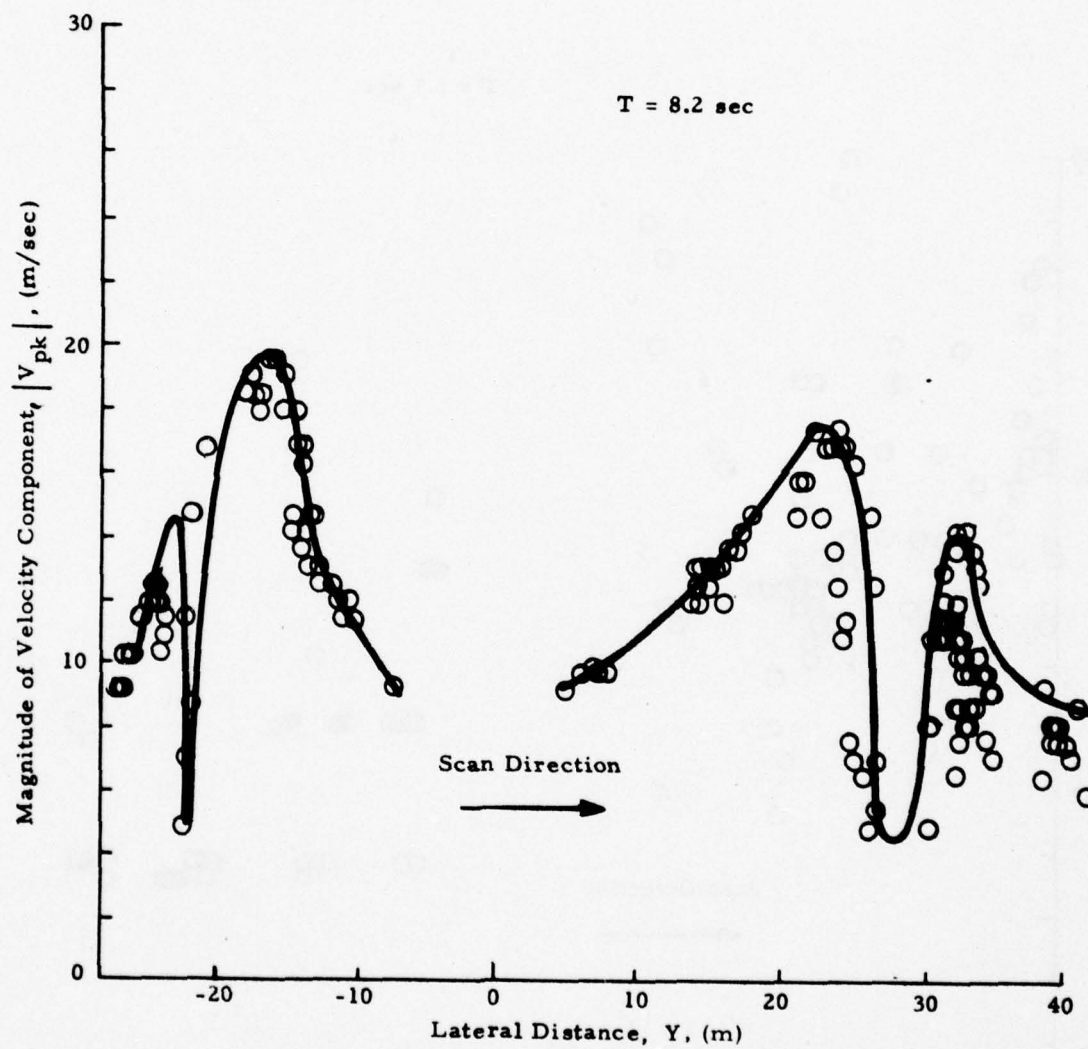


Fig. 13 (Concluded)

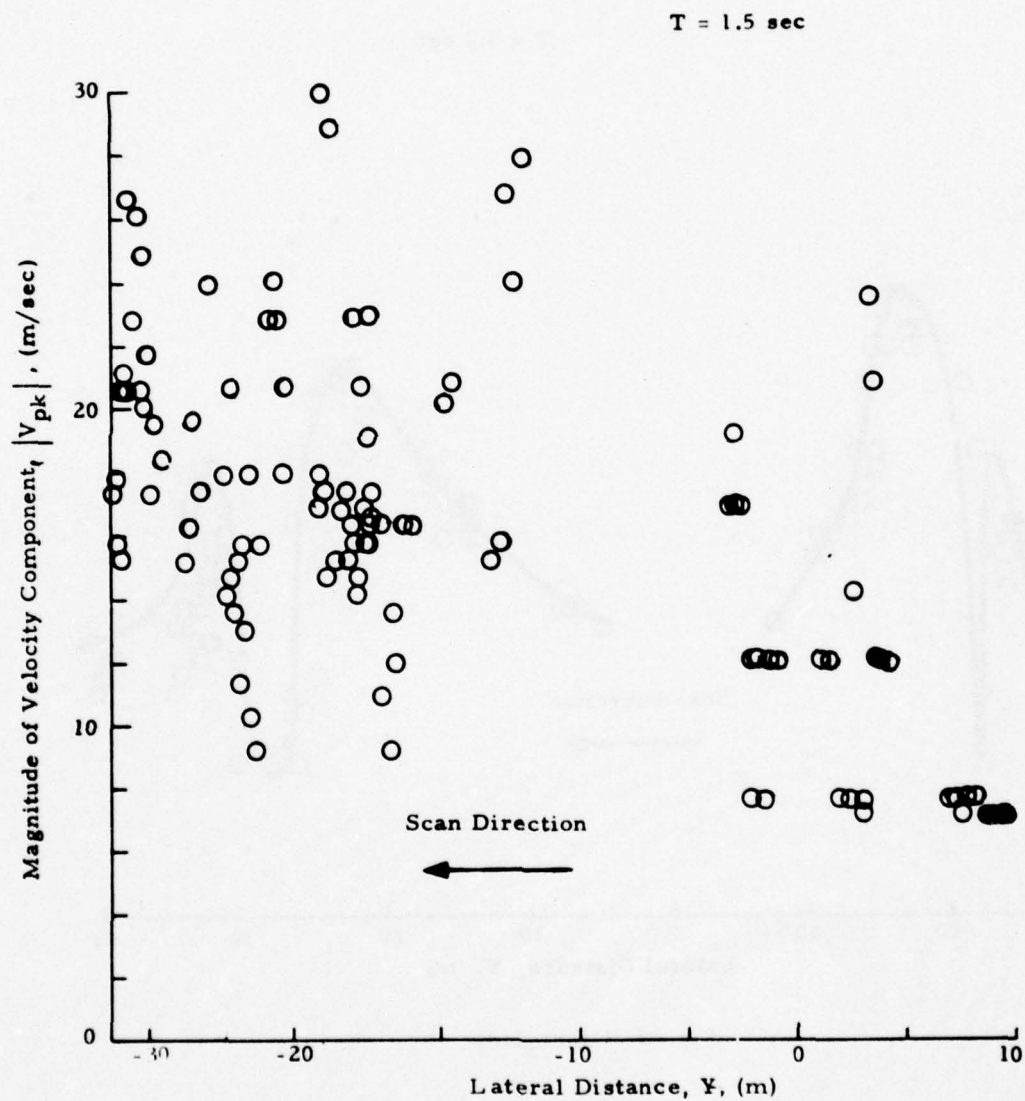


Fig.14 - $|V_{pk}|$ as a Function of Lateral Distance for Rosamond B-747 Flyby 11

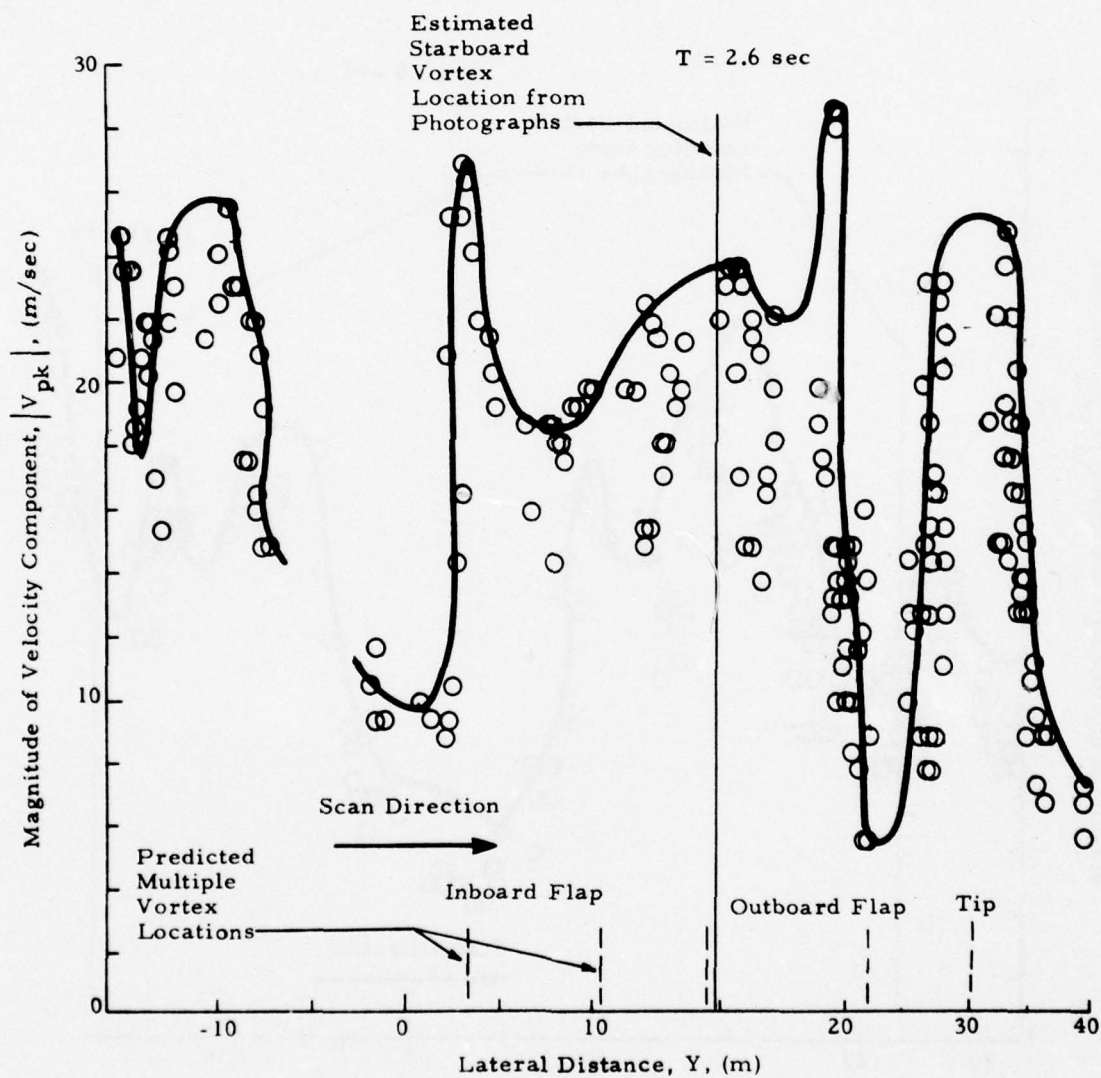


Fig. 14 (Continued)

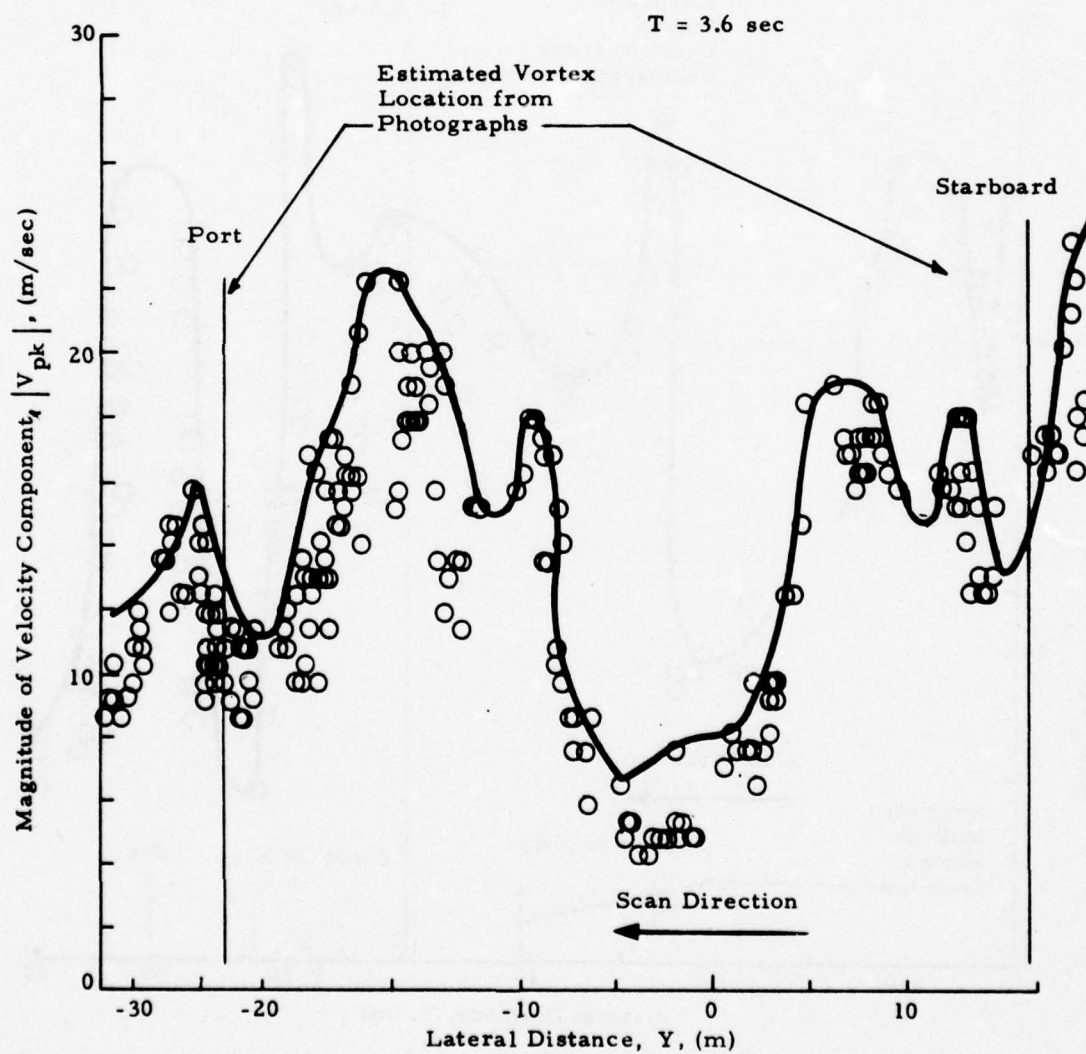


Fig. 14 (Continued)

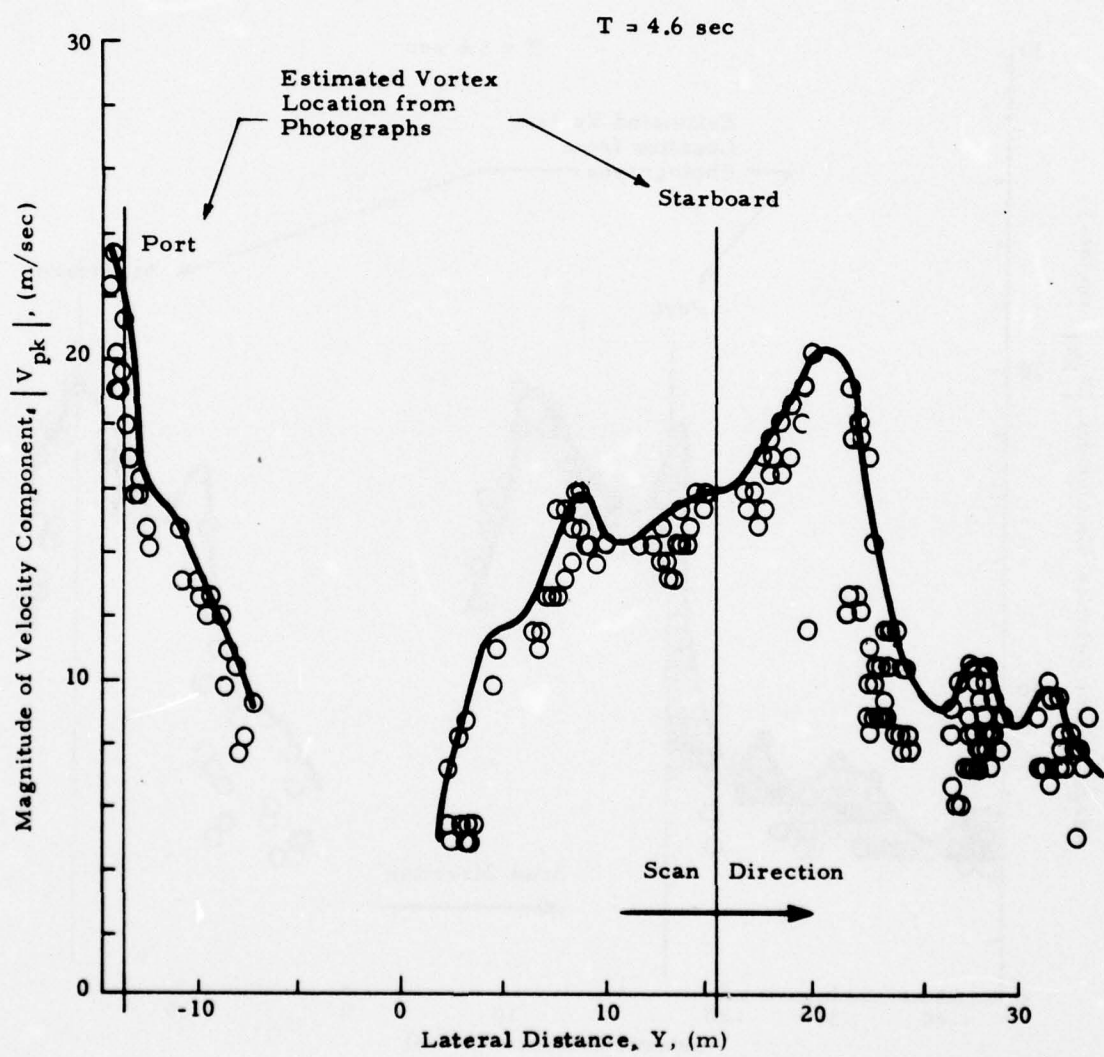


Fig. 14 (Continued)

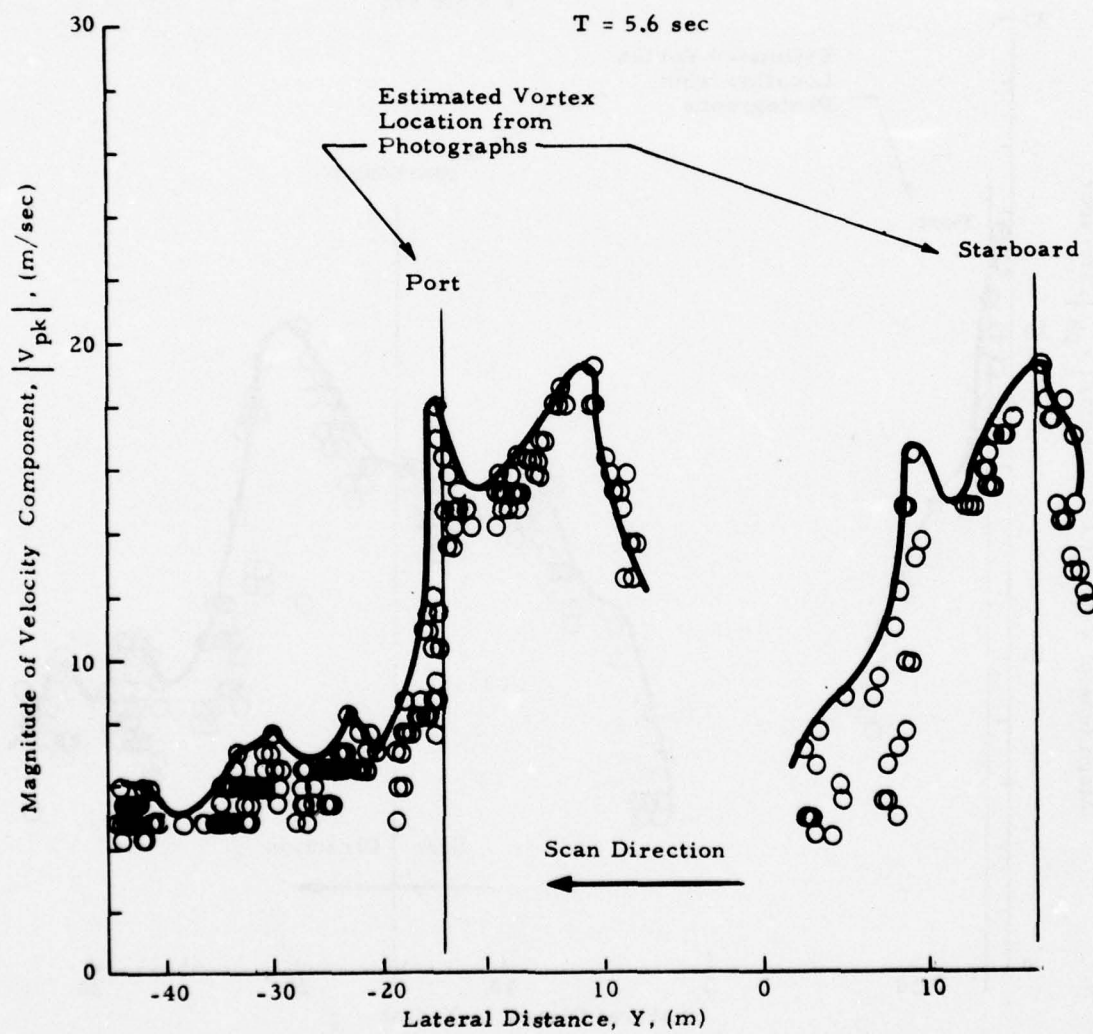


Fig. 14 (Continued)

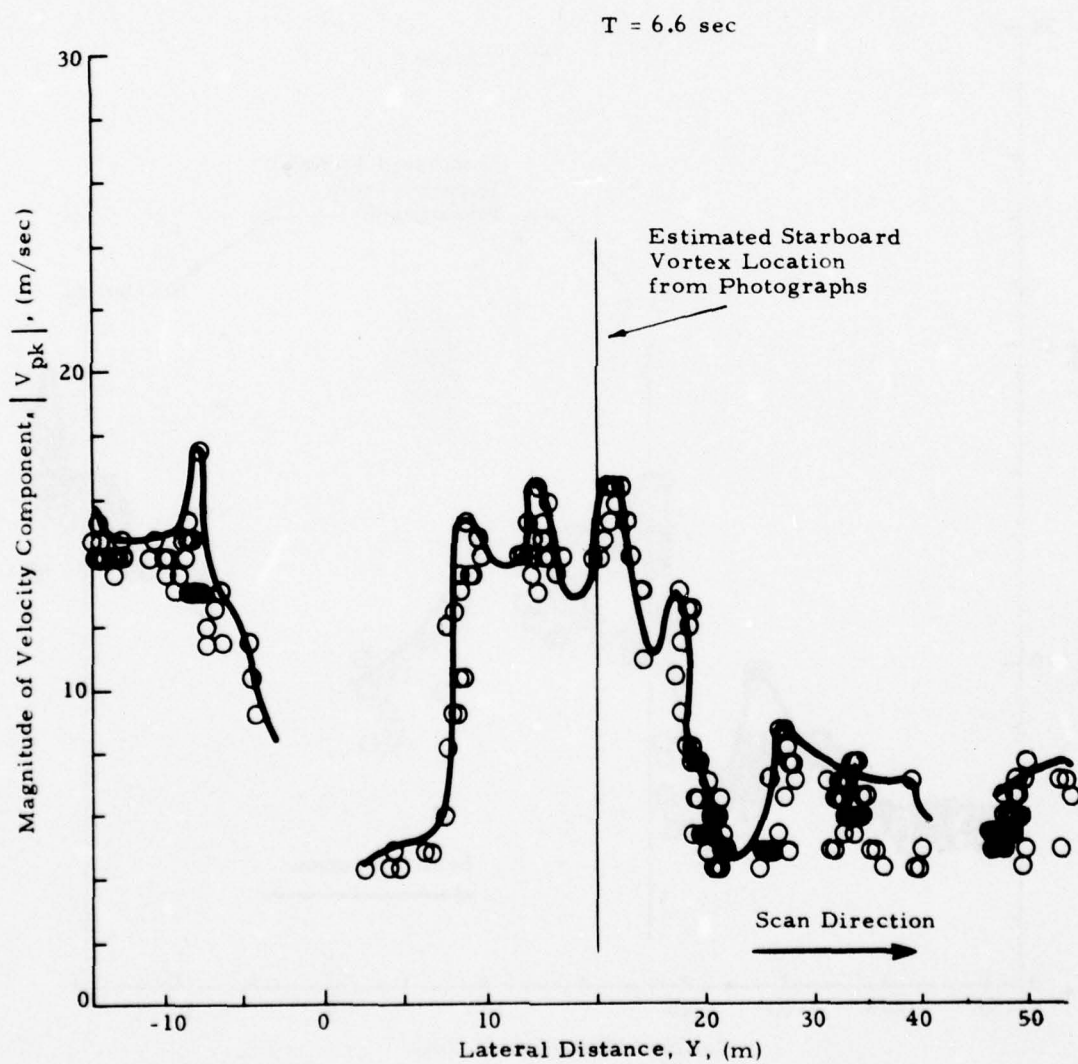


Fig. 14 (Continued)

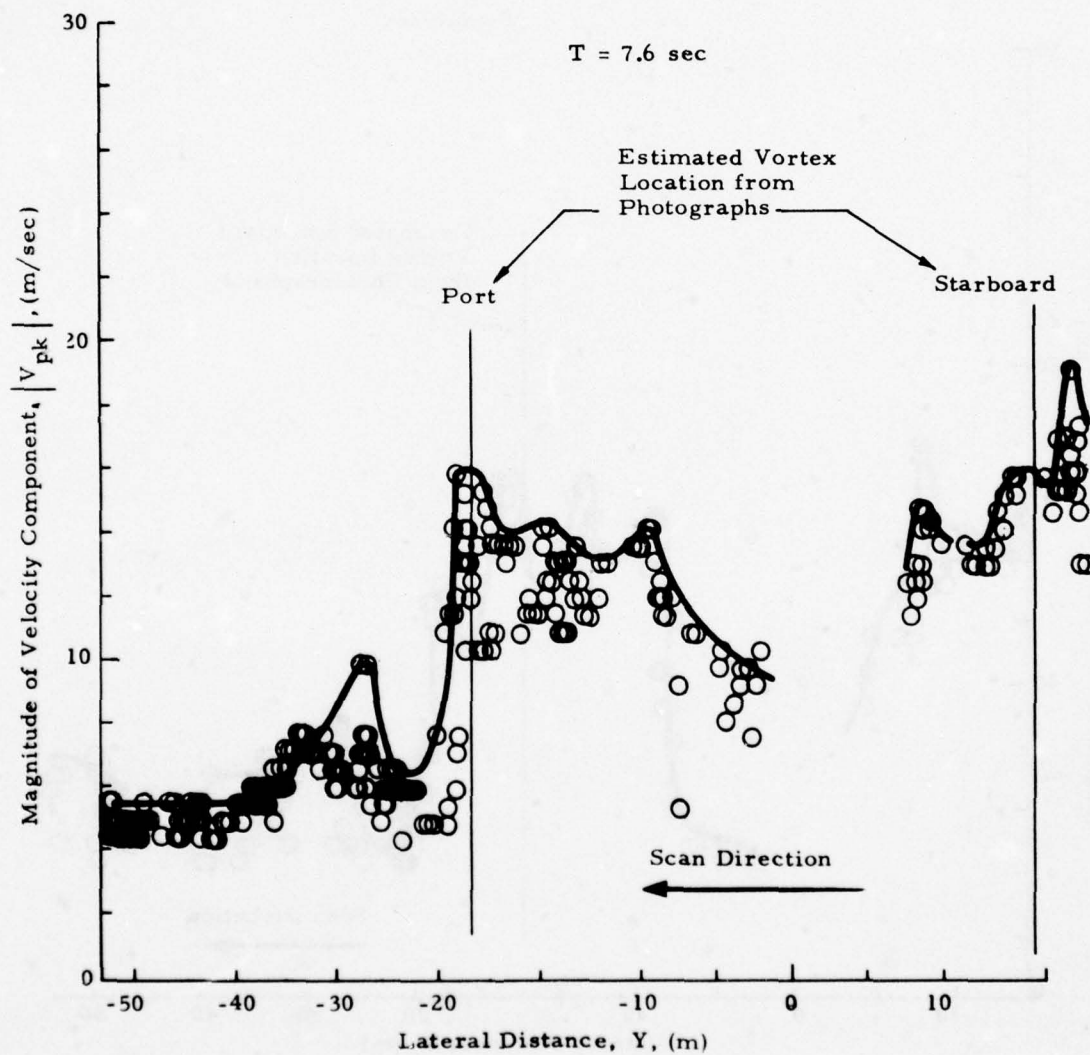


Fig. 14 (Continued)

T = 8.7 sec

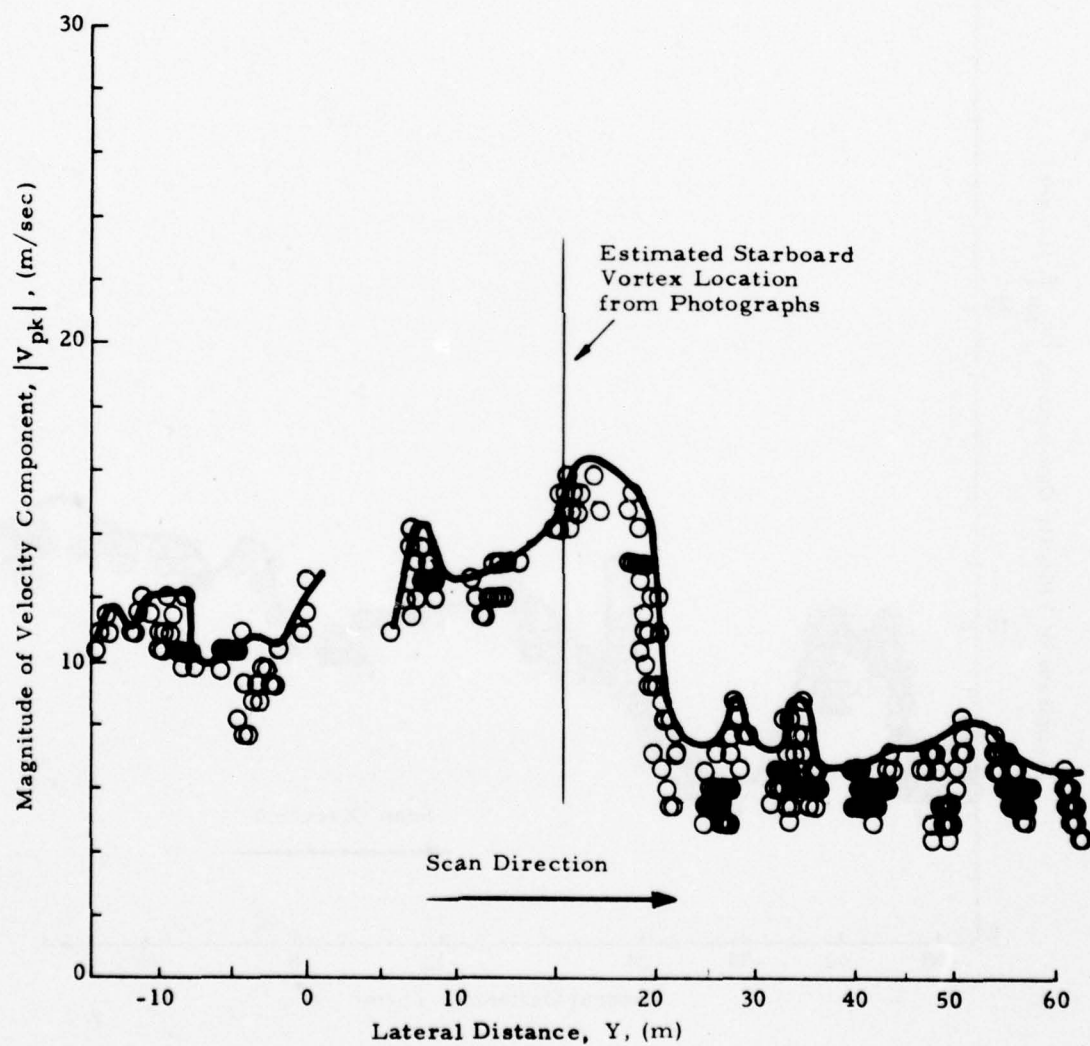


Fig. 14 (Continued)

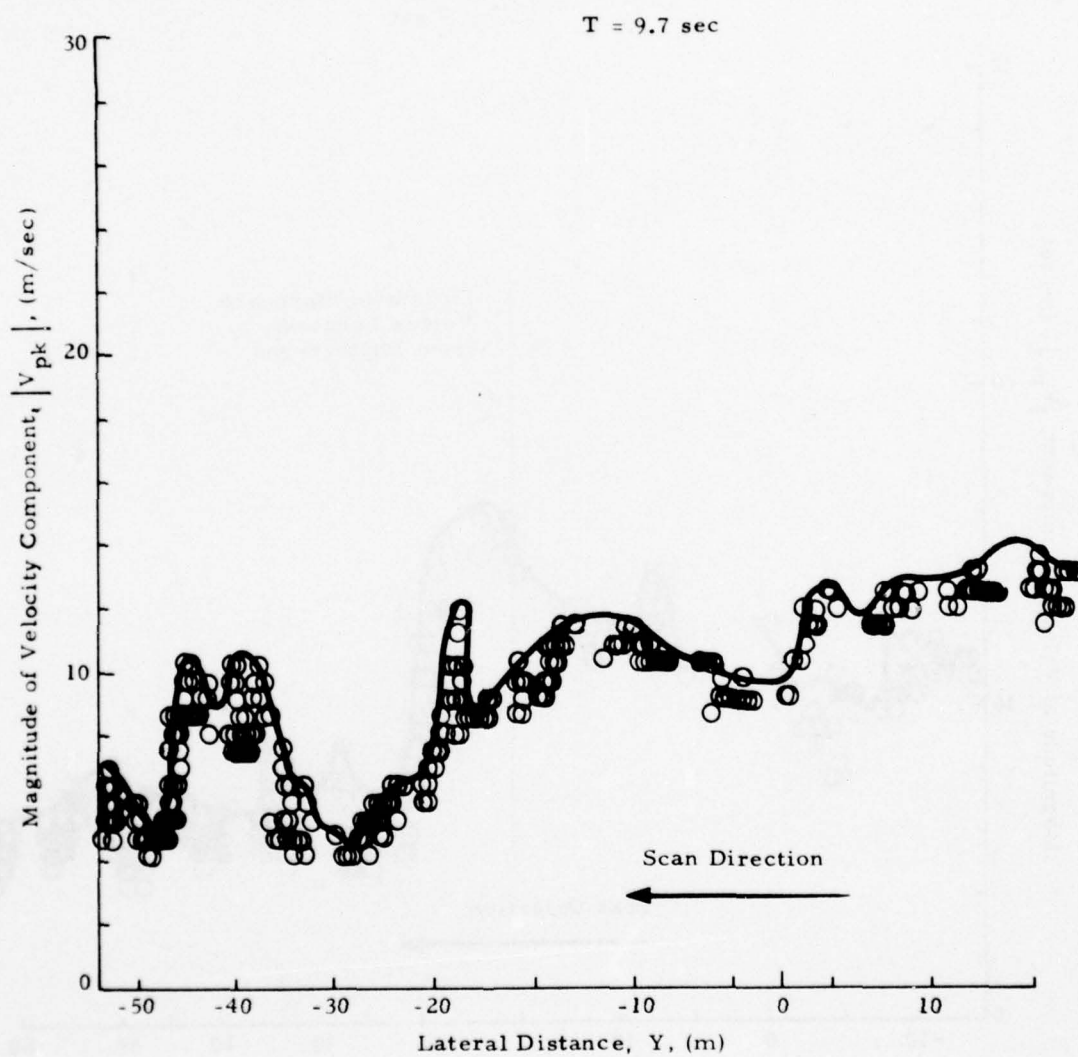


Fig.14 (Concluded)

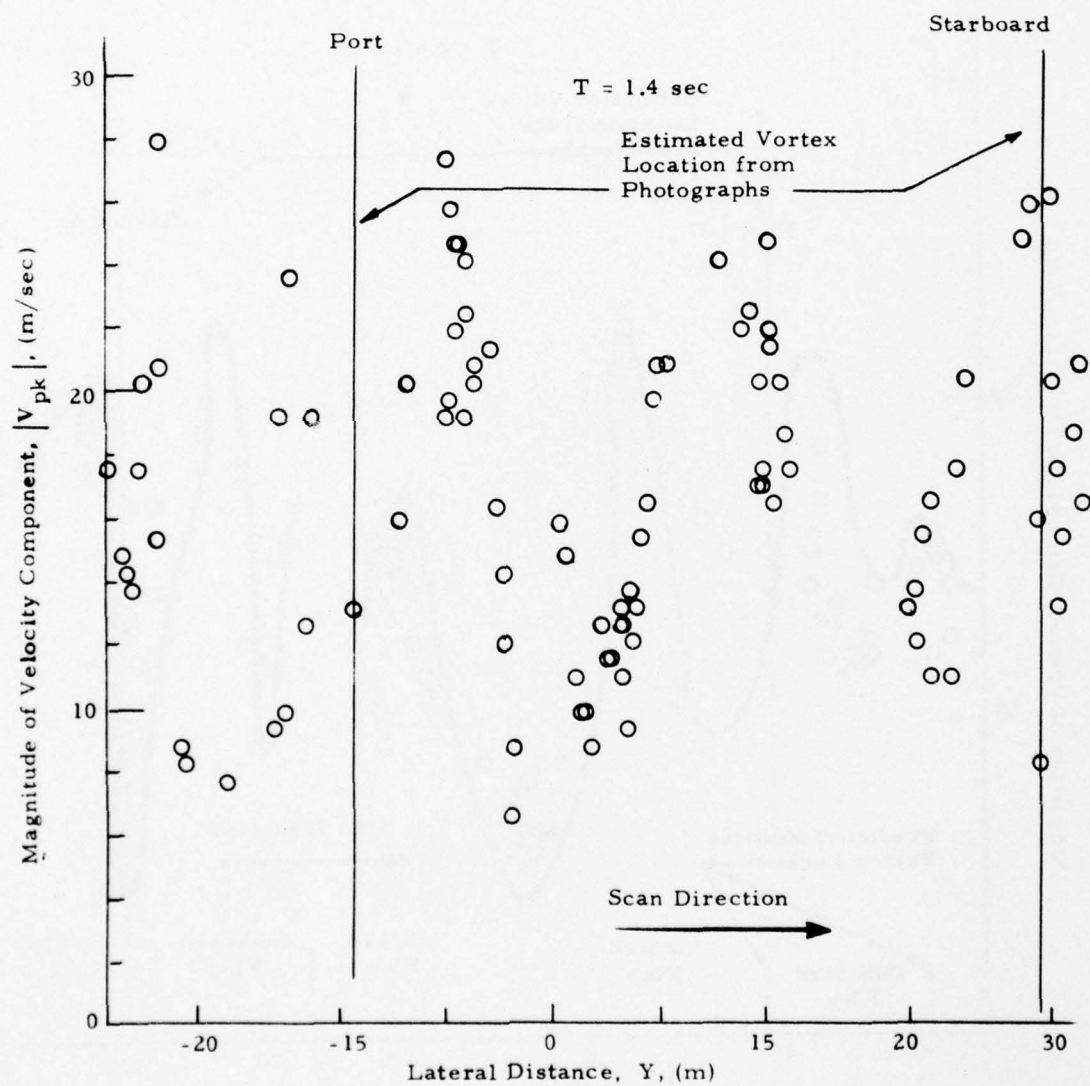


Fig. 15 - $|V_{pk}|$ as a Function of Lateral Distance for Rosamond B-747 Flyby 12

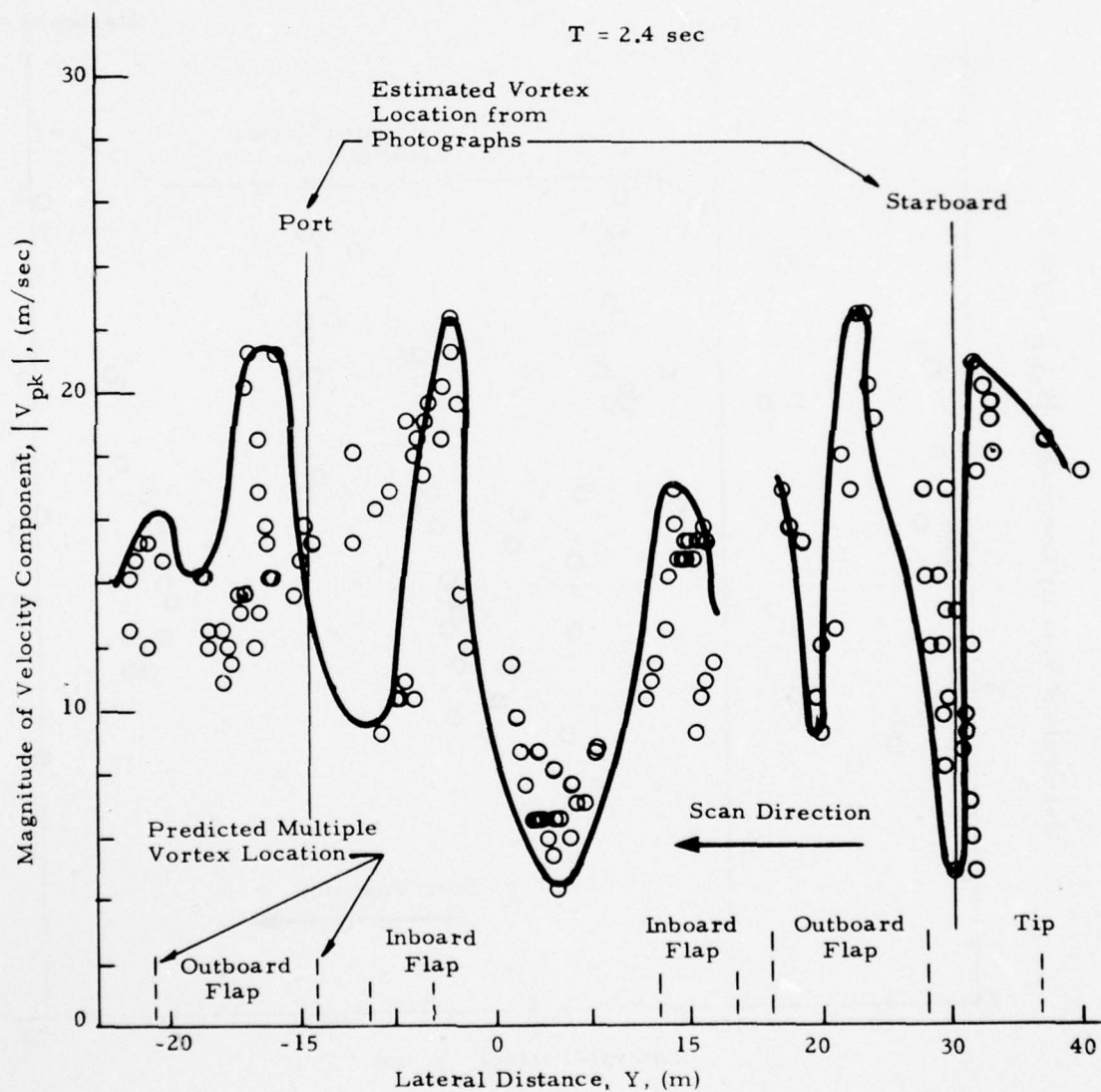


Fig.15 (Continued)

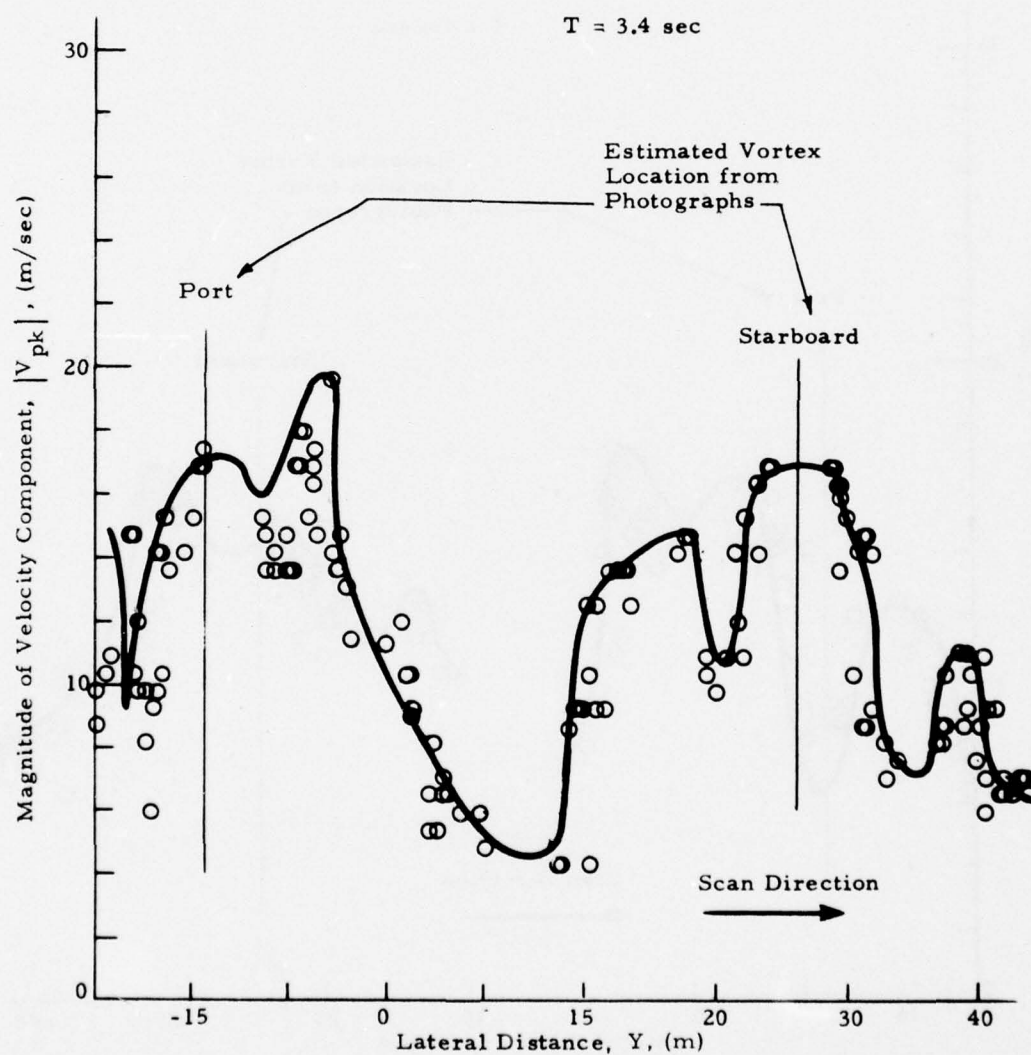


Fig. 15 (Continued)

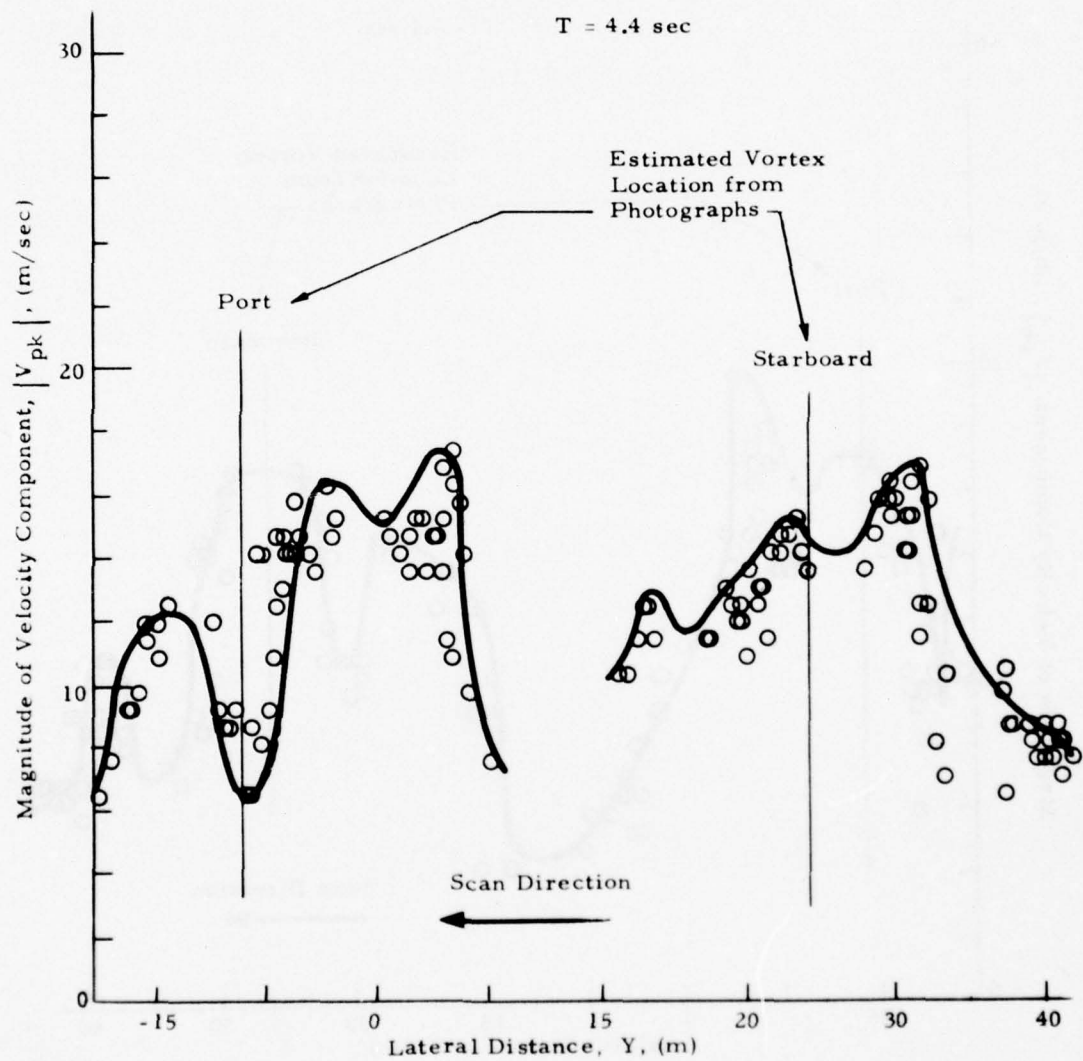


Fig. 15 (Continued)

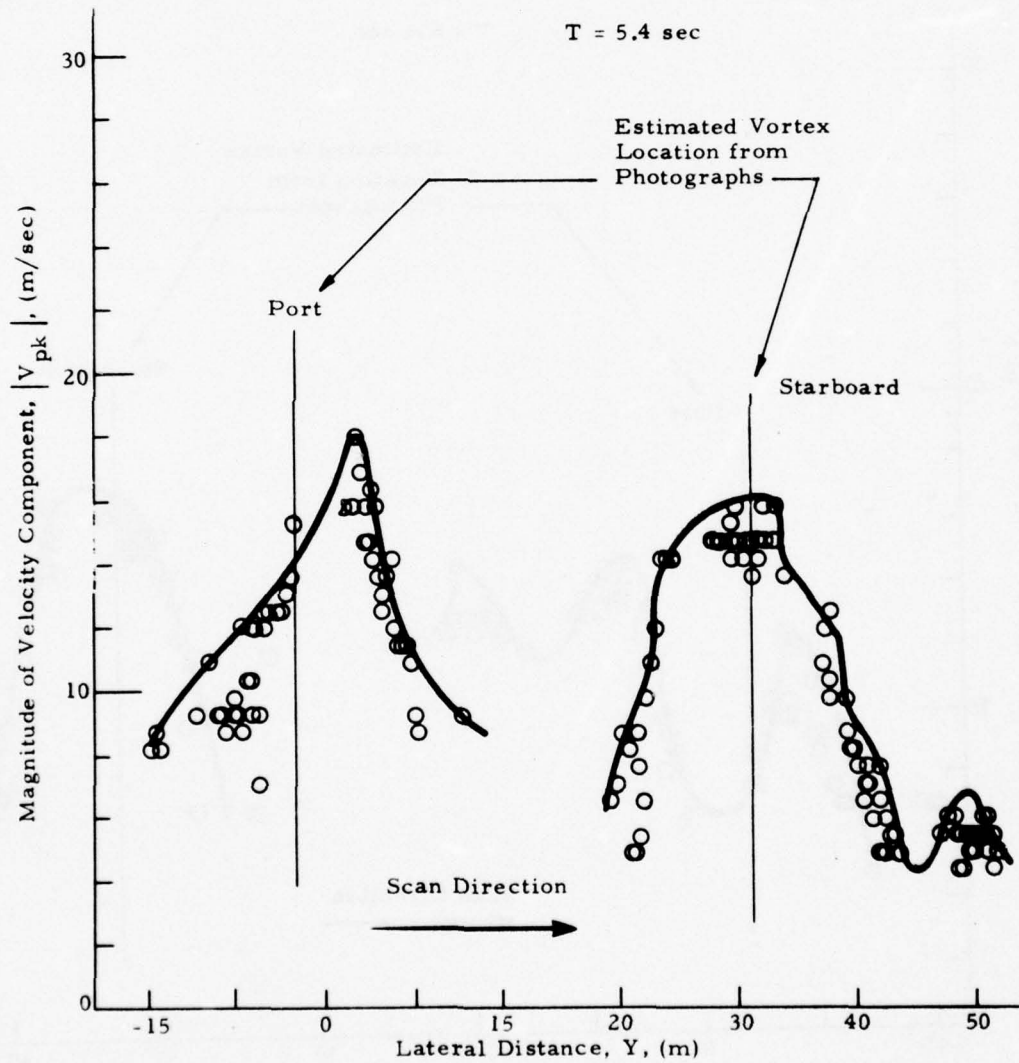


Fig. 15 (Continued)

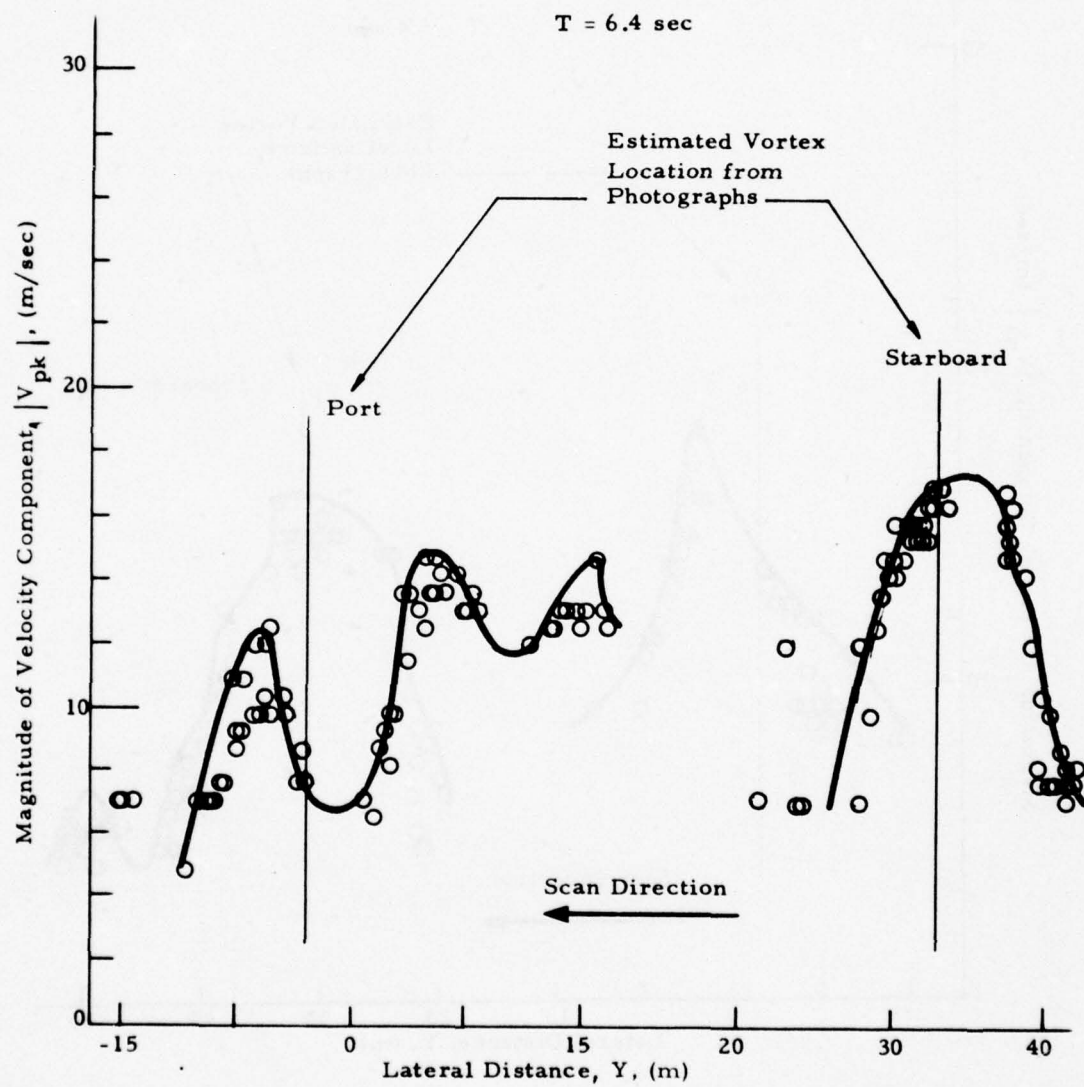


Fig. 15 (Continued)

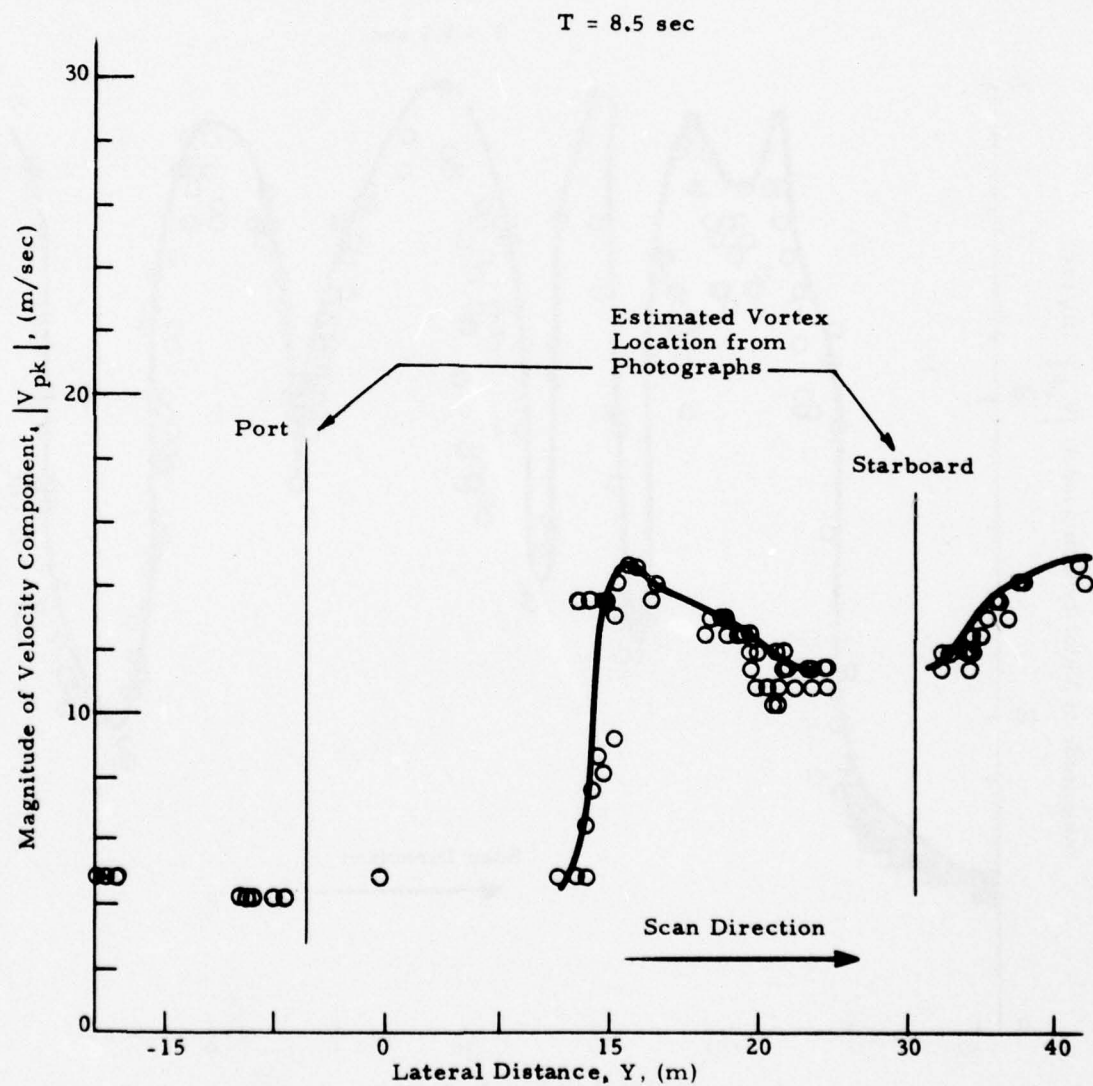


Fig. 15 (Concluded)

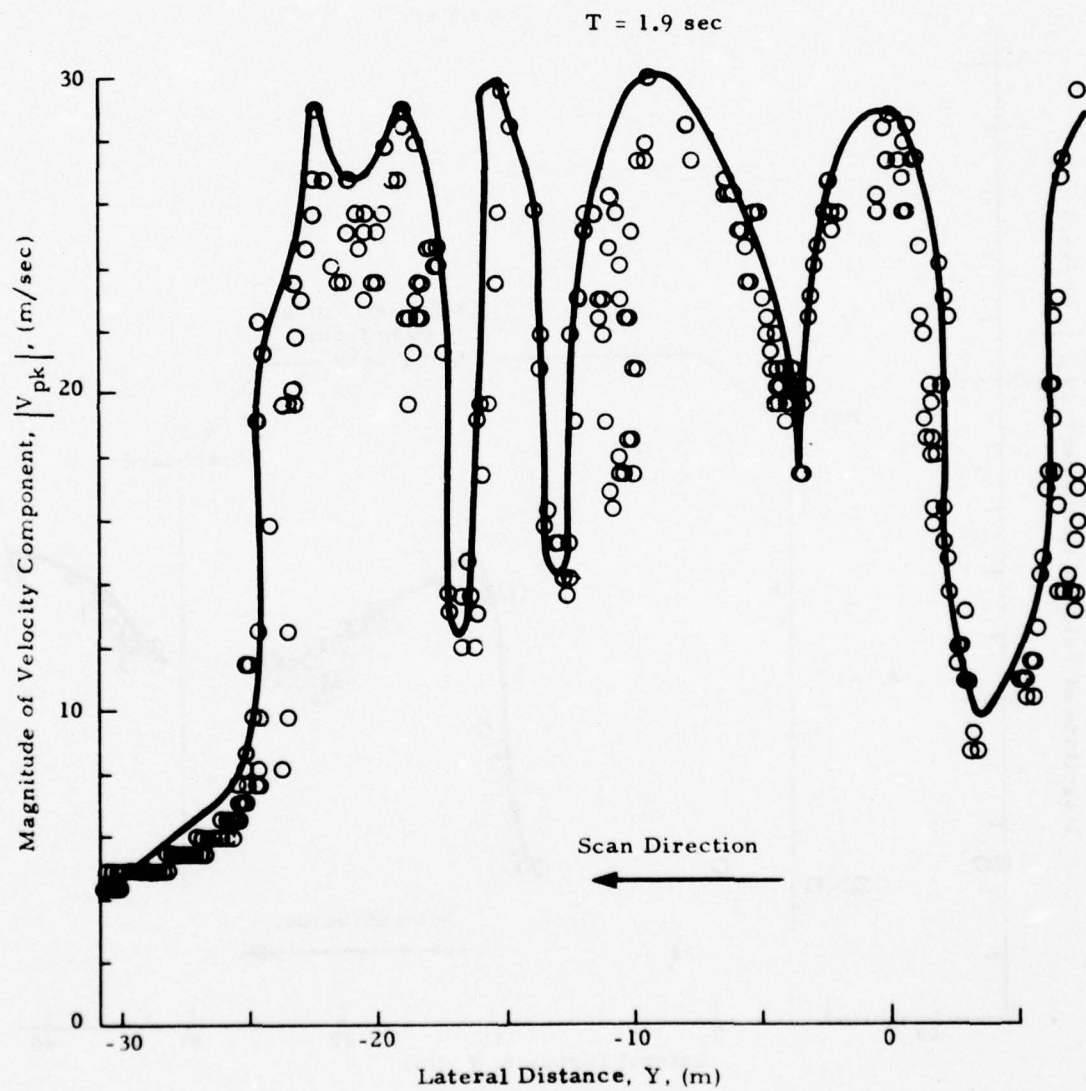


Fig. 16 - $|V_{pk}|$ as a Function of Lateral Distance for Rosamond B-747
Flyby 13

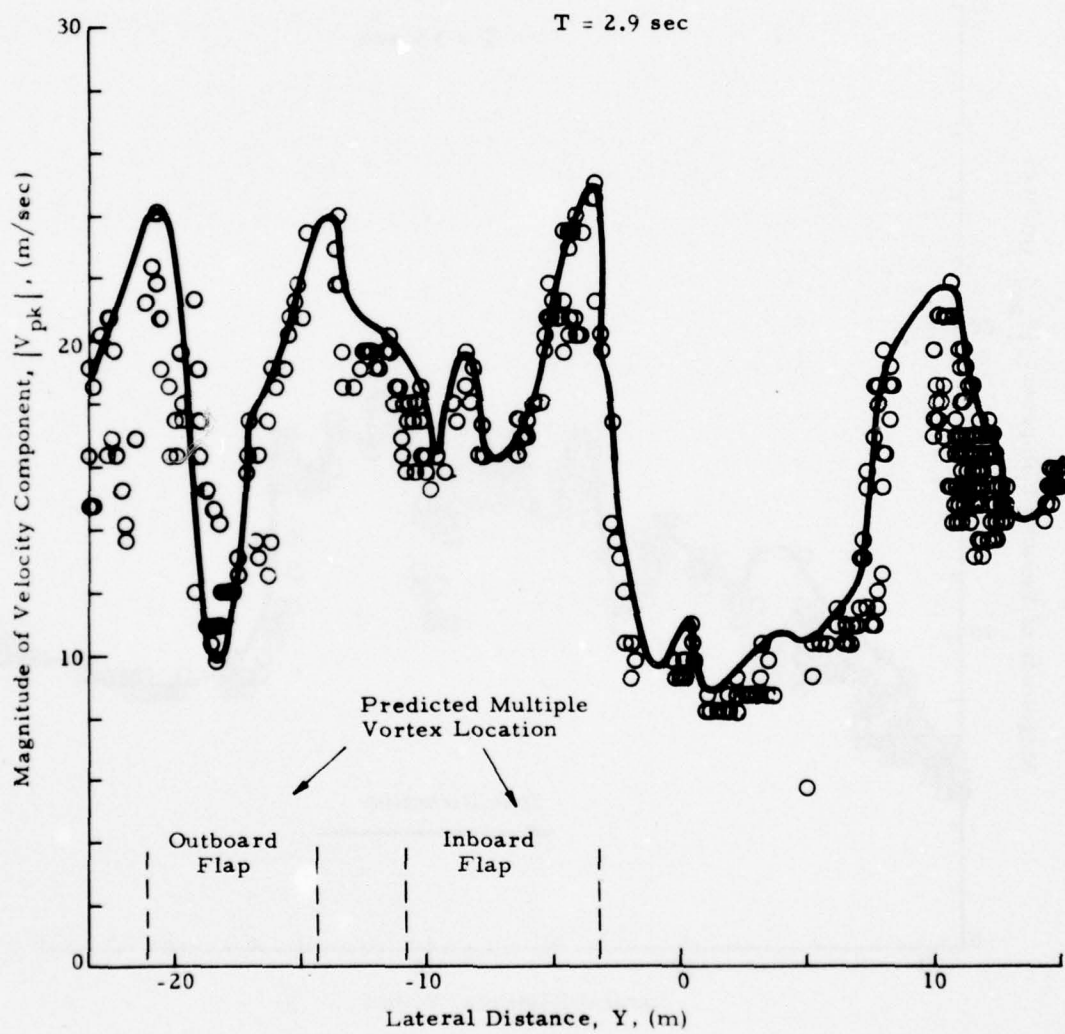


Fig. 16 (Continued)

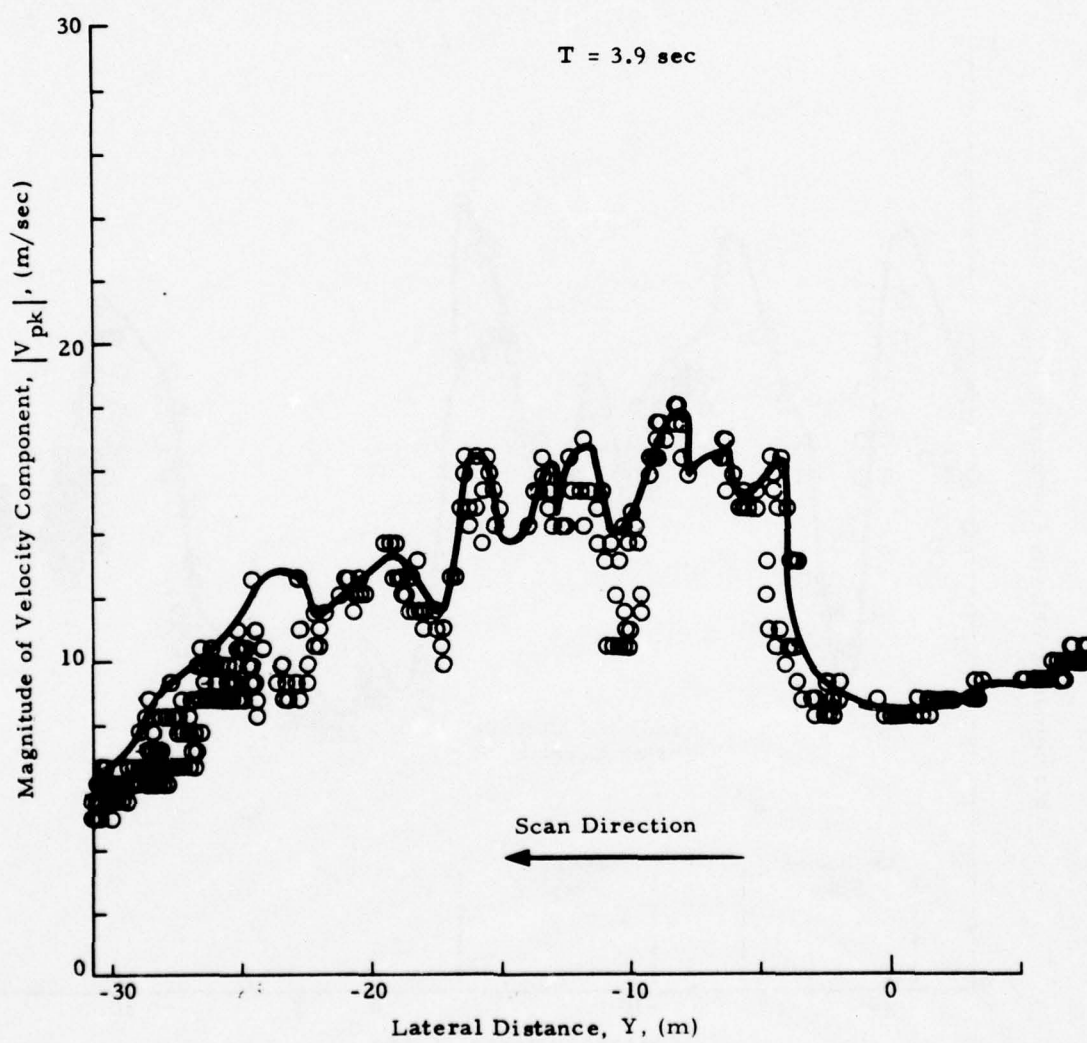


Fig. 16 (Continued)

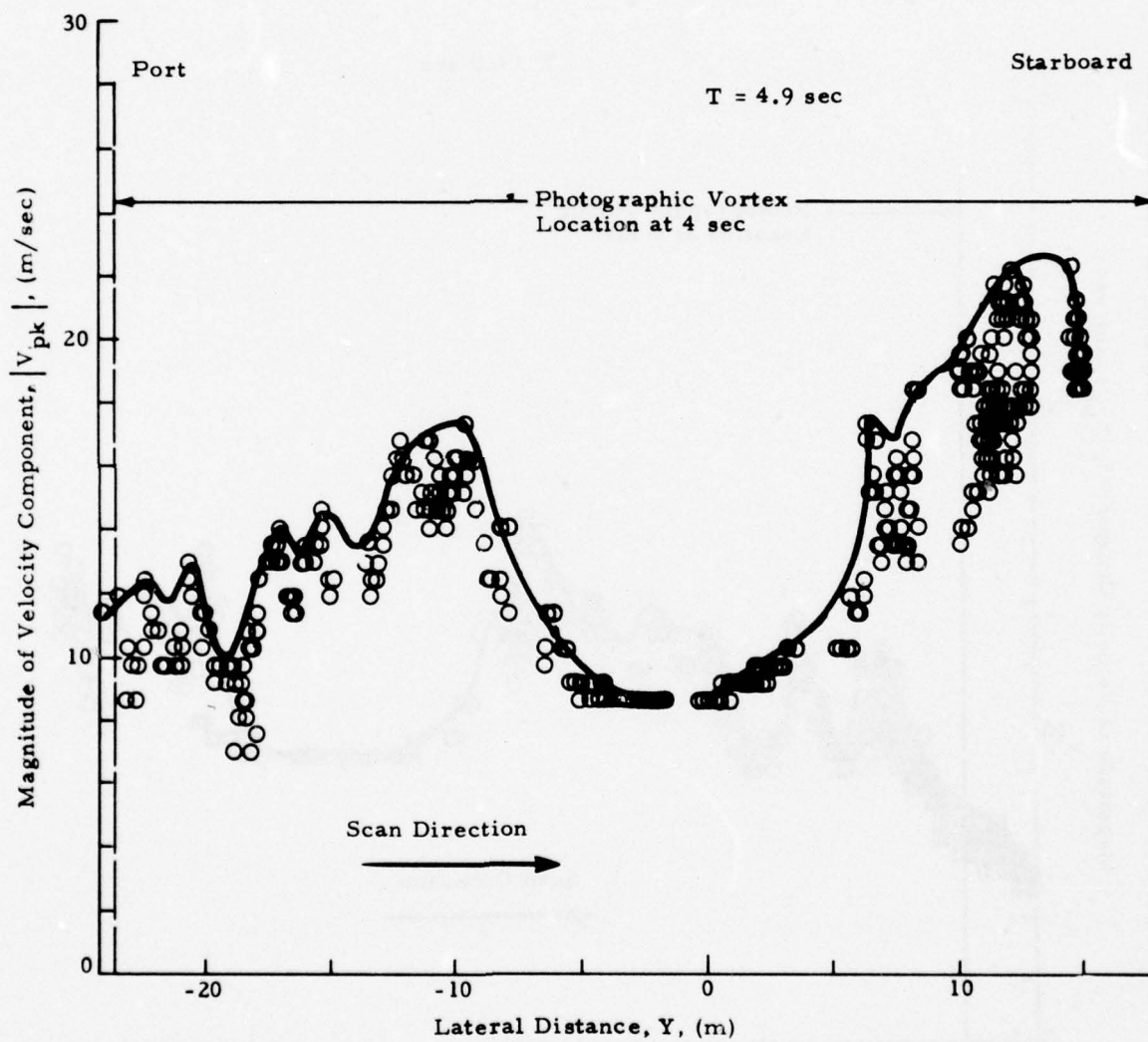


Fig. 16 (Continued)

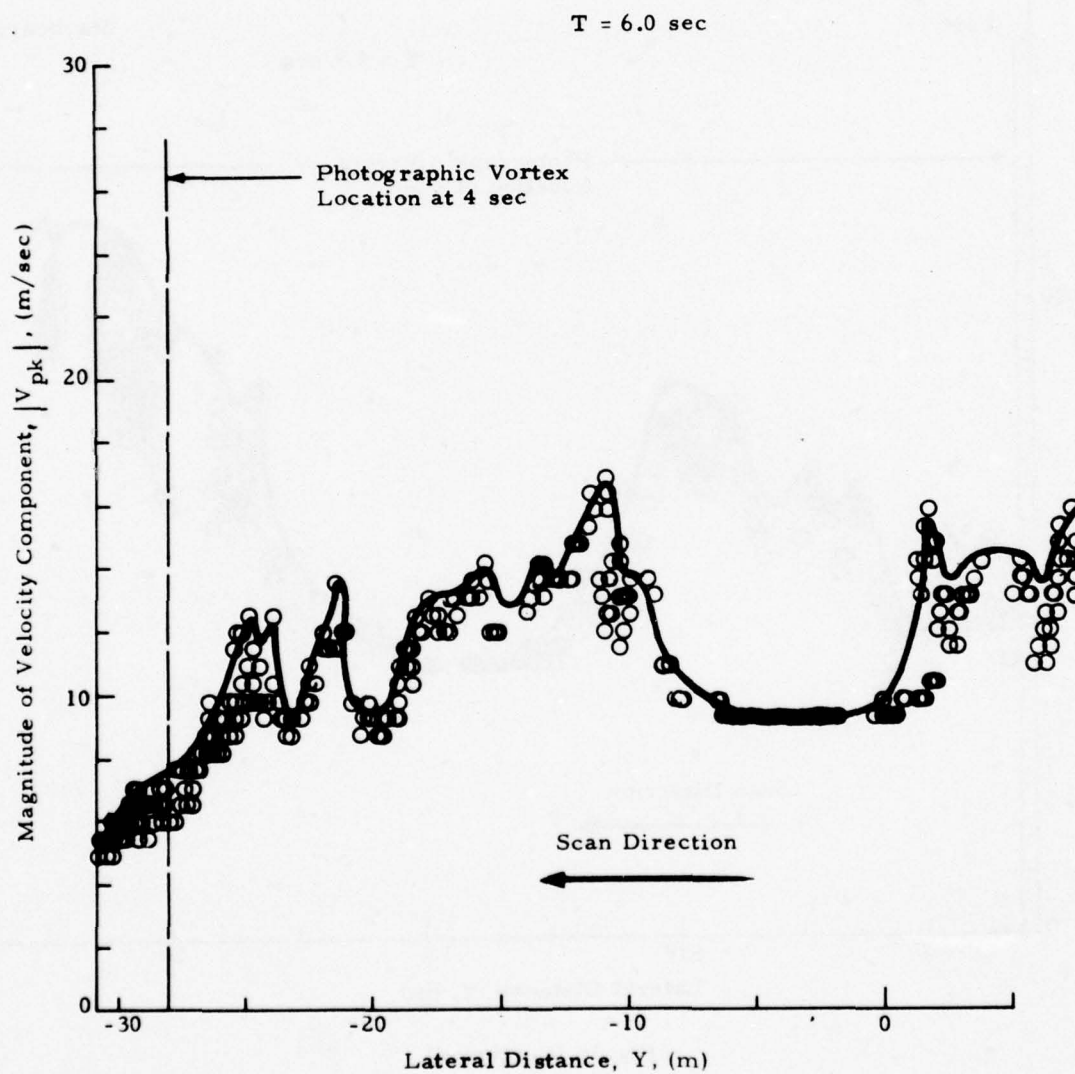


Fig.16 (Continued)

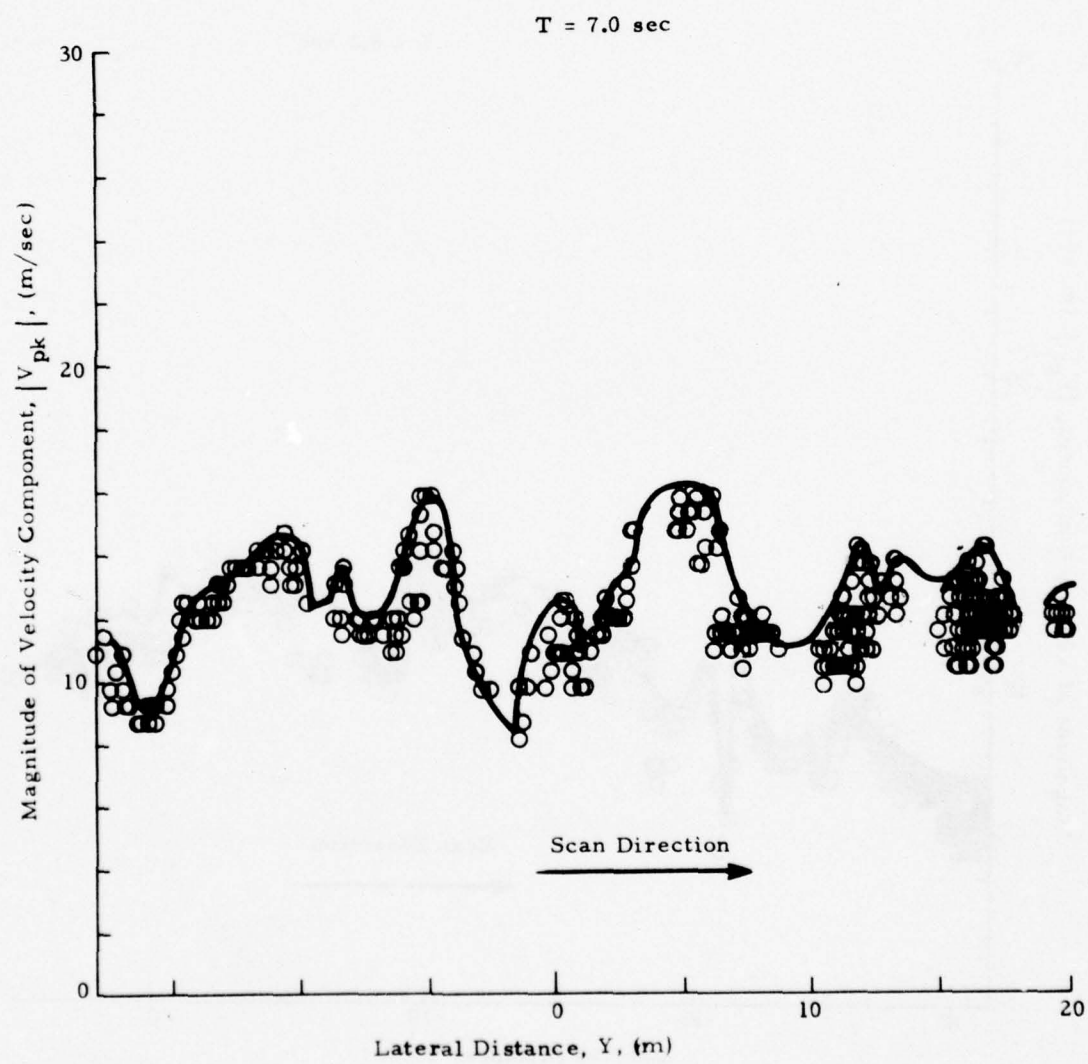


Fig. 16 (Continued)

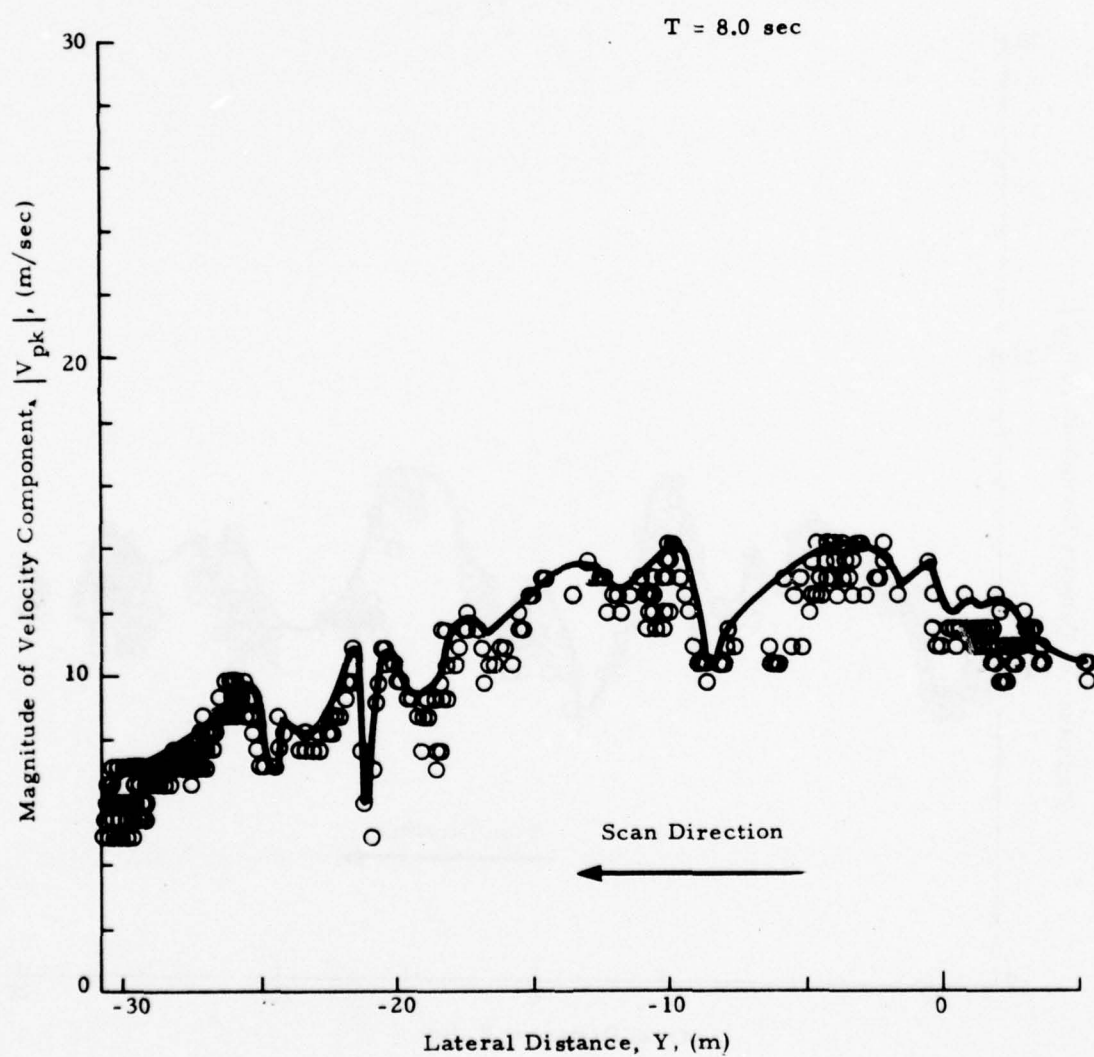


Fig. 16 (Concluded)

measurements, θ , where $y = -R \cos\theta$. This resulted in a nonlinear lateral scale at extended distances from the flight path centerline.

To illustrate the maximum downwash or upwash velocities in the aircraft near wake, the highest values of $|V_{pk}|$ occurring over 1 deg increments were faired by a smooth curve. The solid lines in the plots represent a faired curve through the highest LDV measurements given by the circles. Since the arc-scan measurements were made at an initial range equal or somewhat less than the airplane height, and since the maximum descent rate of the trailing vortices was on the order of 2 m/sec, the wake vortex remained essentially in the focal volume of the LDV system over the time period of 0 to 8 sec. Thus, the solid lines shown in Figs. 13 through 16 are indicative of the peak velocities observed with the LDV system in the aircraft near wake.

Available measurements of vortex lateral position obtained from a triangulation of simultaneous photographs or estimated from overhead photographs are also shown in Figs. 13, 14, and 15.

The spanwise downwash distribution for flyby 8, the 0-spoiler configuration, shows a well defined double-peak signature in most of the plots shown in Fig. 13 which is suggestive of a coherent vortex. For example, in Fig. 13 at $t = 2.2$ sec, two broad peaks are observed separated by a spacing of 0.76 wingspan. The lack of signature in the inboard regions may be attributed to the lack of high velocities or aerosols near the flight path centerline. The two broad peaks become more well defined at later times ($t = 3.3$ to 8.2 sec), showing a double-peak signature characteristic of the rotational velocity profile of a viscous vortex. The lateral separation and the maximum speed for the two double-peak signatures do not change significantly over this time range.

In contrast to the coherent wake structure observed earlier for the 0-spoiler configuration (Fig. 13), the downwash field for flybys 11, 12 and 13, where the two outer spoilers were deployed, shows a broad high amplitude region composed of narrower closely spaced peaks. This is suggestive of multiple

vortices and an incomplete vortex roll-up phase. These measurements indicate that the deployment of spoilers has a marked effect on the near-wake structure, tending to retard the early formation of a coherent trailing vortex pair. Analysis of the downwash field shown in Figs. 13 through 16 has been carried out to determine the basic characteristics of single and multiple vortices such as location, circulation strength, and the magnitude of the velocity component.

4.1.2 Vortex Pair Characteristics

For the 0-spoiler configuration, the spanwise downwash distribution in the wake shows a well defined double-peak signature (Fig. 13). A double-peak signature is predicted theoretically when a vortex pair is interrogated in the arc-scan mode. For example, the magnitude of the line-of-sight velocity component for Rosamond flyby 11 at $t \sim 2$ sec assuming a fully rolled-up vortex pair is shown in Fig. 17. The magnitude of the line-of-sight velocity generated by a distribution of N line vortices with the LDV located at the origin is given by

$$|V_{los}| = \frac{1}{2\pi} \sum_{n=1}^N \Gamma_n \frac{[(Y_n - Y_o) X_o + (X_o - X_n) Y_o]}{[(X_o - X_n)^2 + (Y_o - Y_n)^2]^{1/2} [X_n^2 + Y_n^2]^{1/2}} \quad (3)$$

where (X_o, Y_o) is the location of the centroid of the focal volume, and (X_n, Y_n) and Γ_n are the coordinate and circulation strength of the n^{th} vortex, respectively.

In Fig. 17, the magnitude of the computed line-of-sight velocity is shown for a pair of line vortices with spacing $b' = Kb = 41.8$ m and circulation strength $\Gamma = U_\infty \bar{c} C_L / 2K = 606 \text{ m}^2/\text{sec}$ where the spanwise loading coefficient, wingspan, flight velocity, mean chord, and lift coefficient are taken to be $K = 0.7$, $b = 59.7$ m, $U = 72.5 \text{ m/sec}$, $\bar{c} = 8.3$ m, $C_L = 1.41$. The vortex pair was assumed to be located at an altitude of 180 m and the selected arc scan range was 183 m. The magnitude of the computed line-of-sight velocity for the vortex pair shows the characteristic double peak signatures noted earlier in the LDV measurements. The magnitude of the peak velocity is determined by the separation distance between

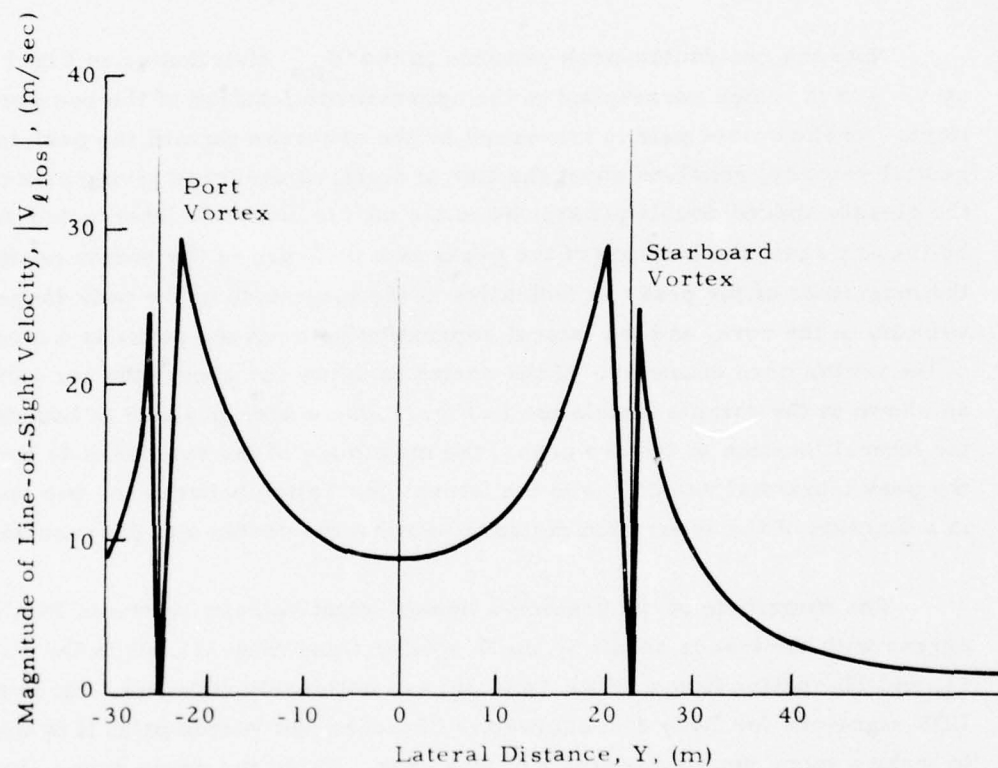


Fig. 17 - Magnitude of Line-of-Sight Velocity Component for Rosamond B-747 Flyby 11 at $t \sim 2$ sec, Computed Assuming a Fully Rolled-Up Vortex Pair

the vortex pair and the scan arc. The slight asymmetry in the double peaks results from the velocity contribution of the adjoining vortex, the scan geometry, and the decrease in the contribution of the vortex rotational velocity along the line of sight at extended lateral distances from the centerline.

Note the two double-peak patterns in the V_{los} distribution in Fig. 17 at $y = \pm 23$ m which correspond to the approximate location of the two vortices. As the vortex pair is traversed by the arc-scan pattern, the peak tangential velocity, resolved about the line of sight, is observed giving rise to the closely spaced double peaks. When the vortex center is intersected exactly by the arc scan, the location of the peaks is a measure of the vortex position, the magnitude of the peaks is indicative of the magnitude of the peak tangential velocity in the core, and the lateral separation between the peaks is a measure of the vortex core diameter. If the vortex is below (or above) the arc-scan, as shown in the sample simulation in Fig. 17, the vortex position is bounded by the lateral location of the two peaks, the magnitude of the two peaks is less than the peak tangential velocity, and the lateral separation between the two peaks is a function of the separation distance between the vortex and the scan arc.

The magnitude of the predicted line-of-sight velocity shown in Fig. 17 agrees with the trends shown by the 0-spoiler flyby (Fig. 13), while the 1, 2, 11, and 12-spoiler flybys (Figs. 14 to 16) are noticeably different. Since the LDV signature for flyby 8 is suggestive of a coherent vortex pair, it is useful to make a more detailed analysis of this case. From the seven scans shown in Fig. 13 the earliest scan showing the two double peak signatures was selected ($t = 3.3$ sec); the minimum points were used to determine the lateral position of the port vortex (vortex altitude was assumed to be the scan range $R = 240$ m), and the peak velocity magnitudes observed by the LDV for the port vortex were plotted as a function of radius about the vortex center in Fig. 18. For comparison, the magnitude of the velocity for a potential line vortex and a turbulent viscous vortex are also shown in Fig. 18 matched to the experimentally measured core circulation and core velocity.

LDV Measurements of Port Vortex, Flyby 8

Time = 3.3 sec

Core Radius = 4.5 m

Circulation = 565 m²/sec

○ Starboard Scan

□ Port Scan

Theory

— Hoffman & Joubert Model (Ref.7)

--- 1/r Field for Line Vortex with Circulation
 $\Gamma = 565 \text{ m}^2/\text{sec}$

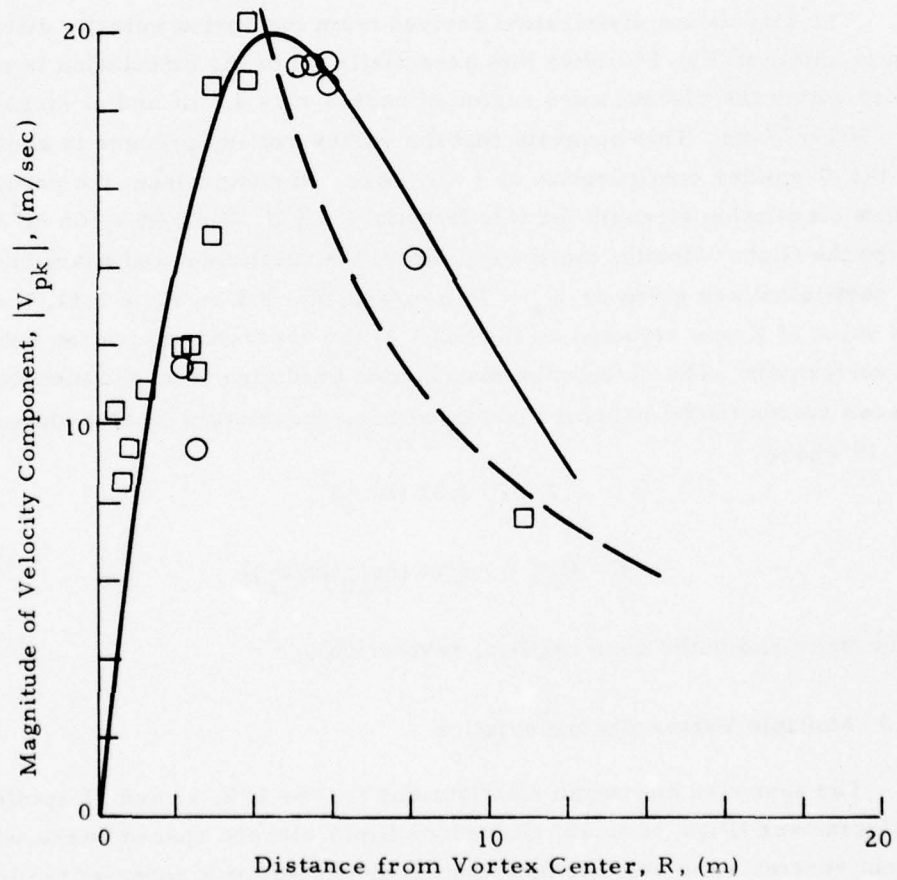


Fig. 18 - Magnitude of Wake Vortex Velocity Distribution with 0 Spoilers

The results in Fig. 18 indicate that the velocity distribution observed with the LDV is in general agreement with the theoretical model of Hoffman and Joubert near the core region of the vortex. In the outer flow region, the experimental velocity distribution decreases more rapidly than the theoretical logarithmic circulation model and approaches the $1/r$ profile. However, sufficient scatter exists in the LDV data points to make a detailed comparison difficult, and agreement with other theoretical models is possible.

The circulation distribution derived from the vortex velocity distribution is shown in Fig. 19. Note that essentially all of the circulation is contained within the viscous core region of radius $r_c = 4.5$ m and of circulation $\Gamma_c = 565$ m²/sec. This suggests that the vortex roll-up process is complete for the 0-spoiler configuration at $t = 3.3$ sec. In comparison, the predicted vortex circulation strength for this flyby is $\Gamma = \frac{1}{2} U_\infty \bar{c} C_L / K = 565$ m²/sec, where the flight velocity, mean wing chord, lift coefficient and spanwise loading coefficient, are given by $U_\infty = 73.6$ m/sec, $\bar{c} = 8.3$ m, $C_L = 1.41$, $K = 0.762$. The value of K was selected on the basis of the observed separation between the vortex pair. The circulation distribution predicted from the turbulent viscous vortex model using the observed core parameters is also shown in Fig. 19 where

$$\Gamma = \Gamma_c 1.83 (r/r_c)^2,$$

$$\Gamma = \Gamma_c [1 + 2.14 \log_{10} (r/r_c)],$$

in the inner and outer core regions, respectively.

4.1.3 Multiple Vortex Characteristics

The spanwise downwash distributions for the 1, 2, 11, and 12-spoiler configurations (Figs. 14 to 16) showed multiple closely spaced peaks which did not resemble the velocity distribution predicted for a coherent trailing vortex pair (Fig. 17). Since the multiple high-velocity peaks in the near-wake downwash field are found in multiple vortex wakes; and the 1, 2, 11, and 12-spoiler configurations (flybys 11, 12, and 13) have been analyzed to identify possible multiple vortex characteristics.

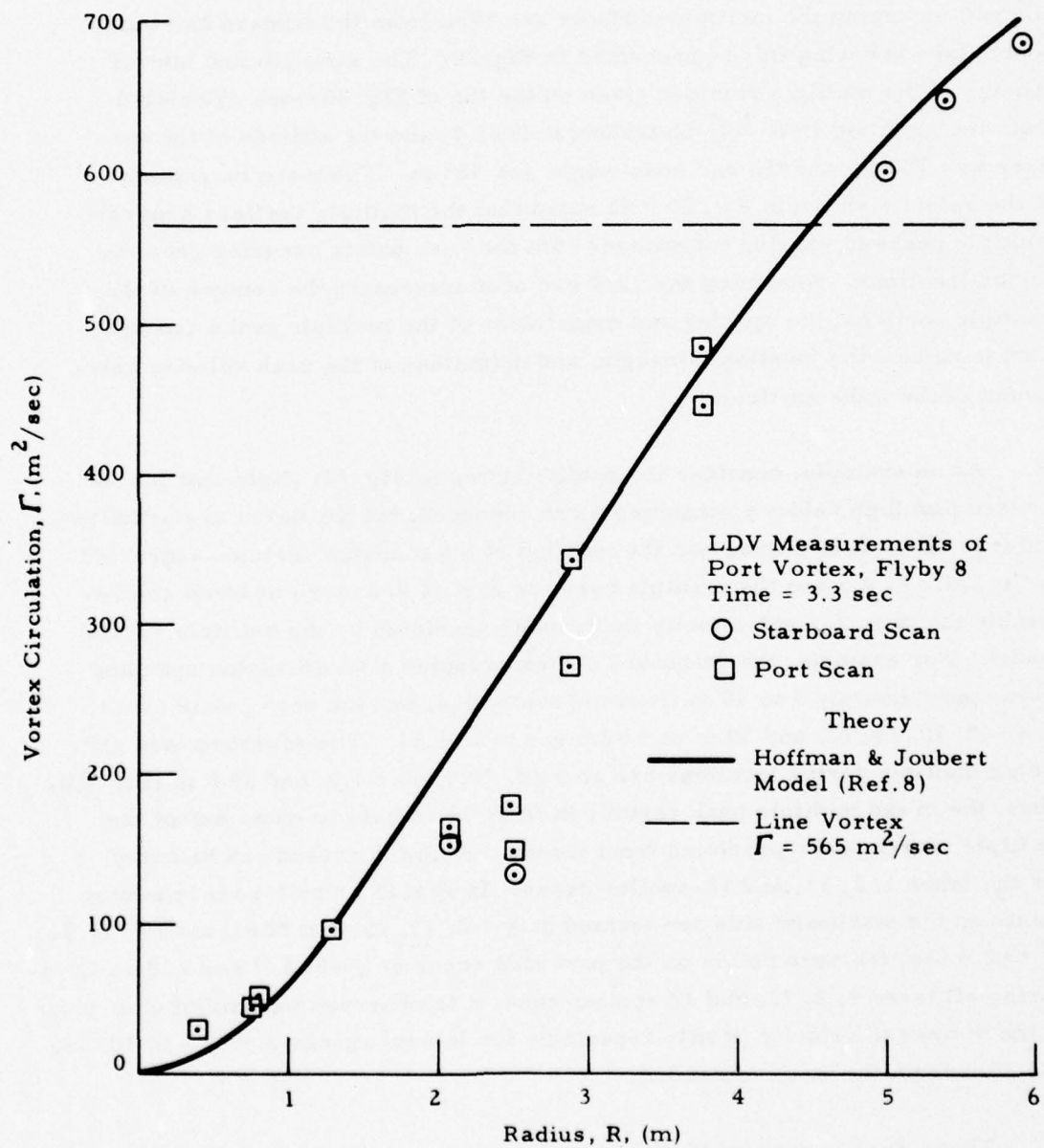


Fig. 19 - Circulation as a Function of Radius for 0 Spoiler Flight Configuration

The magnitude line-of-sight velocity component predicted for a B-747 aircraft assuming the multiple vortices are shed from the inboard and outboard flaps and wing tips is presented in Fig. 20. The strength and lateral spacing of the multiple vortices given on the top of Fig. 20 were calculated from the modified Betz roll-up technique (Ref. 9) and the altitude of the vortices was 180 m, and the arc scan range was 183 m. From the magnitudes of the velocity shown in Fig. 20 it is noted that the multiple vortices generate multiple peaks of varying magnitudes with the zero points occurring near the vortex locations. Assuming the LDV arc scan intersects the centers of the multiple vortices, the spacing and magnitudes of the multiple peaks can be used to deduce the location, strength, and magnitude of the peak velocity component of the wake vortices.

As an example, consider the profile shown in Fig. 14. Note that for the 1.5-sec plot high velocity magnitudes are recorded, but the peaks are scattered and it is difficult to distinguish the location of the multiple vortices suggested in Fig. 20. At 2.6 sec the multiple peaks in Fig. 14 are more ordered and resemble the line-of-sight velocity magnitudes predicted by the multiple vortex model. For example, the starboard vortex occupies a broad region spanning from approximately 3 to 40 m from the centerline, and the zero points occur at $y \sim 0, 10, 15, 22,$ and 30 m at $t = 2.6$ sec in Fig. 14. The superimposed predicted multiple vortex locations are at $y = 3, 10.4, 14, 21.3,$ and 29.6 m (Fig. 20). Thus, the broad multiple peak regions in flyby 11 contain to some extent the multiple vortex peaks predicted from theory. A similar trend can be noted for the other 1, 2, 11, and 12-spoiler cases. In Fig. 15 at $t = 2.4$ sec, the zero points on the starboard side are located at $y \sim 0, 17, 25,$ and 32 m, and in Fig. 18 at $t = 2.9$ sec, the zero points on the port side occur at $y \sim 0, 5, 10$ and 18 m. Comparing all three 1, 2, 11, and 12 spoiler runs, it is observed that minimums occur in the downwash velocity profile repeatedly for lateral spacings of $y \sim 0, 10, 15,$ and 25 m from the wake centerline.

These results suggest that three or four merged vortices are present in the near wake for each semispan. A more detailed analysis of the LDV measurements may establish the strength and core radii of these vortices.

$\Gamma_1 = 62.3 \text{ m}^2/\text{sec}$, $\Gamma_2 = 433.5 \text{ m}^2/\text{sec}$, $\Gamma_3 = -158.4 \text{ m}^2/\text{sec}$, $\Gamma_4 = 298 \text{ m}^2/\text{sec}$, $\Gamma_5 = -16.2 \text{ m}^2/\text{sec}$
 $\Gamma_6 = -62.3 \text{ m}^2/\text{sec}$, $\Gamma_7 = -433.5 \text{ m}^2/\text{sec}$, $\Gamma_8 = 158.4 \text{ m}^2/\text{sec}$, $\Gamma_9 = -298 \text{ m}^2/\text{sec}$, $\Gamma_{10} = 16.2 \text{ m}^2/\text{sec}$
 $y_1 = 29.6 \text{ m}$, $x_1 = 180 \text{ m}$, $y_2 = 21.3 \text{ m}$, $x_2 = 180 \text{ m}$, $y_3 = 14 \text{ m}$, $x_3 = 180 \text{ m}$, $y_4 = 10.4 \text{ m}$, $x_4 = 180 \text{ m}$,
 $y_5 = 3 \text{ m}$, $x_5 = 180 \text{ m}$, $y_6 = -29.6 \text{ m}$, $x_6 = 180 \text{ m}$, $y_7 = -21.3 \text{ m}$, $x_7 = 180 \text{ m}$, $y_8 = -14 \text{ m}$, $x_8 = 180 \text{ m}$,
 $y_9 = -10.4 \text{ m}$, $x_9 = 180 \text{ m}$, $y_{10} = -3 \text{ m}$, $x_{10} = 180 \text{ m}$
 (Subscripts 1-5 Starboard Vortices, 6-10 Port Vortices)

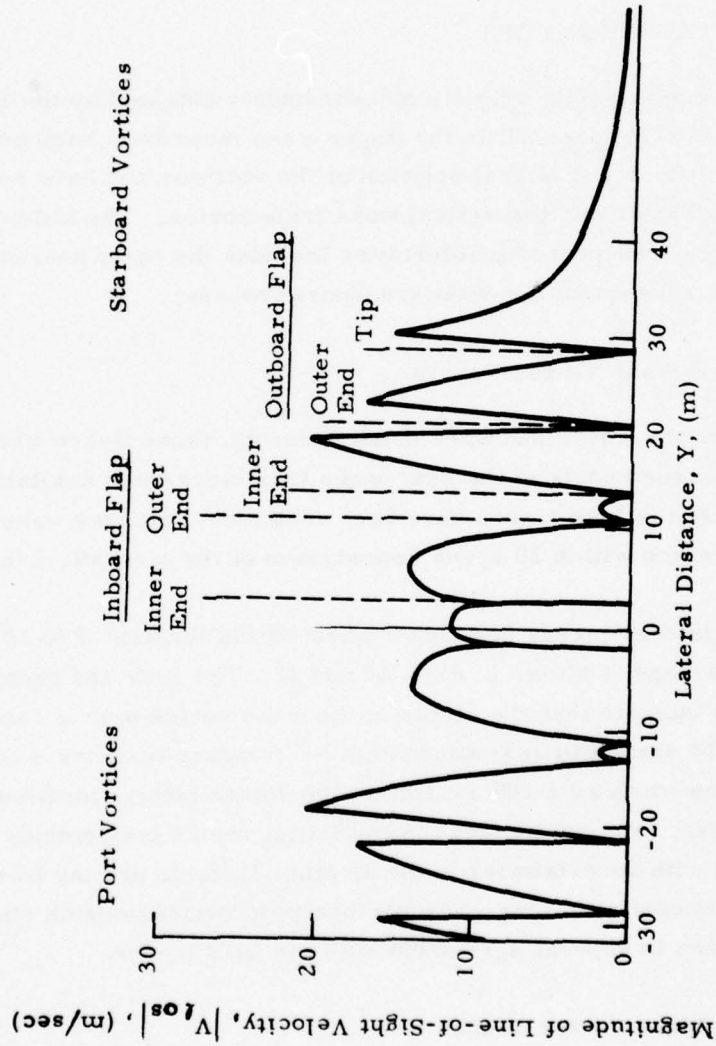


Fig. 20 - Magnitude of Line-of-Sight Velocity Component for Rosamond B-747
 Flyby 11 at $t \sim 2$ sec, Computed Assuming Multiple Wake Vortices

However, the LDV measurements have shown that multiple vortices exist in the near wake of the B-747 aircraft when spoilers are deployed, whereas a coherent rolled-up trailing vortex pair exists in the near wake for 0 spoilers.

4.2 VORTEX TRANSPORT

The line-of-sight velocity measurements obtained by the LDV in the wake of the B-747 aircraft in the finger-scan mode have been processed to yield the altitude and lateral position of the vortices, and have been compared with photographic and theoretical wake trajectories. The following analysis of the vortex transport characteristics includes the early near-wake flow as well as the subsequent far-wake transport process.

4.2.1 Near-Wake Vortex Tracks

From the Rosamond wake measurements, those flybys where photographic measurements of the near-wake trajectory were available for comparison with the LDV tracks have been selected. The near wake was assumed to be the region within 20 spans downstream of the aircraft, $x/b \leq 20$.

The lateral versus horizontal wake vortex location 5 to 10 sec after aircraft passage is shown in Figs. 21 and 22. The LDV and photographic measurements indicate that the center of the wake vortex pair is located at approximately 80% semispan and descends at ~ 1.5 m/sec over the 4 to 10 sec interval. However, as much as a 15% scatter in the vortex lateral location and 50% scatter in the descent rate can be noted in the initial vortex trajectories which may be associated with uncertainties in the airplane location or may be due to the different flight configurations. The photographic measurements shown in Figs. 21 and 22 are in general agreement with the LDV trends.

4.2.2 Far Wake Vortex Tracks

The line-of-sight velocity measurements obtained with the LDV system in the finger-scan mode have been processed with the VAD and Vortex Track Program and the I_{pk} program to determine the far-wake vortex trajectories.

Solid Symbols Photo, Open
Symbols LDV Measurements

Flyby	Aircraft Alt. (m)
○ 27	67
◇ 28	66
△ 30	66

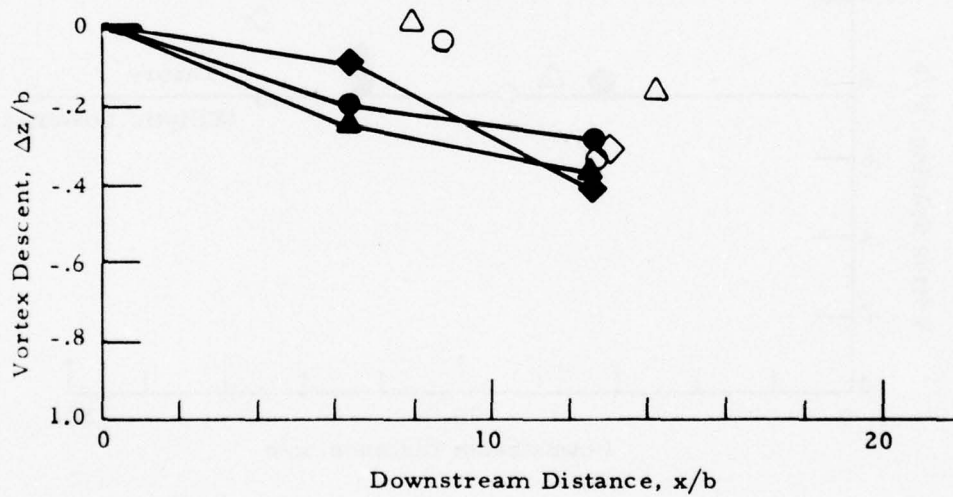


Fig. 21 - Vortex Descent as a Function of Downstream Distance
for Flybys with 30/30 Flaps, 0 Spoilers

Solid Symbols Photo, Open
Symbols LDV Measurements

Flyby

○ 27

◇ 28

△ 30

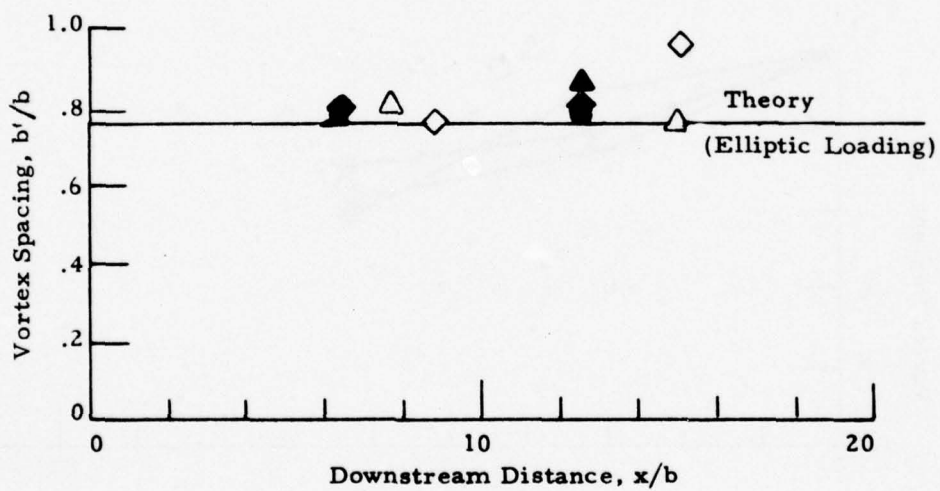


Fig. 22 - Vortex Spacing as a Function of Downstream Distance
for Flybys with 30/30 Flaps, 0 Spoilers

The regions of the maximum backscatter intensity were used to locate the vortex core region. The wake vortex tracks from the Rosamond tests include the results from the low-speed data and high-speed data.

4.2.2.1 Low-Speed Data

The wake vortex trajectories from the low-speed LDV measurements are presented in Appendix D. From the wake vortex trajectories presented in Appendix D, the following wake transport characteristics can be noted: (1) the wake vortex descends nearly vertically with very little horizontal motion; (2) the initial descent rate over the period 0 through 20 sec after aircraft passage is in general agreement with the prediction; and (3) the wake descent diminishes after 20 sec and the vortex tends to remain at a constant altitude in ground effect. In addition to the above trends, some scatter is noted in the location of the vortices. Since both the photographic and LDV tracks show the vortex wandering in lateral position and altitude, particularly at late times, this is believed to be the effect of random atmospheric winds and gusts. However, in some cases, a large scatter is noted in the LDV vortex tracks which is not seen in the corresponding photographic measurements. This has been investigated using the high-speed data since accurate determination of the vortex position is a prerequisite in determining other relevant parameters such as the decay of the vortex rotational velocity and circulation strength.

4.2.2.2 High-Speed Data

The wake vortex tracks computed from the high-speed LDV data using the I_{pk} algorithm are given in Appendix E for flybys 27, 28, 44, 47, 48, and 49. The vertical and lateral vortex trajectories computed from the high-speed data show the same trends as the low-speed tracks discussed earlier.

Comparison of the high-speed wake vortex measurements with the observed photographic vortex position is shown in the V_{pk} versus elevation angle curves in Figs. 23 and 24. With the exception of any dominant low

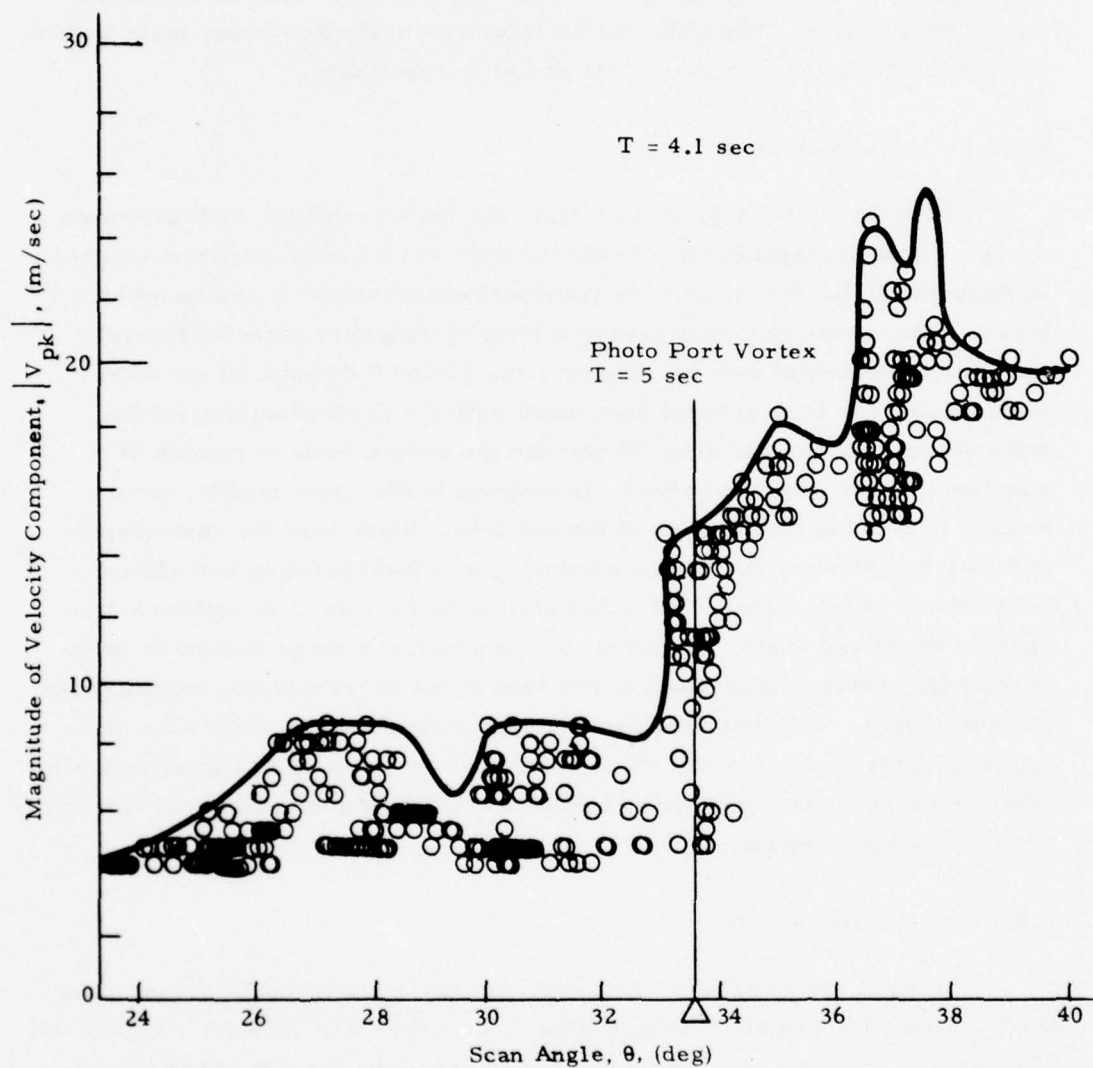


Fig. 23 - Comparison of Photographic and LDV Measurements for Rosamond B-747 Flyby 27

Flyby 27

T = 6.6 sec

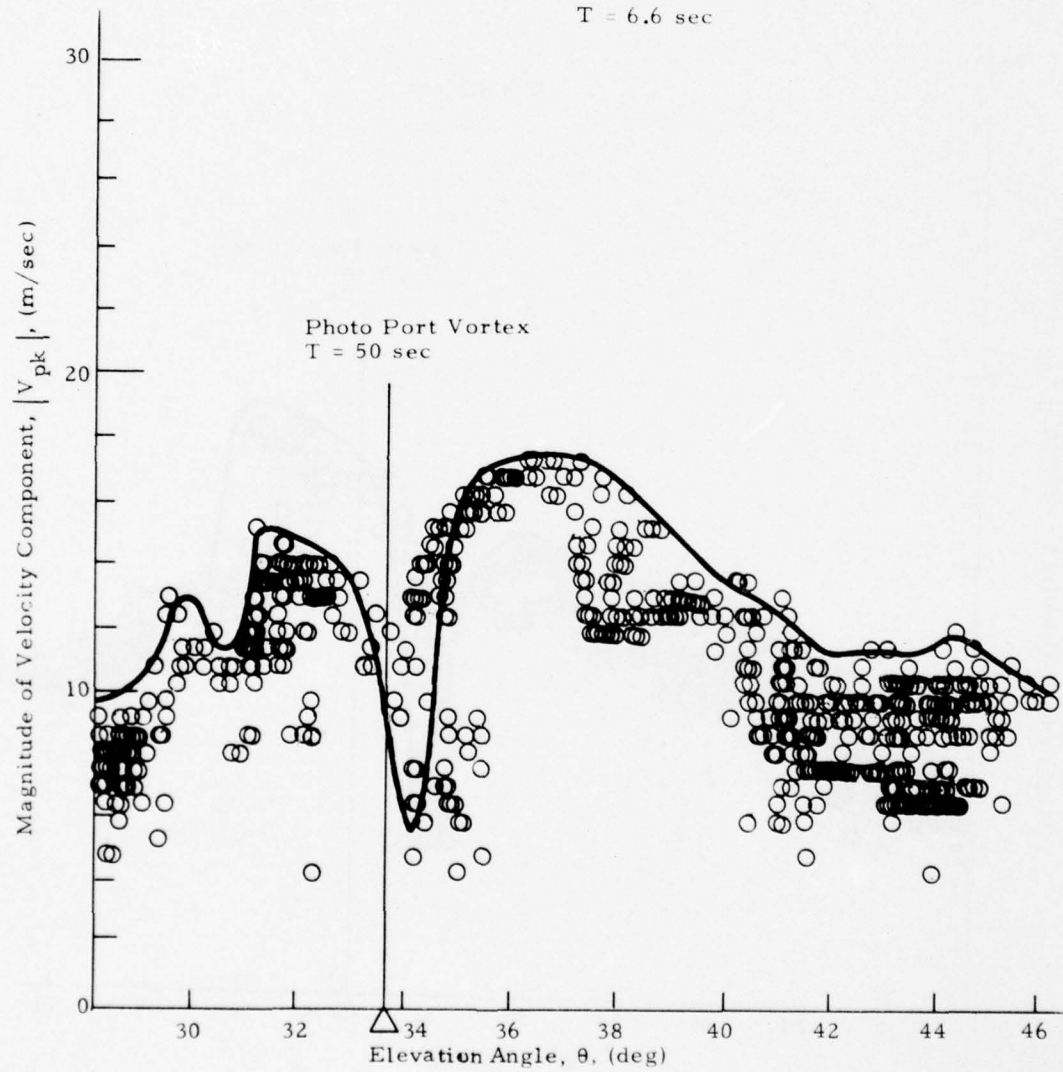


Fig. 23 (Continued)

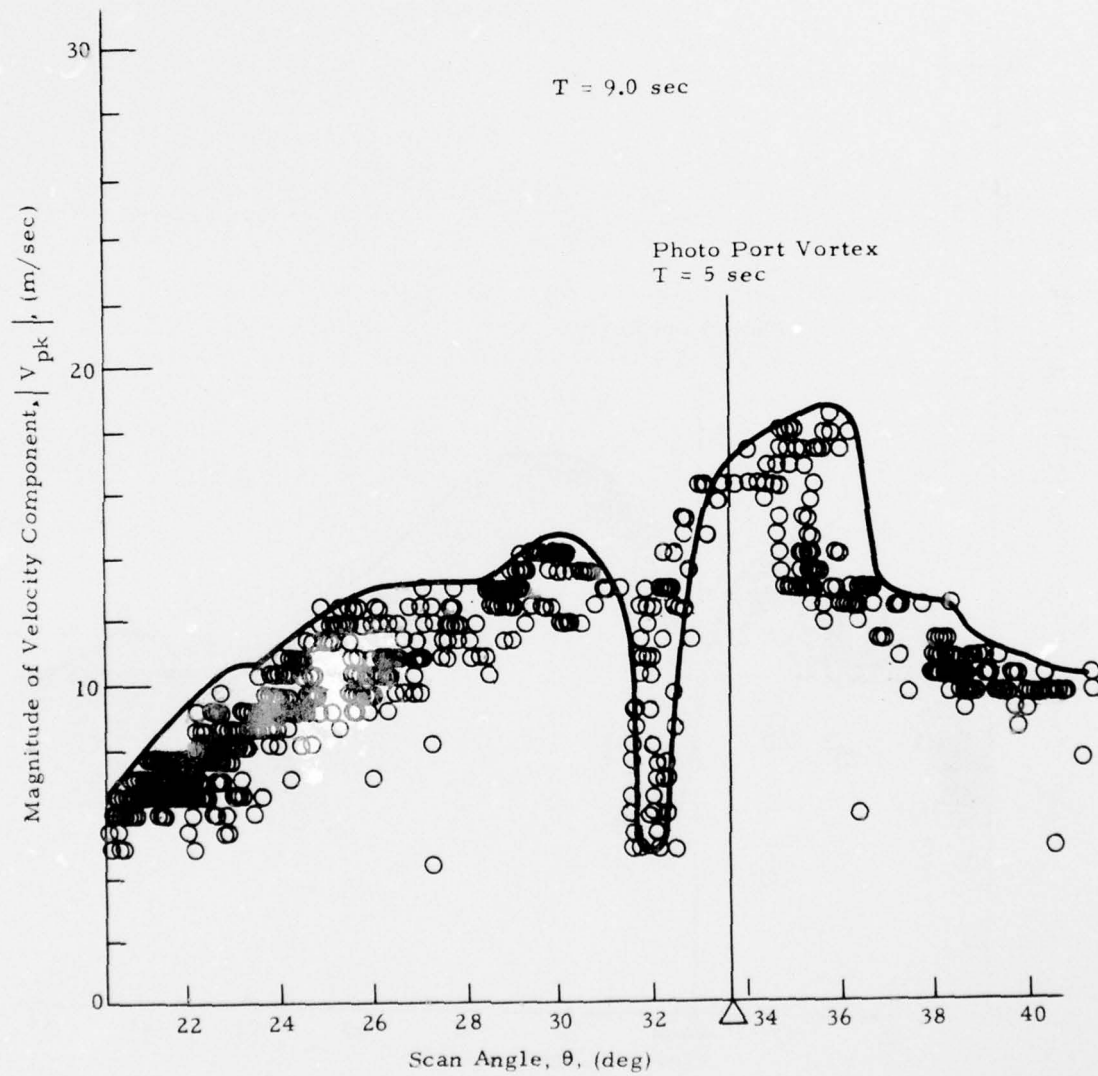


Fig. 23 (Continued)

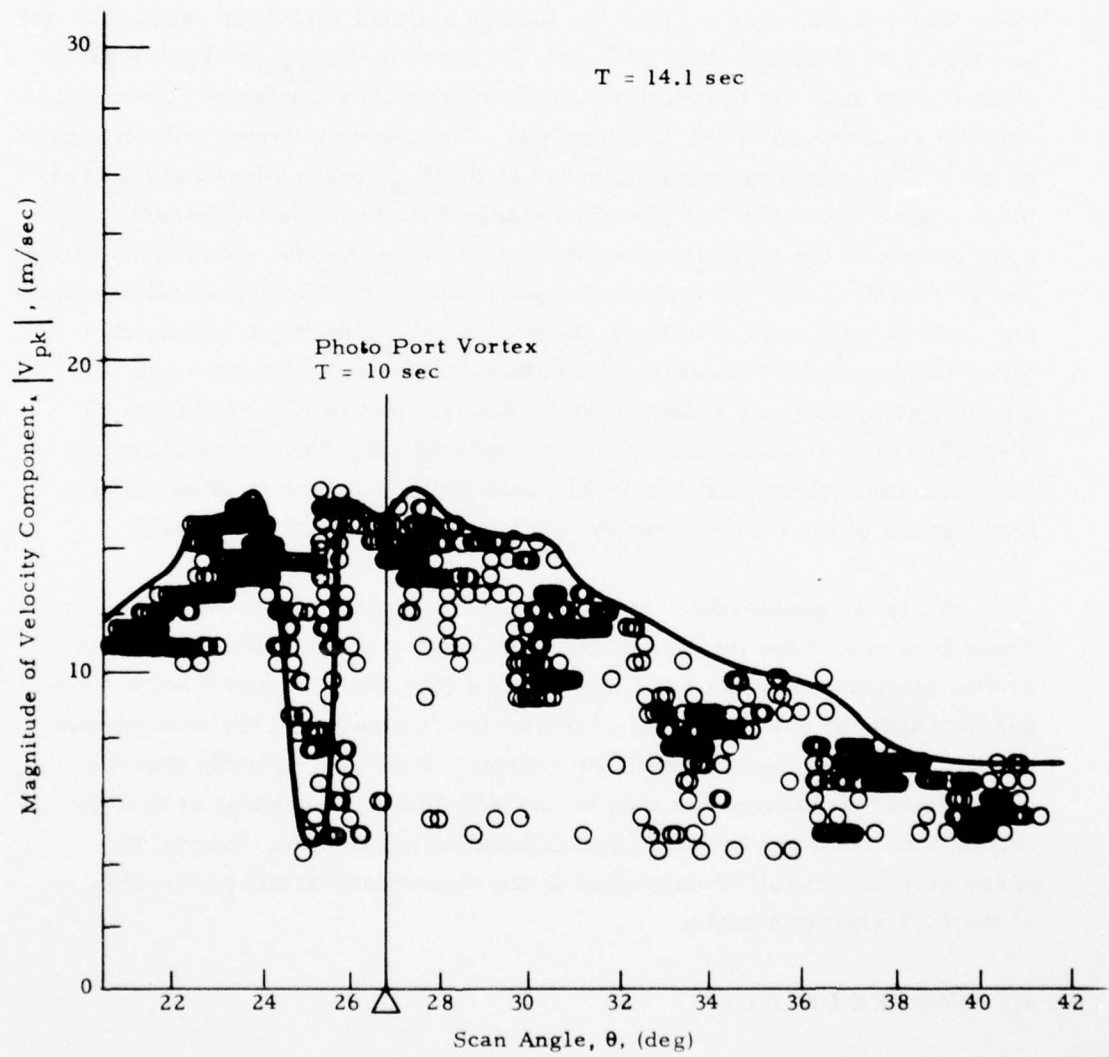


Fig.23 (Concluded)

magnitude spikes, the solid line in the plots connects the maximum values of $|V_{pk}|$ observed by the LDV in the finger scan mode for one scan between the two elevation angle limits (i.e., it represents the maximum value of $|V_{pk}|$ for many finger-scan lobes). Since the LDV is scanned rapidly in range (3.5 Hz) and slowly in elevation angle (0.2 Hz), the peaks in the $|V_{pk}|$ versus elevation-angle curves indicate the elevation angle at which the maximum line-of-sight velocity is observed by the LDV system. Thus, when a vortex is interrogated by the LDV system, two maxima occur in the $|V_{pk}|$ versus elevation angle at those angles where the line of sight is tangent to the vortex core and a minimum occurs at the mid-elevation angle, or in other words, a double-peak signature results. The low magnitude spike bounded by the high amplitude peaks marks the vortex core, and here, the minimum $|V_{pk}|$ points are connected. For a number of LDV measurements, this double-peak signature can be clearly recognized; for example, at $t = 6.6, 9.0$ and 14.1 sec for flyby 23 (Fig. 27) and at $t = 4.2$ and 14.2 sec for flyby 28 (Fig. 24). In addition, the elevation angle at which these double-peak patterns occur is often within a few degrees of the vortex elevation angle measured photographically.

While the photographic and LDV measurements agree well for some scans in terms of the location of the vortex signature, for other scans, the scatter in elevation angle is as high as 6 deg (Fig. 24, $t = 5$ and 9 sec). It is possible that the core diameter of the vortex is small, and the scan pattern misses the peak-tangential velocity regions. It is also possible that the photographic measurements may be subjected to some errors, or that the smoke does not mark the exact vortex location accurately. Lastly, the error may be a result of anomalies in the determination and processing of the LDV elevation angle.

4.3 VORTEX DECAY

Information regarding the decay of wake vortices such as the time history of the peak tangential velocity, circulation and viscous core radius is contained in the line-of-sight velocity magnitudes measured by the LDV system.

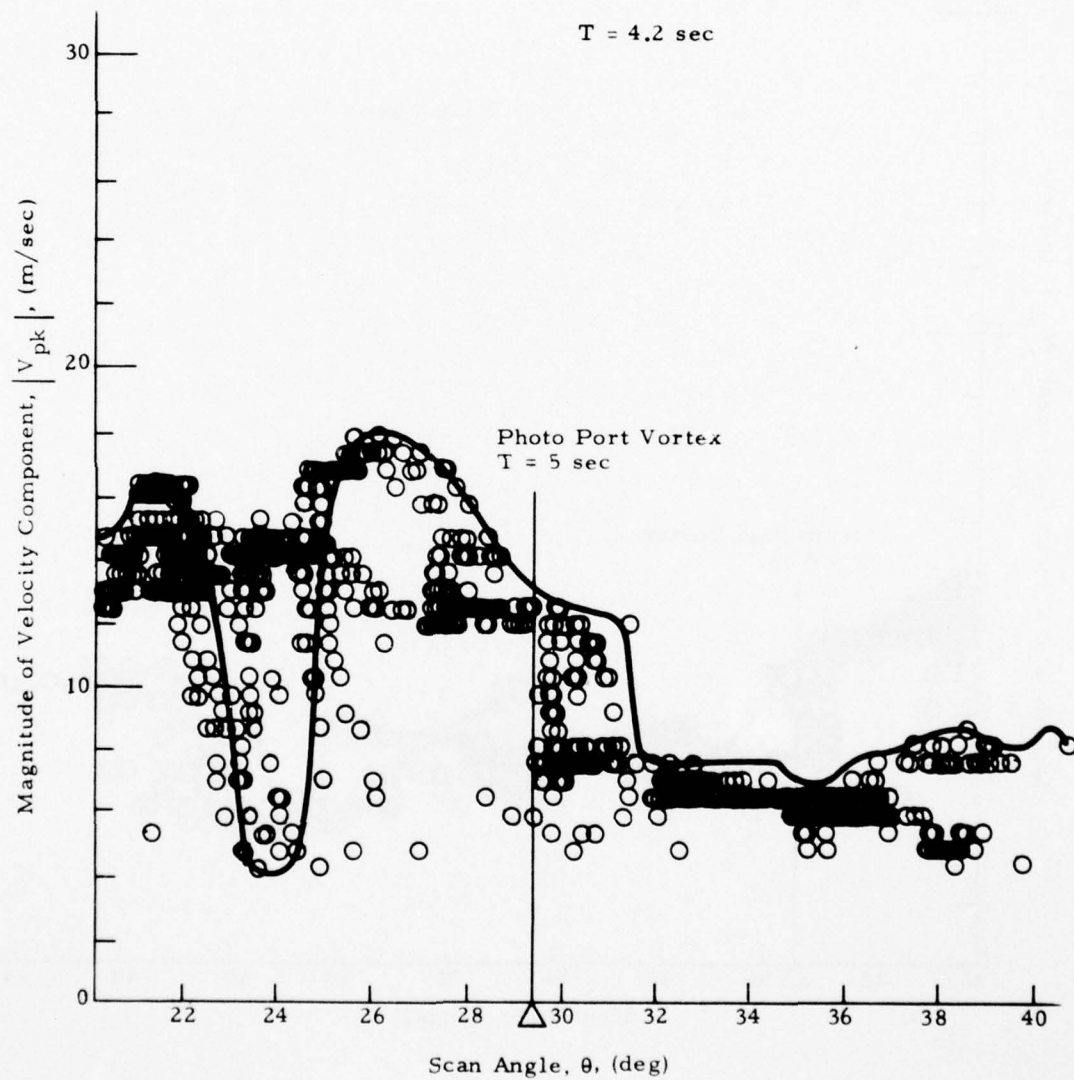


Fig. 24 - Comparison of Photographic and LDV Measurements for Rosamond B-747 Flyby 28

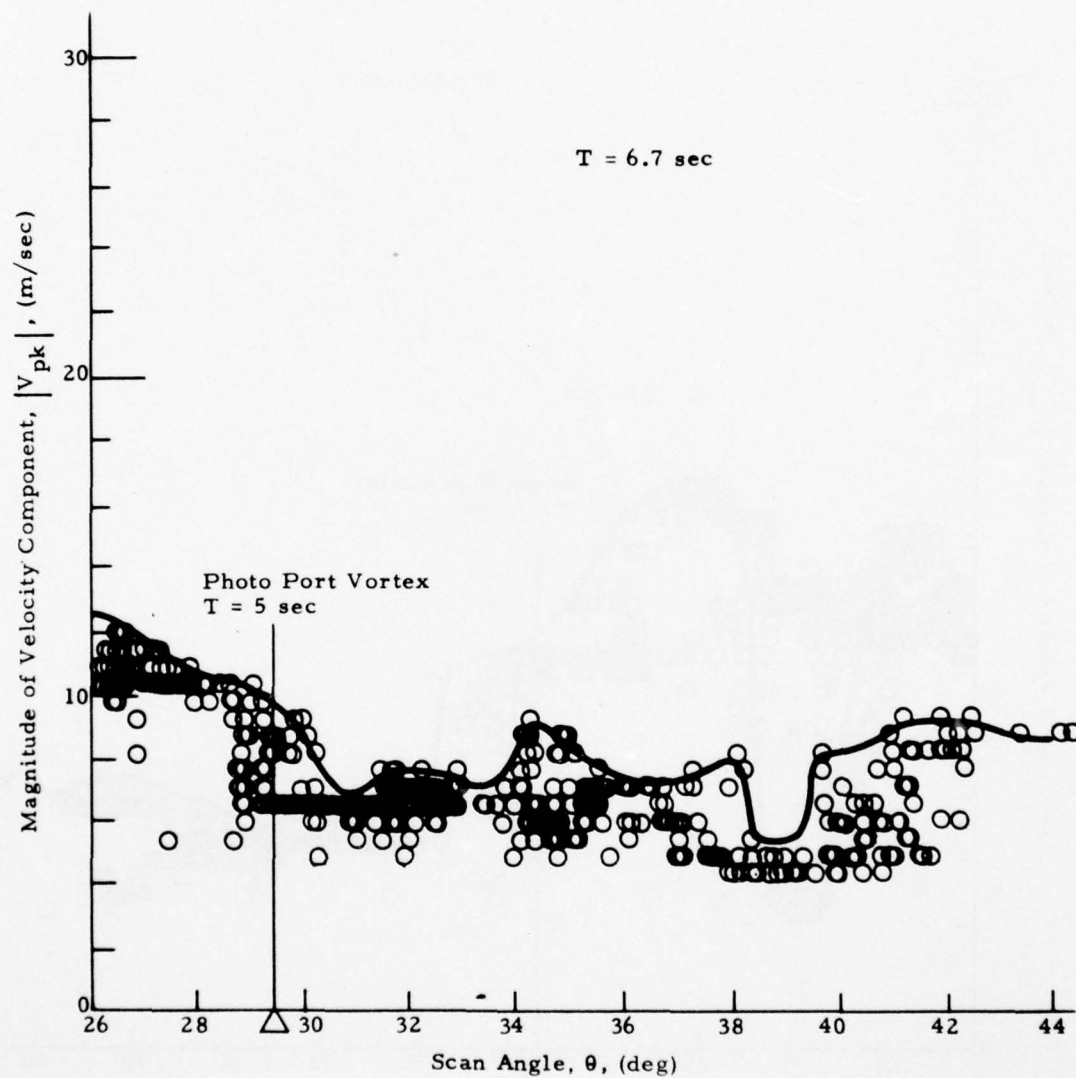


Fig. 24 (Continued)

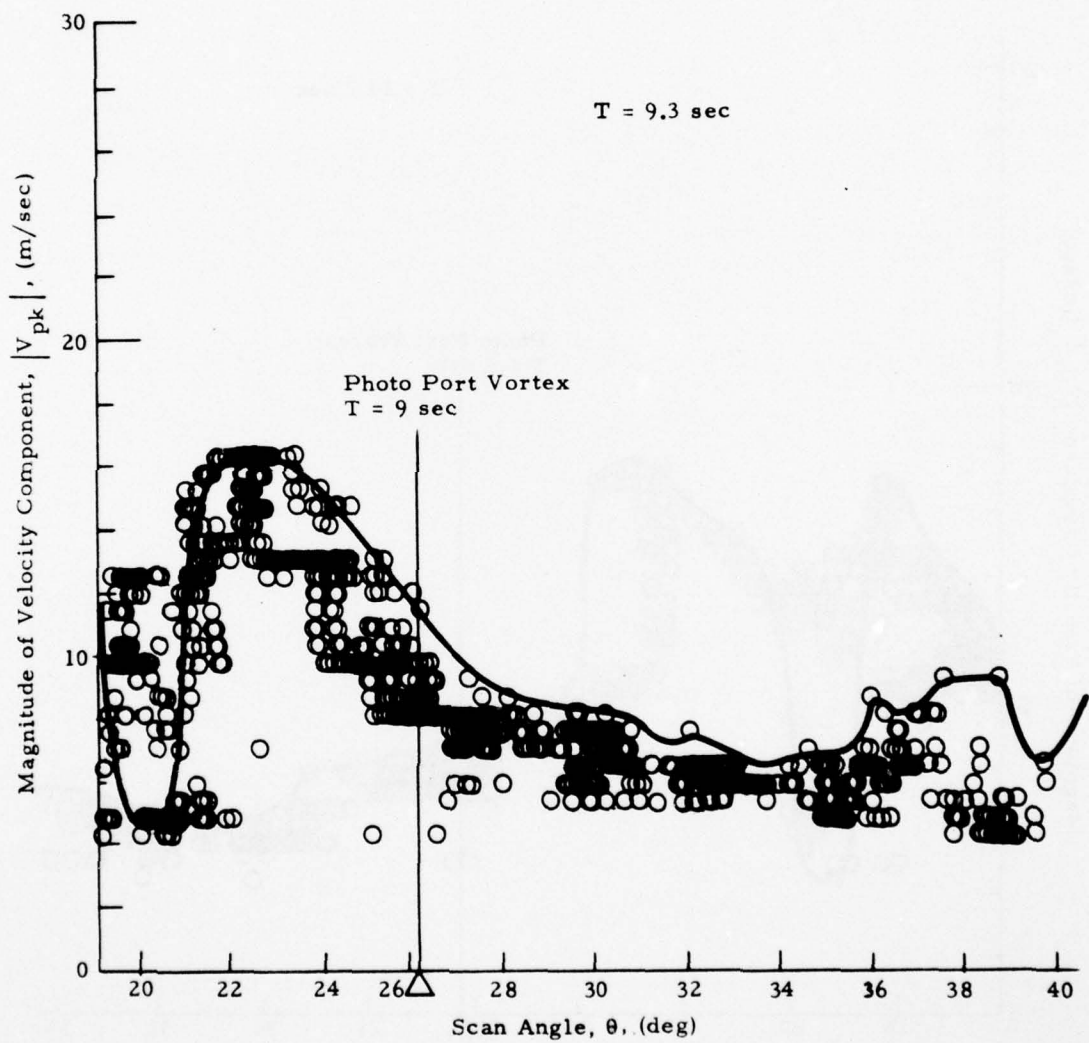


Fig. 24 (Continued)

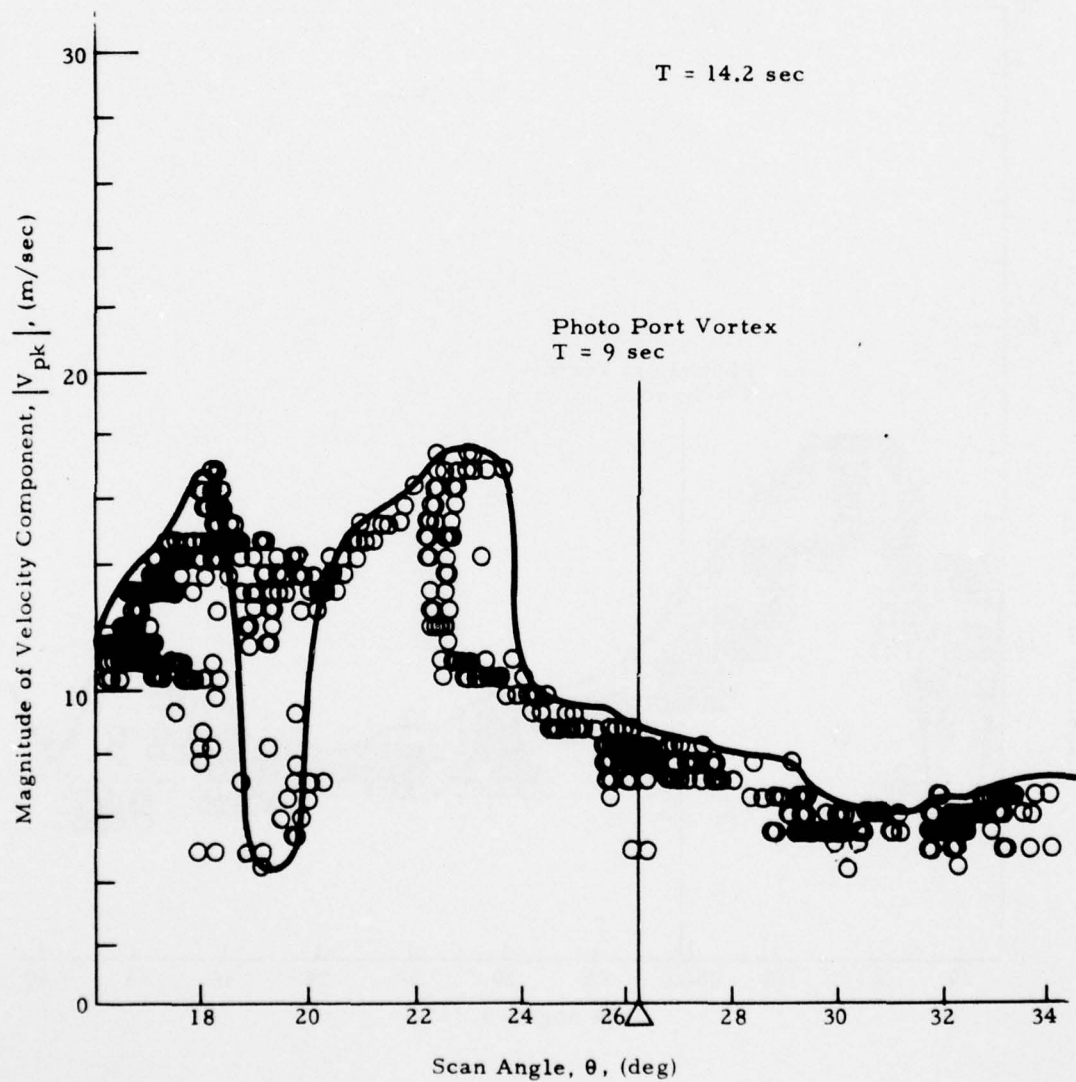


Fig. 24 (Concluded)

4.3.1 Decay of Vortex Rotational Velocity

To determine the decay of the wake vortex rotational velocity from the LDV line-of-sight velocity magnitudes, two basic methods were used to pick out the maximum tangential velocity of the vortex:

- a. Selection of the maximum value of $|V_{pk}|$ (or $|V_{ms}|$) occurring during each scan between minimum and maximum elevation settings.
- b. Selection of the maximum value of $|V_{pk}|$ occurring within ± 3 deg of the known elevation angle of the vortex.

For both techniques, the maximum value of $|V_{pk}|$ is a good measure of the magnitude of the peak tangential velocity of the vortex if the LDV line of sight is tangent at some point with the circular core region of the vortex, and the vortex range falls within the focal volume. However, in the first approach, the $|V_{pk}|$ time history becomes meaningless if the vortex drifts out of the scan area. To eliminate this uncertainty, in the second approach, other information, i.e., photographic vortex position, is used to establish the approximate location of the vortices. These regions are then searched for the maximum $|V_{pk}|$ values which are associated with the vortex phenomena.

The $|V_{pk}|$ and $|V_{ms}|$ time histories determined using the first technique are shown in Appendix F. A bandwidth criterion of $N \geq 2$ was used in the analysis to filter out random high-frequency noise (i.e., at least two of the 100 frequency bins had to be activated for the data to be used). A sample of the results, presented in Fig. 25, indicates that the wake vortex rotational velocity is nearly constant approximately 50 spans downstream of the aircraft followed by $1/\text{time}$ decay. Some scatter which may be associated with the uncertainty in vortex location may be noted in the velocity decay curve.

Using the photographic vortex tracks to determine the approximate vortex location (the second technique above), the $|V_{pk}|$ time history has been

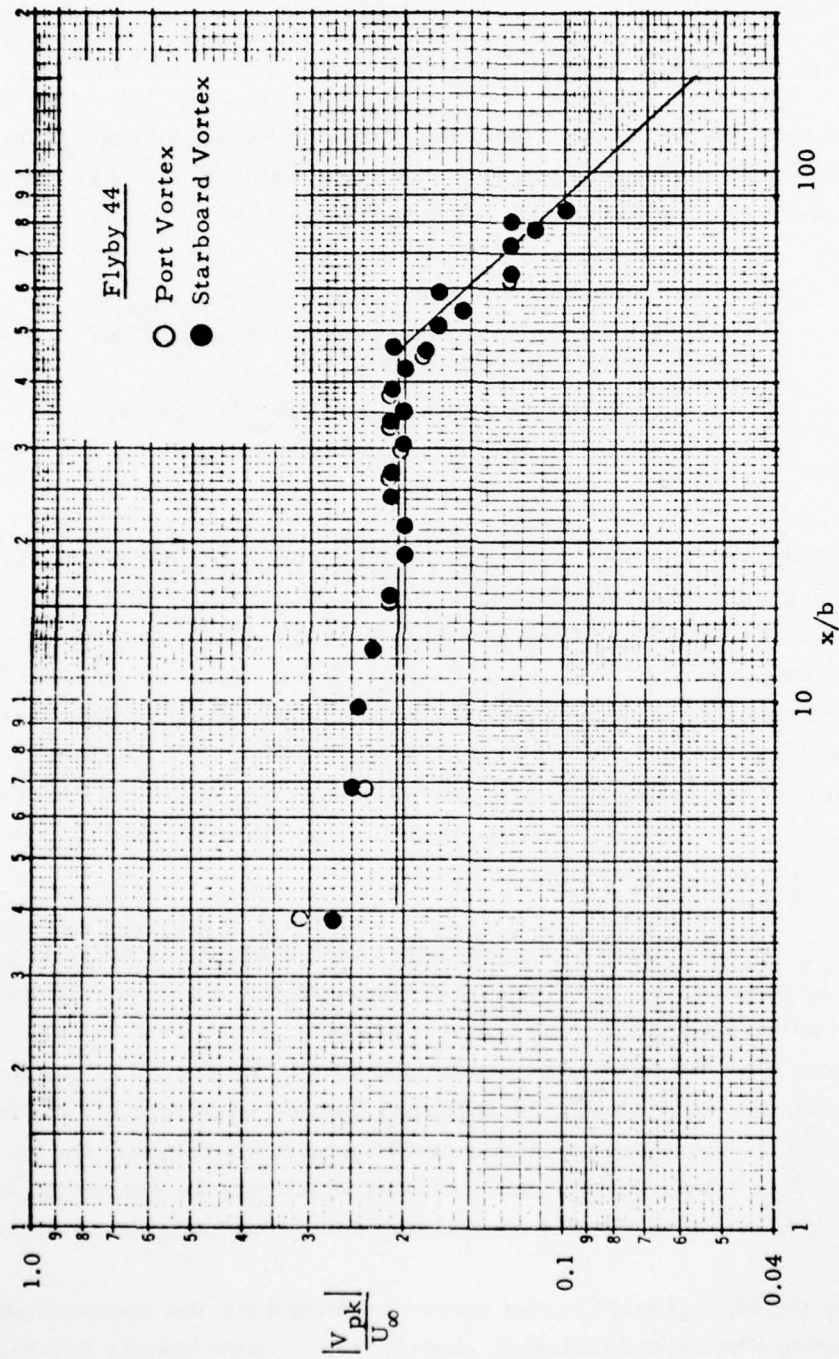


Fig. 25 - Decay of Magnitude of Wake Vortex Rotational Velocity Component for Flyby 44

recomputed for flybys 27 and 28 and is presented in Figs. 26 and 27. The results shown in Figs. 26 and 27 also indicate a nearly constant magnitude of the vortex velocity component within 50 spans downstream of the aircraft. Less scatter occurs in $|V_{pk}|$ versus time plots when the photographic tracks are used to establish the vortex center. Unfortunately, photographic measurements were not available at late times to establish the final vortex decay process.

4.3.2 Core Radius Time History

The vortex core radius was determined from the observed variations in $|V_{pk}|$ with range and elevation angle according to the technique discussed earlier in Section 2.1.2. The computed vortex core radius time history for flybys 27, 28, and 44 is given in Figs. 28, 29, and 30, respectively. Photographic vortex tracks were compared with LDV $|V_{pk}|$ distributions to compute the core radius time history in Figs. 28 and 29, while the predicted vortex tracks were used to compute the core radius time history in Fig. 30. The LDV wake vortex measurements show that the vortex core radius is approximately constant in the aircraft near wake. The observed core radius ranges from 1 to 4 m, and the mean core radius is approximately 2 m.

4.3.3 Circulation Decay

The circulation time history was computed from the observed LDV line-of-sight velocity distribution using: (1) the vortex tracks from the low-speed data, and (2) the photographic tracks to determine the vortex location. In the first technique, the circulation was determined from the average moment of the line-of-sight velocity components within a correlation radius of the computer vortex center. In the second technique, the circulation was computed from the moment of the two maximum $|V_{pk}|$ values adjacent to the center of the vortex as outlined earlier in Section 2.1.2, and the photographic vortex tracks were used to determine the vortex location. It was found that this technique was very sensitive to errors in core radius.

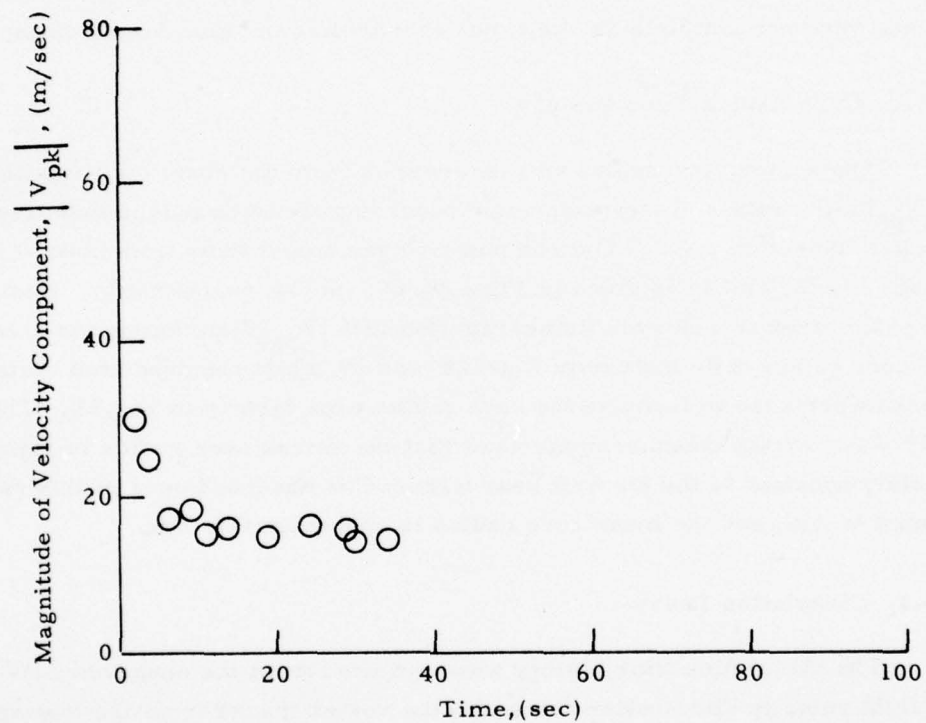


Fig. 26 - $|V_{pk}|$ as a Function of Time for Flyby 27 Using Photographic Tracks to Locate the Vortex Center

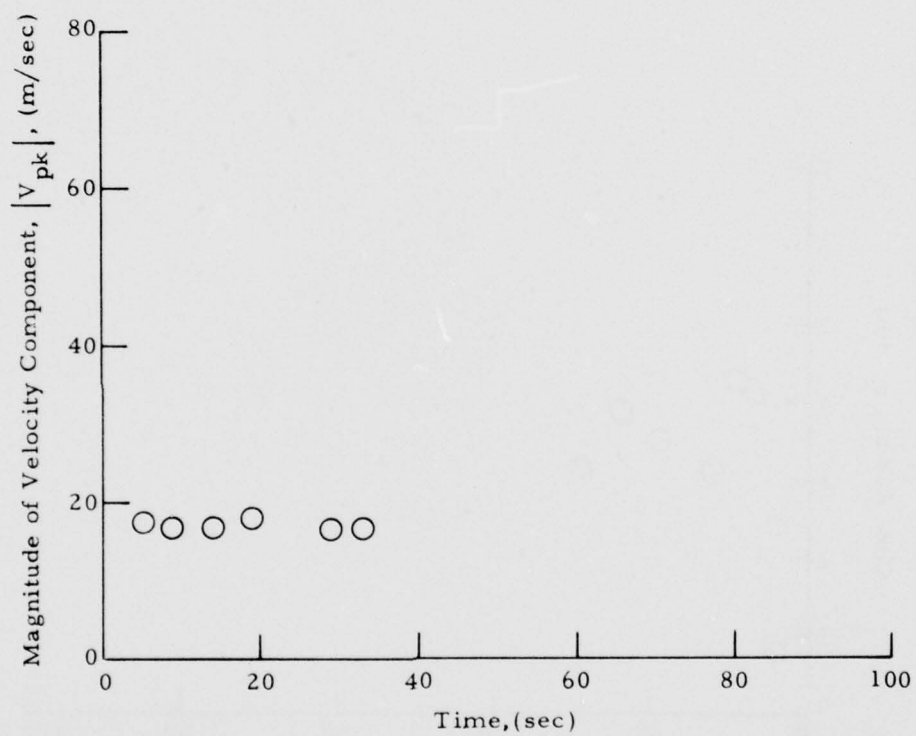


Fig. 27 - $|V_{pk}|$ as a Function of Time for Flyby 28 Using Photographic Tracks to Locate the Vortex Center

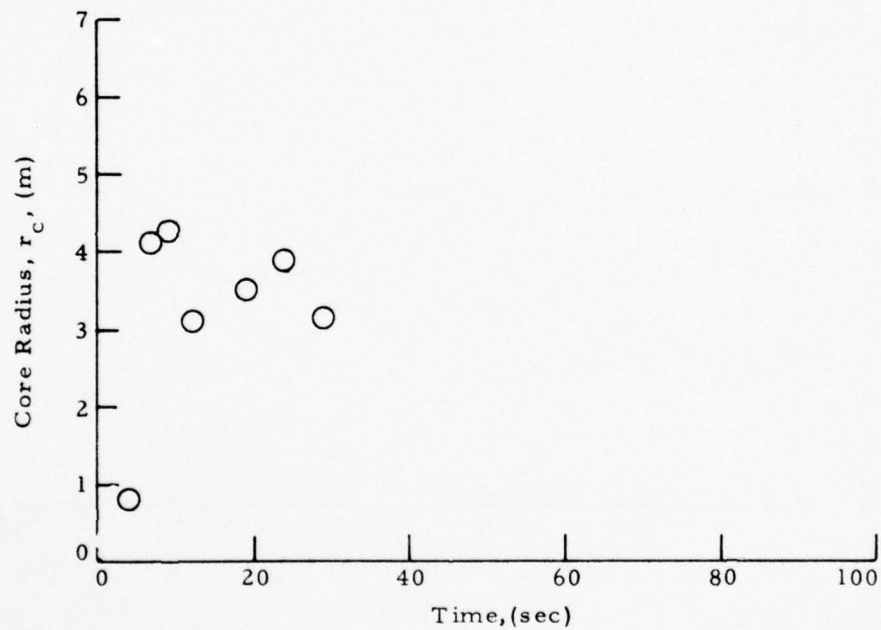


Fig. 28 - Vortex Core Radius as a Function of Time for Flyby 27

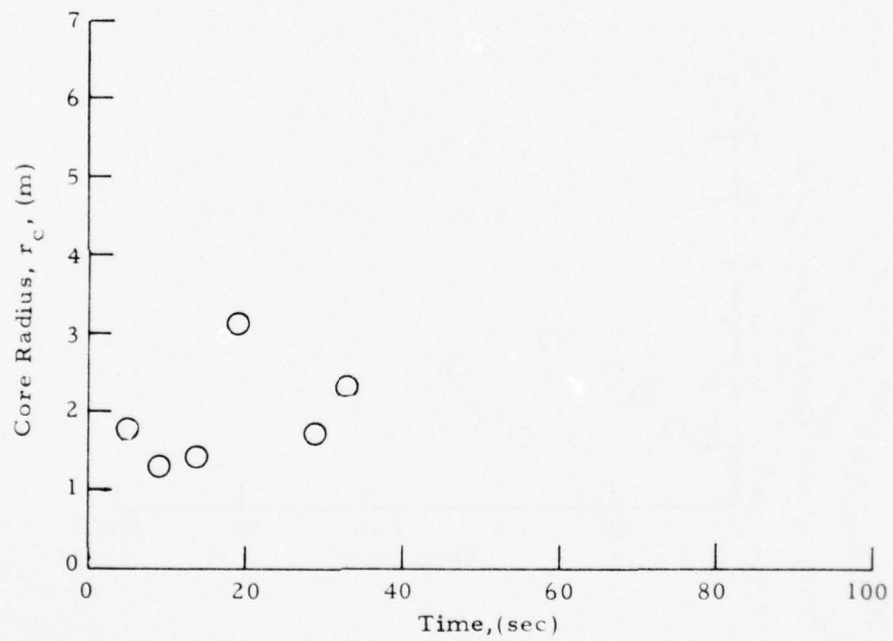


Fig. 29 - Vortex Core Radius as a Function of Time for Flyby 28

AD-A048 275

LOCKHEED MISSILES AND SPACE CO INC HUNTSVILLE ALA HU--ETC F/G 1/1
LASER DOPPLER VELOCIMETER MEASUREMENTS OF B-747 WAKE VORTEX CHA--ETC(U)
SEP 77 M R BRASHEARS, A D ZALAY

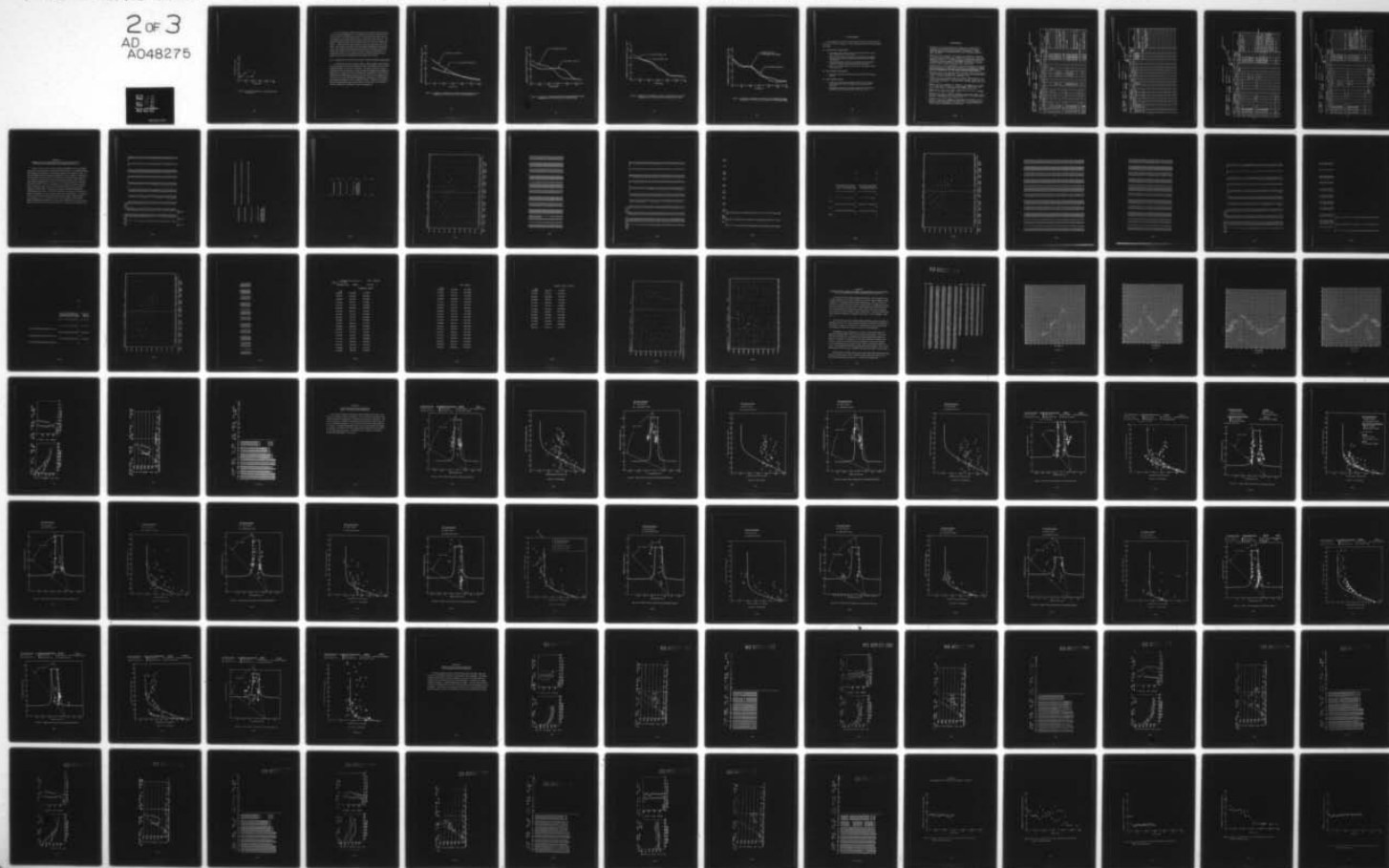
UNCLASSIFIED

LMSC-HREC-TR-D496975

FAA-RD-77-85

NL

2 OF 3
AD
A048275



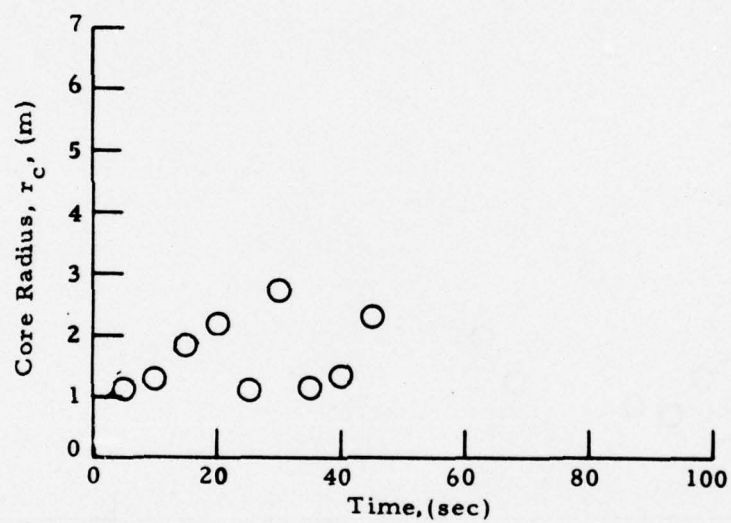


Fig. 30 - Vortex Core Radius as a Function of Time for Flyby 44

The circulation time history computed from the low-speed data vortex tracks is shown in Appendix G. The computed circulation is shown from 20 sec to the time of the last measurement. At periods earlier than a few sec, circulations are not shown since the vortex may not be fully rolled up. The general circulation decay trend is similar to the velocity decay trends noted earlier - relatively small decay initially followed by rapid decay in the far wake. More scatter is evident in the circulation distributions than the velocity or core radius distributions presented earlier because the circulation involves the product of the scatter of the previous two measurements. To reduce this scatter, the circulation has been recomputed using the photographic vortex tracks to define the vortex center more closely.

4.3.4 Comparison of Vortex Decay Trends for Different Flight Configurations

To determine the vortex decay trends for different flight configurations, the time history of the vortex rotational velocity, circulation, and core radius presented earlier can be cross correlated. The decay of the wake vortex rotational velocity for different spoiler and flap and landing gear settings and flight paths is compared in Figs. 31 through 34, respectively. These results indicate that the deployment of spoilers decreases the vortex rotational velocity in the near wake while flap and landing gear settings and aircraft flight path angle do not appear to have a significant effect. However, care must be used in interpreting the above results since for some of the runs the wake vortices drifted out of the field of view (see Appendix D).

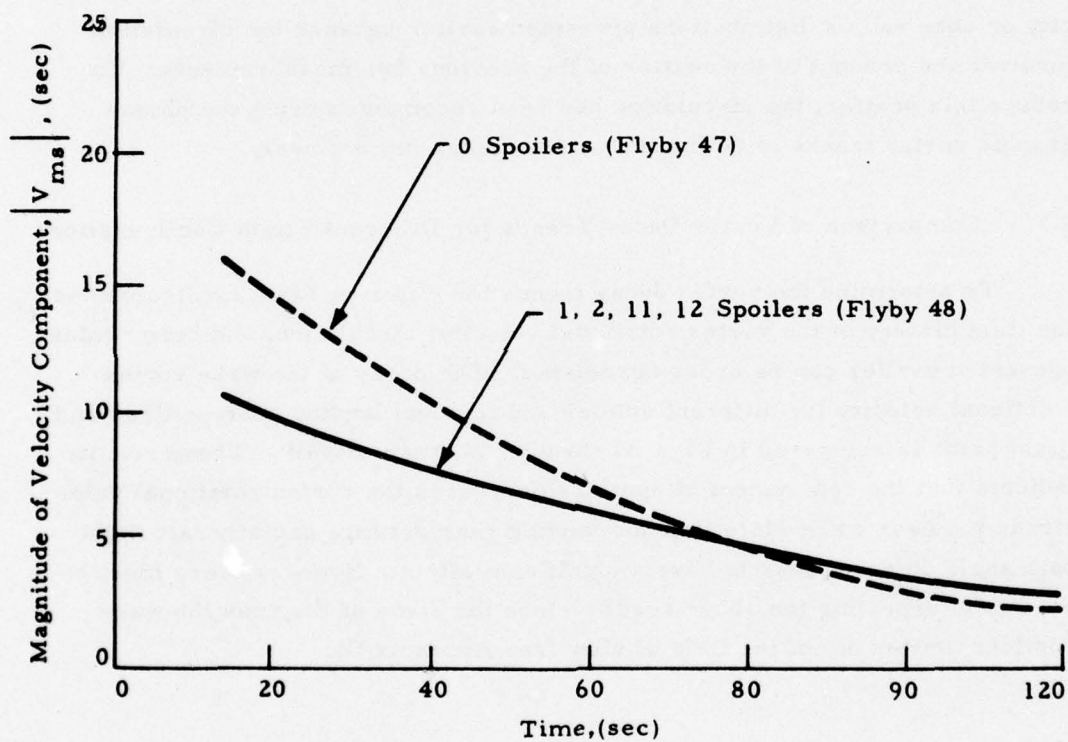


Fig. 31 - Comparison of Magnitude of Wake Vortex Rotational Velocity Component for B-747 Flybys With and Without Spoilers

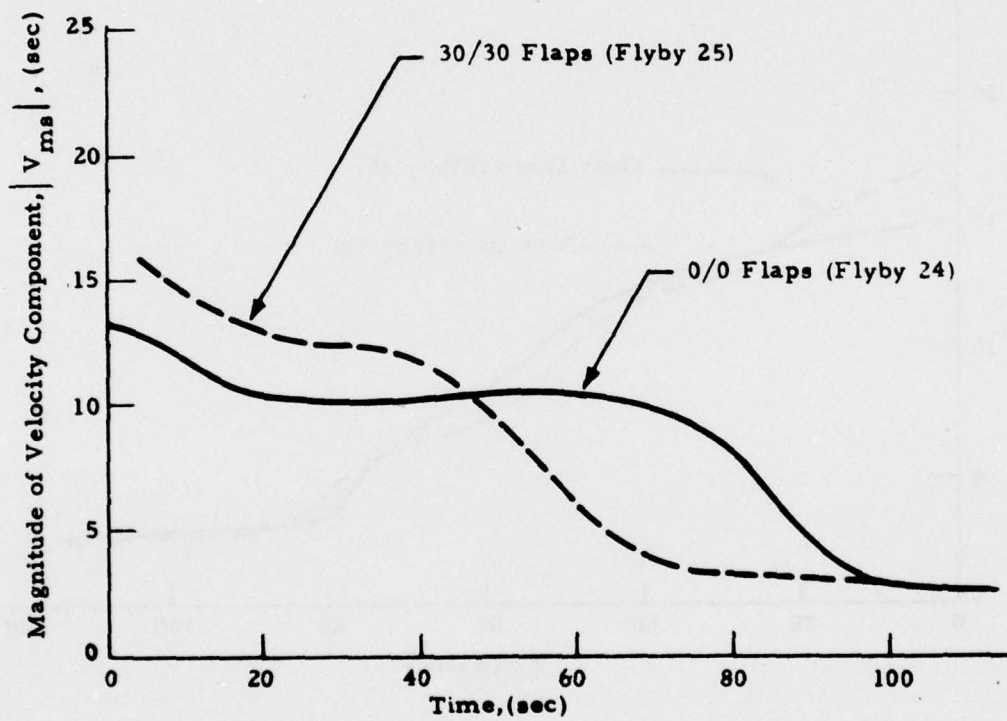


Fig. 32 - Comparison of Magnitude of Wake Vortex Rotational Velocity Component for B-747 Flyby With and Without Flaps

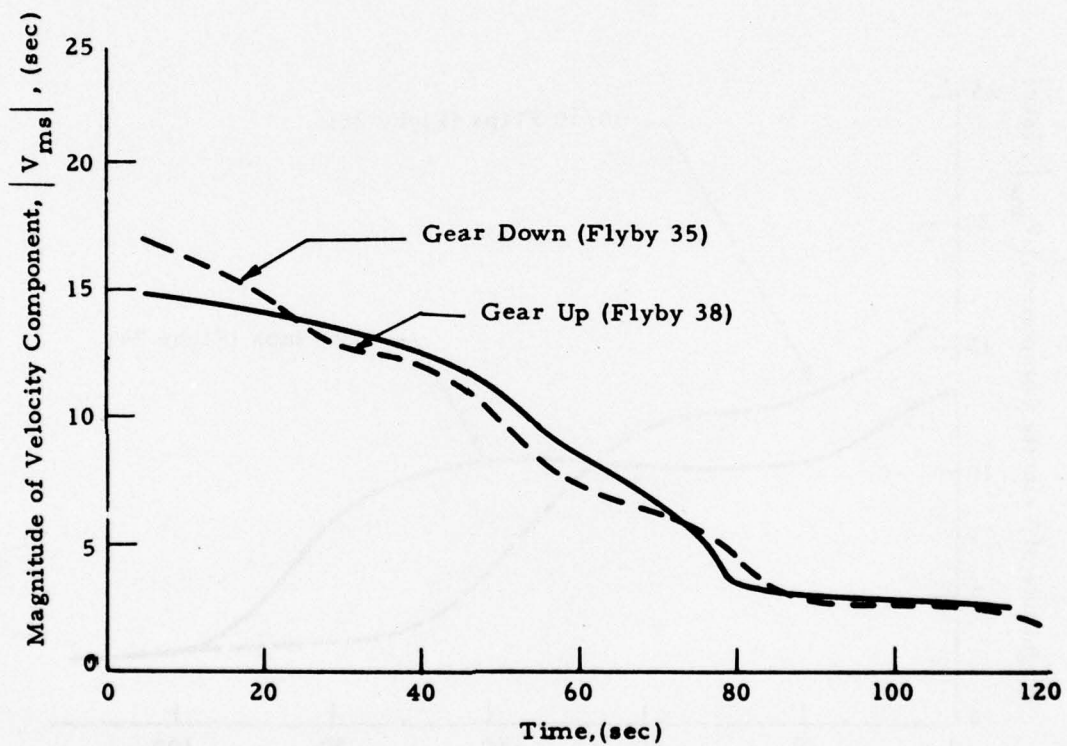


Fig. 33 - Comparison of Magnitude of Wake Vortex Rotational Velocity Component for B-747 Flybys With and Without Gear Down

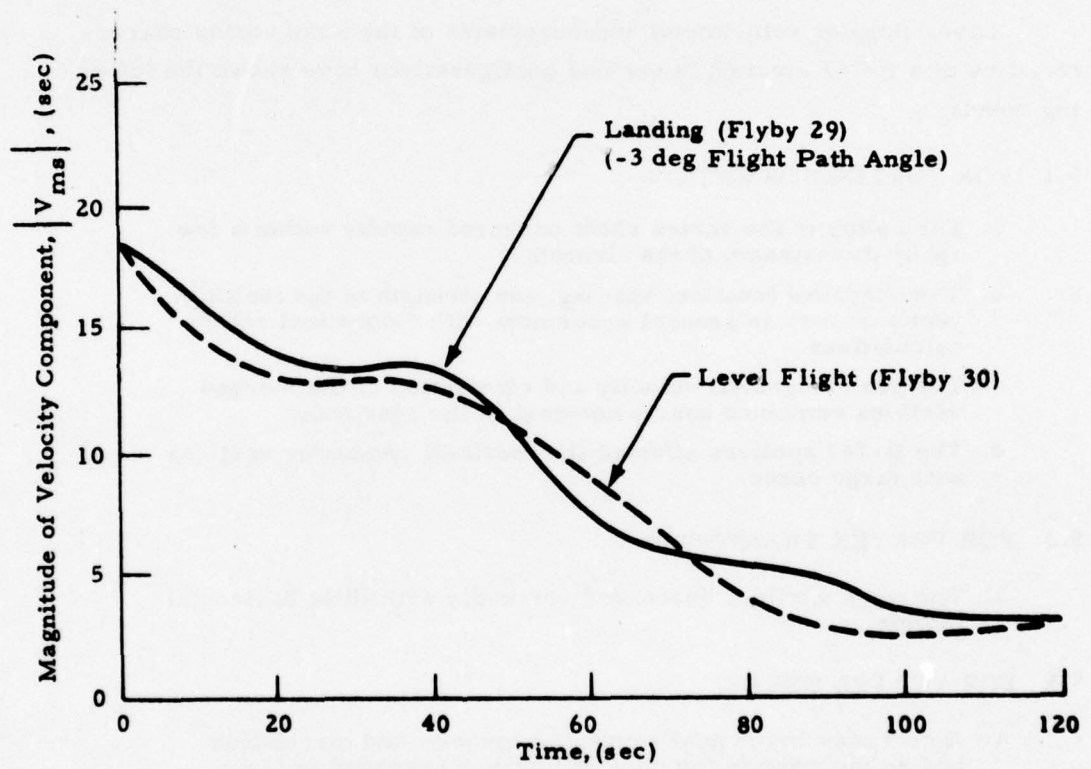


Fig. 34 - Comparison of Magnitude of Wake Vortex Rotational Velocity Component for B-747 in Level Flight and in Descending Flight

5. CONCLUSIONS

Laser Doppler velocimeter measurements of the wake vortex characteristics of a B-747 aircraft in various configurations have shown the following trends.

5.1 FOR VORTEX FORMATION:

- a. The rollup of the vortex sheet occurred rapidly within a few spans downstream of the aircraft.
- b. The observed location, spacing, and strength of the multiple vortices were in general agreement with theoretical rollup calculations.
- c. The peak tangential velocity and circulation of the merged vortices remained nearly constant in the near wake.
- d. The B-747 spoilers affected the vortices, producing vortices with large cores.

5.2 FOR VORTEX TRANSPORT:

- a. The wake vortices descended vertically with little horizontal motion.

5.3 FOR VORTEX DECAY:

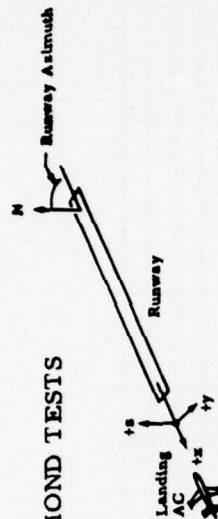
- a. A decrease in the peak tangential velocity and circulation and an increase in the core radius was observed in the far wake.
- b. Deployment of spoilers and flaps enhanced the vortex peak tangential velocity decay process in the near wake.

REFERENCES

1. Krause, M.C., L.K. Morrison, C.E. Craven, N.A. Logan and T.R. Lawrence, "Development of Theory and Experiments to Improve Understanding of Laser Doppler Systems - Final Report," LMSC-HREC TR D306632, Lockheed Missiles & Space Company, Huntsville, Ala., June 1973.
2. Wilson, D.J., M.C. Krause, E.W. Coffey, C-C. Huang, B.B. Edwards, C.E. Craven, K.R. Shrider, J.L. Jetton and L.K. Morrison, "Development and Testing of Laser Doppler System Components for Wake Vortex Monitoring - Volume I - Scanner Development, Laboratory and Field Testing and System Modeling," LMSC-HREC TR D390159-1, Lockheed Missiles & Space Company, Huntsville, Ala., August 1974.
3. Lawrence, T.R. et al., "Application of a Laser Velocimeter for Remote Wind Velocity and Turbulence Measurements," Proceedings of the International Conference on Aerospace and Aeronautical Meteorology, 22-26 May 1972, Washington, D.C., The American Meteorological Society.
4. Brashears, M.R., T.R. Lawrence and A.D. Zalay, "Mobile Laser Doppler System Check Out and Calibration," FAA-RD-77-48, Lockheed Missiles & Space Company, Huntsville, Ala., September 1976.
5. Garodz, L.J., D.M. Lawrence and N. J. Miller, "Measurement of the Trailing Vortex Systems of Large Transport Aircraft, Using Tower Fly-by and Flow Visualization," FAA-RD-75-127, NAFEC, Atlanta City, N. J., January 1976.
6. Bilbro, J.W., H.B. Jeffreys, E.A. Weaver, R.M. Huffaker, G.D. Craig, R.W. George, and P.J. Marrero, "Laser Doppler Velocimeter Wake Tests," FAA-RD-76-11 (also NASA TM X 64988), March 1976.
7. Hoffman, E.R., and P.M. Joubert, "Turbulent Line Vortices," J. Fluid Mech., Vol. 16, Part 3, July 1963, p. 395.
8. Snedeker, R.S., and A.J. Bilanin, "Analysis of the Vortex Wakes of the Boeing 727, Lockheed L-1011, McDonnell Douglas DC-10, and Boeing 747 Aircraft," ARAP Report No. 245, July 1975.
9. Brashears, M.R., N.A. Logan, S.J. Robertson, K.R. Shrider, and C.D. Walters, "Analysis of Predicted Aircraft Wake Vortex Transport and Comparison with Experiment," FAA-RD-74-74, Lockheed Missiles & Space Company, Huntsville, Ala., April 1974.

Appendix A

EXTERNAL LOGS FOR ROSAMOND TESTS



Location: Rosamond 10 10 10
 Date: 12/2/55 15 15 15
 Sheet 1 of 2

Runway Azimuth: _____
 Mirror Azimuth
 for Switch _____

Van X Position: _____
 Ref. Pt. _____
 Van Y Position: _____
 Ref. Pt. _____

Run ID	Spectrum Analyzer				Scanner			Computer		Time		Estimated Wind Azimuth (from)	Comments
	AC Type No.	B.W. (kHz)	Log Lin	Freq. Span (MHz) Min. f _c Max.	Rate (msec)	Range Min. Rate Max.	Elevation Min. Rate Max.	Tape No.	No. Records	Start	Stop		
1	VAD	10	10	0 10cm .5	1			2001		7:40:00	7:41:30	42°	Alt. at 31, 40, 61, 70, 91, 122, 244, 400 at 1 Rev/alt.
2	VAD									7:40:00	7:41:30		same alt.
3	AC 1	30		1 0 2		57	62° 15 3			7:04:00	7:06:00		
4	AC 2	100		1 0 6						7:04:30	7:06:00		
5	AC 3									7:04:30	7:06:00		
6	AC 4			0 10cm 5		60				7:04:30	7:06:00		
7	AC 5					118	63 20			7:04:30	7:06:00		
8	AC 6	30				118	63 03			7:04:30	7:06:00		
9	AC 7					240	63 30			7:04:30	7:06:00		
10	AC 8						63 21			7:04:30	7:06:00		
11	VAD	10		0 .5	1					7:04:30	7:06:00		Time mark on tape, not human giving 5:10° past 90°
12	AC 9	30		0 1/2cm 5		56	63 13			7:04:30	7:06:00		Run ship comp. half Gen. fail, 5:11 No. 6
13	AC 10					120	63 15			7:04:30	7:06:00		Alt. 42° (222°)
14	AC 11					183	63 25			7:04:30	7:06:00		Same alt. as run 1. Sync. check 07:25:00
15	AC 12					240	62 35			7:04:30	7:06:00		222° azimuth
16	AC 13					57	62 03			7:04:30	7:06:00		
17	AC 14					57				7:04:30	7:06:00		precisely in middle of analog tape run out
18	AC 15					57				7:04:30	7:06:00		for 1/2 min (corrected) still 200.
19	AC 16					66				7:04:30	7:06:00		Range, 68 m, 45-47-48; Amplitude threshold
20	VAD	10		0 1/2cm .5						7:04:30	7:06:00		not changed.
21	AC 17	30		0 10cm 5		35	62 03			7:04:30	7:06:00		same alt. as run 1.
22	AC 18									7:04:30	7:06:00		Alt. 42° Corrected time code this run.
23	AC 19									7:04:30	7:06:00		Repeat of previous run (run 17)

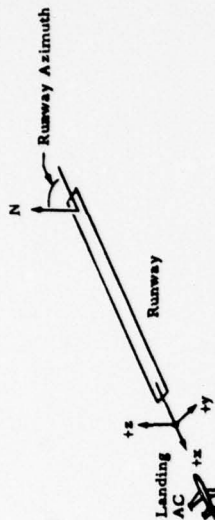
Location: Mountain View
 Date: 12/2/75 - 0-4
 Sheet 2 of 2
 Van X Position: _____
 Ref. Pt. _____
 Van Y Position: _____
 Ref. Pt. _____
 Center of RW _____

Van X Position:
Ref. Pt.

Van Y Position:
Ref. Pt.

Runway Asimuth:
Mirror Asimuth
for Switch

A-2



Appendix A (Continued)

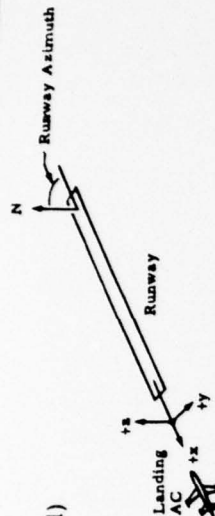
Location: Runway 01, 1st
 Date: 12/3/75 - 04/2
 Sheet 1 of 2

Van X Position: 200' N of RW
 Van Y Position: 200' N of RW

Runway Azimuth:
 Mirror Azimuth for Switch:

Run ID		Spectrum Analyzer				Scanner				Computer		Time		Estimated Wind Azimuth (from)	Comments
AC Type or VAD No.	B.W. (kHz)	Log Lin	Freq. Span (MHz)		Rate (insec)	Range			Elevation		Tape No.	No. Records	Start	Stop	
			Min.	f _c	Max.		Max.	Min.	Rate	Max.	Min.	Rate			
1	VAD	10	0	2cm	.5	1							6:29	6:35	alt. at 31.46, 31.76, 31.12, 31.24, 488 at 1 rev. alt.
2	AC 23	30	0	1cm	5	1	140	35	3.5	63	10	.2	6:55:46	6:57:03	PRECISE 180. not updated for run 3 (AC run 24)
3	AC 24												6:57:04	7:01:12	
4	AC 25												7:03:30	7:06:30	
5	AC 26												7:07:47	7:10:04	
6	AC 27									45	17		7:12:33	7:14:41	
7	AC 28									40	17		7:16:50	7:18:58	
8	AC 29												7:21:23	7:23:37	
9	AC 30									45	17		7:25:17	7:27:18	
10	VAD	10	0	2cm	.5								7:31	7:37	alt. same as run 1.
11	AC 31	30	0	2cm	5		140	35	3.5	45	17	.2	7:50:49	7:58:30	plot came in at 33 ft. instead of 200.
12	AC 32												8:00:47	8:04:11	alt. same as run 1. not this run but
13	AC 33									55	30		8:06:09	8:09:36	to work at. before run started.
14	AC 34												8:11:12	8:17:06	Run AC 33: plot came in at 20 ft. alt.
15	AC 35												8:18:44	8:21:57	Met switch run no. in previous to 34 during run.
16	AC 36												8:26:47	8:27:45	Run AC 35: during run not this run.
17	AC 37												8:35:17	8:37:19	Run AC 36: last 300 feet during run 36. plug to maintain pulled out
18	AC 38												8:38:30	8:42:35	Retired at 8:42:30. Also, car time "work" and AV "work" not synchronous for run 36.
19	VAD	10	0	15cm	.5								8:34	8:46	alt. same as run 1.

Appendix A (Concluded)



Location: 12/5/55 - 1st
 Date: 12/5/55 - 1st
 Sheet 2 of 2

Van X Position: 200' N of RW
 Ref. Pt. 200' N of RW

Runway Azimuth:
 Mirror Azimuth for Switch:

Run ID	Spectrum Analyzer					Scanner					Computer		Time		Estimated Wind Azimuth (from)	Comments	
	AC Type or VAD	B.W. (kHz)	Log Lin	Freq. Span (MHz)	Rate (msec)	Max.	Min.	Rate	Max.	Min.	Elevation	Tape No.	No. Records	Start			Stop
20	AC 39	30	W	0	5	1	140	35	35	55	23			9:01:11	9:02:39	at 1000 ft	
21	AC 40													9:06:52	9:08:57		
22	AC 41													9:12:30	9:14:34		
23	AC 42													9:18:06	9:20:10		
24	AC 43						150	35						9:23:27	9:25:31		
25	AC 44						160	35						9:28:40	9:30:55		
26	AC 45													9:33:57	9:36:46		
27	AC 46						180	35						9:39:09	9:42:11		
28	VAD	10		0	200	.5								9:44	9:52		at 1000 ft. Same as run 1. (Sheet 1)
29	AC 47	30		0	800	5	140	35	35	63	23			10:10:53	10:13:11		1000 ft. Same as run 1. (Sheet 1)
30	AC 48						160	35						10:15:23	10:17:41		1000 ft. Same as run 1. (Sheet 1)
31	AC 49													10:20:16	10:22:34		1000 ft. Same as run 1. (Sheet 1)
32	AC 50						140	35						10:24:49	10:27:07		1000 ft. Same as run 1. (Sheet 1)
33	AC 51													10:29:31	10:31:49		1000 ft. Same as run 1. (Sheet 1)
34	AC 52													10:33:57	10:36:15		1000 ft. Same as run 1. (Sheet 1)
35	AC 53													10:37:50	10:40:50		1000 ft. Same as run 1. (Sheet 1)
36	AC 54													10:41:53	10:44:56		1000 ft. Same as run 1. (Sheet 1)
37	VAD	10		0	200	.5								10:49:00	10:51:15		1000 ft. Same as run 1. (Sheet 1)
NOTES: TIME CHECK & END OF SPOT 4																	
OUR TIME AV TIME																	
10:46:13 10:48:10																	

Range check at end of Spot 9
 TIME CHECK at end of Spot 9
 OUR TIME 10:40:13
 AU TIME 10:48:10
 Range check at end of runs O.K.

Appendix B
SAMPLE OUTPUT FROM VELOCITY AZIMUTH DISPLAY AND
VORTEX TRACKER PROGRAM FOR ROSAMOND FLYBY 25

Page B-2 indicates the relative intensity (INTENSITY) and V_{ms} (SPEED (ft/sec)) of the LDV signal as a function of time and space for one sweep between the minimum and maximum elevation-angle setting in the finger-scan mode. A list of the data sorted according to INTENSITY is given on page B-3 followed by the list of the values selected for determining the vortex location on page B-4. A "scatter plot" showing the location of the intensity points in units of ft and their relative magnitude (on a scale of A to 0) is given on page B-5 along with the selected center of the two correlation circles (labeled Z) and the centroid of the correlation circles (the vortex locations labeled P and S for port and starboard, respectively). On page B-6, the points used in determining the vortex location are listed. The data are printed out on pages B-7 through B-12 and B-13 through B-17 for two other sample scans during flyby 25. A summary of the port and starboard locations from each of the scans is given on pages B-18 through B-20. The vortex trajectories are displayed on the last two pages of Appendix B, including time versus lateral displacement of the vortices (page B-21) and time versus vertical location as a function of time (page B-22).

3.272 SEC.									
4.841 SEC.									
4.056 SEC.									
IP	TIME	RANGE	ANGLE	YP	DELTA TIME	C WIND	SPEED	IFREQ	INTENSITY
1	3.272	386.2	62.6	22.1	.784	.00	15.65	18	286
2	3.287	359.2	62.3	33.2	.769	.00	13.04	15	190
3	3.302	426.9	62.0	46.3	.754	.00	18.52	19	158
4	3.317	293.8	61.8	61.0	.740	.00	18.26	21	200
5	3.332	259.7	61.6	78.3	.725	.00	19.13	22	112
6	3.351	487.6	59.5	64.4	.605	.00	23.47	27	126
7	3.446	491.0	59.3	51.6	.590	.00	13.04	15	126
8	3.496	350.1	58.8	18.4	.560	.00	16.52	19	124
9	3.511	380.4	58.6	1.6	.545	.00	13.91	14	128
10	3.541	437.9	58.1	-31.6	.515	.00	27.82	32	124
11	3.795	319.1	53.9	12.0	.261	.00	20.87	24	126
12	3.810	341.7	53.6	-2.8	.247	.00	8.69	10	198
13	3.825	376.4	53.4	-24.6	.232	.00	16.52	19	158
14	3.855	432.6	52.9	-61.2	.202	.00	29.56	34	126
15	3.869	434.6	52.5	-64.4	.187	.00	35.65	41	124
16	3.884	418.5	52.3	-55.7	.172	.00	23.47	27	144
17	3.899	391.2	52.1	-40.1	.157	.00	28.95	31	166
18	3.914	360.5	51.8	-22.8	.142	.00	39.99	46	112
19	3.929	331.7	51.5	-8.4	.127	.00	35.65	41	126
20	3.944	310.2	51.4	6.3	.112	.00	10.43	12	126
21	3.959	274.4	51.2	27.9	.097	.00	15.65	18	120
22	3.974	440.0	51.0	46.8	.082	.00	16.52	19	128
23	4.079	262.2	49.1	28.3	.037	.00	46.95	54	184
24	4.094	292.1	48.9	8.0	.022	.00	46.08	53	220
25	4.108	322.0	48.6	-13.1	.052	.00	50.43	58	256
26	4.123	348.1	48.3	-31.6	.067	.00	42.60	49	256
27	4.138	375.3	48.1	-50.5	.082	.00	36.52	42	192
28	4.153	402.2	47.9	-69.5	.097	.00	30.43	35	280
29	4.168	434.0	47.7	-91.9	.112	.00	26.08	30	318
30	4.183	438.8	47.4	-97.2	.127	.00	13.04	15	320
31	4.198	425.6	47.2	-84.4	.142	.00	9.84	11	190
32	4.213	401.4	47.0	-73.9	.157	.00	9.56	11	192
33	4.228	371.4	46.7	-54.6	.172	.00	29.56	34	222
34	4.243	348.9	46.6	-39.9	.187	.00	7.82	9	320
35	4.258	308.0	46.1	-13.5	.202	.00	33.04	38	164
36	4.273	277.6	45.9	7.0	.217	.00	24.34	28	168
37	4.467	393.9	42.8	-89.2	.411	.00	17.39	20	158
38	4.482	420.7	42.6	-104.9	.426	.00	20.87	24	128
39	4.497	438.9	42.3	-124.5	.441	.00	16.52	19	174
40	4.512	427.5	42.0	-117.9	.456	.00	17.39	20	128
41	4.527	406.9	41.8	-103.5	.471	.00	16.52	19	192
42	4.781	384.1	37.6	-104.4	.725	.00	8.69	10	128
43	4.796	405.6	37.4	-125.5	.740	.00	8.69	10	118
44	4.811	437.7	37.2	-148.8	.754	.00	9.56	11	196
45	4.826	435.6	36.8	-148.9	.769	.00	8.69	10	190
46	4.841	414.7	36.6	-133.0	.784	.00	8.69	10	174

ORDER	VELOCITY	INTENSITY
1	25	30
2	23	34
3	24	29
4	26	28
5	18	1

6	27	25
7	15	26
8	19	33
9	35	24
10	28	4
11	14	44
12	33	27
13	10	32
14	17	41
15	29	2
16	36	31
17	6	45
18	16	23
19	11	39
20	38	46
21	5	36
22	4	17
23	37	35
24	40	3
25	3	13
26	8	37
27	13	12
28	22	16
29	39	9
30	41	22
31	1	38
32	21	40
33	9	42
34	2	6
35	7	7
36	30	11
37	20	14
38	31	19
39	32	20
40	44	8
41	12	10
42	42	15
43	43	21
44	45	43
45	46	5
46	34	18

	11	113	N1	N2	R2
30	29		2	2	30.15
30	28		3	3	1355.06
30	32		4	4	1405.40
30	41		5	5	2727.48
30	31		6	6	171.75
30	39		7	7	1492.69
30	17		8	8	3453.66
30	37		9	9	3134.18
30	16	10	10	10	1796.11
30	38	11	11	11	1633.05
30	40	12	12	12	1798.91
30	14	13	13	13	1782.36
30	15	14	14	14	1556.26

11	113	N1	N2	R2
24	23	2	2	897.96
24	36	3	3	425.12
24	35	4	4	463.56
24	12	5	5	3123.12
24	22	6	6	2803.32
24	6	7	7	3296.32
24	7	8	8	2819.10
24	11	9	9	1438.20
24	19	10	10	1772.64
24	20	11	11	499.09
24	21	12	12	440.48
AV = 2	JJJ = 24	YC =	15.2	ZC = 229.4

[illegible]

NPV#	4	KD=	244	RANGE#	293.44	ANGLE#	45.62	NSAMPL=	10	RANGE1=	294.59	RANGEM=	245.09
NPV#	5	KD=	254	RANGE#	351.49	ANGLE#	48.62	NSAMPL=	11	RANGE1=	347.77	RANGEM=	301.56
NPV#	6	KD=	258	RANGE#	407.88	ANGLE#	49.05	NSAMPL=	13	RANGE1=	403.87	RANGEM=	434.71
NPV#	7	KD=	259	RANGE#	435.10	ANGLE#	49.93	NSAMPL=	13	RANGE1=	434.71	RANGEM=	437.66
NPV#	8	KD=	260	RANGE#	435.54	ANGLE#	49.62	NSAMPL=	12	RANGE1=	437.66	RANGEM=	419.95
NPV#	9	KD=	261	RANGE#	416.27	ANGLE#	49.83	NSAMPL=	14	RANGE1=	419.95	RANGEM=	393.70
NPV#	10	KD=	244	RANGE#	332.55	ANGLE#	50.62	NSAMPL=	12	RANGE1=	336.29	RANGEM=	305.12
NPV#	11	KD=	275	RANGE#	291.67	ANGLE#	53.30	NSAMPL=	24	RANGE1=	283.14	RANGEM=	315.94
NPV#	12	KD=	277	RANGE#	345.14	ANGLE#	53.82	NSAMPL=	10	RANGE1=	341.86	RANGEM=	374.67
NPV#	13	KD=	278	RANGE#	381.86	ANGLE#	54.06	NSAMPL=	30	RANGE1=	374.67	RANGEM=	393.62
NPV#	14	KD=	279	RANGE#	408.18	ANGLE#	54.33	NSAMPL=	32	RANGE1=	398.62	RANGEM=	428.48
NPV#	15	KD=	280	RANGE#	438.03	ANGLE#	54.73	NSAMPL=	32	RANGE1=	428.48	RANGEM=	428.48
NPV#	16	KD=	1	RANGE#	435.45	ANGLE#	54.87	NSAMPL=	35	RANGE1=	440.62	RANGEM=	425.85
NPV#	17	KD=	2	RANGE#	416.75	ANGLE#	55.07	NSAMPL=	37	RANGE1=	425.85	RANGEM=	401.25
NPV#	18	KD=	3	RANGE#	390.35	ANGLE#	55.28	NSAMPL=	41	RANGE1=	401.25	RANGEM=	374.67
NPV#	19	KD=	4	RANGE#	360.89	ANGLE#	55.57	NSAMPL=	42	RANGE1=	374.67	RANGEM=	341.86
NPV#	20	KD=	5	RANGE#	329.96	ANGLE#	55.88	NSAMPL=	39	RANGE1=	341.86	RANGEM=	311.35
NPV#	21	KD=	6	RANGE#	297.67	ANGLE#	56.09	NSAMPL=	43	RANGE1=	311.35	RANGEM=	279.53
NPV#	22	KD=	7	RANGE#	272.57	ANGLE#	56.24	NSAMPL=	21	RANGE1=	279.53	RANGEM=	246.39
NPV#	23	KD=	17	RANGE#	297.93	ANGLE#	58.54	NSAMPL=	35	RANGE1=	274.90	RANGEM=	308.40
NPV#	24	KD=	18	RANGE#	320.95	ANGLE#	58.89	NSAMPL=	45	RANGE1=	308.40	RANGEM=	336.29
NPV#	25	KD=	19	RANGE#	381.24	ANGLE#	59.09	NSAMPL=	47	RANGE1=	336.29	RANGEM=	368.11
NPV#	26	KD=	20	RANGE#	375.79	ANGLE#	59.26	NSAMPL=	30	RANGE1=	368.11	RANGEM=	393.70
NPV#	27	KD=	21	RANGE#	405.09	ANGLE#	59.98	NSAMPL=	39	RANGE1=	393.70	RANGEM=	422.90
NPV#	28	KD=	22	RANGE#	430.70	ANGLE#	59.78	NSAMPL=	44	RANGE1=	422.90	RANGEM=	440.62
NPV#	29	KD=	23	RANGE#	436.37	ANGLE#	60.07	NSAMPL=	35	RANGE1=	440.62	RANGEM=	428.48
NPV#	30	KD=	24	RANGE#	419.37	ANGLE#	60.27	NSAMPL=	37	RANGE1=	428.48	RANGEM=	403.87
NPV#	31	KD=	25	RANGE#	395.17	ANGLE#	60.48	NSAMPL=	39	RANGE1=	403.87	RANGEM=	381.56
NPV#	32	KD=	26	RANGE#	370.74	ANGLE#	60.74	NSAMPL=	34	RANGE1=	381.56	RANGEM=	349.74
NPV#	33	KD=	27	RANGE#	339.06	ANGLE#	61.07	NSAMPL=	35	RANGE1=	349.74	RANGEM=	319.23
NPV#	34	KD=	28	RANGE#	305.17	ANGLE#	61.28	NSAMPL=	42	RANGE1=	319.23	RANGEM=	285.76
NPV#	35	KD=	29	RANGE#	273.09	ANGLE#	61.48	NSAMPL=	39	RANGE1=	285.76	RANGEM=	263.28

54	25.069	491.0	42.3	-5.6	398.0	-.754	.00	17.78	17	158
55	25.099	491.7	42.8	16.4	364.1	-.784	.00	18.26	21	190
56	25.114	376.6	42.8	27.6	341.8	-.799	.00	20.87	24	126
ORDER	VELOCITY	INTENSITY								
1	11	26								
2	13	37								
3	15	11								
4	18	12								
5	14	49								
6	9	13								
7	8	23								
8	20	24								
9	23	27								
10	10	41								
11	16	29								
12	24	31								
13	25	7								
14	7	22								
15	26	40								
16	18	21								
17	6	25								
18	12	30								
19	27	39								
20	31	50								
21	34	53								
22	28	55								
23	56	9								
24	30	46								
25	49	36								
26	29	28								
27	47	47								
28	5	10								
29	32	54								
30	33	15								
31	50	14								
32	55	51								
33	37	1								
34	22	2								
35	38	20								
36	51	35								
37	39	3								
38	52	8								
39	41	14								
40	44	17								
41	53	17								
42	54	38								
43	36	5								
44	40	6								
45	43	18								
46	4	32								
47	4	33								
48	17	43								
49	46	44								
50	21	48								
51	45	52								
52	48	56								

11	113	1	14
20	37	4	2
20	11	4	3
20	12	4	4
20	13	5	5
20	23	6	6
20	24	7	7
20	27	8	8
20	41	9	9
20	44	10	10
20	40	11	11
20	45	12	12
20	39	13	13
20	9	14	14
20	28	15	15
20	10	16	16
20	14	17	17
20	38	18	18
20	32	19	19
20	36	20	20

323.2

11	11	11
31	31	30
46	46	46
31	31	36
31	31	47
31	31	35
17	17	17
19	19	19
5	5	5
6	6	6
16	16	16
32	32	32
33	33	33
44	44	44
48	48	48
45	45	45
39	39	39
31	31	31
2	2	2
44	44	44

Yr	Yr	Yr
1	2	3
4	5	6
7	8	9
10	11	12
13	14	15
16	17	18
19	20	21
22	23	24
25	26	27
28	29	30
31	32	33
34	35	36
37	38	39
40	41	42
43	44	45
46	47	48
49	50	51
52	53	54
55	56	57
58	59	60
61	62	63
64	65	66
67	68	69
70	71	72
73	74	75
76	77	78
79	80	81
82	83	84
85	86	87
88	89	90
91	92	93
94	95	96
97	98	99
100	101	102
103	104	105
106	107	108
109	110	111
112	113	114
115	116	117
118	119	120
121	122	123
124	125	126
127	128	129
130	131	132
133	134	135
136	137	138
139	140	141
142	143	144
145	146	147
148	149	150
151	152	153
154	155	156
157	158	159
160	161	162
163	164	165
166	167	168
169	170	171
172	173	174
175	176	177
178	179	180
181	182	183
184	185	186
187	188	189
190	191	192
193	194	195
196	197	198
199	200	201
202	203	204
205	206	207
208	209	210
211	212	213
214	215	216
217	218	219
220	221	222
223	224	225
226	227	228
229	230	231
232	233	234
235	236	237
238	239	240
241	242	243
244	245	246
247	248	249
250	251	252
253	254	255
256	257	258
259	260	261
262	263	264
265	266	267
268	269	270
271	272	273
274	275	276
277	278	279
280	281	282
283	284	285
286	287	288
289	290	291
292	293	294
295	296	297
298	299	300
301	302	303
304	305	306
307	308	309
310	311	312
313	314	315
316	317	318
319	320	321
322	323	324
325	326	327
328	329	330
331	332	333
334	335	336
337	338	339
340	341	342
343	344	345
346	347	348
349	350	351
352	353	354
355	356	357
358	359	360
361	362	363
364	365	366
367</		

H. 527 • 37

NPV# 4	KU= 479	RANGE#	244.61	ANGLE#	61.76	NSAMPL= 20	RANGE1=	256.56	RANGE#	221.78
NPV# 5	KD= 280	RANGE#	214.83	ANGLE#	61.56	NSAMPL= 20	RANGE1=	221.78	RANGE#	221.78
NPV# 6	KD= 5	RANGE#	209.80	ANGLE#	60.77	NSAMPL= 13	RANGE1=	205.71	RANGE#	237.20
NPV# 7	KU= 6	RANGE#	245.00	ANGLE#	60.10	NSAMPL= 24	RANGE1=	237.20	RANGE#	269.69
NPV# 8	KD= 7	RANGE#	278.56	ANGLE#	59.73	NSAMPL= 33	RANGE1=	269.69	RANGE#	298.59
NPV# 9	KU= 8	RANGE#	305.63	ANGLE#	59.54	NSAMPL= 29	RANGE1=	296.59	RANGE#	327.76
NPV# 10	KU= 9	RANGE#	335.79	ANGLE#	59.34	NSAMPL= 31	RANGE1=	327.76	RANGE#	353.67
NPV# 11	KD= 10	RANGE#	361.82	ANGLE#	59.09	NSAMPL= 27	RANGE1=	353.67	RANGE#	383.86
NPV# 12	KD= 11	RANGE#	391.95	ANGLE#	58.74	NSAMPL= 29	RANGE1=	383.86	RANGE#	411.75
NPV# 13	KD= 12	RANGE#	420.04	ANGLE#	58.54	NSAMPL= 32	RANGE1=	411.75	RANGE#	437.66
NPV# 14	KU= 15	RANGE#	403.30	ANGLE#	57.73	NSAMPL= 33	RANGE1=	411.75	RANGE#	464.15
NPV# 15	KD= 16	RANGE#	379.45	ANGLE#	57.53	NSAMPL= 34	RANGE1=	386.15	RANGE#	490.61
NPV# 16	KD= 17	RANGE#	347.46	ANGLE#	57.33	NSAMPL= 34	RANGE1=	357.61	RANGE#	517.16
NPV# 17	KD= 18	RANGE#	318.99	ANGLE#	57.15	NSAMPL= 27	RANGE1=	327.76	RANGE#	543.67
NPV# 18	KD= 19	RANGE#	283.56	ANGLE#	56.86	NSAMPL= 35	RANGE1=	295.26	RANGE#	569.18
NPV# 19	KD= 20	RANGE#	250.89	ANGLE#	56.54	NSAMPL= 32	RANGE1=	261.81	RANGE#	594.69
NPV# 20	KD= 21	RANGE#	217.85	ANGLE#	56.34	NSAMPL= 30	RANGE1=	227.69	RANGE#	620.19
NPV# 21	KU= 26	RANGE#	207.05	ANGLE#	55.15	NSAMPL= 24	RANGE1=	199.80	RANGE#	645.69
NPV# 22	KD= 27	RANGE#	240.91	ANGLE#	54.87	NSAMPL= 32	RANGE1=	229.99	RANGE#	671.19
NPV# 23	KD= 28	RANGE#	289.99	ANGLE#	54.55	NSAMPL= 23	RANGE1=	264.11	RANGE#	696.70
NPV# 24	KD= 30	RANGE#	300.20	ANGLE#	54.34	NSAMPL= 32	RANGE1=	289.70	RANGE#	722.21
NPV# 25	KD= 31	RANGE#	330.09	ANGLE#	54.14	NSAMPL= 30	RANGE1=	322.51	RANGE#	747.77
NPV# 26	KD= 32	RANGE#	358.24	ANGLE#	53.88	NSAMPL= 31	RANGE1=	347.77	RANGE#	773.28
NPV# 27	KD= 33	RANGE#	388.25	ANGLE#	53.54	NSAMPL= 30	RANGE1=	381.56	RANGE#	798.79
NPV# 28	KD= 34	RANGE#	414.71	ANGLE#	53.35	NSAMPL= 25	RANGE1=	403.87	RANGE#	824.30
NPV# 29	KD= 35	RANGE#	409.97	ANGLE#	52.69	NSAMPL= 28	RANGE1=	417.34	RANGE#	849.81
NPV# 30	KD= 37	RANGE#	384.00	ANGLE#	52.34	NSAMPL= 28	RANGE1=	391.08	RANGE#	875.32
NPV# 31	KD= 38	RANGE#	357.71	ANGLE#	52.15	NSAMPL= 26	RANGE1=	365.81	RANGE#	900.83
NPV# 32	KD= 39	RANGE#	326.40	ANGLE#	51.95	NSAMPL= 24	RANGE1=	334.65	RANGE#	926.34
NPV# 33	KD= 40	RANGE#	293.72	ANGLE#	51.70	NSAMPL= 26	RANGE1=	302.17	RANGE#	951.85
NPV# 34	KD= 41	RANGE#	260.98	ANGLE#	51.35	NSAMPL= 26	RANGE1=	269.69	RANGE#	977.36
NPV# 35	KD= 42	RANGE#	228.27	ANGLE#	51.15	NSAMPL= 24	RANGE1=	236.22	RANGE#	1002.87
NPV# 36	KD= 43	RANGE#	229.23	ANGLE#	49.73	NSAMPL= 17	RANGE1=	223.43	RANGE#	1028.38
NPV# 37	KD= 49	RANGE#	263.43	ANGLE#	49.35	NSAMPL= 23	RANGE1=	257.55	RANGE#	1053.89
NPV# 38	KD= 50	RANGE#	290.68	ANGLE#	49.15	NSAMPL= 23	RANGE1=	283.14	RANGE#	1079.40
NPV# 39	KD= 51	RANGE#	321.53	ANGLE#	48.95	NSAMPL= 23	RANGE1=	315.94	RANGE#	1104.91
NPV# 40	KD= 52	RANGE#	346.42	ANGLE#	48.76	NSAMPL= 18	RANGE1=	340.22	RANGE#	1130.42
NPV# 41	KD= 53	RANGE#	379.46	ANGLE#	48.52	NSAMPL= 20	RANGE1=	374.67	RANGE#	1155.93
NPV# 42	KD= 54	RANGE#	406.17	ANGLE#	48.15	NSAMPL= 23	RANGE1=	398.62	RANGE#	1181.44
NPV# 43	KD= 55	RANGE#	392.37	ANGLE#	47.17	NSAMPL= 17	RANGE1=	374.67	RANGE#	1206.95
NPV# 44	KD= 59	RANGE#	369.50	ANGLE#	46.77	NSAMPL= 15	RANGE1=	340.22	RANGE#	1232.46
NPV# 45	KD= 60	RANGE#	334.73	ANGLE#	46.76	NSAMPL= 18	RANGE1=	309.71	RANGE#	1257.97
NPV# 46	KD= 61	RANGE#	304.25	ANGLE#	46.54	NSAMPL= 16	RANGE1=	275.59	RANGE#	1283.48
NPV# 47	KD= 62	RANGE#	270.77	ANGLE#	46.17	NSAMPL= 15	RANGE1=	243.44	RANGE#	1308.99
NPV# 48	KD= 63	RANGE#	238.08	ANGLE#	45.97	NSAMPL= 16	RANGE1=	209.97	RANGE#	1334.50
NPV# 49	KD= 64	RANGE#	204.57	ANGLE#	45.77	NSAMPL= 16	RANGE1=	185.04	RANGE#	1360.01
NPV# 50	KD= 65	RANGE#	191.47	ANGLE#	44.76	NSAMPL= 20	RANGE1=	151.31	RANGE#	1385.52
NPV# 51	KD= 69	RANGE#	223.48	ANGLE#	44.57	NSAMPL= 14	RANGE1=	117.81	RANGE#	1411.03
NPV# 52	KD= 70	RANGE#	258.67	ANGLE#	44.32	NSAMPL= 19	RANGE1=	84.31	RANGE#	1436.54
NPV# 53	KD= 71	RANGE#	284.06	ANGLE#	43.97	NSAMPL= 15	RANGE1=	50.81	RANGE#	1462.05
NPV# 54	KD= 72	RANGE#	315.03	ANGLE#	43.76	NSAMPL= 20	RANGE1=	17.31	RANGE#	1487.56
NPV# 55	KD= 73	RANGE#	341.40	ANGLE#	43.57	NSAMPL= 15	RANGE1=	17.31	RANGE#	1513.07
NPV# 56	KD= 74	RANGE#	375.07	ANGLE#	43.32	NSAMPL= 20	RANGE1=	17.31	RANGE#	1538.58
NPV# 57	KD= 75	RANGE#	399.81	ANGLE#	42.96	NSAMPL= 19	RANGE1=	17.31	RANGE#	1564.09
NPV# 58	KD= 76	RANGE#	428.61	ANGLE#	42.76	NSAMPL= 20	RANGE1=	17.31	RANGE#	1589.60
NPV# 59	KD= 77	RANGE#	457.41	ANGLE#	42.56	NSAMPL= 22	RANGE1=	17.31	RANGE#	1615.11
NPV# 60	KD= 78	RANGE#	486.21	ANGLE#	42.36	NSAMPL= 22	RANGE1=	17.31	RANGE#	1640.62

PHV= 61	KD= 79	RANGE=	420.44	ANGLE=	42.36	NSAMPL= 22	RANGEI=	425.85	RANGE=	401.25
PHV= 62	KD= 80	RANGE=	395.97	ANGLE=	42.10	NSAMPL= 24	RANGEI=	401.25	RANGE=	379.27
PHV= 63	KD= 81	RANGE=	372.97	ANGLE=	41.76	NSAMPL= 20	RANGEI=	379.27	RANGE=	347.77
PHV= 64	KD= 82	RANGE=	342.03	ANGLE=	41.56	NSAMPL= 19	RANGEI=	347.77	RANGE=	317.59
PHV= 65	KD= 83	RANGE=	311.38	ANGLE=	41.36	NSAMPL= 18	RANGEI=	317.59	RANGE=	283.14
PHV= 66	KD= 84	RANGE=	276.57	ANGLE=	41.12	NSAMPL= 20	RANGEI=	283.14	RANGE=	250.33
PHV= 67	KD= 85	RANGE=	243.91	ANGLE=	40.76	NSAMPL= 19	RANGEI=	250.33	RANGE=	216.54
PHV= 68	KD= 86	RANGE=	212.85	ANGLE=	40.58	NSAMPL= 11	RANGEI=	216.54	RANGE=	183.07
PHV= 69	KD= 87	RANGE=	184.60	ANGLE=	39.08	NSAMPL= 30	RANGEI=	183.07	RANGE=	149.61
PHV= 70	KD= 88	RANGE=	152.79	ANGLE=	38.74	NSAMPL= 29	RANGEI=	149.61	RANGE=	116.11
PHV= 71	KD= 89	RANGE=	121.42	ANGLE=	38.54	NSAMPL= 30	RANGEI=	116.11	RANGE=	82.61
PHV= 72	KD= 90	RANGE=	90.53	ANGLE=	38.33	NSAMPL= 33	RANGEI=	82.61	RANGE=	49.11
PHV= 73	KD= 91	RANGE=	60.05	ANGLE=	38.13	NSAMPL= 35	RANGEI=	49.11	RANGE=	15.61
PHV= 74	KD= 92	RANGE=	30.38	ANGLE=	37.85	NSAMPL= 38	RANGEI=	15.61	RANGE=	0.01
PHV= 75	KD= 93	RANGE=	0.25	ANGLE=	37.55	NSAMPL= 36	RANGEI=	0.01	RANGE=	0.01
PHV= 76	KD= 94	RANGE=	0.25	ANGLE=	37.33	NSAMPL= 26	RANGEI=	0.01	RANGE=	0.01
PHV= 77	KD= 95	RANGE=	0.25	ANGLE=	37.11	NSAMPL= 46	RANGEI=	0.01	RANGE=	0.01
PHV= 78	KD= 96	RANGE=	0.25	ANGLE=	36.85	NSAMPL= 37	RANGEI=	0.01	RANGE=	0.01
PHV= 79	KD= 97	RANGE=	0.25	ANGLE=	36.52	NSAMPL= 42	RANGEI=	0.01	RANGE=	0.01
PHV= 80	KD= 98	RANGE=	0.25	ANGLE=	36.37	NSAMPL= 14	RANGEI=	0.01	RANGE=	0.01
PHV= 81	KD= 99	RANGE=	0.25	ANGLE=	35.97	NSAMPL= 33	RANGEI=	0.01	RANGE=	0.01
PHV= 82	KD= 100	RANGE=	0.25	ANGLE=	35.11	NSAMPL= 45	RANGEI=	0.01	RANGE=	0.01
PHV= 83	KD= 101	RANGE=	0.25	ANGLE=	34.98	NSAMPL= 10	RANGEI=	0.01	RANGE=	0.01
PHV= 84	KD= 102	RANGE=	0.25	ANGLE=	33.98	NSAMPL= 43	RANGEI=	0.01	RANGE=	0.01
PHV= 85	KD= 103	RANGE=	0.25	ANGLE=	33.63	NSAMPL= 44	RANGEI=	0.01	RANGE=	0.01
PHV= 86	KD= 104	RANGE=	0.25	ANGLE=	33.31	NSAMPL= 39	RANGEI=	0.01	RANGE=	0.01
PHV= 87	KD= 105	RANGE=	0.25	ANGLE=	33.12	NSAMPL= 35	RANGEI=	0.01	RANGE=	0.01
PHV= 88	KD= 106	RANGE=	0.25	ANGLE=	32.93	NSAMPL= 21	RANGEI=	0.01	RANGE=	0.01
PHV= 89	KD= 107	RANGE=	0.25	ANGLE=	32.72	NSAMPL= 32	RANGEI=	0.01	RANGE=	0.01
PHV= 90	KD= 108	RANGE=	0.25	ANGLE=	32.54	NSAMPL= 33	RANGEI=	0.01	RANGE=	0.01
PHV= 91	KD= 109	RANGE=	0.25	ANGLE=	32.13	NSAMPL= 32	RANGEI=	0.01	RANGE=	0.01
PHV= 92	KD= 110	RANGE=	0.25	ANGLE=	31.94	NSAMPL= 21	RANGEI=	0.01	RANGE=	0.01
PHV= 93	KD= 111	RANGE=	0.25	ANGLE=	31.72	NSAMPL= 17	RANGEI=	0.01	RANGE=	0.01
PHV= 94	KD= 112	RANGE=	0.25	ANGLE=	31.17	NSAMPL= 12	RANGEI=	0.01	RANGE=	0.01
PHV= 95	KD= 113	RANGE=	0.25	ANGLE=	30.78	NSAMPL= 13	RANGEI=	0.01	RANGE=	0.01
PHV= 96	KD= 114	RANGE=	0.25	ANGLE=	28.17	NSAMPL= 14	RANGEI=	0.01	RANGE=	0.01
PHV= 97	KD= 115	RANGE=	0.25	ANGLE=	27.17	NSAMPL= 16	RANGEI=	0.01	RANGE=	0.01
PHV= 98	KD= 116	RANGE=	0.25	ANGLE=	26.97	NSAMPL= 15	RANGEI=	0.01	RANGE=	0.01
PHV= 99	KD= 117	RANGE=	0.25	ANGLE=	26.77	NSAMPL= 15	RANGEI=	0.01	RANGE=	0.01
PHV= 100	KD= 118	RANGE=	0.25	ANGLE=	26.57	NSAMPL= 11	RANGEI=	0.01	RANGE=	0.01
PHV= 101	KD= 119	RANGE=	0.25	ANGLE=	26.36	NSAMPL= 10	RANGEI=	0.01	RANGE=	0.01
PHV= 102	KD= 120	RANGE=	0.25	ANGLE=	25.98	NSAMPL= 12	RANGEI=	0.01	RANGE=	0.01

[illegible]

B-14

42	21	34
43	22	57
44	23	34
45	24	59
46	25	4
47	26	23
48	27	38
49	28	45
50	29	46
51	31	50
52	47	52
53	48	55
54	53	56
55	60	62
56	30	65
57	34	30
58	37	49
59	43	58
60	44	60
61	45	63
62	46	11
63	55	18
64	57	51
65	65	12
66	66	37
67	67	66

11	113	N1	N2	N2
44	28	2	2	528.17
44	6	3	3	3443.30
44	20	4	4	2028.29
44	32	5	5	539.24
44	19	6	6	1408.77
44	31	7	7	456.58
44	43	8	8	1009.41
44	15	9	9	2470.52
44	47	10	10	1555.29
44	27	11	11	1216.85
44	33	12	12	2144.54
44	29	13	13	2129.44
44	16	14	14	2044.82
44	45	15	15	498.80
44	46	16	16	162.32
44	56	17	17	2007.23
44	30	18	18	2380.44
44	18	19	19	2824.32
44	44	YC	YC	46.4
KV = 1	JJJ = 44			ZC = 198.7

11	113	N1	N2	N2
61	54	2	2	1190.72
61	64	3	3	1888.51
61	53	4	4	1807.21
61	57	5	5	2106.69
61	59	6	6	1481.17
61	50	7	7	1952.76

WASAWANO DRY LAKE DAY 2	W797	12/03/75	WOSAWANO LAKE	MO370.	RUN NO.
9.000-0.02
3.600-0.02
3.200-0.02
2.800-0.02
2.400-0.02
2.000-0.02
1.600-0.02
1.200-0.02
0.800-0.02
0.400-0.02

NPHV= 4	KD= 219	RANGE=	538.75	ANGLE=	48.56	NSAMPL= 12	RANGE1=	411.75	RANGE=	1470.14
NPHV= 5	KD= 224	RANGE=	337.17	ANGLE=	40.22	NSAMPL= 10	RANGE1=	340.22	RANGE=	309.71
NPHV= 6	KD= 227	RANGE=	305.62	ANGLE=	40.42	NSAMPL= 12	RANGE1=	309.71	RANGE=	278.89
NPHV= 7	KD= 228	RANGE=	271.84	ANGLE=	40.42	NSAMPL= 11	RANGE1=	275.59	RANGE=	241.97
NPHV= 8	KD= 229	RANGE=	237.20	ANGLE=	40.45	NSAMPL= 13	RANGE1=	241.47	RANGE=	208.44
NPHV= 9	KD= 230	RANGE=	204.94	ANGLE=	41.22	NSAMPL= 11	RANGE1=	208.44	RANGE=	175.87
NPHV= 10	KD= 235	RANGE=	222.18	ANGLE=	42.12	NSAMPL= 10	RANGE1=	218.83	RANGE=	282.30
NPHV= 11	KD= 234	RANGE=	255.02	ANGLE=	42.62	NSAMPL= 10	RANGE1=	252.30	RANGE=	279.63
NPHV= 12	KD= 237	RANGE=	283.21	ANGLE=	42.80	NSAMPL= 11	RANGE1=	279.53	RANGE=	312.99
NPHV= 13	KD= 238	RANGE=	315.52	ANGLE=	42.78	NSAMPL= 10	RANGE1=	312.99	RANGE=	338.25

NOSAMOND DRY LAKE DAY 2 B747 12/03/75
 TIME IS 7: 3:50
 NOSAMOND LAKE HD270. RUN NO. 4

STARBOARD VORTEX

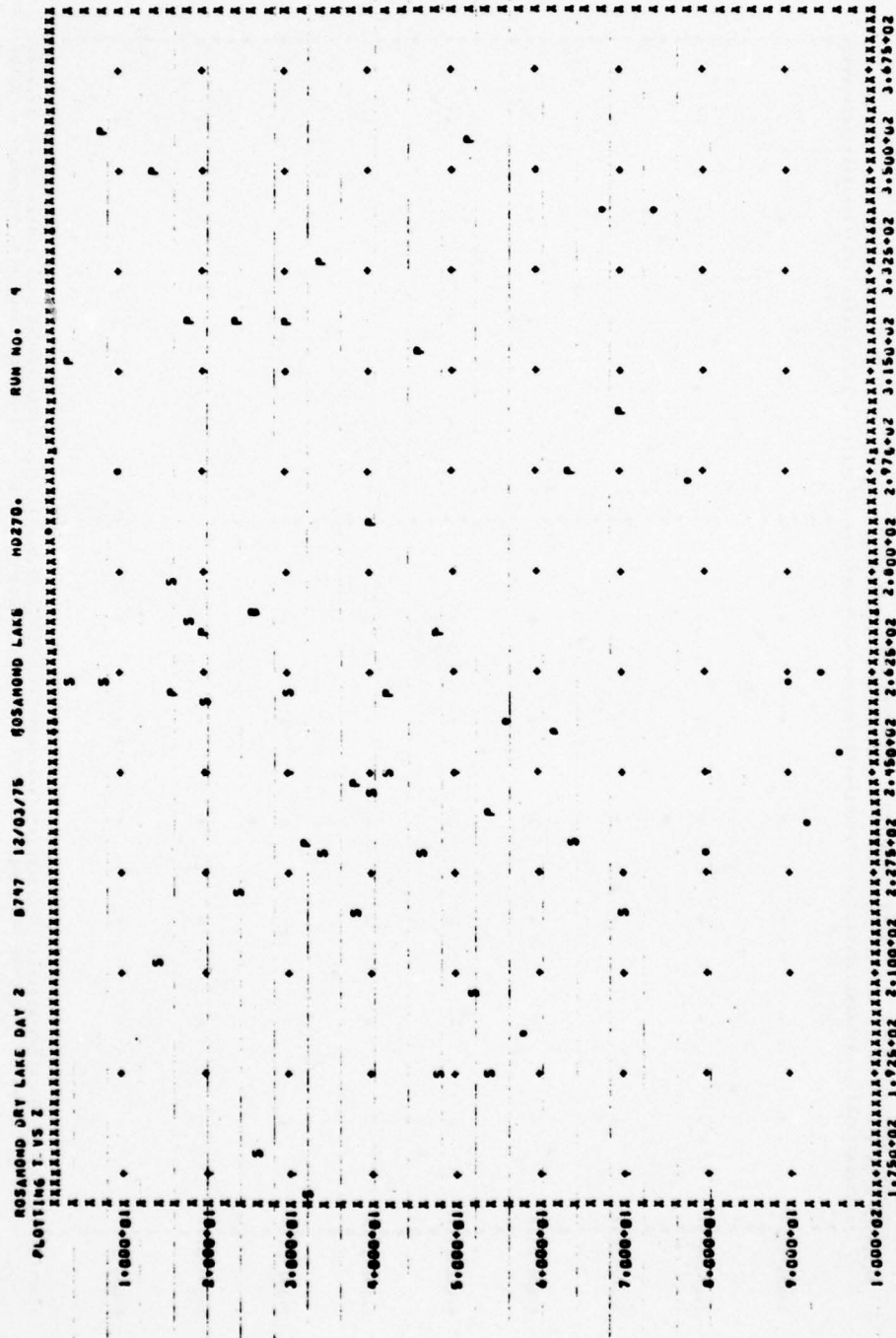
TIME	Z	Y
4.05621	260.652	44.1498
8.27676	260.229	38.5139
13.85668	212.365	47.6868
15.5002	278.173	6.46237
18.7123	271.046	36.3668
20.6620	257.905	26.2682
24.3148	224.413	55.0379
26.2645	177.873	46.3209
29.8949	259.492	26.9209
31.6056	171.146	59.0845
34.7579	230.324	46.7477
37.0064	220.007	5.36603
40.5472	241.469	61.3459
42.5118	244.896	40.6397
45.4176	230.303	52.5408
47.4121	192.493	60.0888
51.1471	205.975	83.2493
53.0743	192.320	58.7777
63.6145	233.186	37.4797
69.2095	220.445	35.1234

PORT VORTEX

TIME	Z	Y
4.05621	316.589	-81.6382
8.27676	357.333	-29.5650
13.8568	349.730	-34.7920
15.5002	258.296	-114.384
18.7123	323.249	-69.0965
20.6620	269.113	-123.139
24.3148	323.246	-60.4487
26.2645	273.360	14.0868
29.8949	323.499	-74.6053
31.6056	232.370	-37.9057
34.7579	334.106	-23.4391
37.0064	243.742	-125.949
40.5472	289.022	-84.2635
42.5118	258.368	-105.767
45.4176	318.621	-45.9242
47.4121	269.746	-97.0168
51.1471	354.548	-20.3668
53.0743	237.969	-126.092
63.6145	297.511	-90.3922
69.2095	308.295	-82.9007

UNKNOWN TYPE OF VORTEX

TIME	Z	Y
2.89089	286.775	31.5946
9.94257	297.216	-87.3446
56.5852	253.098	45.4470
58.5648	198.678	46.4100
61.9412	252.638	67.2202
67.1926	342.761	-433675
73.0118	342.916	-59.9073
77.9868	296.564	-91.7344
80.8926	230.220	-141.526
89.0200	261.570	-43.6382
91.4552	235.365	-136.489
94.5179	262.498	-29.0438
96.8784	248.933	-124.571



Appendix C

SAMPLE OUTPUT FROM NASA-MSFC LASER DOPPLER VELOCIMETER DATA PROCESSING ROUTINES FOR ROSAMOND FLYBY 47

Results from the Rosamond high-speed data are given on page C-2 including a printout of the relative intensity of the LDV signal (IPEAK) and the frequency (or velocity) of the flow field including V_{ms} and V_{pk} in units of meters per second (VMAX and VPEAK, respectively). The sweep count from the start of the flyby is shown by the column labeled SCAN while the lateral and vertical location and range and elevation angle of the focal volume are given by X(m), Y(m), R(m), and T(deg), respectively. The time at which the LDV signal was sampled is contained in the frame count (1 FRAME = 1/500 sec).

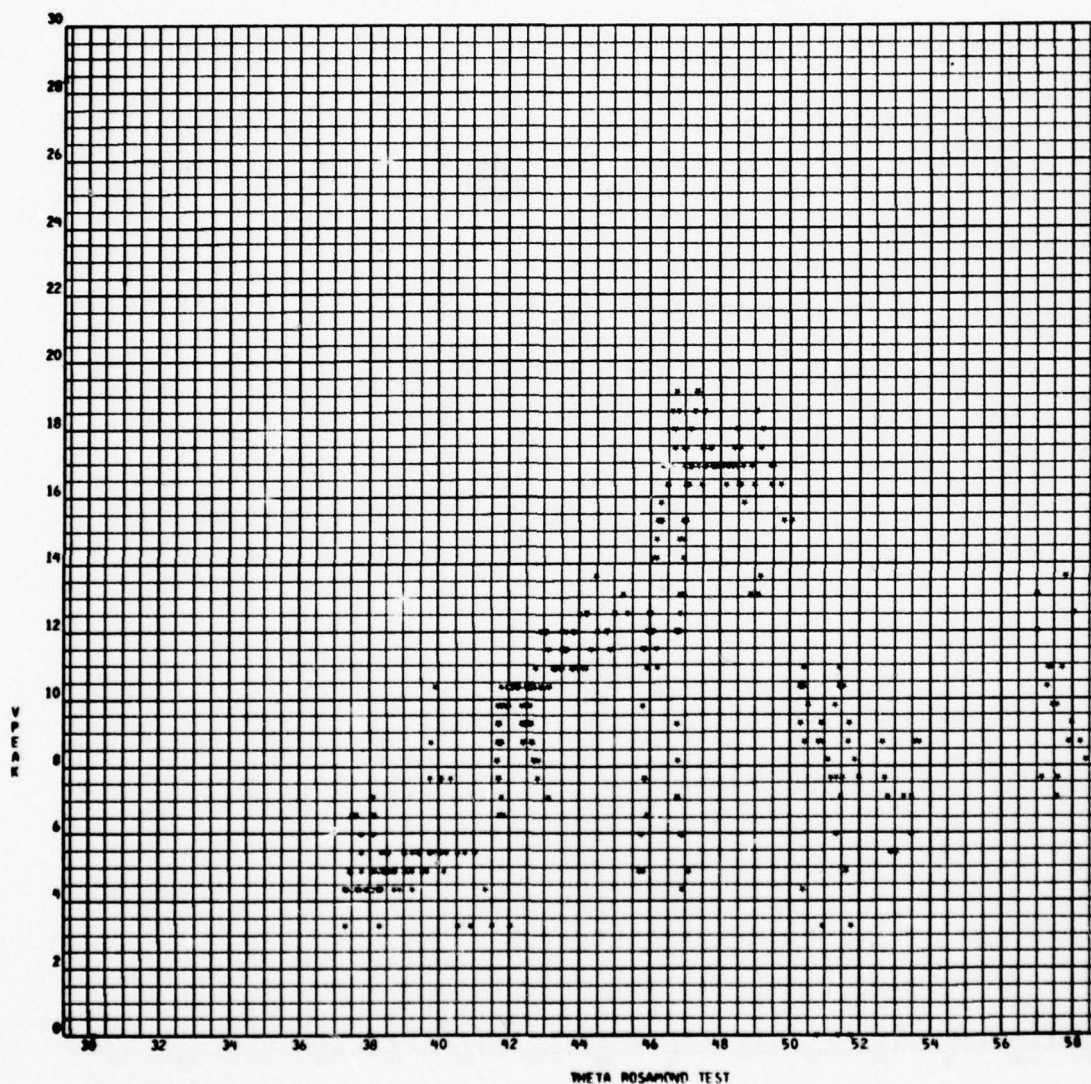
From the array of LDV sample points illustrated on page C-2, plots of VPEAK versus the scan elevation angle in degrees, THETA, are generated as illustrated on pages C-3 through C-6. Note that the characteristic double peak signature of the wake vortex is evident in the sample plots.

Applying the " I_{pk} " algorithm (p. 4-7 of Ref. 7) to the threshold LDV spectrum illustrated above, the vortex location is determined. The vortex trajectory for flyby 47 as computed from the high speed data is shown on pages C-7 through C-9. On page C-7 the vertical and lateral motion of the vortices is given as a function of time, while page C-8 shows the altitude versus lateral position of the wake vortex. Page C-9 lists the vortex locations. For additional information regarding the vortex location, criteria, and coefficients used in the " I_{pk} " algorithm and shown in the plots, refer to Ref. 7.

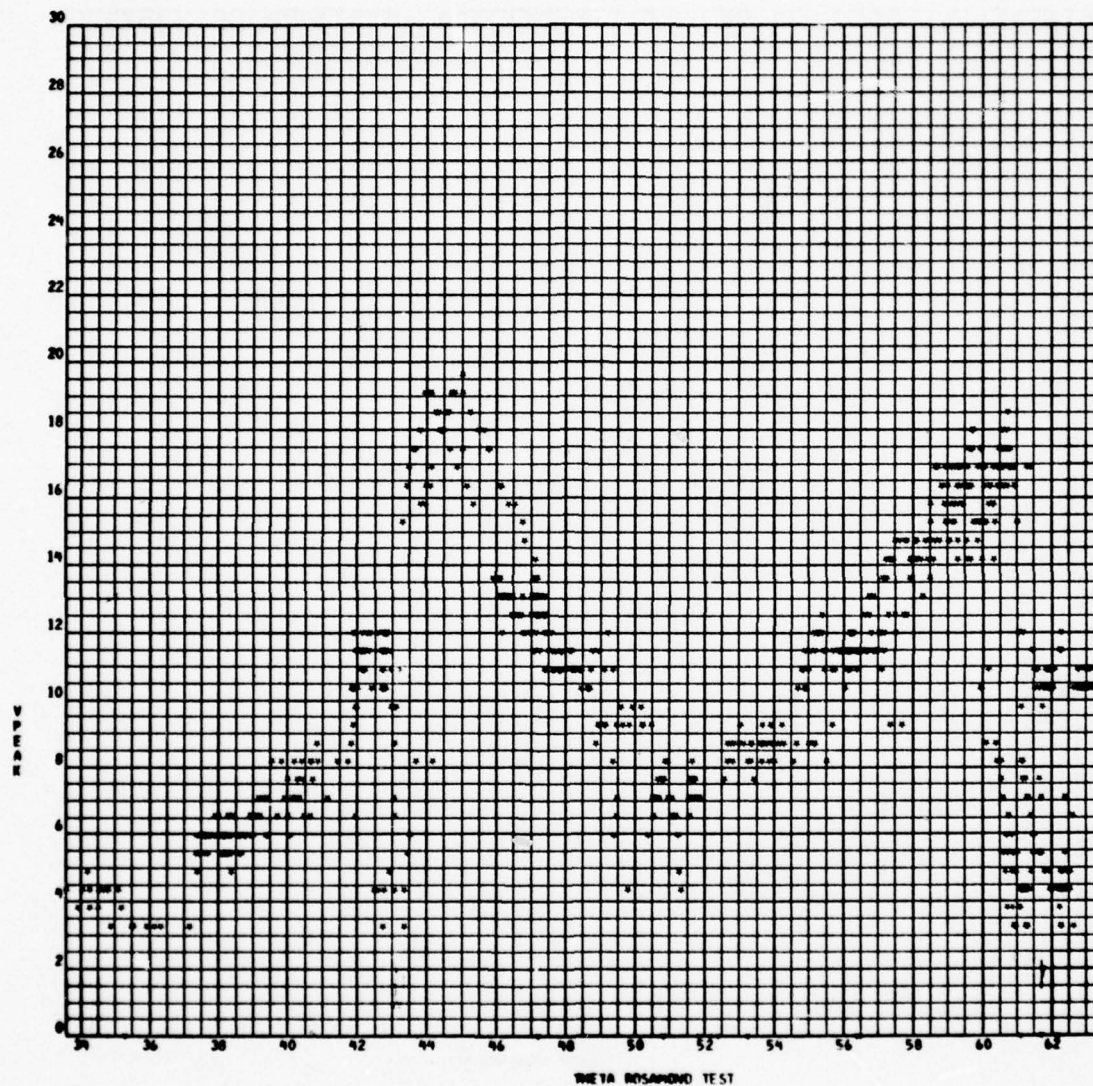
Note that the coordinate system used in the NASA-MSFC data processing routines is not the same as the coordinate system used in the text earlier. The runway centerline is located at $y = -200$ ft in the NASA plots.

BEST AVAILABLE COPY

SCAN	FRAME	X	Y	R	T	IPEAK	VMAX	VPEAK	VAVG	WIDTH
4	4150	219.4	245.0	328.9	48.2	127	9.8	10.9	9.0	8
4	4151	216.9	242.5	325.3	48.2	131	8.2	10.4	8.7	8
4	4152	218.8	240.0	324.7	47.7	134	8.2	10.9	8.8	8
4	4153	216.9	237.5	321.6	47.6	134	9.3	10.4	9.0	8
4	4154	208.7	235.0	314.3	48.4	123	10.4	10.9	9.1	8
4	4155	206.2	232.5	310.8	48.4	121	9.3	10.4	8.5	8
4	4156	208.1	229.4	309.7	47.8	121	10.4	10.4	8.8	8
4	4157	205.0	226.2	305.3	47.8	124	8.2	10.4	8.5	8
4	4158	196.9	223.7	298.0	48.7	118	8.2	10.4	8.2	8
4	4159	199.4	221.2	297.8	48.0	131	8.2	10.9	8.5	9
4	4160	196.9	217.5	293.4	47.8	136	7.1	10.4	8.0	9
4	4161	189.4	215.6	287.0	48.7	128	9.3	10.4	8.7	7
4	4162	186.2	212.5	282.6	48.8	125	9.3	10.9	9.4	8
4	4163	187.5	209.4	281.1	48.2	116	10.9	10.9	9.1	8
4	4164	185.6	206.9	277.9	48.1	123	8.7	10.9	8.8	5
4	4165	178.1	204.4	271.1	48.9	117	8.7	10.9	9.4	5
4	4166	179.4	201.2	269.6	48.3	111	7.1	10.4	7.8	4
4	4167	177.5	198.7	266.5	48.2	116	9.3	10.4	9.0	6
4	4168	169.4	195.6	258.8	49.1	118	9.3	9.8	8.8	5
4	4169	166.2	192.5	254.4	49.2	131	8.7	9.3	8.5	4
4	4170	169.4	190.6	255.0	48.4	119	8.7	10.9	8.8	4
4	4171	166.2	187.5	250.6	48.4	130	8.7	10.4	8.9	5
4	4172	158.7	185.0	243.8	49.4	126	8.7	8.7	8.3	3
4	4173	155.6	181.4	239.4	49.4	131	8.2	8.7	8.2	3
4	4174	158.1	179.4	239.1	48.6	136	8.2	10.4	8.5	5
4	4175	155.0	176.2	234.7	48.7	128	8.7	10.4	7.5	6
4	4176	147.5	173.1	227.4	49.6	129	8.7	9.8	8.1	5
4	4177	145.0	170.6	223.9	49.6	136	8.7	9.3	8.1	6
4	4178	146.9	168.1	223.2	48.9	120	8.2	8.7	7.5	5
4	4179	139.4	165.0	216.8	49.8	132	7.6	8.7	7.7	4
4	4180	136.2	161.9	211.6	49.9	134	8.2	9.3	8.0	5
4	4181	138.7	159.4	211.3	49.0	128	8.2	8.7	7.5	6
4	4182	136.2	156.3	207.3	48.9	130	8.2	8.7	8.4	2
4	4183	128.1	153.2	208.1	50.2	130	8.2	9.3	8.1	5
4	4184	126.2	151.2	197.0	50.1	117	9.3	9.3	8.5	5
4	4185	128.1	148.1	195.8	49.1	121	7.6	8.7	7.8	4
4	4186	125.6	145.0	191.9	49.1	116	6.0	9.3	7.3	5
4	4187	118.1	141.9	184.6	50.2	106	8.2	8.2	8.2	1
4	4188	115.0	139.4	180.7	50.5	115	8.2	8.7	8.2	2
4	4189	117.5	136.9	180.4	49.4					
4	4190	115.0	134.4	176.9	49.4					
4	4191	107.5	131.2	169.7	50.7					
4	4192	109.4	127.5	168.0	49.4					
4	4193	106.9	125.0	164.5	49.5					
4	4194	99.4	121.9	157.3	50.8					
4	4195	96.2	120.0	153.8	51.3					
4	4196	99.4	117.5	153.9	49.8					
4	4197	96.2	114.4	149.5	49.9					
4	4198	88.7	111.2	142.3	51.4					
4	4199	85.6	108.7	138.4	51.8					

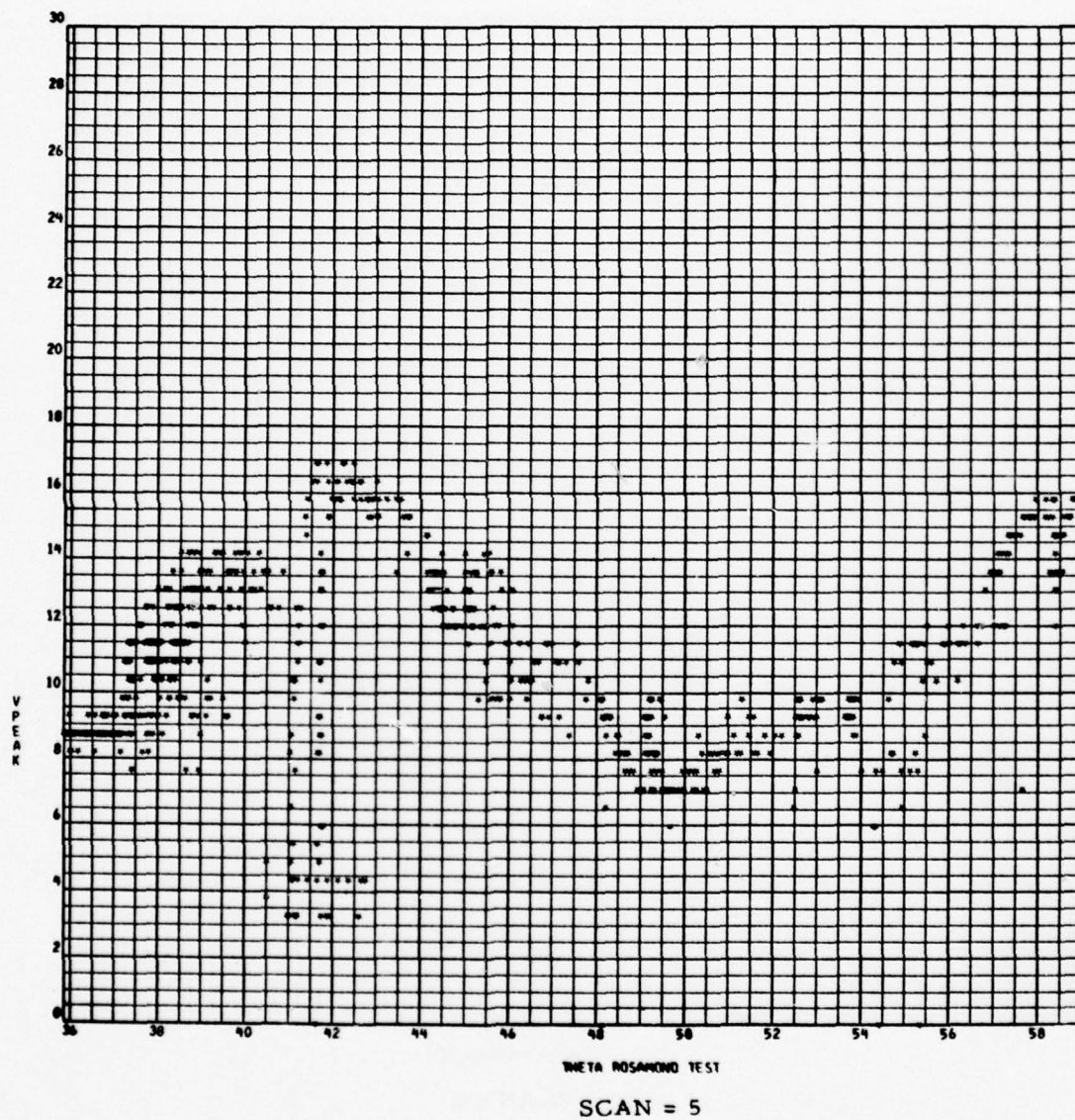


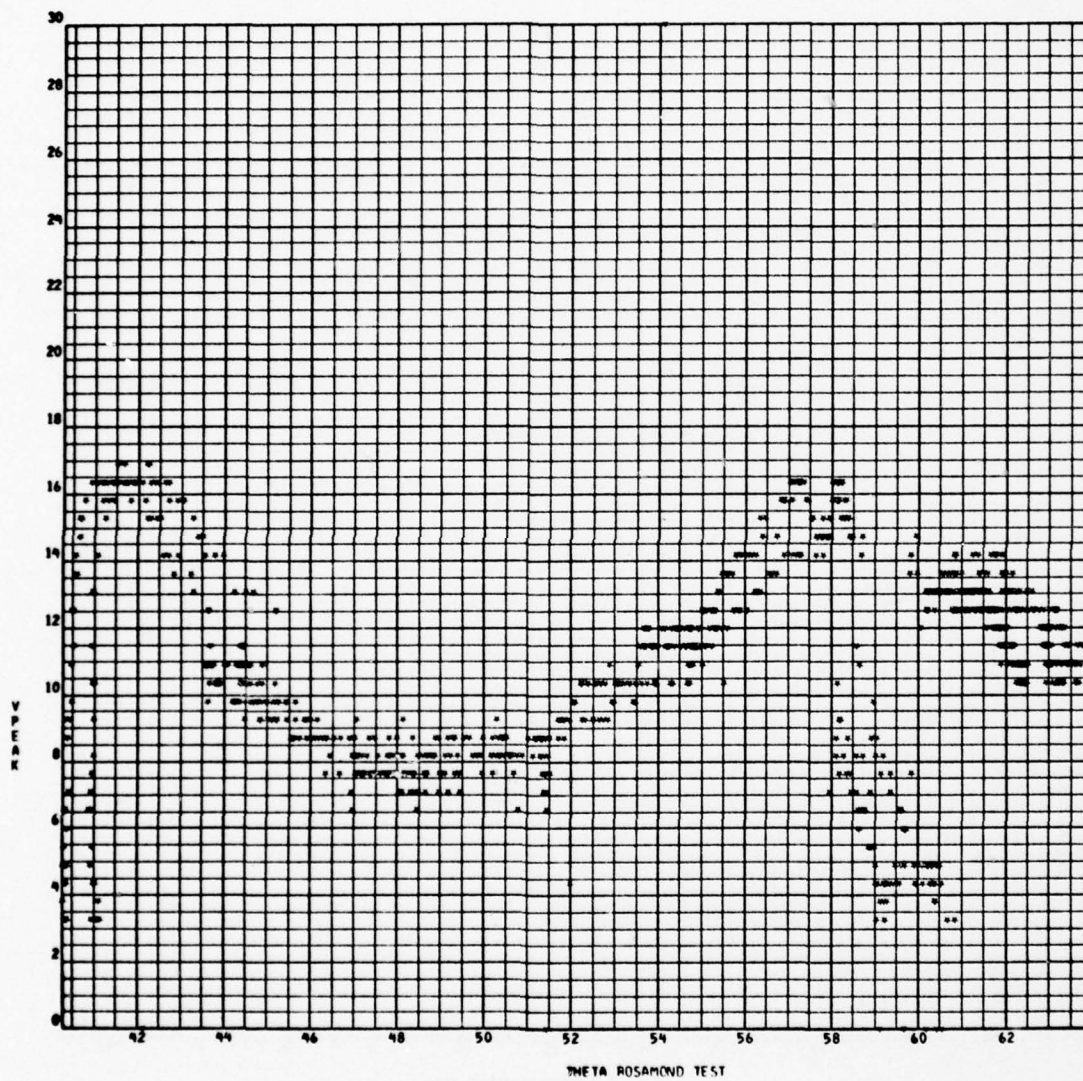
SCAN = 3



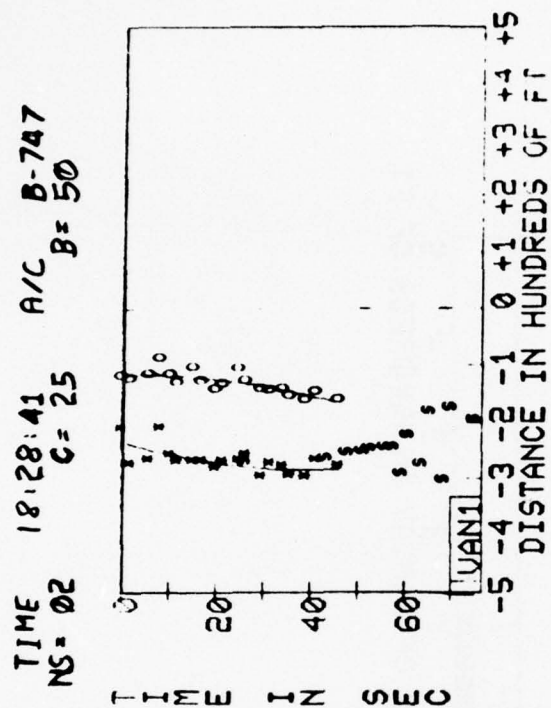
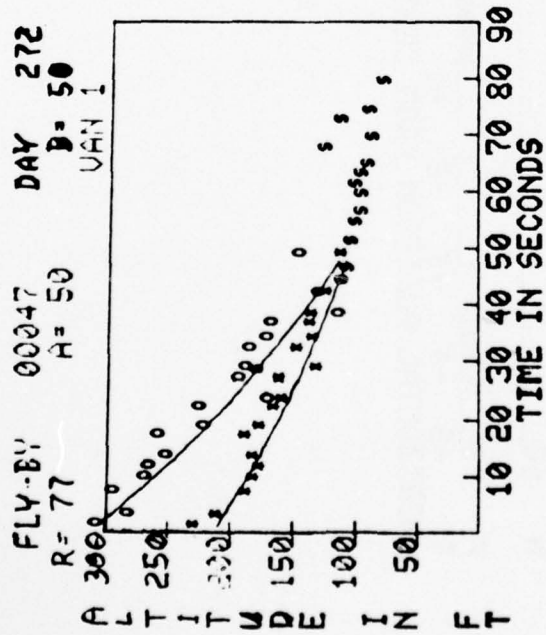
THETA ROSINONE TEST

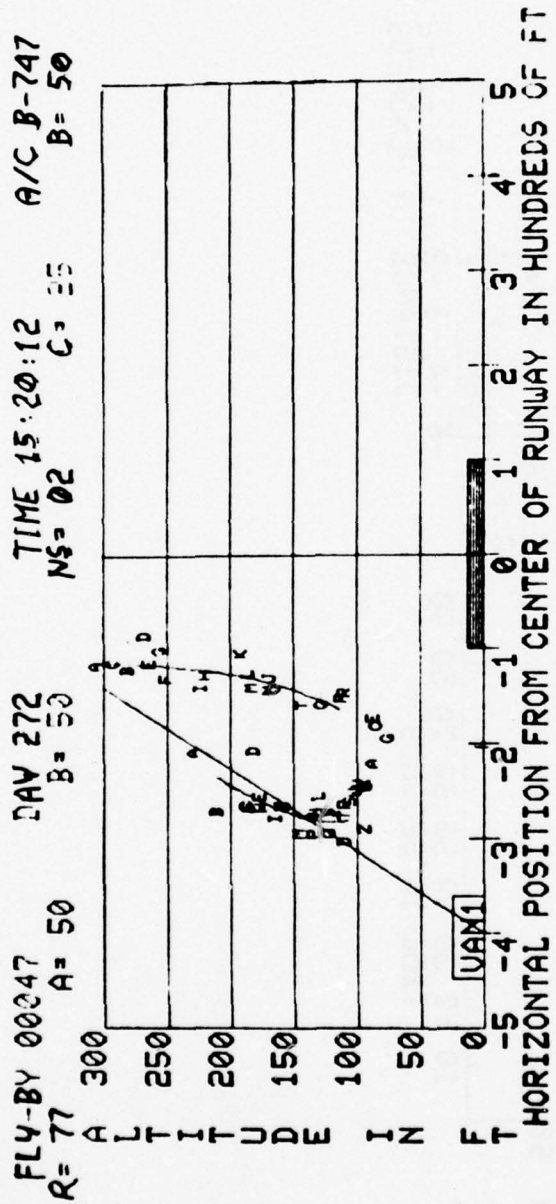
SCAN = 4





SCAN = 6





Appendix D

WAKE VORTEX TRACKS COMPUTED FROM LOW-SPEED MEASUREMENTS

The circles, triangles and diamond symbols represent the port, starboard and undefined vortex, respectively. For each flyby, the predicted wake vortex trajectory assuming zero crosswind is shown by the solid lines. The vortex tracks were computed from the predicted model described in Ref. 10 for a circulation strength of $\Gamma = 662 \text{ m}^2/\text{sec}$ and an initial vortex spacing of $b' = 41.8 \text{ m}$. Available photographic and acoustic measurements also appear on the plots, the solid circles and triangles representing the former and the x's the latter measurements. The dashed line is a smooth curve drawn through the photographic vortex tracks.

<u>LDV Measurement</u>	<u>Photographic Measurement</u>	<u>MAVSS</u>	<u>Theory</u>
○ Port Vortex	● Port Vortex	□ Port Vortex	— Predictive Model
△ Starboard Vortex	▲ Starboard Vortex	× Starboard Vortex	

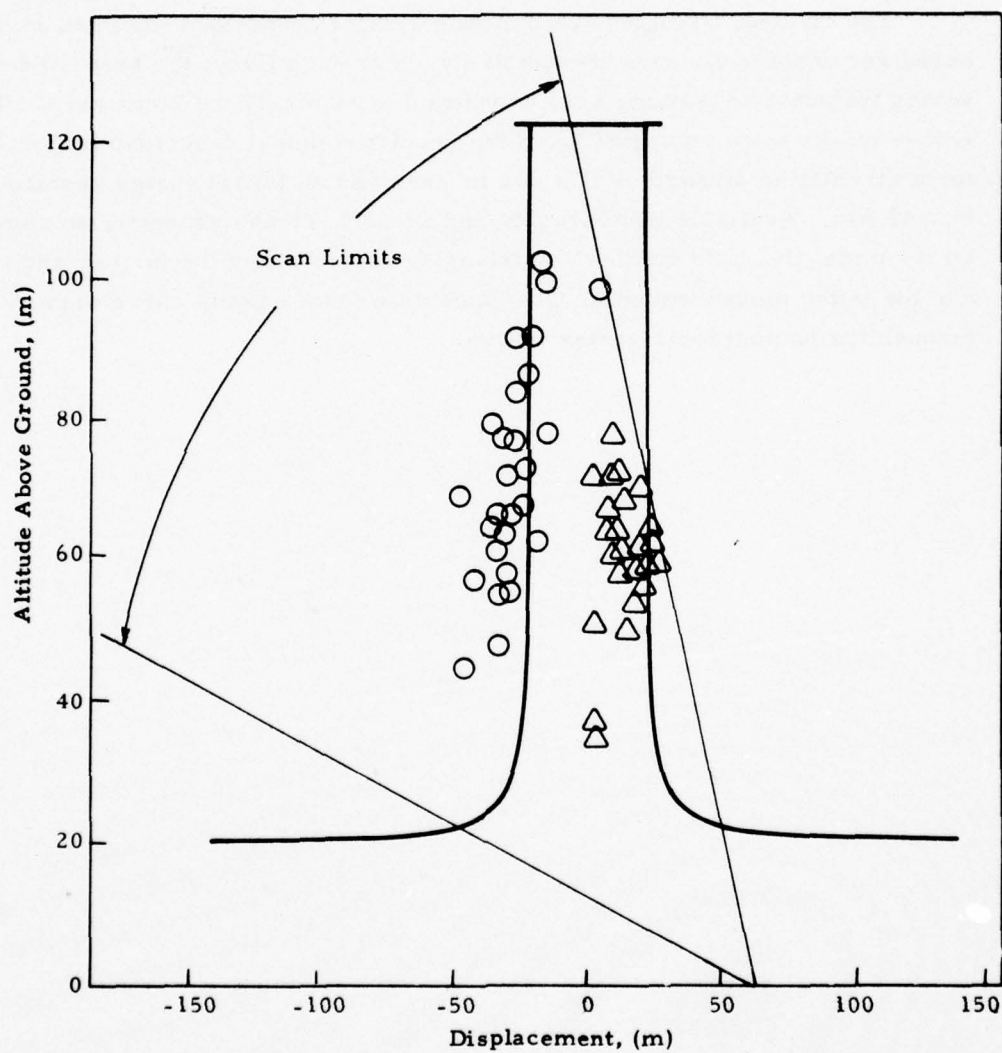


Fig. D-1 - Wake Vortex Trajectory for Rosamond Flyby 23

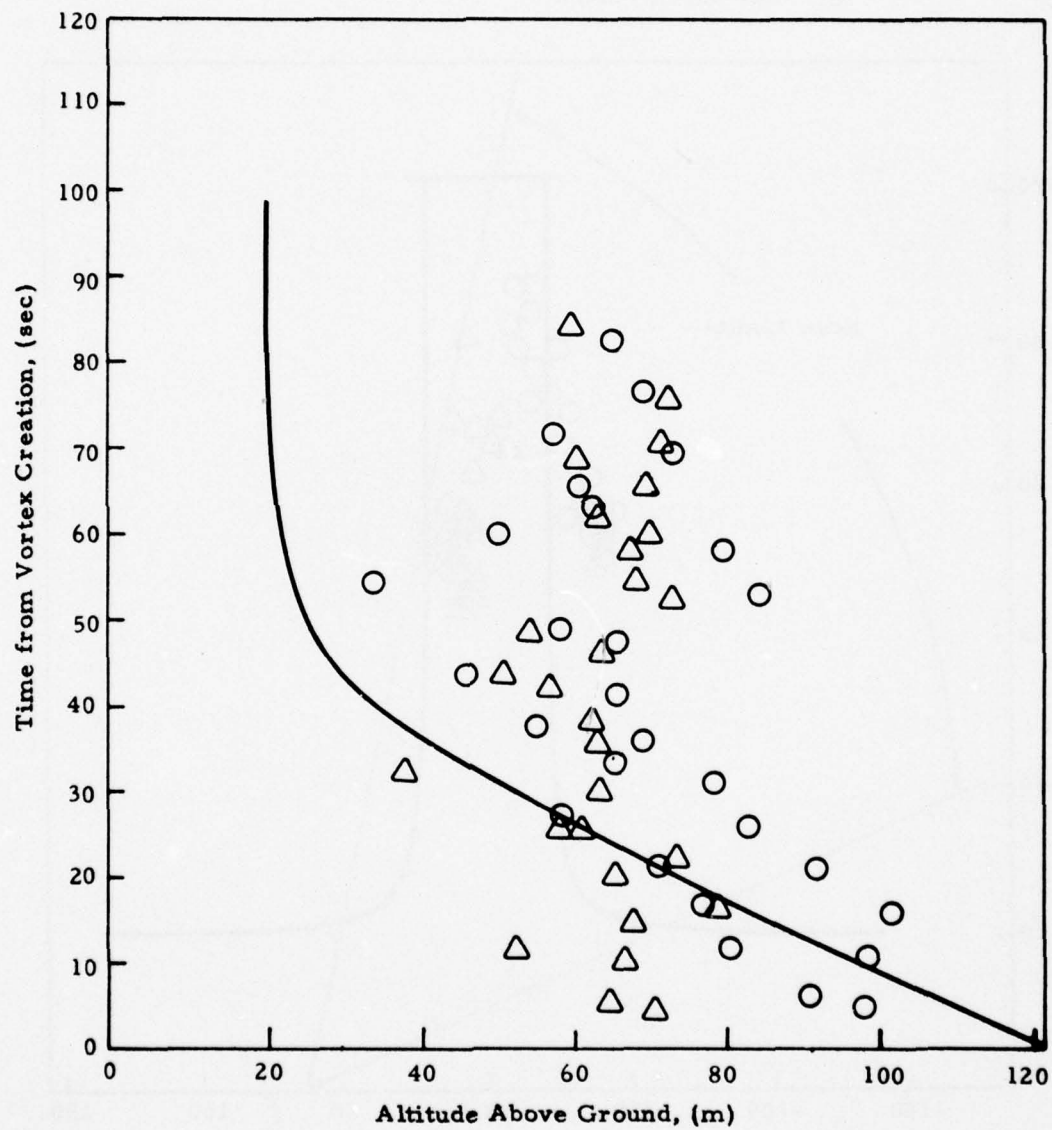


Fig. D-1 - (Concluded)

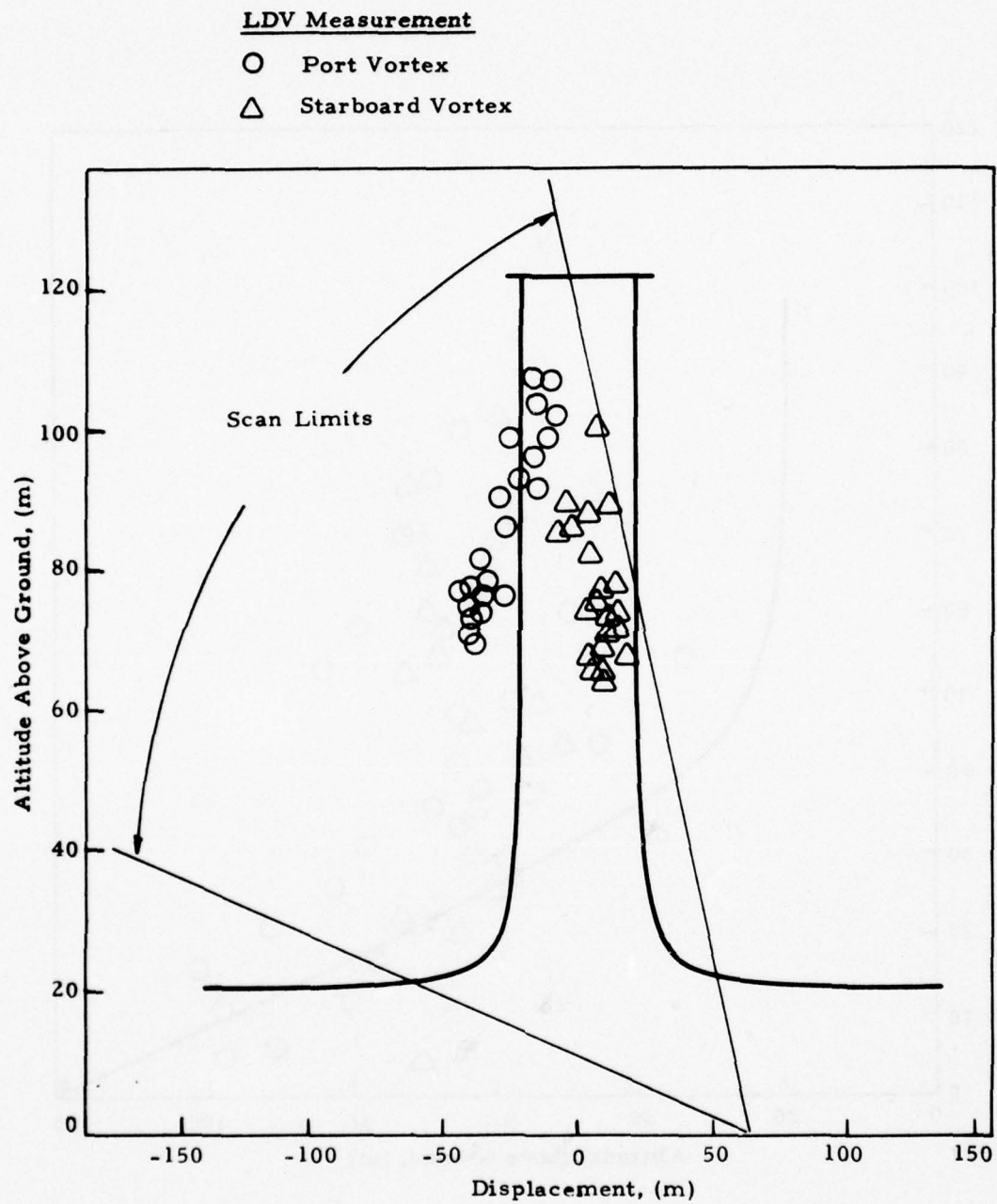


Fig.D-2 - Wake Vortex Trajectory for Rosamond Flyby 24

LDV Measurement

○ Port Vortex

△ Starboard Vortex

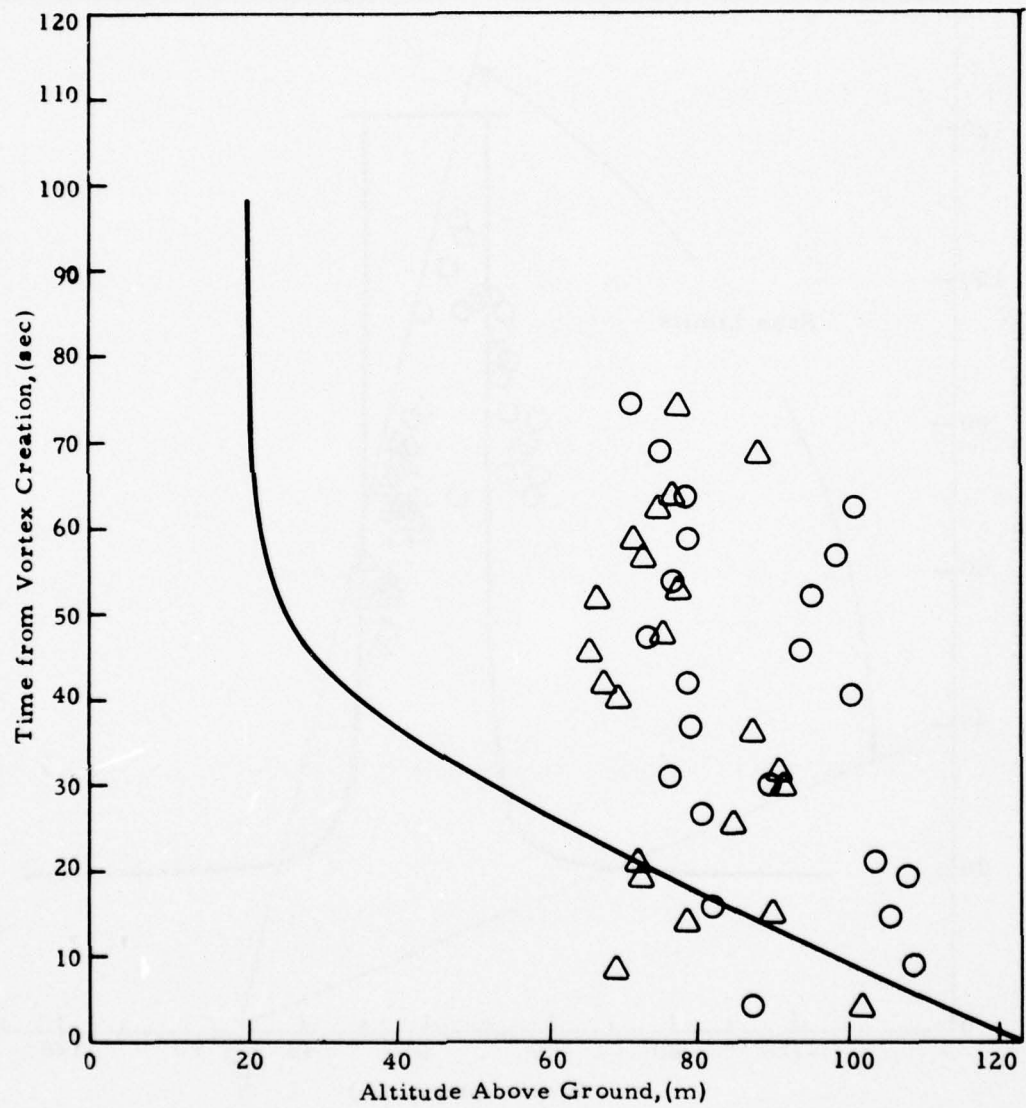


Fig. D-2 - (Concluded)

LDV Measurement

○ Port Vortex

△ Starboard Vortex

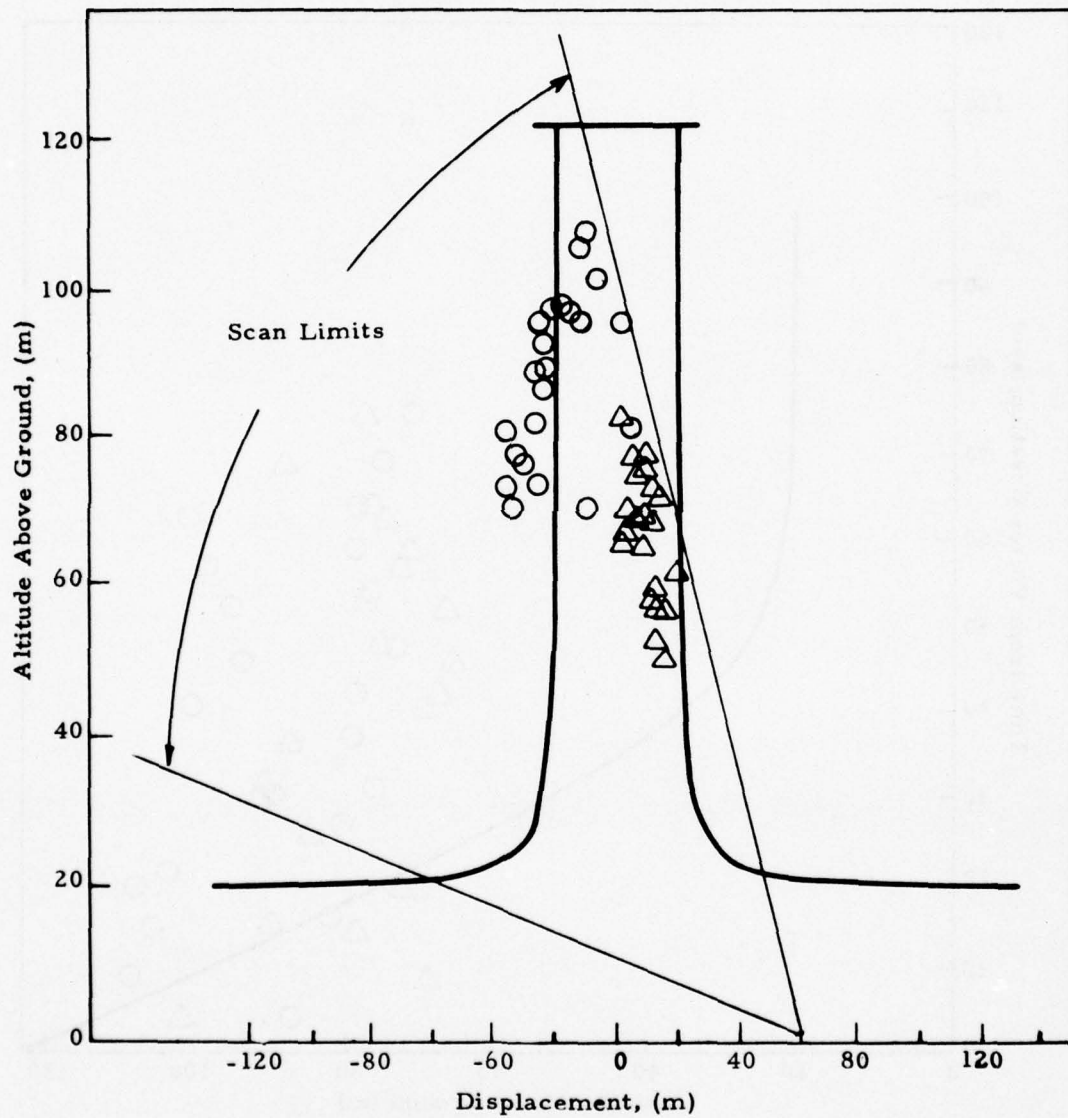


Fig.D-3 - Wake Vortex Trajectory for Rosamond Flyby 25

LDV Measurement

○ Port Vortex

△ Starboard Vortex

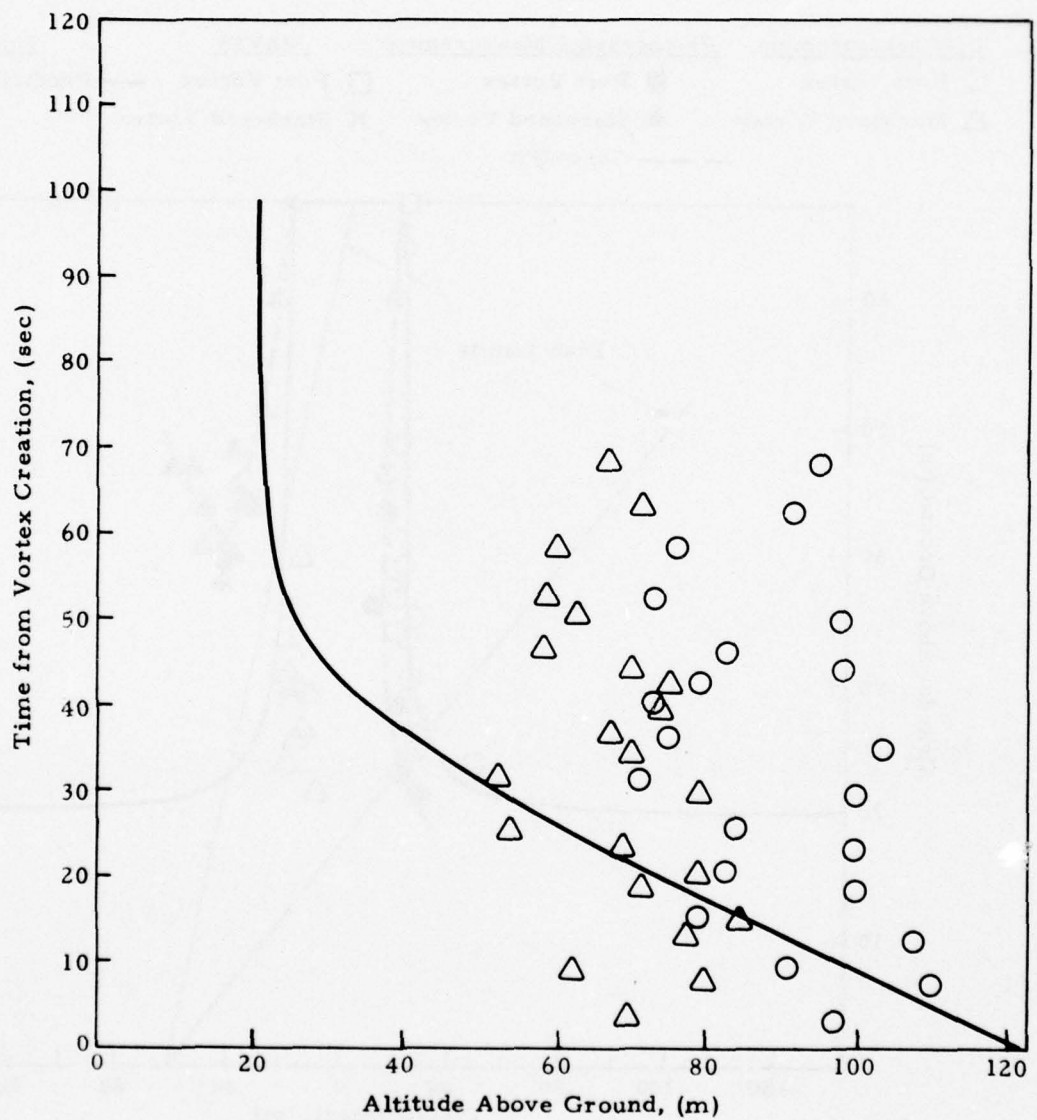


Fig. D-3 - (Concluded)

<u>LDV Measurement</u>	<u>Photographic Measurement</u>	<u>MAVSS</u>	<u>Theory</u>
○ Port Vortex	● Port Vortex	□ Port Vortex	— Predictive Model
△ Starboard Vortex	▲ Starboard Vortex	× Starboard Vortex	
		--- Curve Fit	

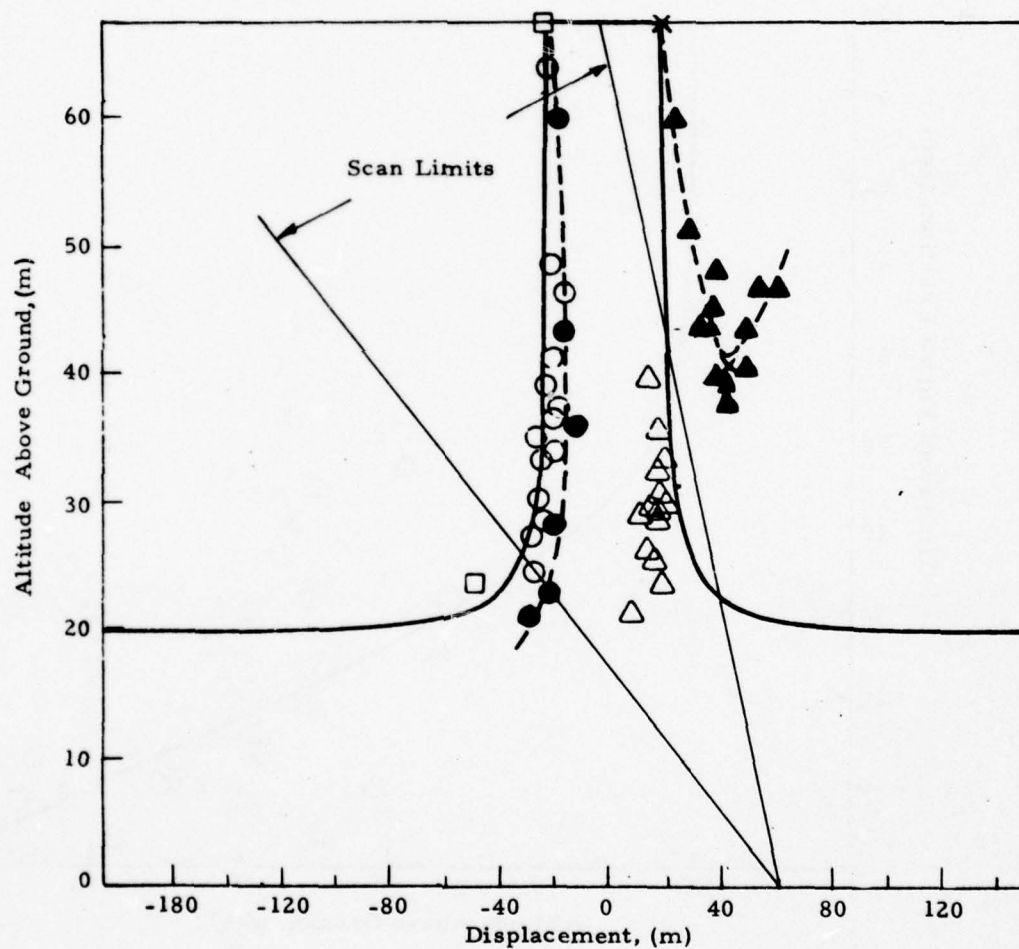


Fig. D-4 - Wake Vortex Trajectory for Rosamond Flyby 27

LDV Measurement	Photographic Measurement	MAVSS	Theory
○ Port Vortex	● Port Vortex	□ Port Vortex	— Predictive Model
△ Starboard Vortex	▲ Starboard Vortex	× Starboard Vortex	
	— — — Curve Fit		

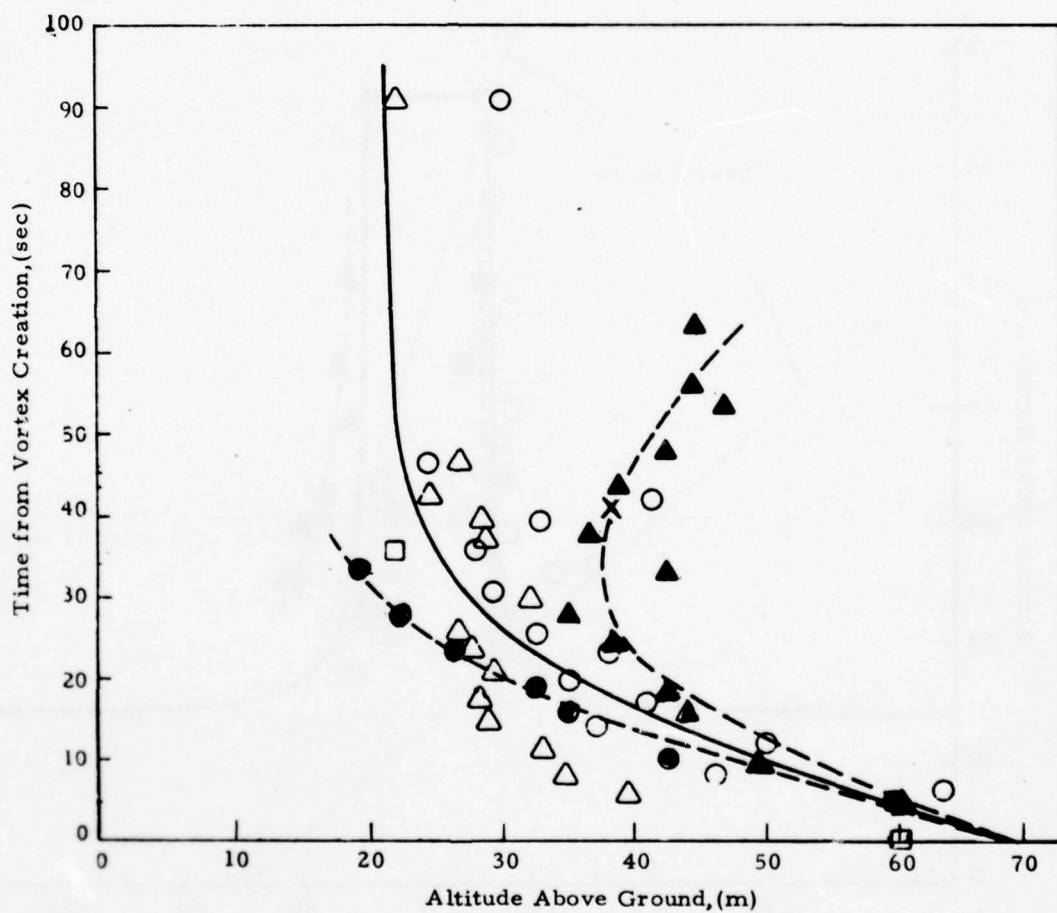


Fig. D-4 - (Concluded)

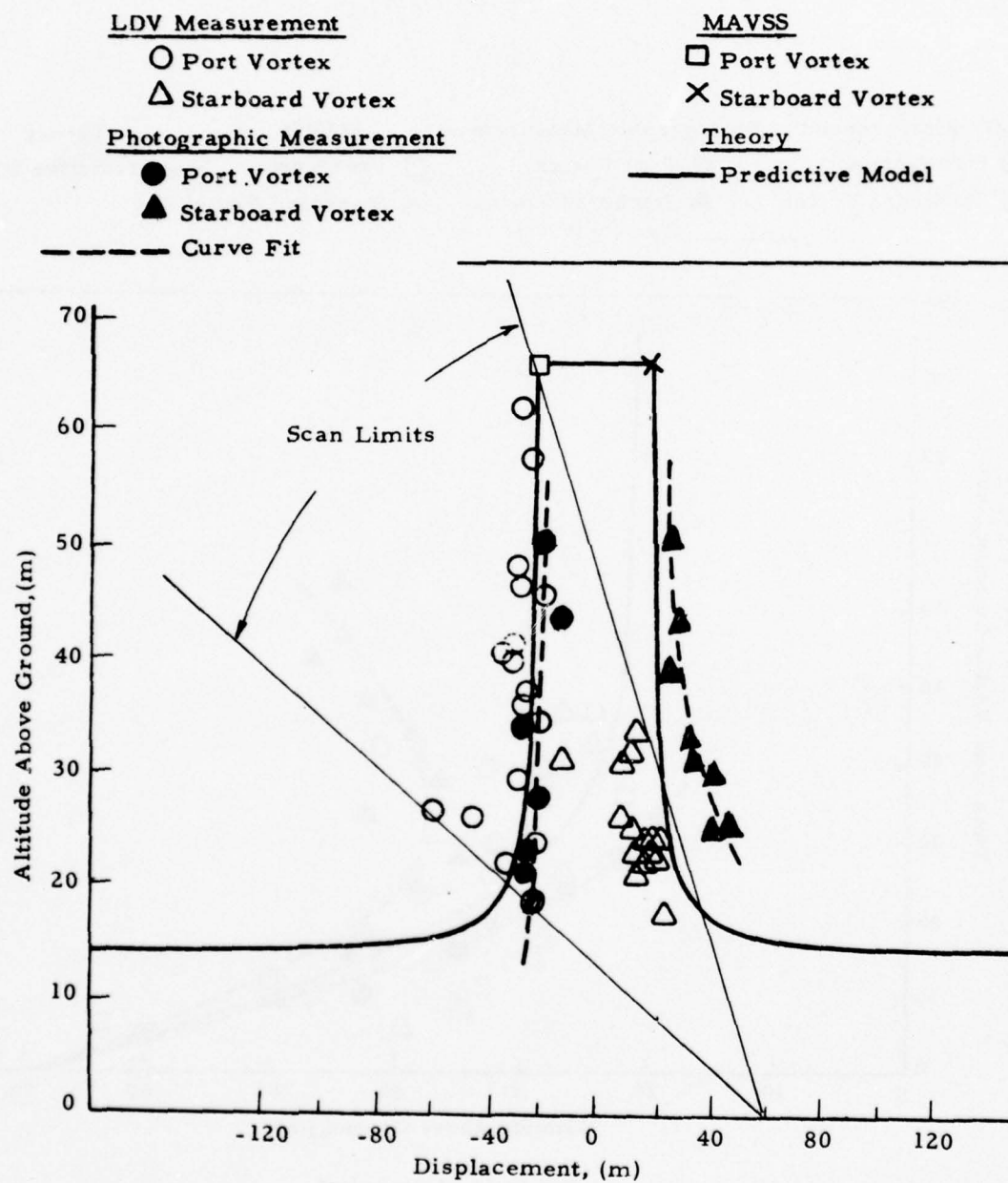


Fig. D-5 - Wake Vortex Trajectory for Rosamond Flyby 28

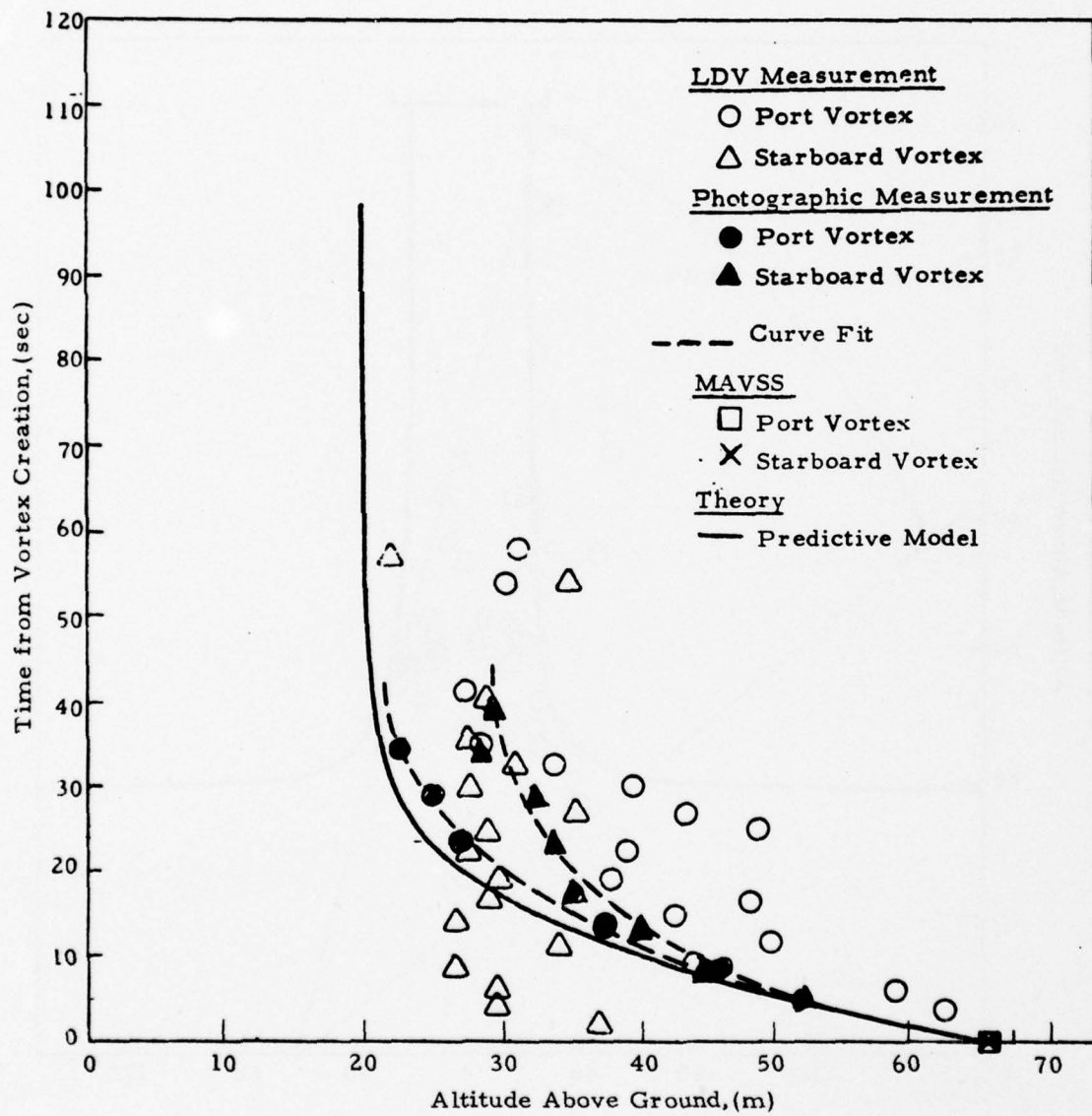


Fig. D-5 - (Concluded)

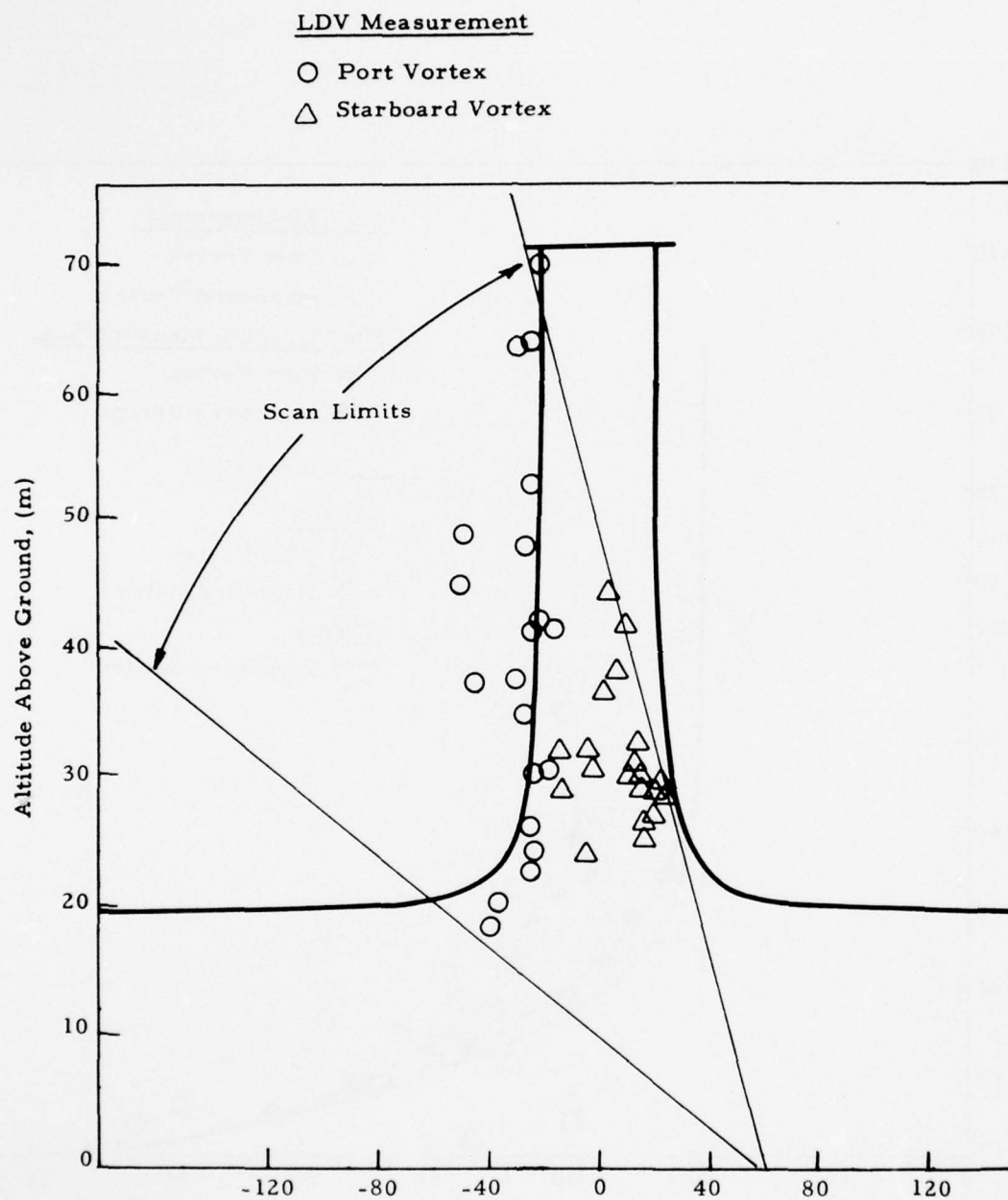


Fig. D-6 - Wake Vortex Trajectory for Rosamond Flyby 29

LDV Measurement

○ Port Vortex

△ Starboard Vortex

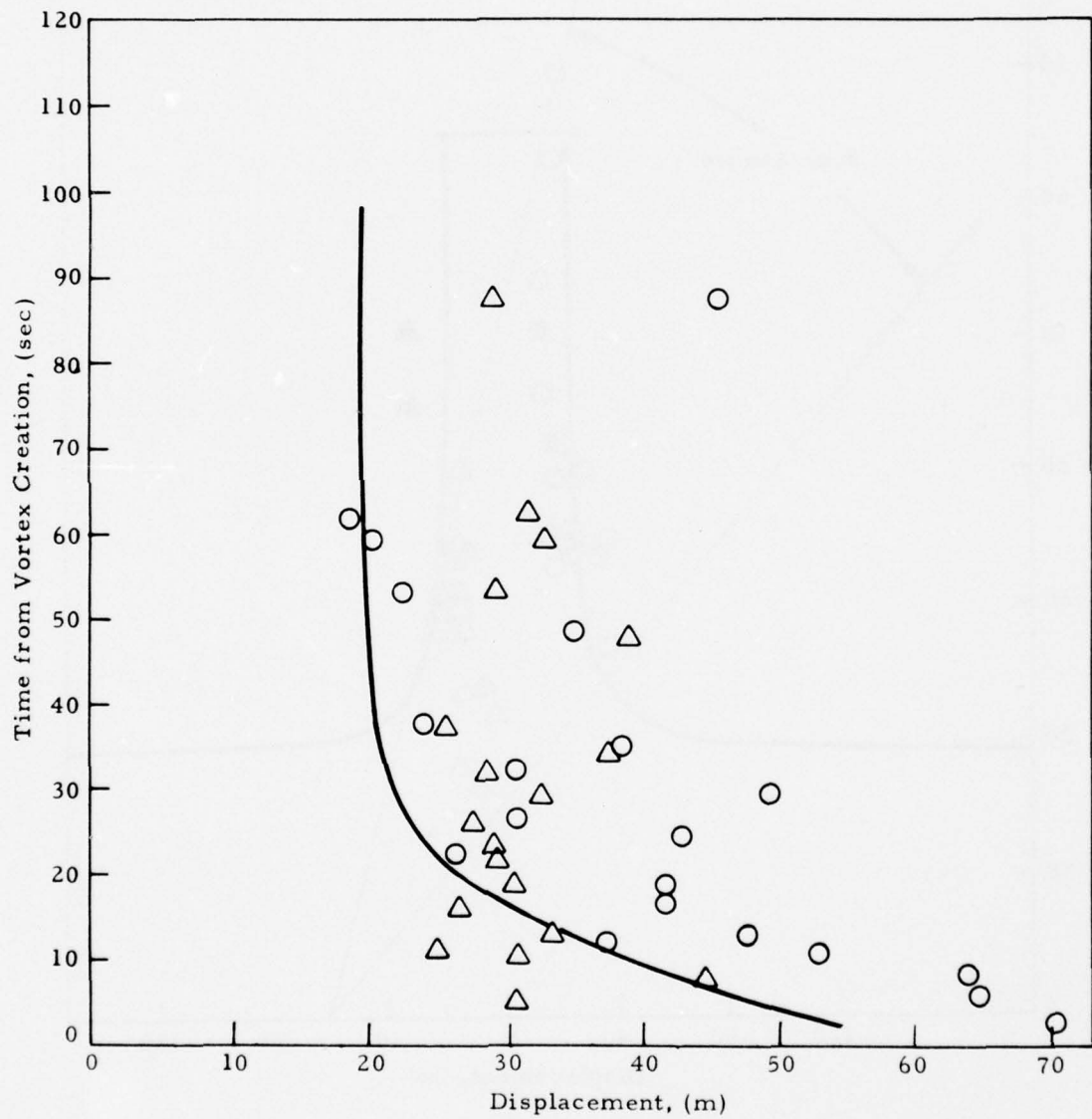


Fig. D-6 - (Concluded)

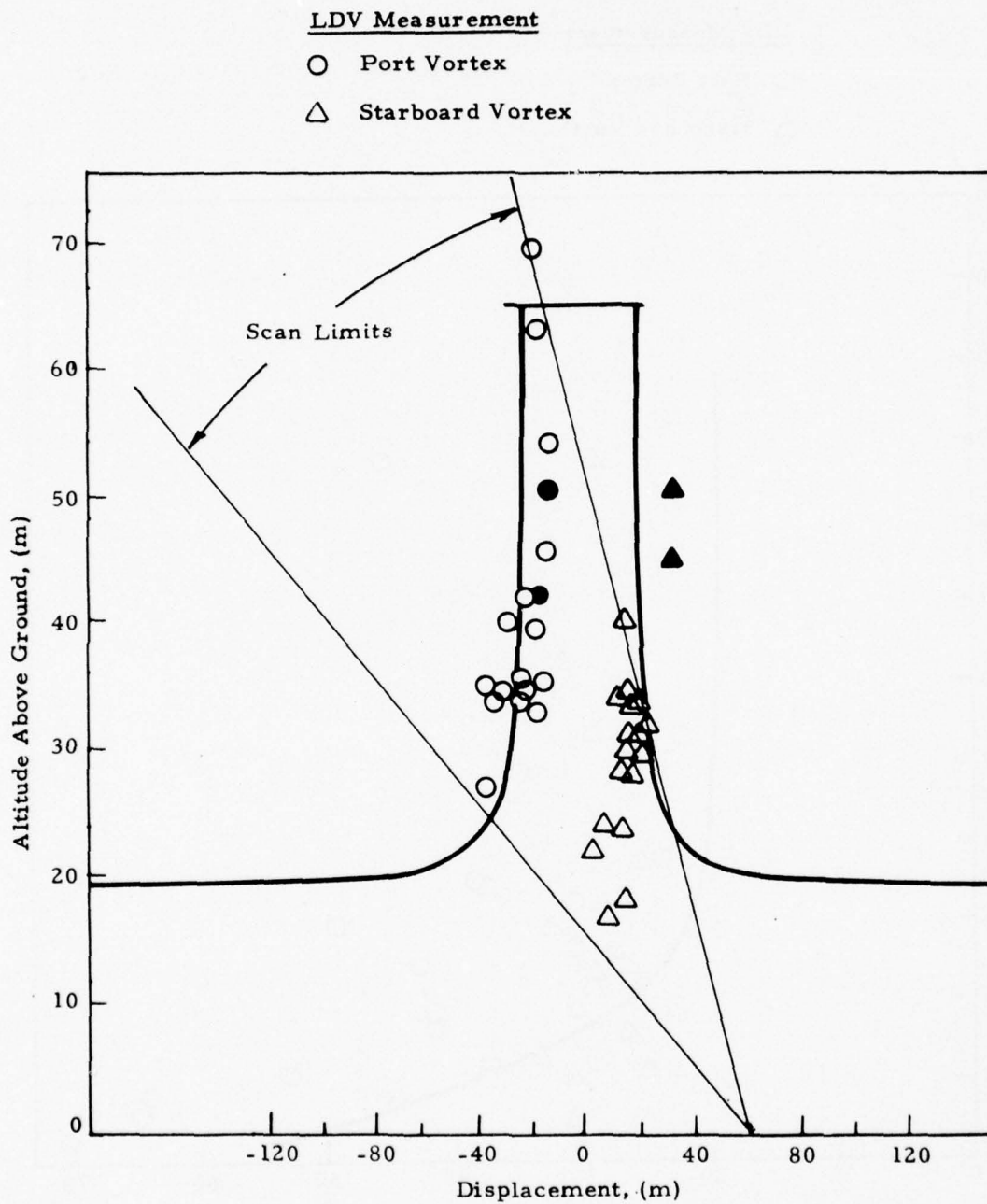


Fig.D-7 - Wake Vortex Trajectory for Rosamond Flyby 30

LDV Measurement

○ Port Vortex

△ Starboard Vortex

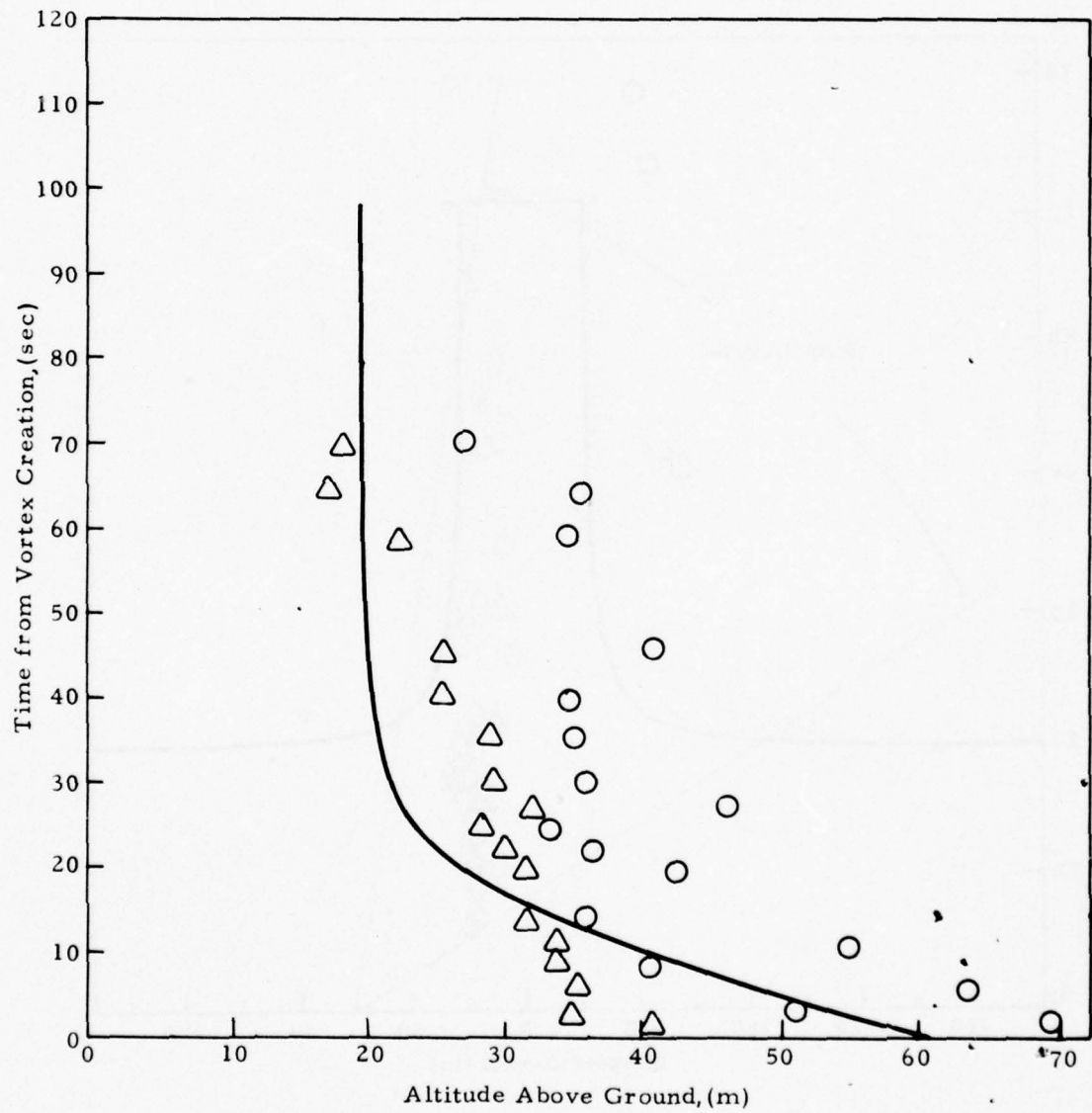


Fig. D-7 - (Concluded)

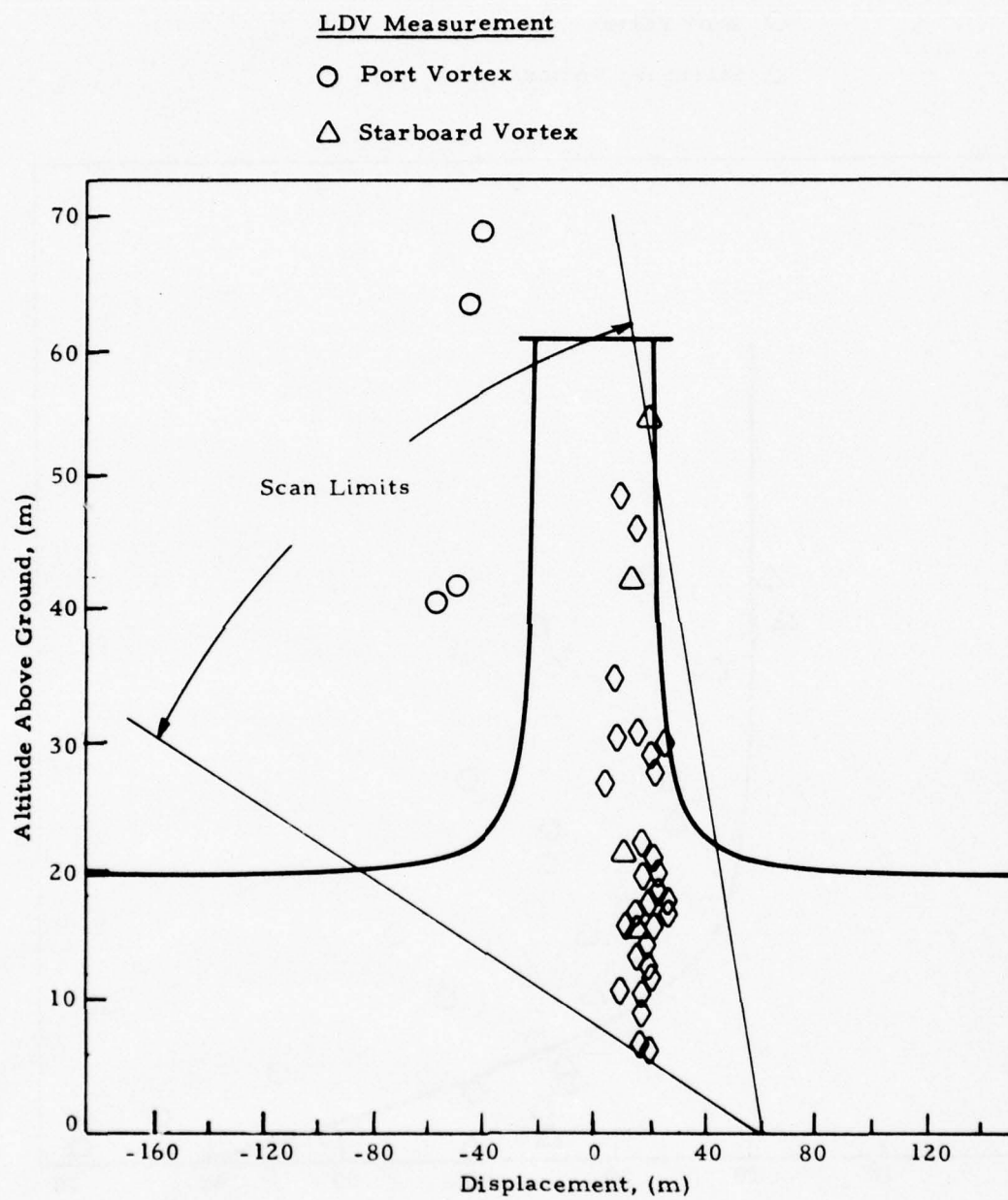


Fig. D-8 - Wake Vortex Trajectory for Rosamond Flyby 40

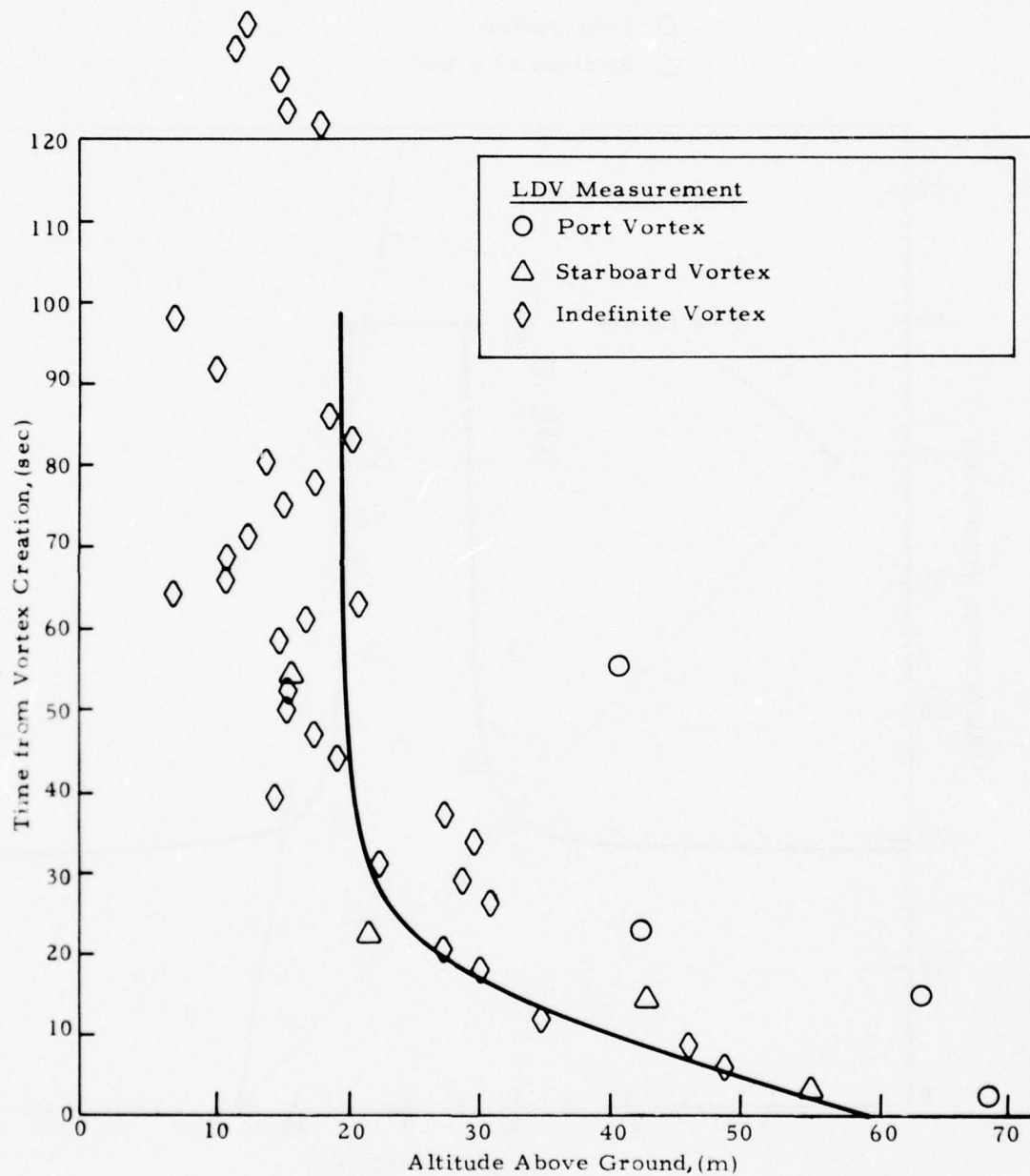


Fig. D-8 - (Concluded)

LDV Measurement

○ Port Vortex

△ Starboard Vortex

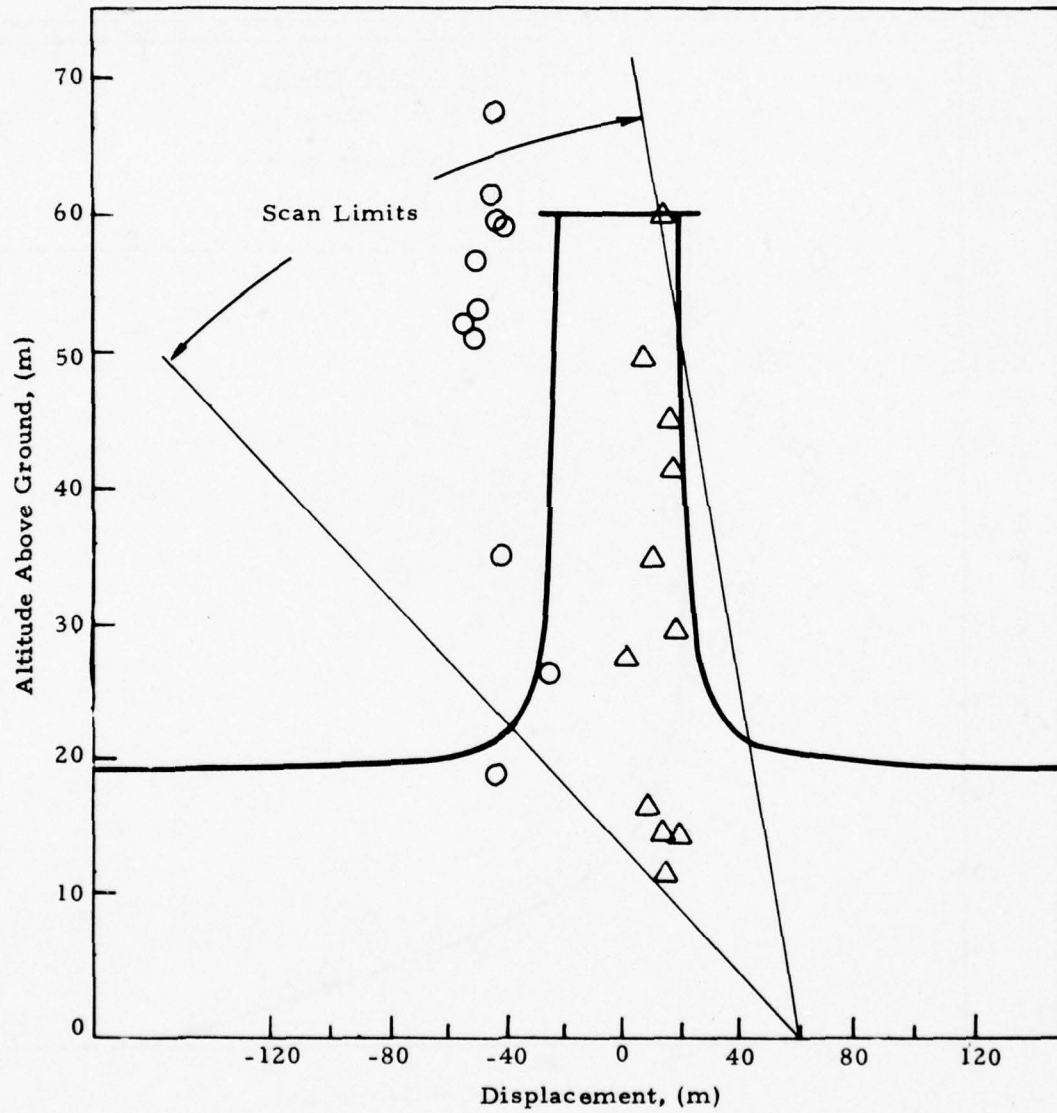


Fig. D-9 - Wake Vortex Trajectory for Rosamond Flyby 42

LDV Measurement

○ Port Vortex

△ Starboard Vortex

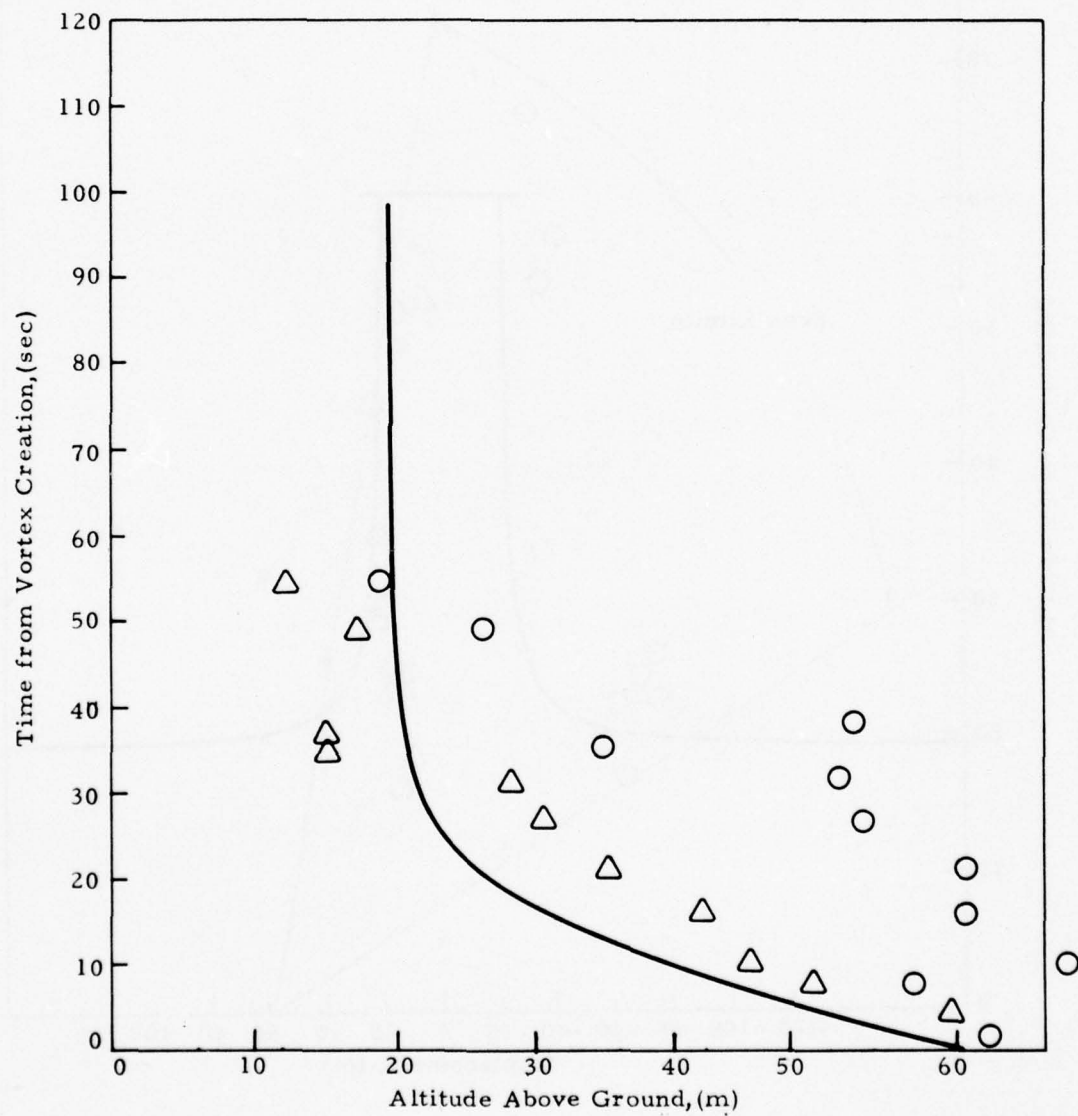


Fig. D-9 - (Concluded)

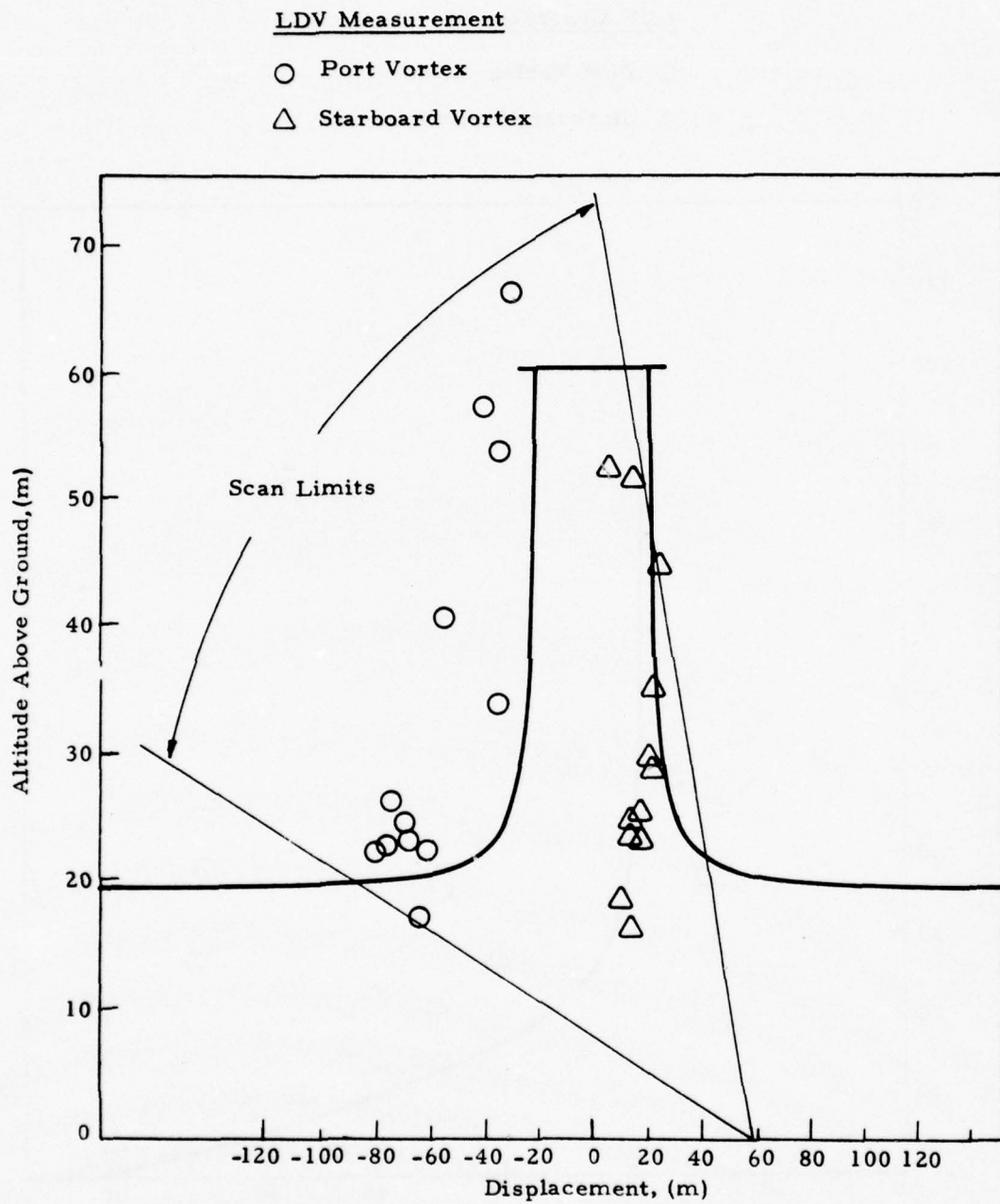


Fig. D-10 - Wake Vortex Trajectory for Rosamond Flyby 44

LDV Measurement

- Port Vortex
△ Starboard Vortex

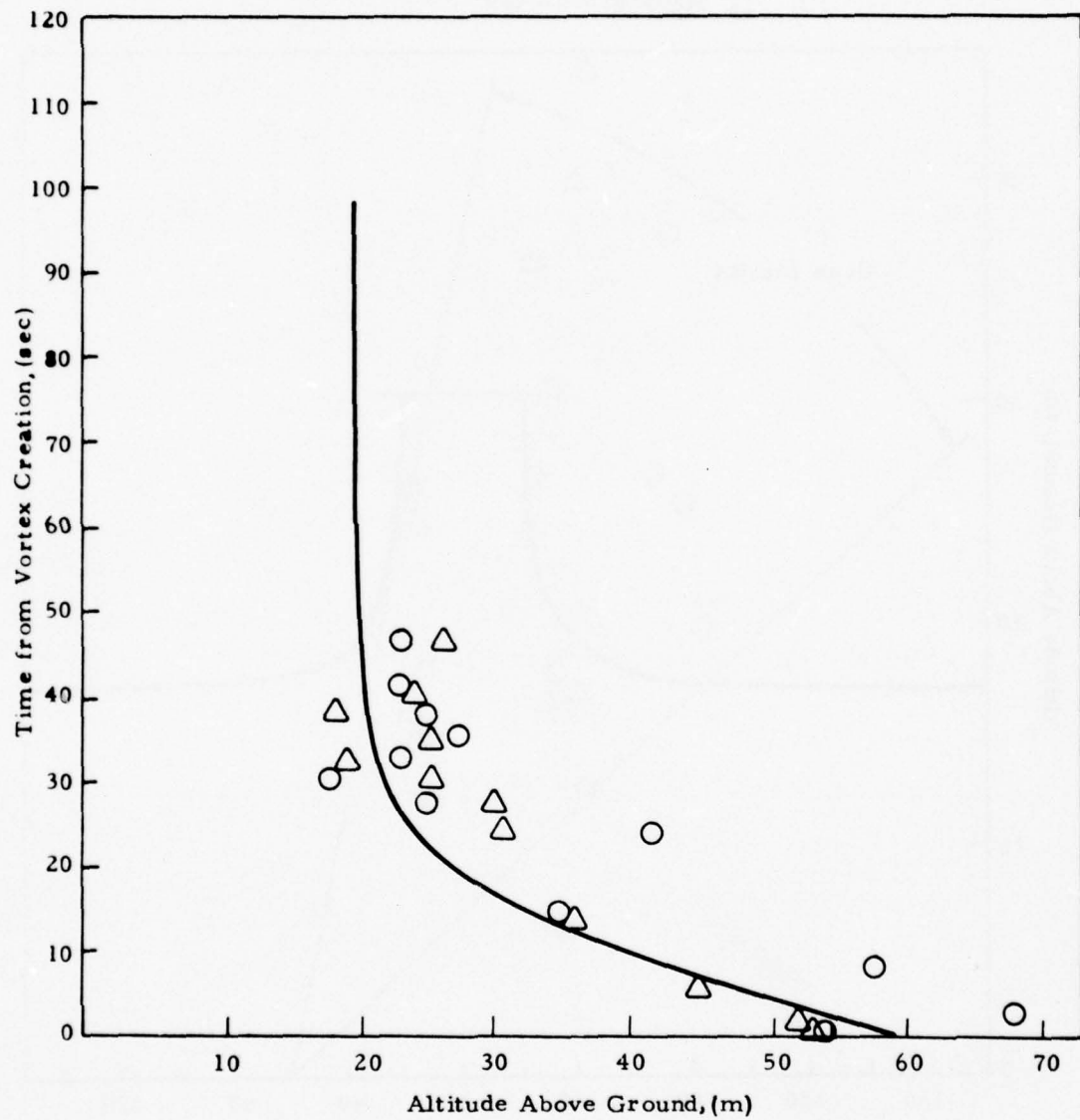


Fig. D-10 - (Concluded)

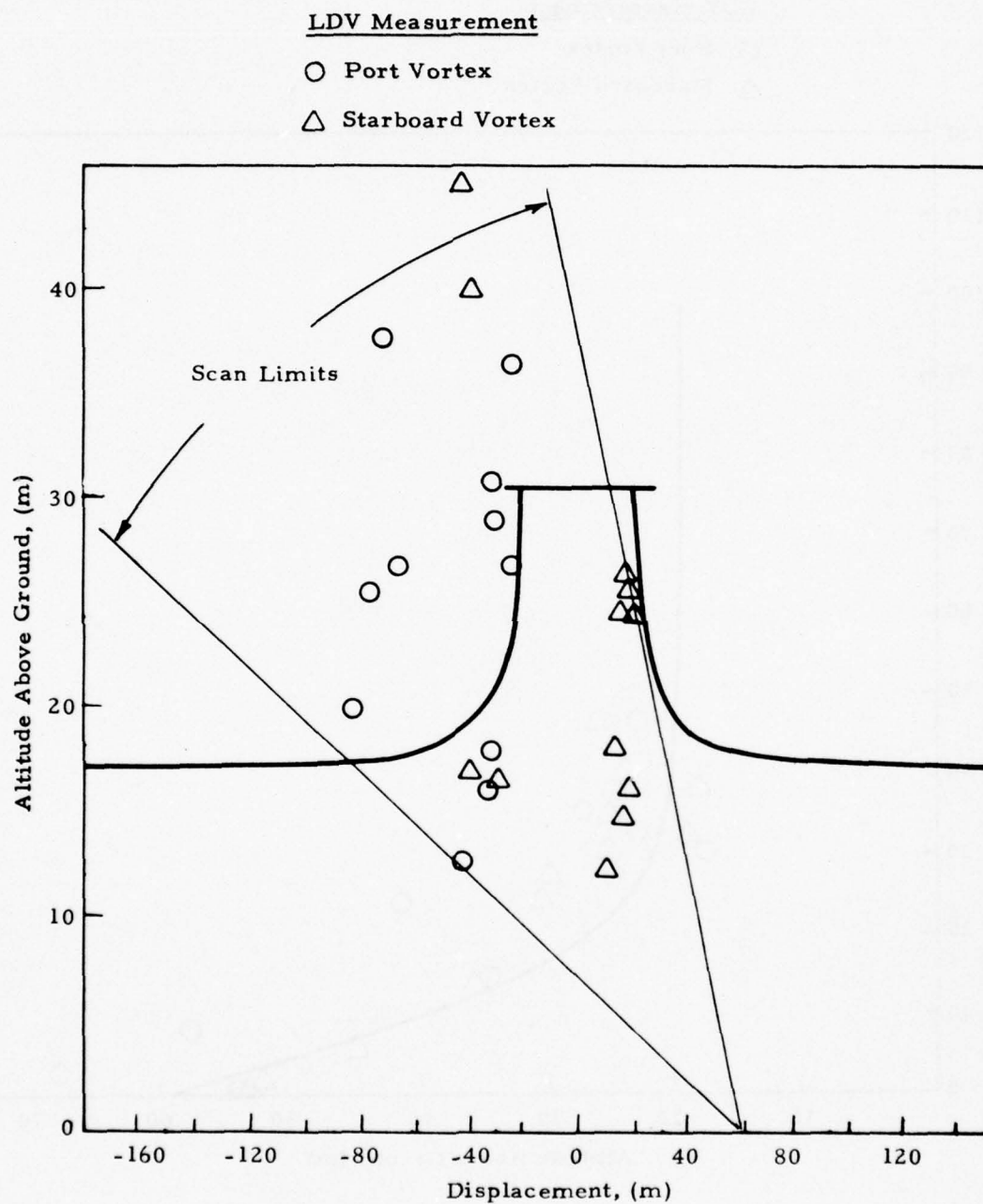


Fig. D-11 - Wake Vortex Trajectory for Rosamond Flyby 46

LDV Measurement

- Port Vortex
△ Starboard Vortex

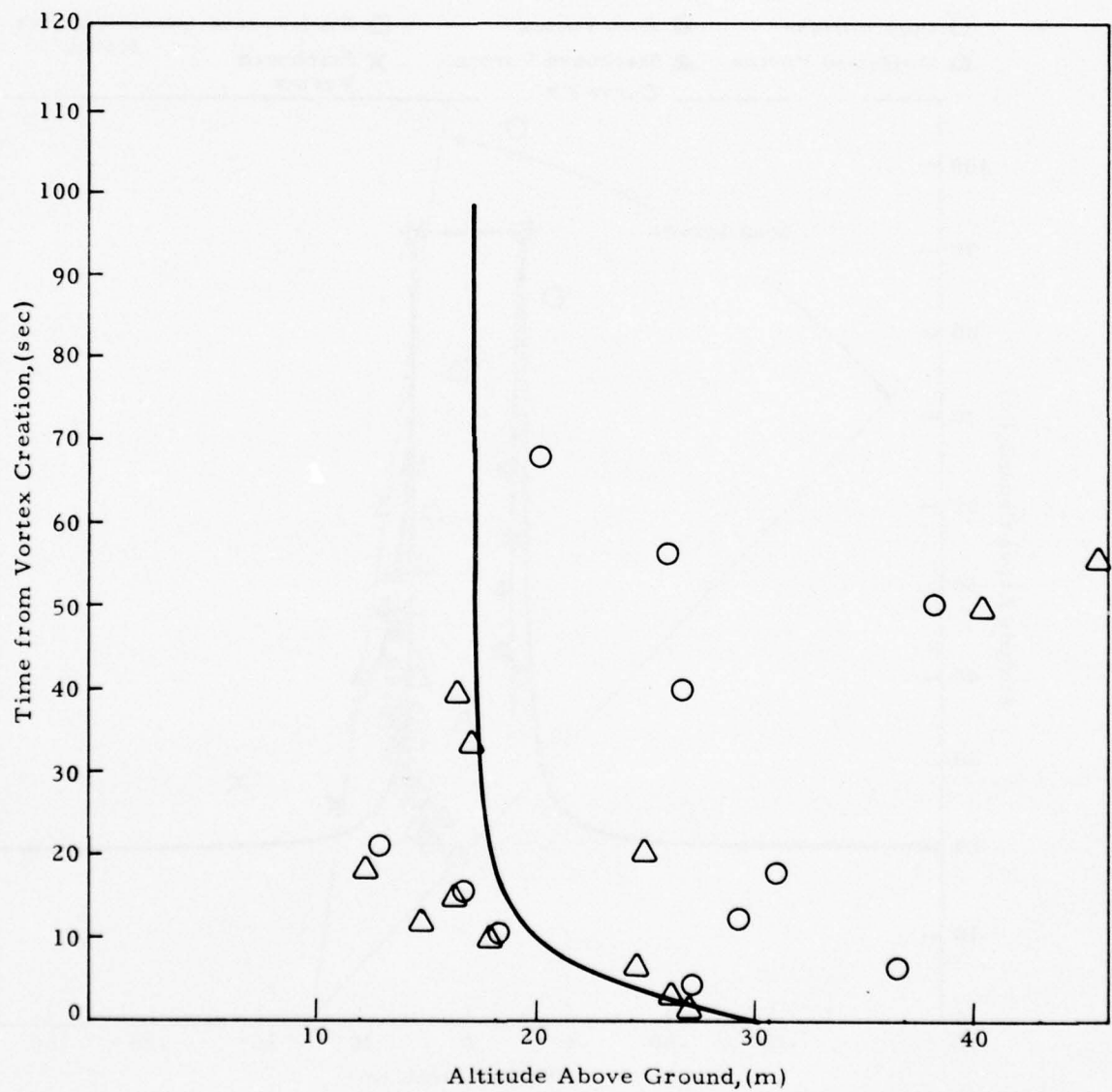


Fig.D-11 - (Concluded)

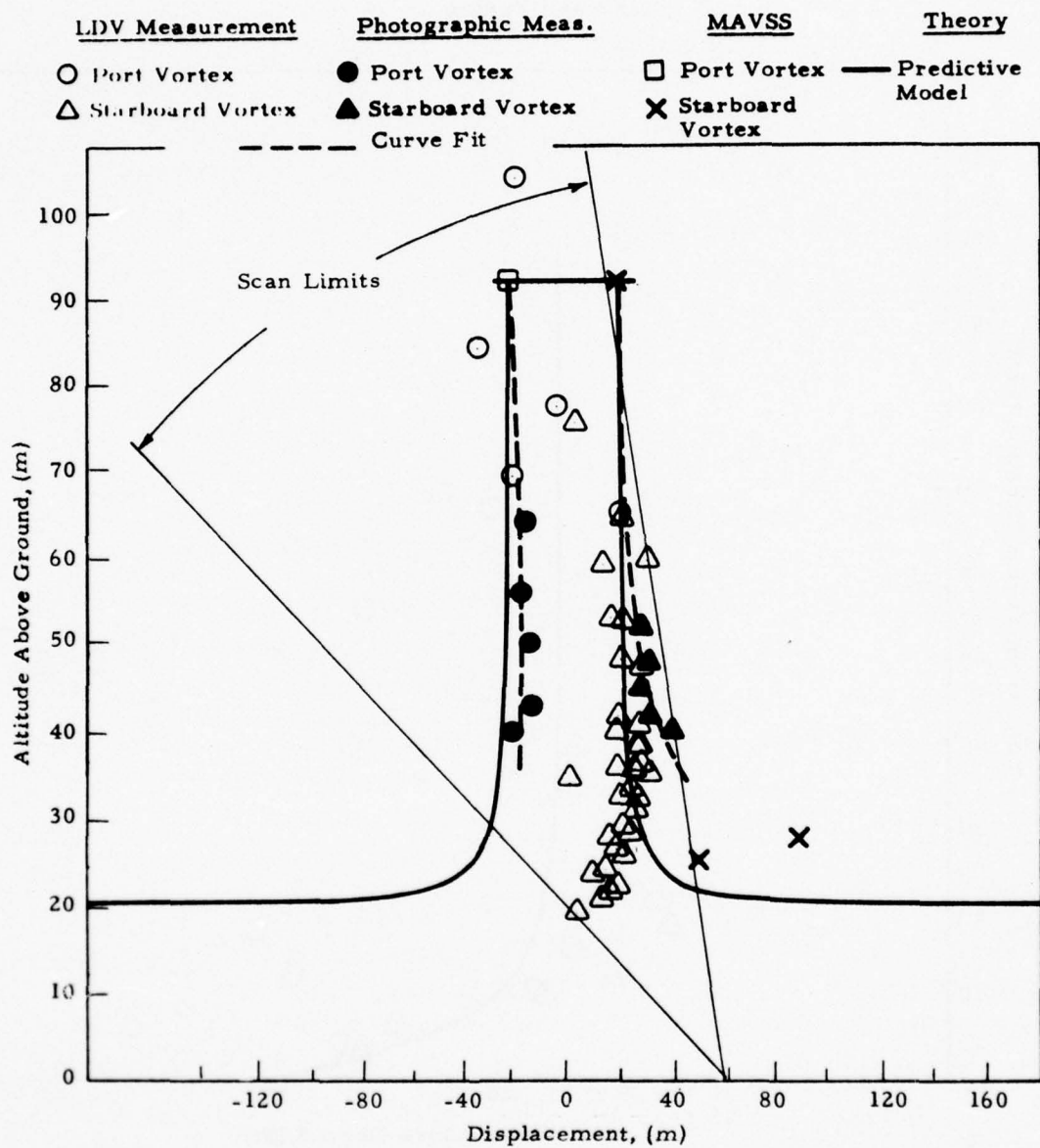
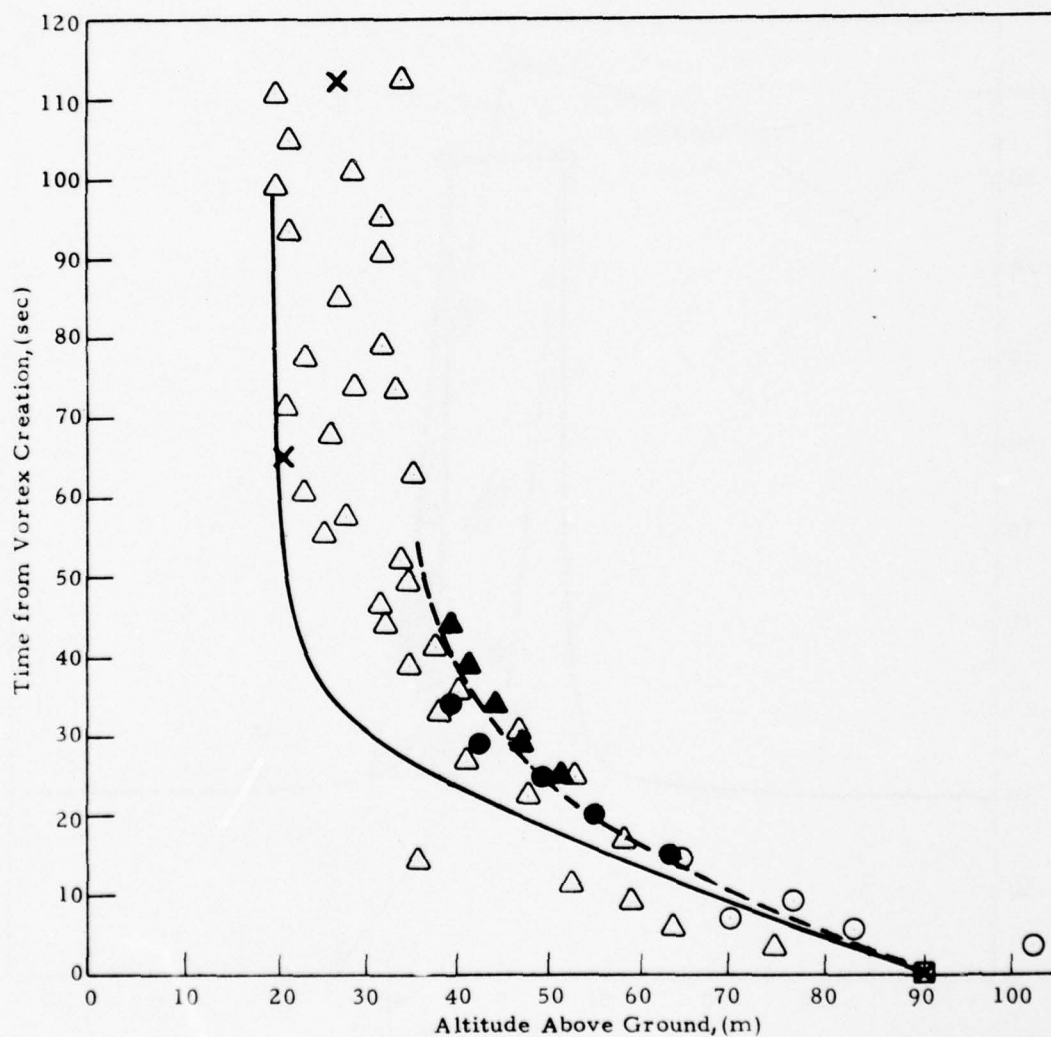


Fig. D-12 - Wake Vortex Trajectory for Rosamond Flyby 47



D-25

<u>LDV Measurement</u>	<u>Photographic Measurement</u>	<u>MAVSS</u>	<u>Theory</u>
○ Port Vortex	● Port Vortex	□ Port Vortex	— Predictive Model
△ Starboard Vortex	▲ Starboard Vortex	× Starboard Vortex	

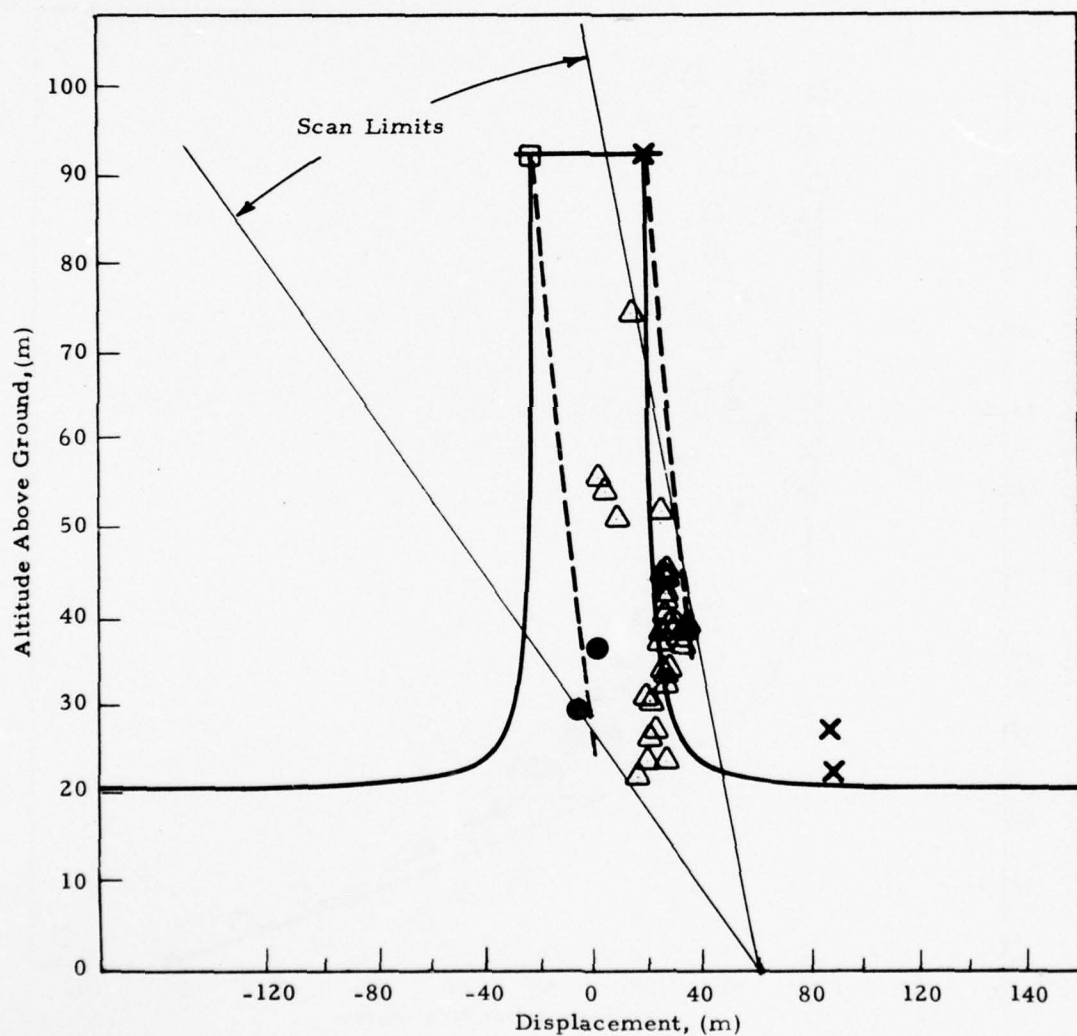


Fig. D-13 - Wake Vortex Trajectory for Rosamond Flyby 48

<u>LDV Measurement</u>	<u>Photographic Measurement</u>	<u>MAVSS</u>	<u>Theory</u>
○ Port Vortex	● Port Vortex	□ Port Vortex	— Predictive Model
△ Starboard Vortex	▲ Starboard Vortex	× Starboard Vortex	

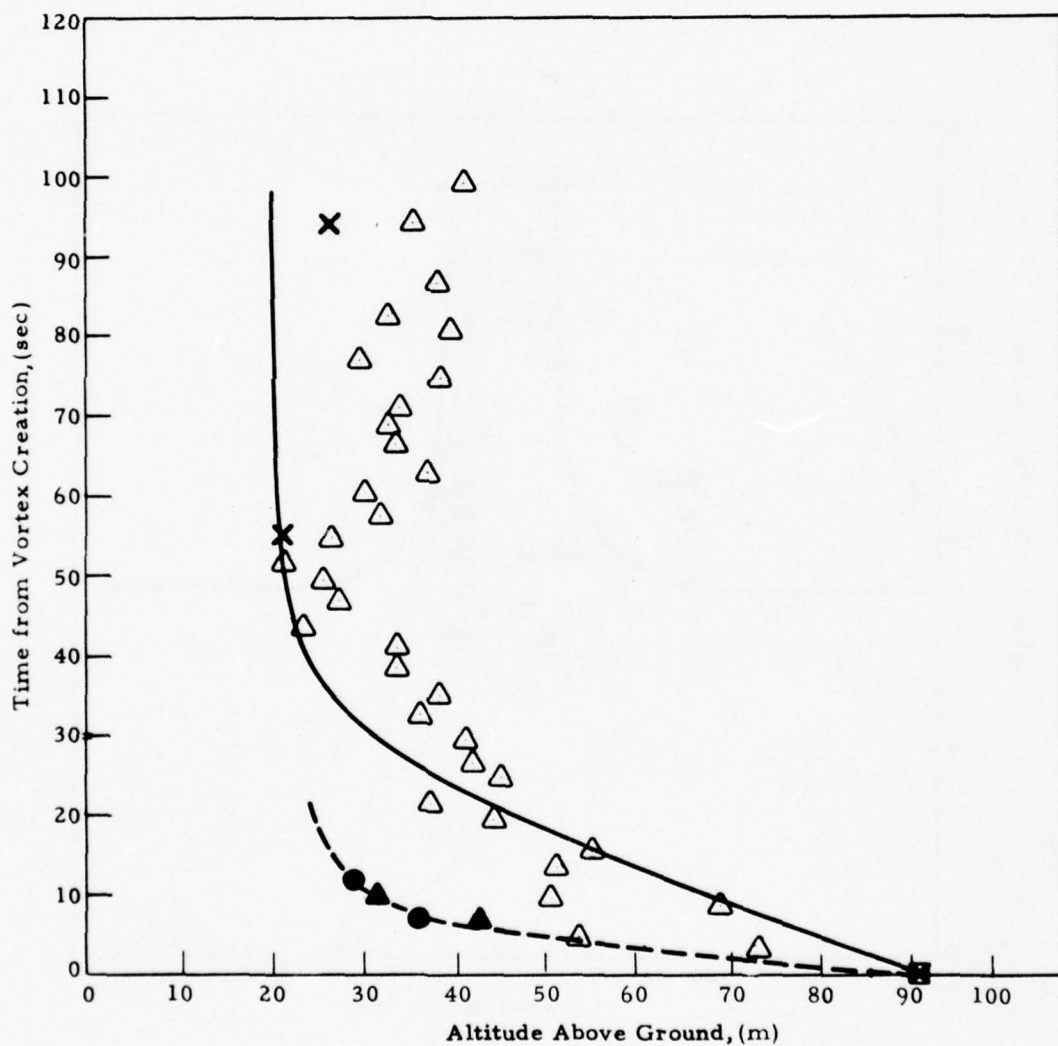


Fig. D-13 - (Concluded)

<u>LDV Measurement</u>	<u>Photographic Measurement</u>	<u>MAVSS</u>	<u>Theory</u>
○ Port Vortex	● Port Vortex	□ Port Vortex	— Predictive Model
△ Starboard Vortex	▲ Starboard Vortex	× Starboard Vortex	

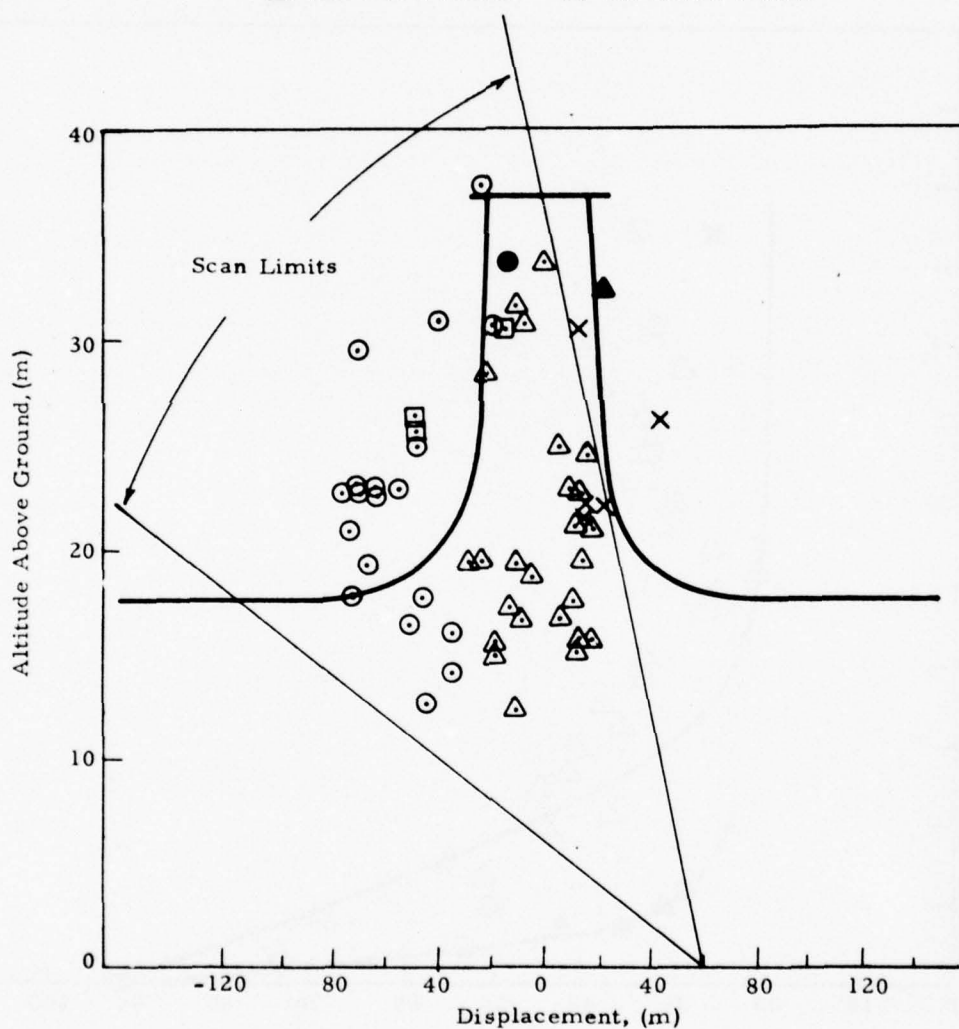


Fig. D-14 - Wake Vortex Trajectory for Rosamond Flyby 49

<u>LDV Measurement</u>	<u>Photographic Measurement</u>	<u>MAVSS</u>	<u>Theory</u>
○ Port Vortex	● Port Vortex	□ Port Vortex	— Predictive Model
△ Starboard Vortex	▲ Starboard Vortex	× Starboard Vortex	

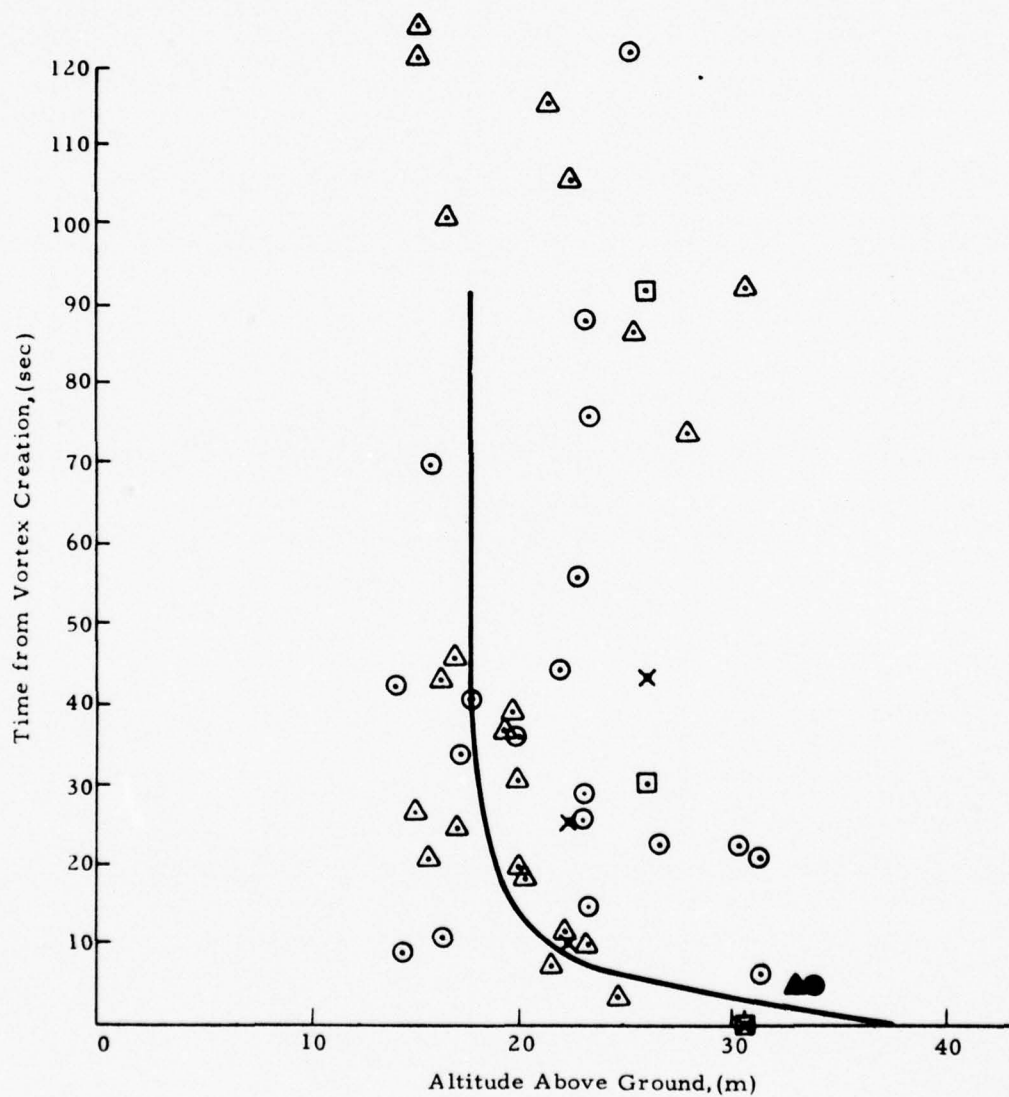
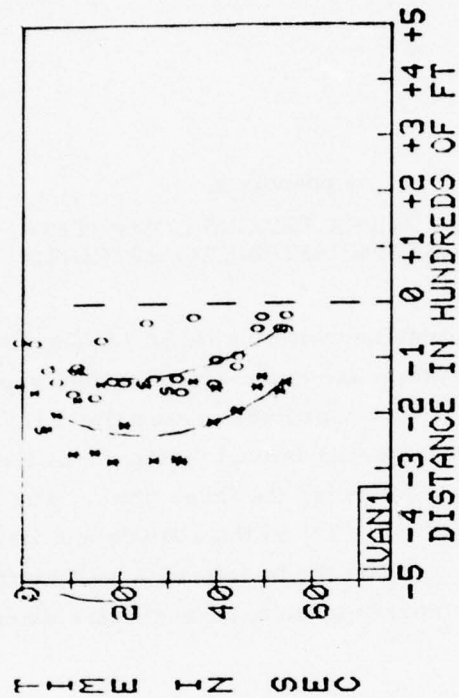
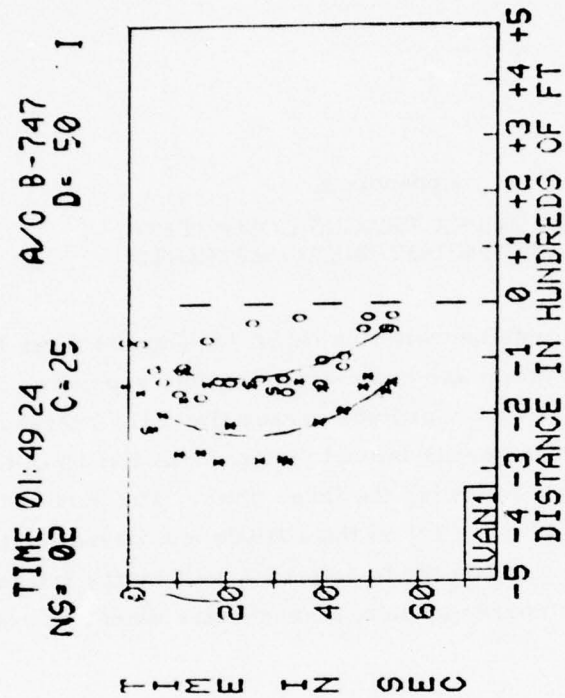


Fig. D-14 - (Concluded)

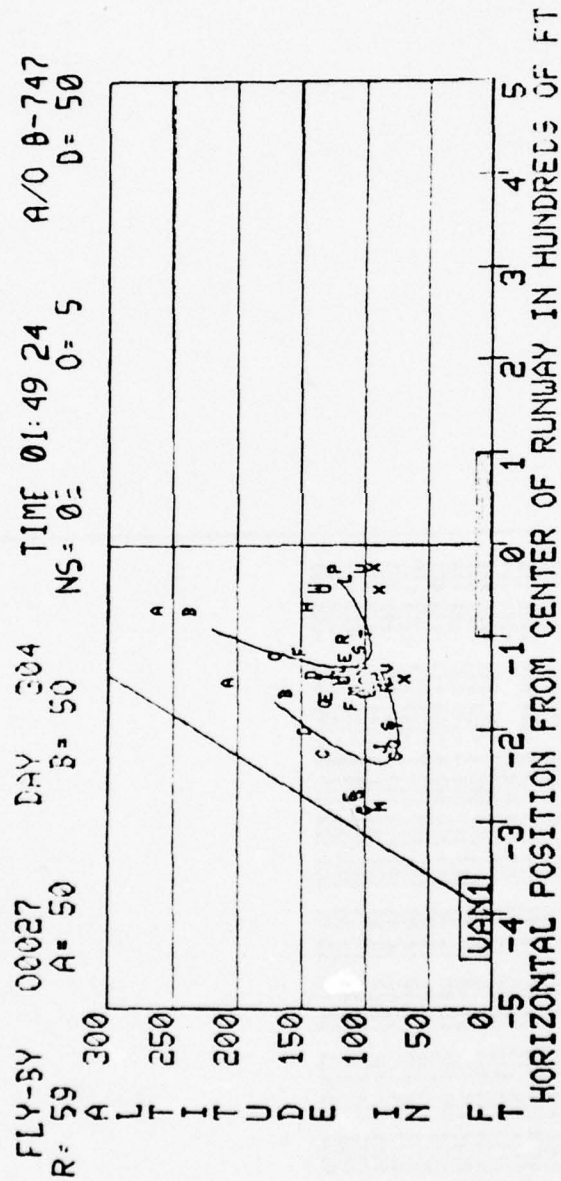
Appendix E
WAKE VORTEX TRACKS COMPUTED
FROM HIGH-SPEED MEASUREMENTS

The measurements obtained with the NASA high-speed filter bank and processor and software system are summarized in this appendix. The output consists of three plots: (1) vortex altitude versus time; (2) lateral distance versus time; and (3) altitude versus lateral distance. A listing of the vortex locations is given in a table following the three plots. The port and starboard vortices are indicated by (0*) and (*) on the altitude and lateral distance versus time plots. The vortices are labeled by letters A to Z on the lateral distance plots (each pair of letters corresponds to a successive elevation scan frame).

BEST AVAILABLE COPY



BEST AVAILABLE COPY

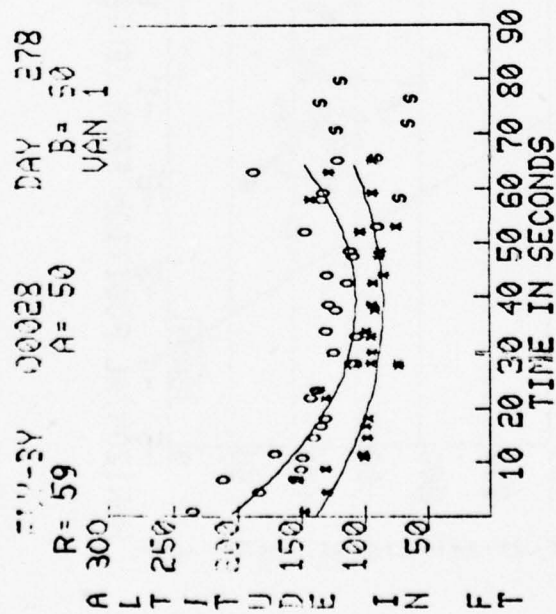
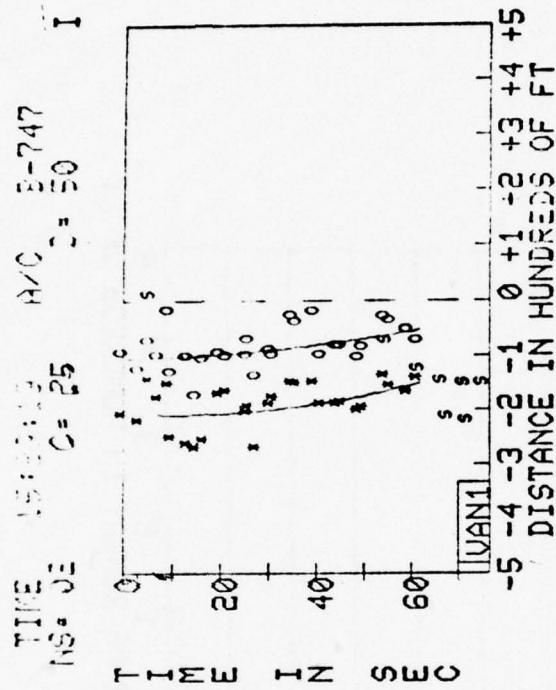


BEST AVAILABLE COPY

FLY-BY 00027 DAY 304 TIME 01 49 24- A/C B-747 I
 00 33 A= 50 B= 50 NG= 02 C= 25 D= 50

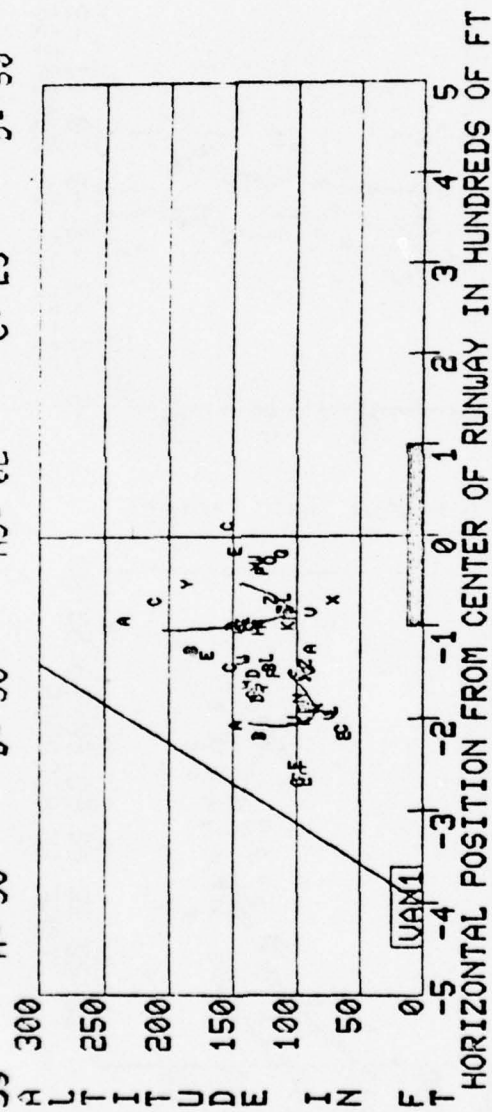
[illegible]

BEST AVAILABLE COPY



BEST AVAILABLE COPY

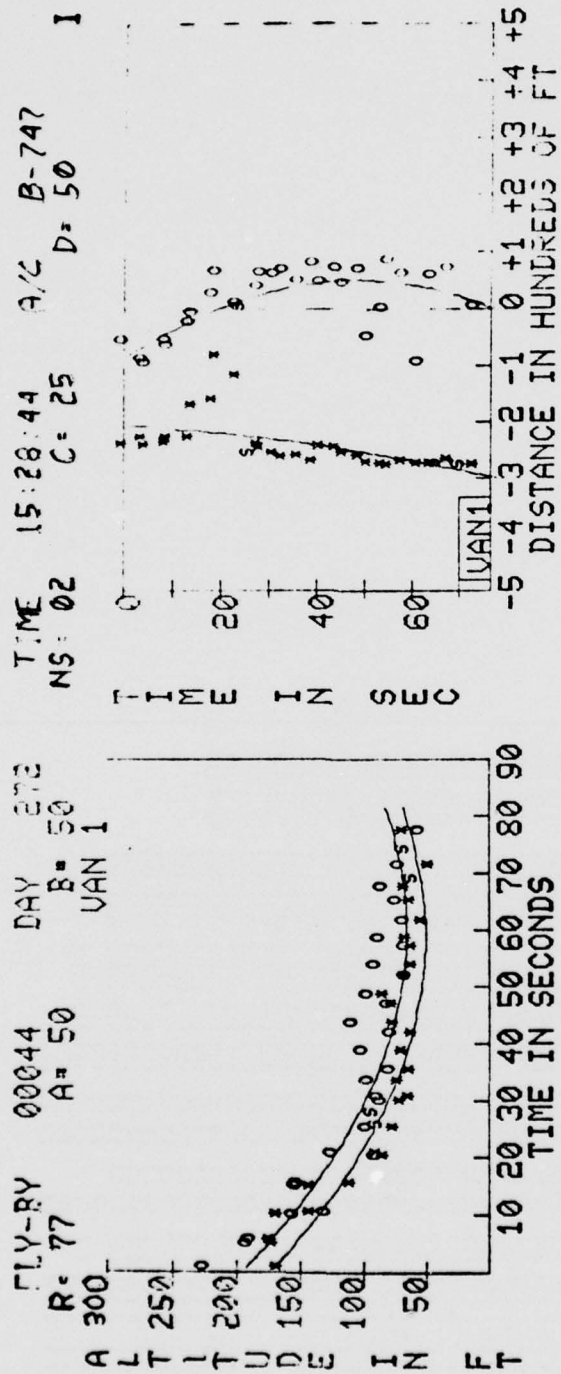
FLY-BY 00028 DAY 278 TIME 15 26:05 A/C B-747
 R-59 A= 50 B= 50 C= 25 D= 50 I



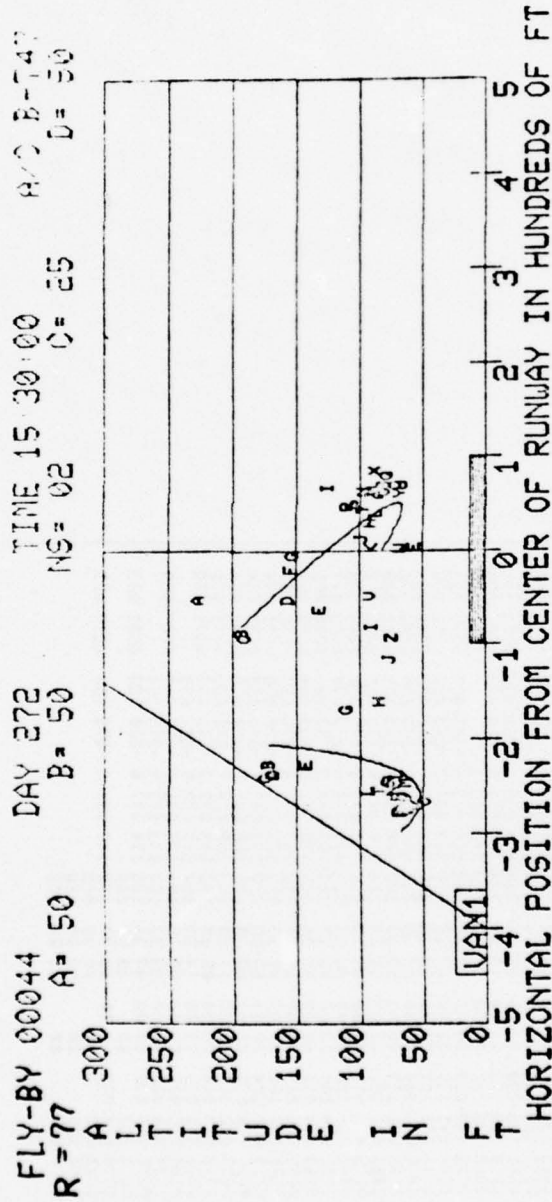
BEST AVAILABLE COPY

[illegible][illegible]

BEST AVAILABLE COPY

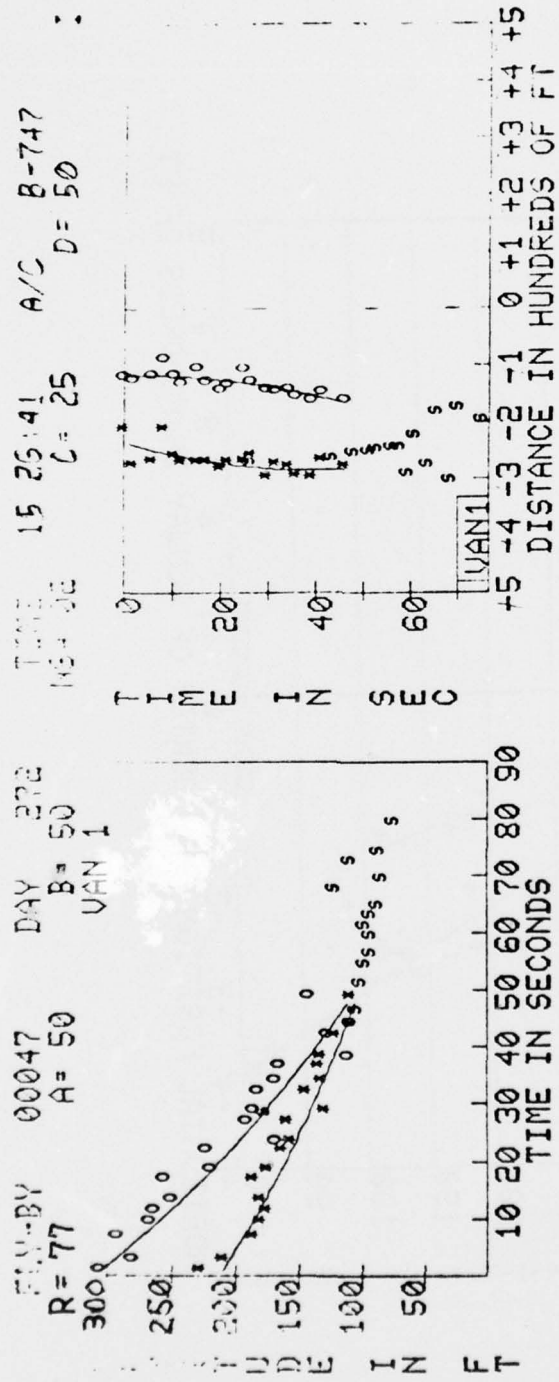


BEST AVAILABLE COPY



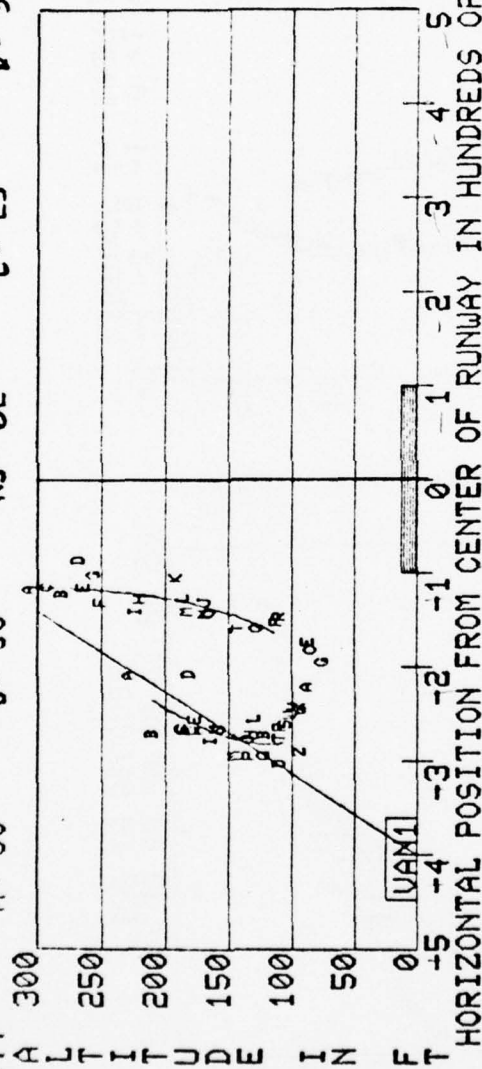
[illegible]

BEST AVAILABLE COPY



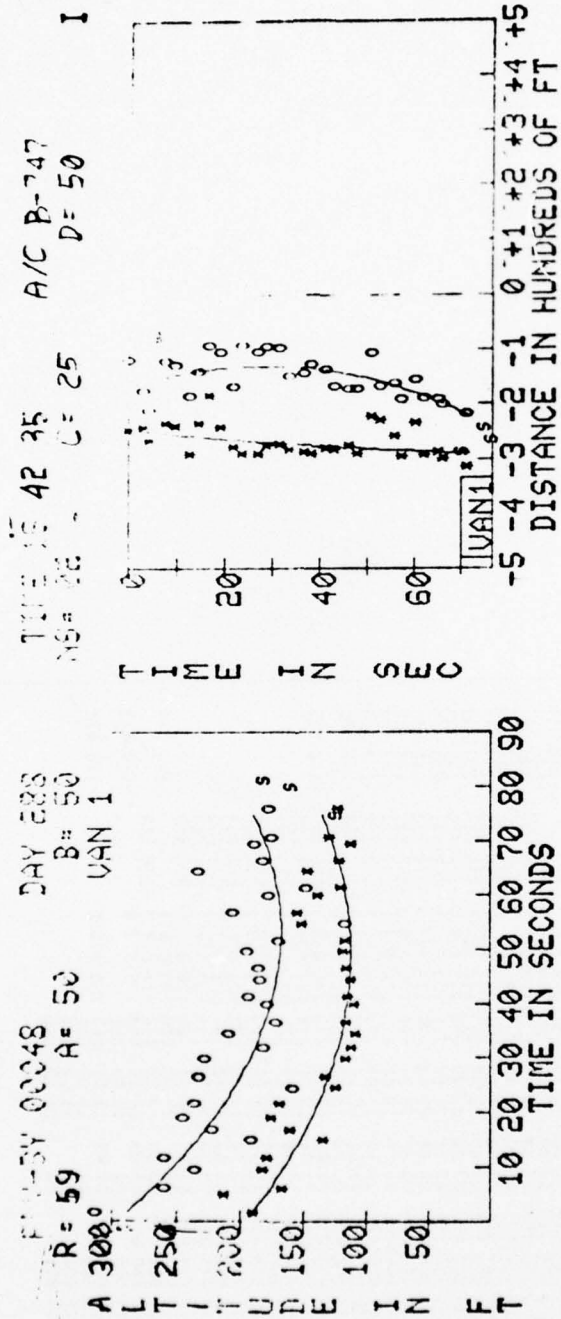
BEST AVAILABLE COPY

FLY-BY 00047 DAY 272 TIME 15:30.12 A/C B-747
 R= 77 A= 50 NS= 02 C= 25 D= 50

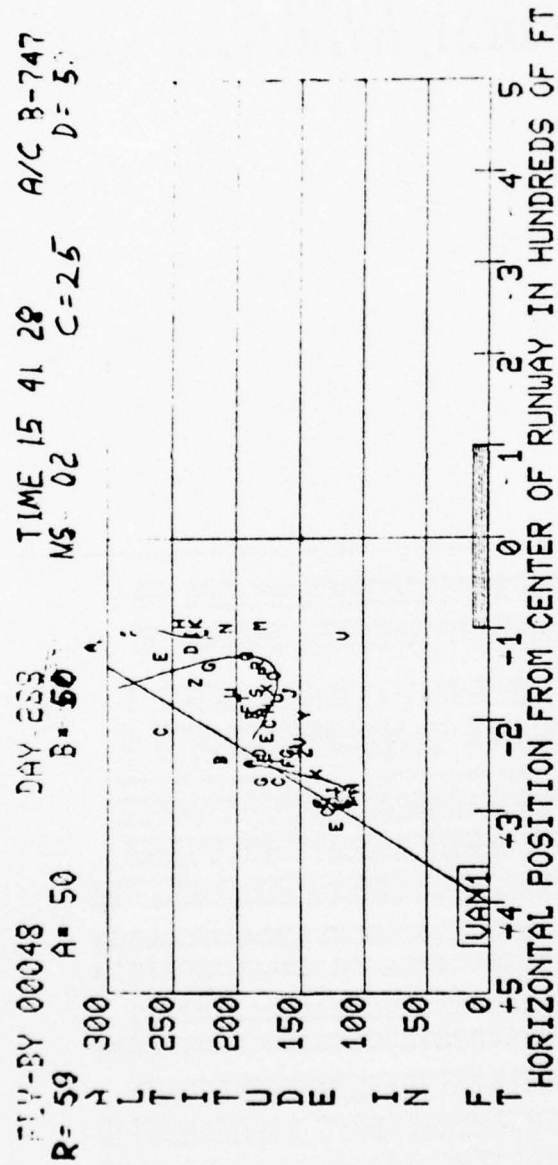


[illegible]

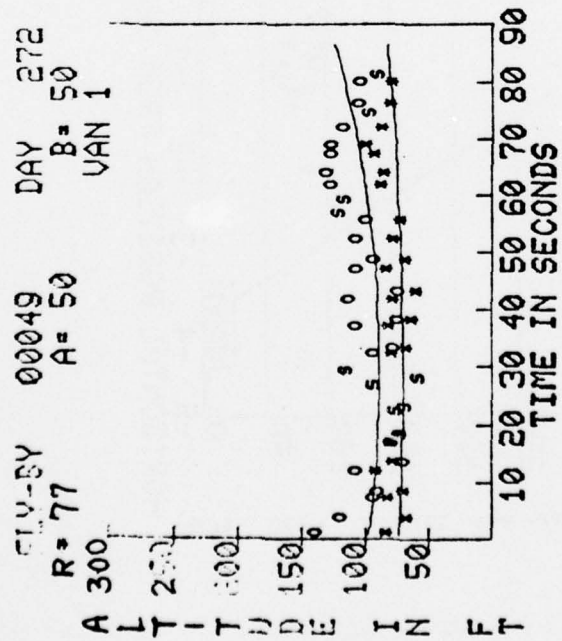
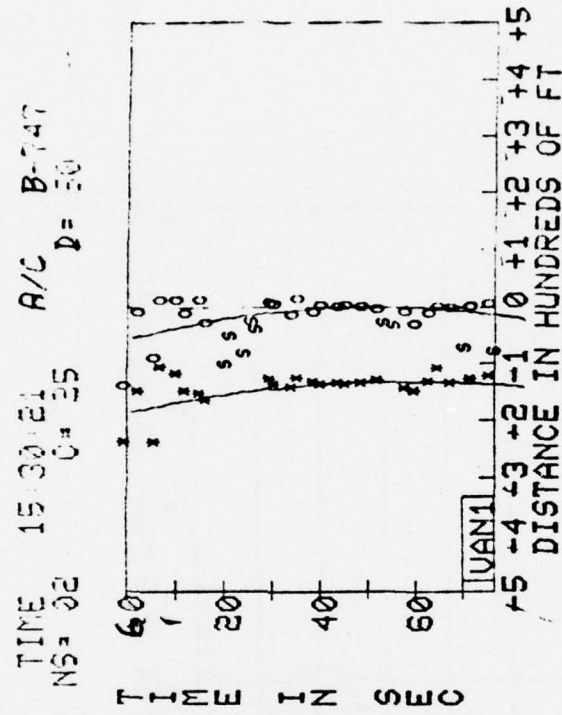
BEST AVAILABLE COPY



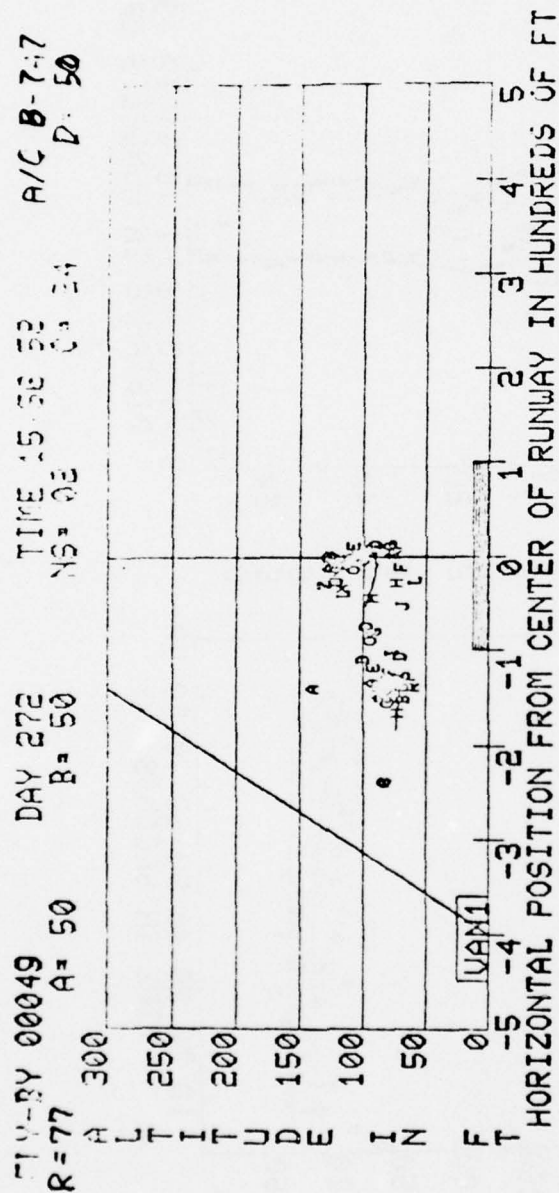
BEST AVAILABLE COPY



BEST AVAILABLE COPY



BEST AVAILABLE COPY



Appendix F
TIME HISTORY OF VORTEX ROTATIONAL VELOCITY

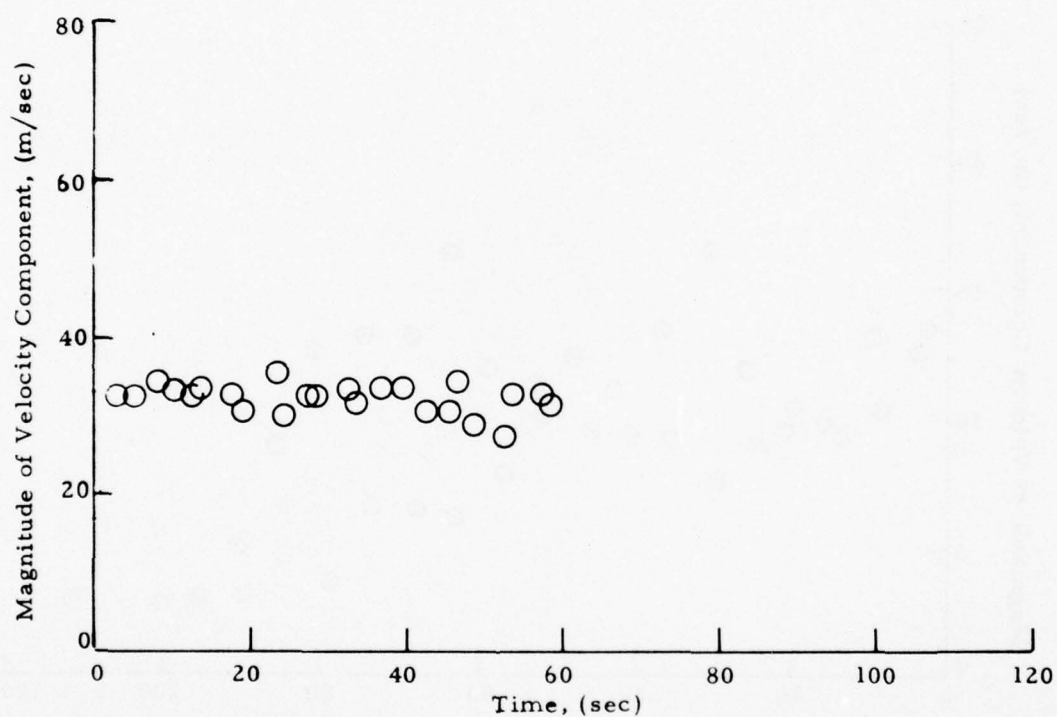


Fig. F-1 $-|V_{pk}|$ as a Function of Time for Rosamond B-747 Flyby 24
(from High-Speed Data)

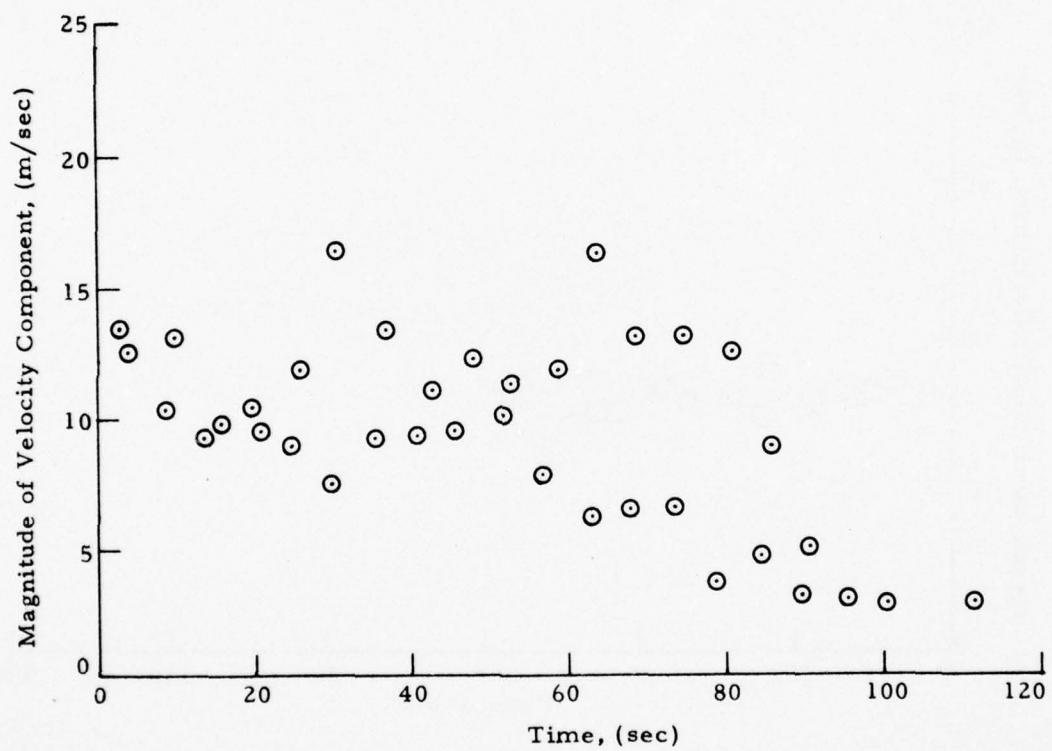


Fig. F-2 $|V_{ms}|$ as a Function of Time for Rosamond B-747 Flyby 24
(from Low-Speed Data)

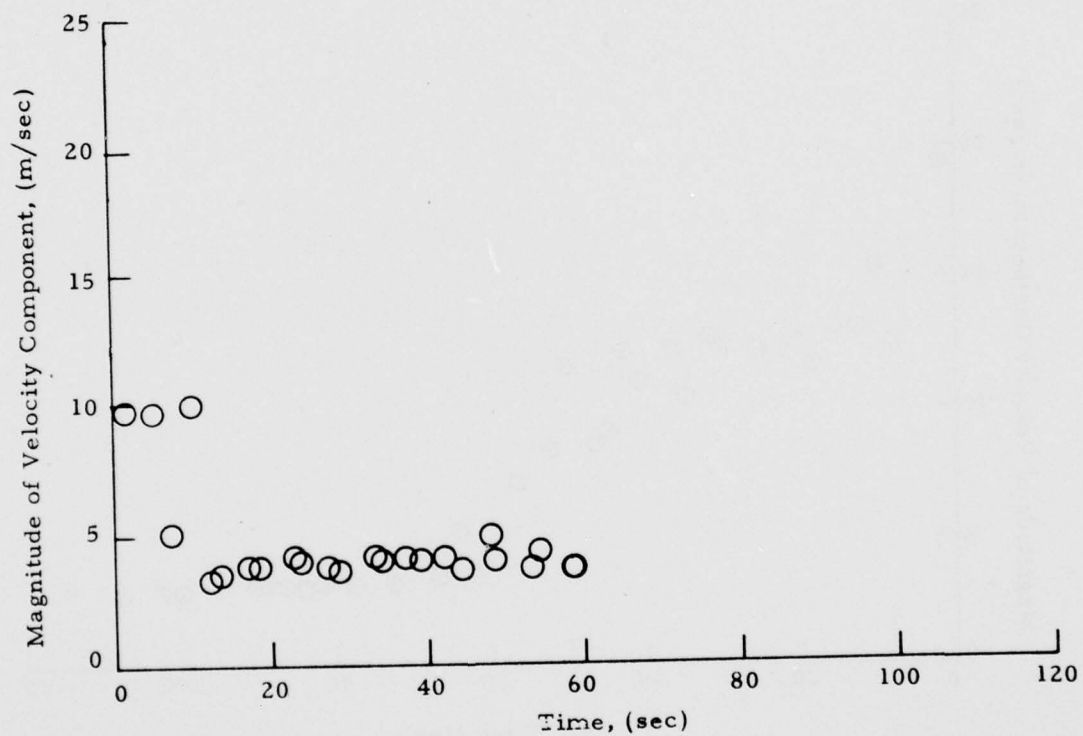


Fig. F-3 $-|V_{ms}|$ as a Function of Time for Rosamond B-747 Flyby 24
(from High-Speed Data)

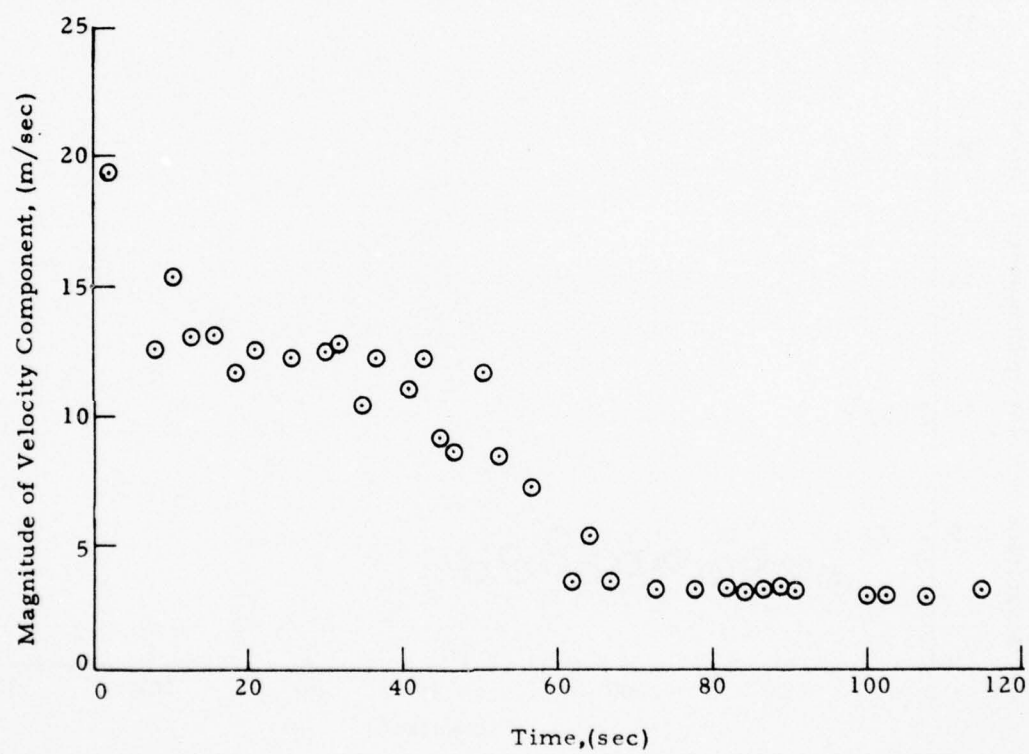


Fig. F-4 - $|V_{ms}|$ as a Function of Time for Rosamond B-747 Flyby 25
(from Low-Speed Data)

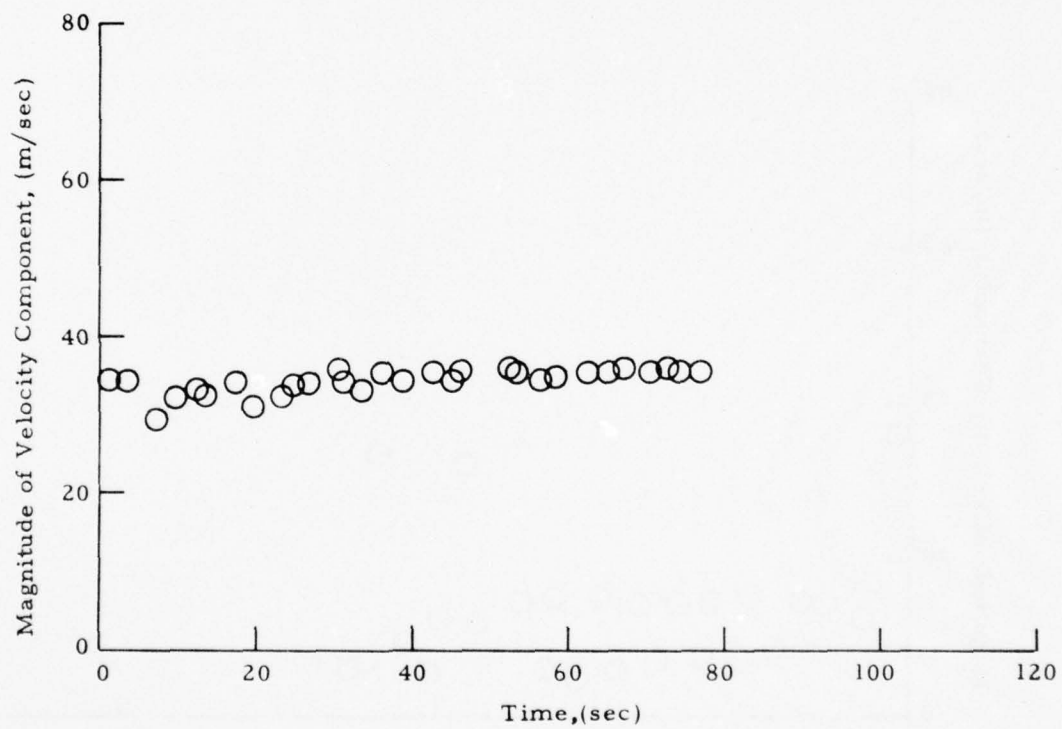


Fig. F-5 - $|V_{pk}|$ as a Function of Time for Rosamond B-747 Flyby 27
(from high speed data)

AD-A048 275

LOCKHEED MISSILES AND SPACE CO INC HUNTSVILLE ALA HU--ETC F/G 1/1
LASER DOPPLER VELOCIMETER MEASUREMENTS OF B-747 WAKE VORTEX CHA--ETC(U).
SEP 77 M R BRASHEARS, A D ZALAY DOT-TSC-1145

UNCLASSIFIED

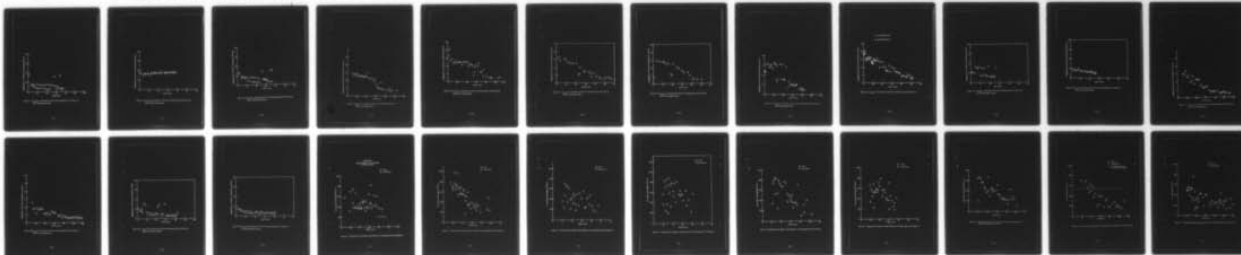
LMSC-HREC-TR-D496975

FAA-RD-77-85

NL

3 OF 3

AD
A048275



END
DATE
FILMED

2- 78

DDC

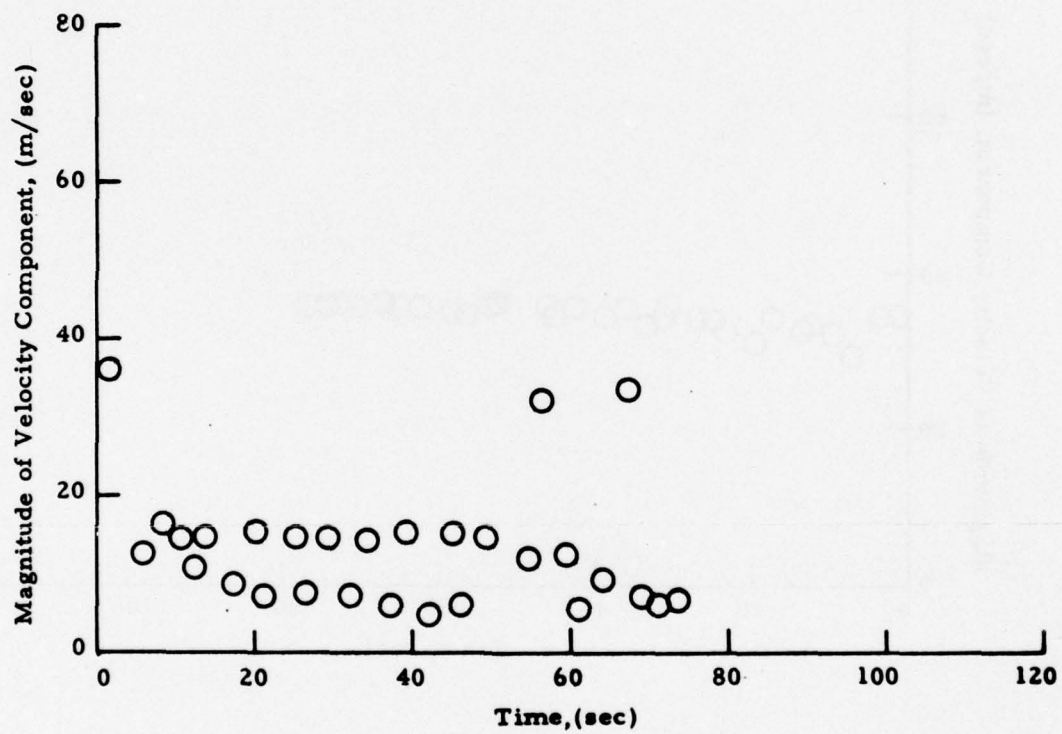


Fig. F-6 - $|V_{ms}|$ as a Function of Time for Rosamond B-747 Flyby 27
(from High-Speed Data)

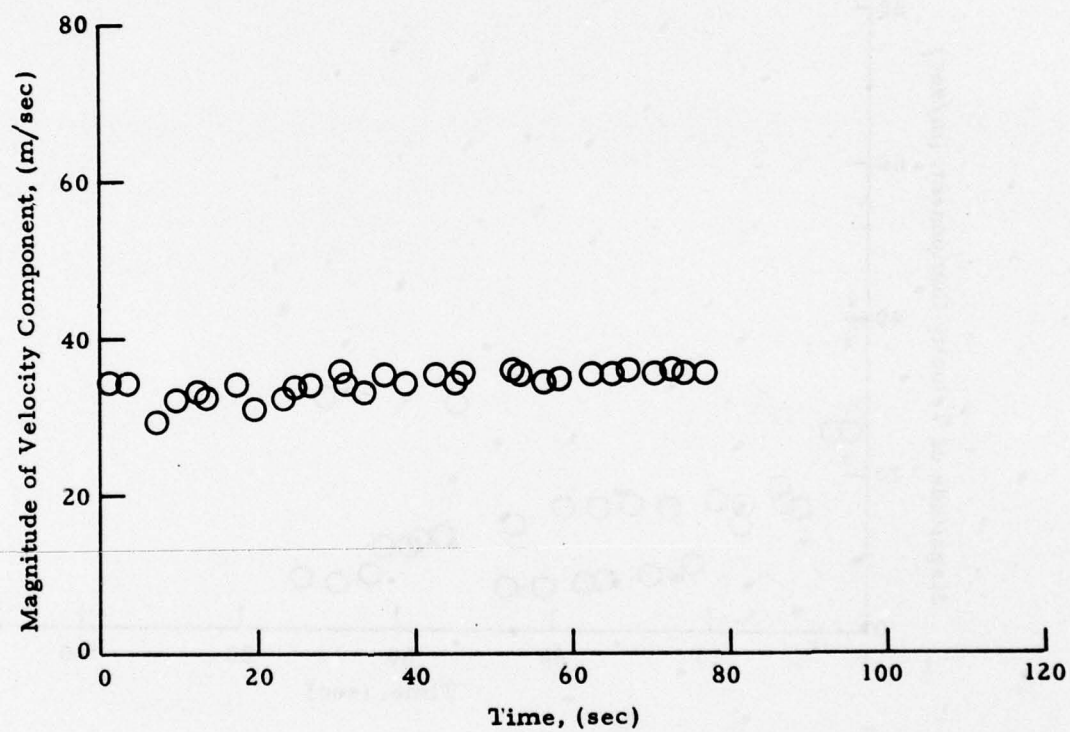


Fig. F-7 - $|V_{pk}|$ as a Function of Time for Rosamond B-747 Flyby 28
(from High-Speed Data)

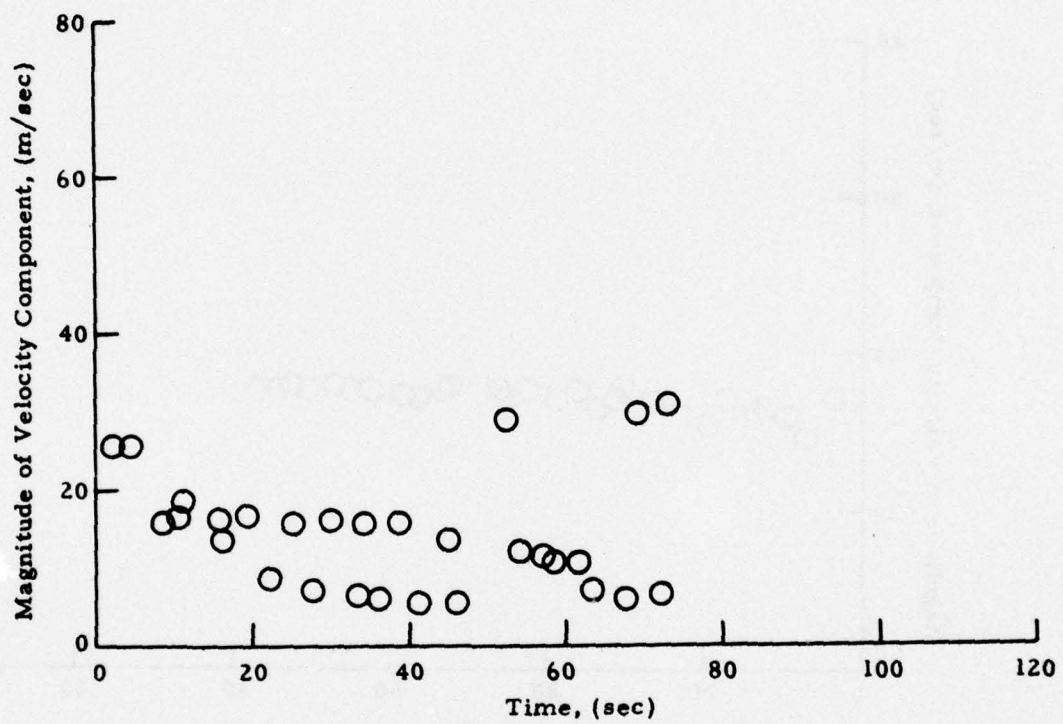


Fig. F-8 - $|V_{ms}|$ as a Function of Time for Rosamond B-747 Flyby 28
(from High-Speed Data)

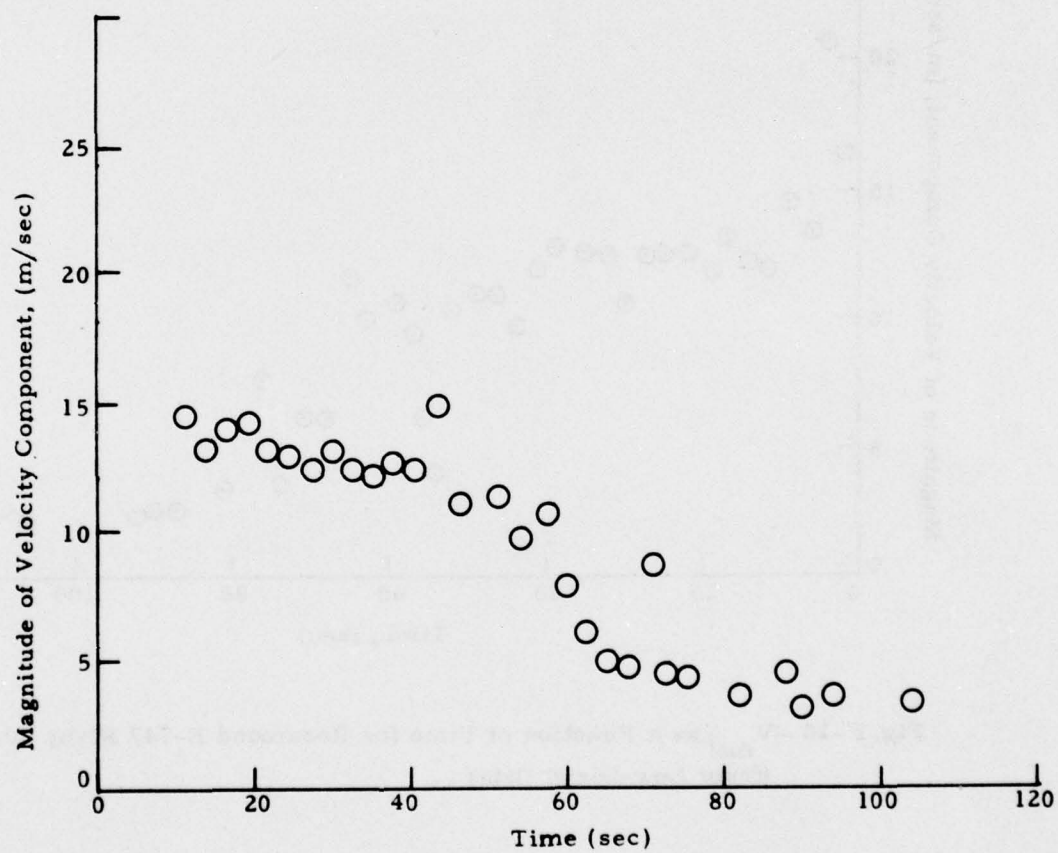


Fig. F-9 $-|V_{ms}|$ as a Function of Time for Rosamond Flyby 29
(from Low-Speed Data)

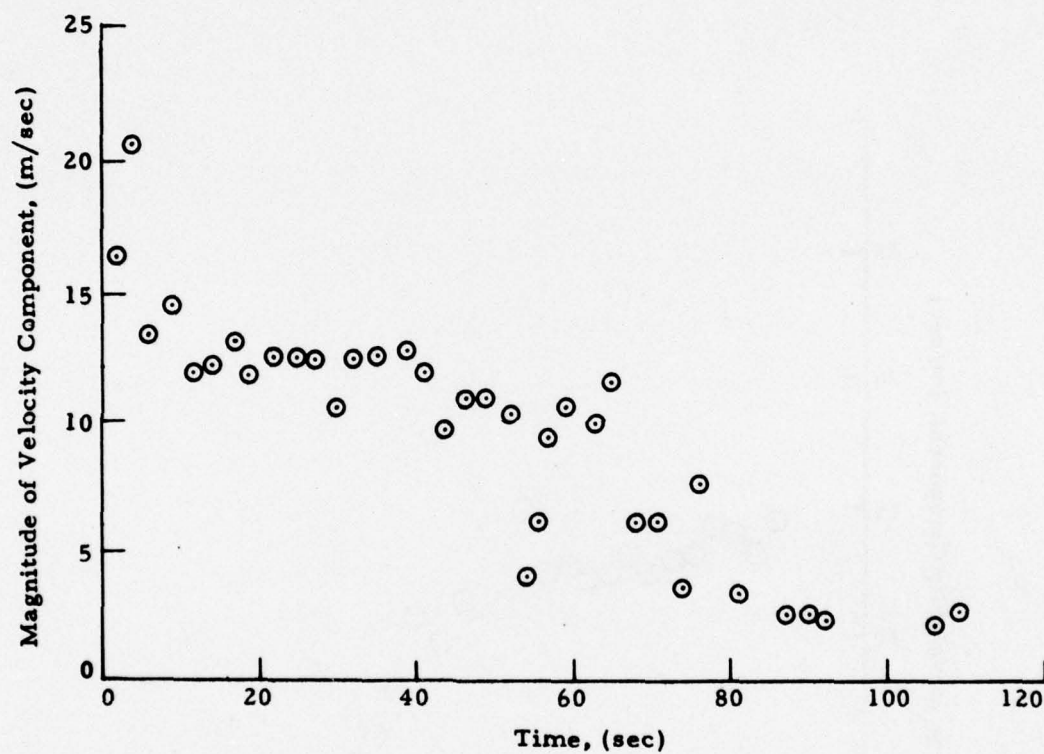


Fig. F-10 $-|V_{ms}|$ as a Function of Time for Rosamond B-747 Flyby 30
(from Low-Speed Data)

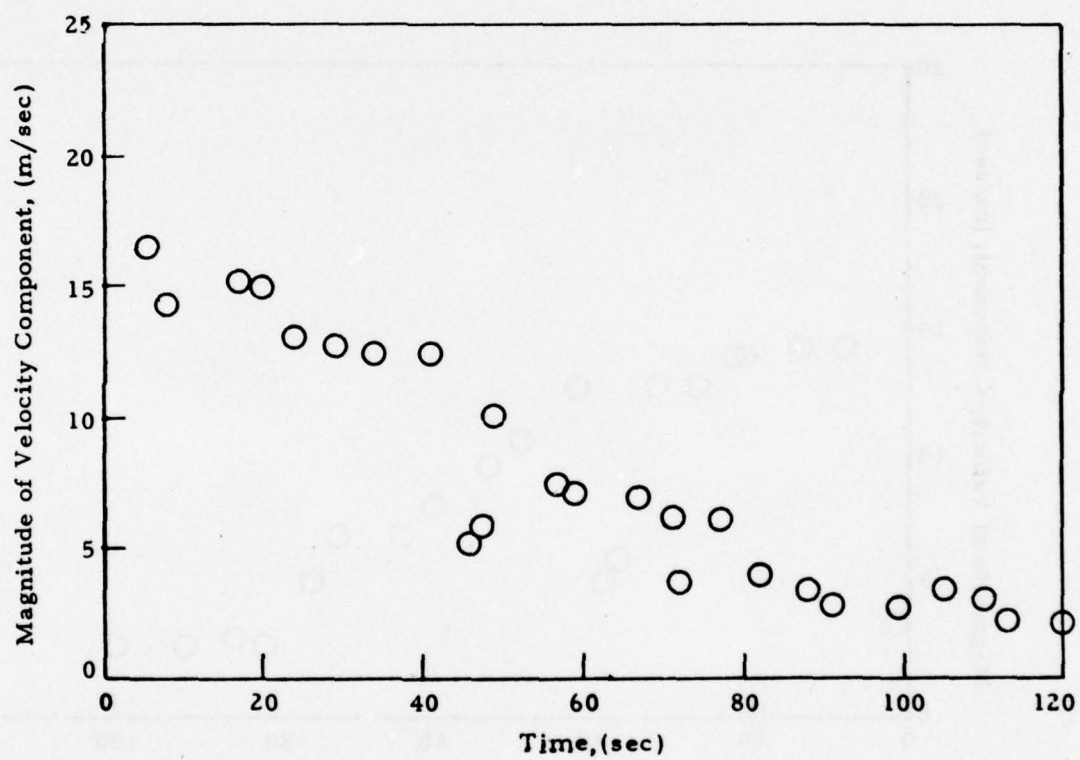


Fig. F-11 - $|V_{ms}|$ as a Function of Time for Rosamond B-747 Flyby 35
(from Low-Speed Data)

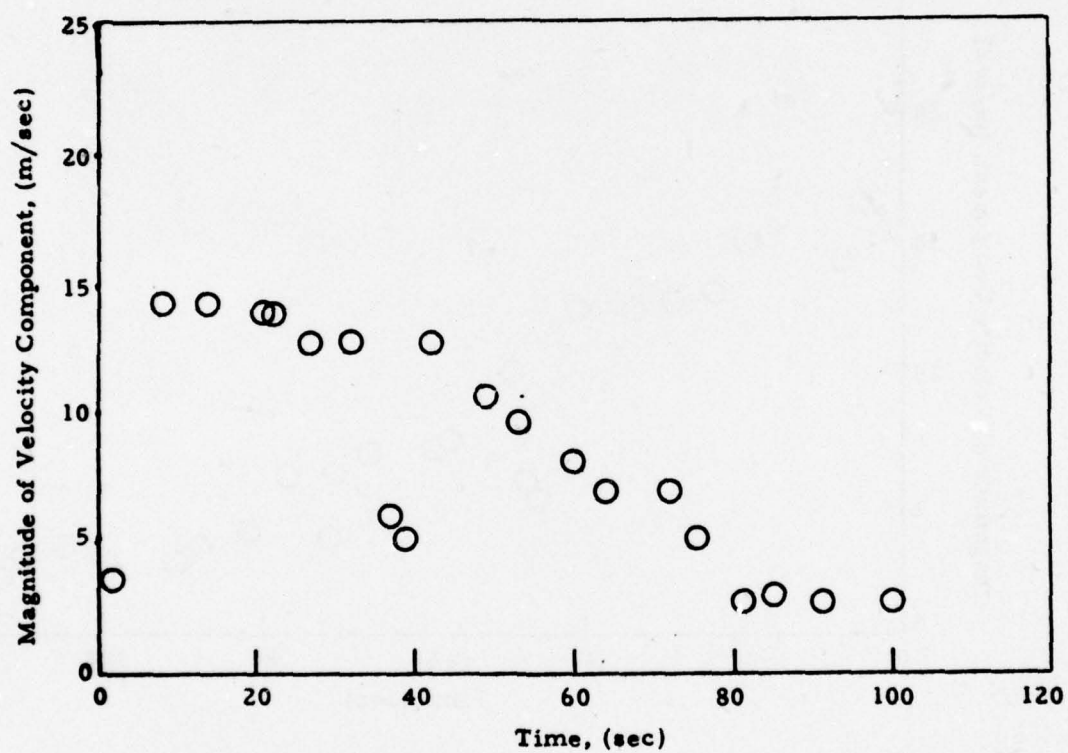


Fig. F-12 - $|V_{ms}|$ as a Function of Time for Rosamond B-747 Flyby 38
(from Low-Speed Data)

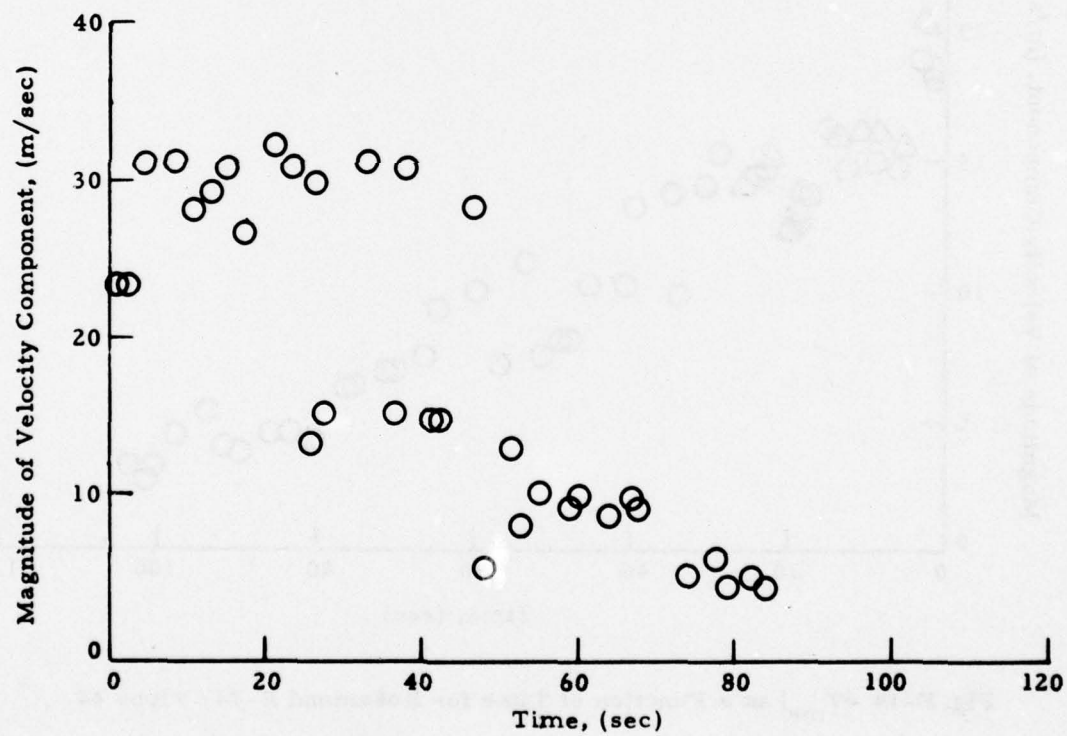


Fig. F-13 - $|V_{pk}|$ as a Function of Time for Rosamond B-747 Flyby 44
(from High Speed Data)

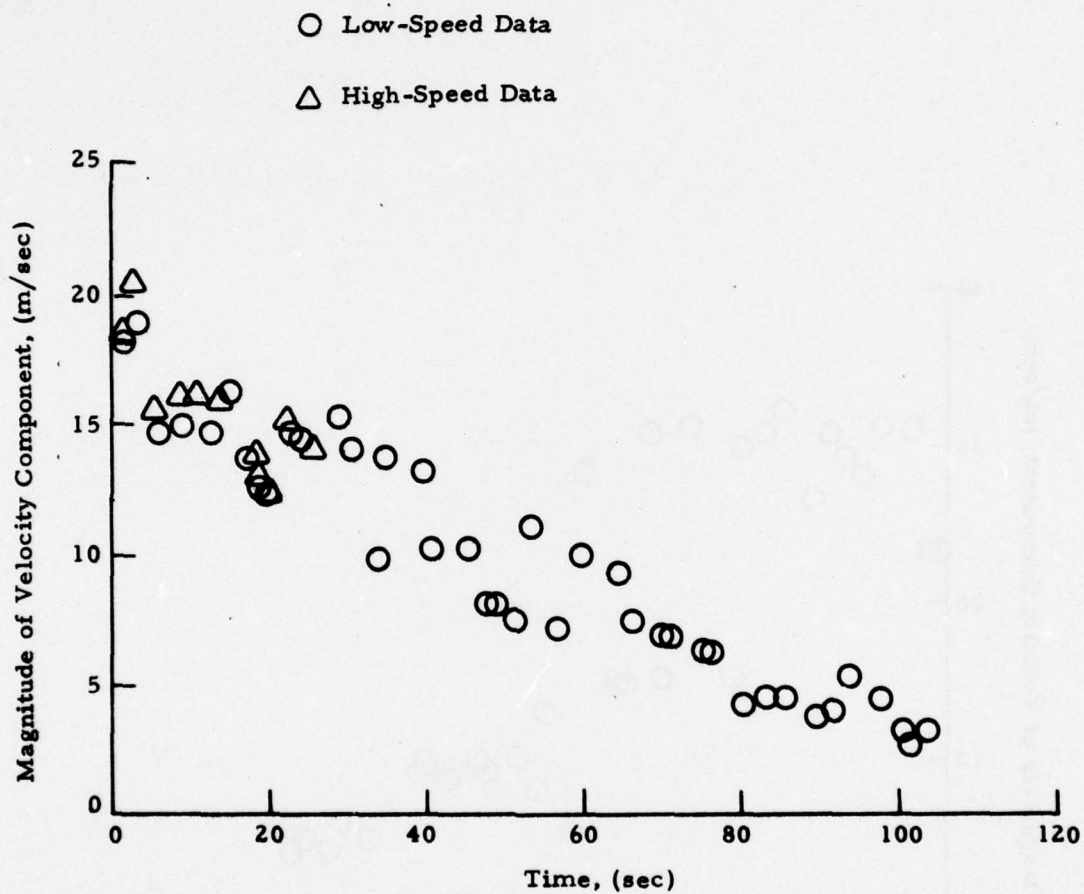


Fig. F-14 $-|V_{ms}|$ as a Function of Time for Rosamond B-747 Flyby 44

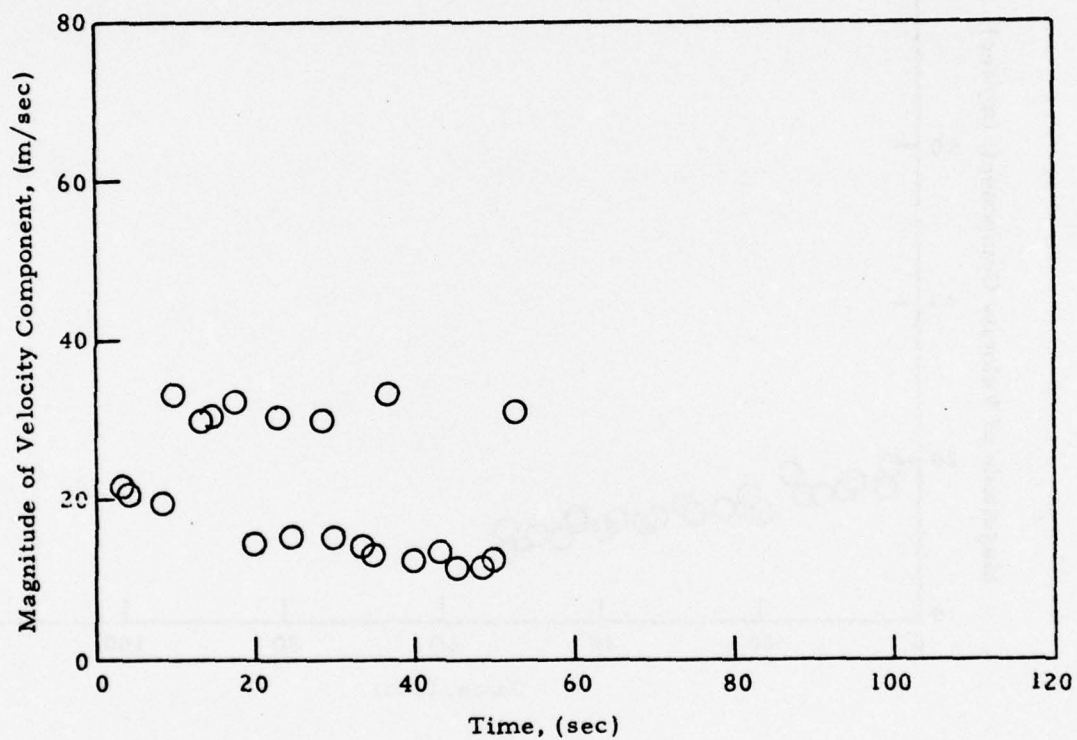


Fig. F-15 - $|V_{pk}|$ as a Function of Time for Rosamond B-747 Flyby 47
(from High-Speed Data)

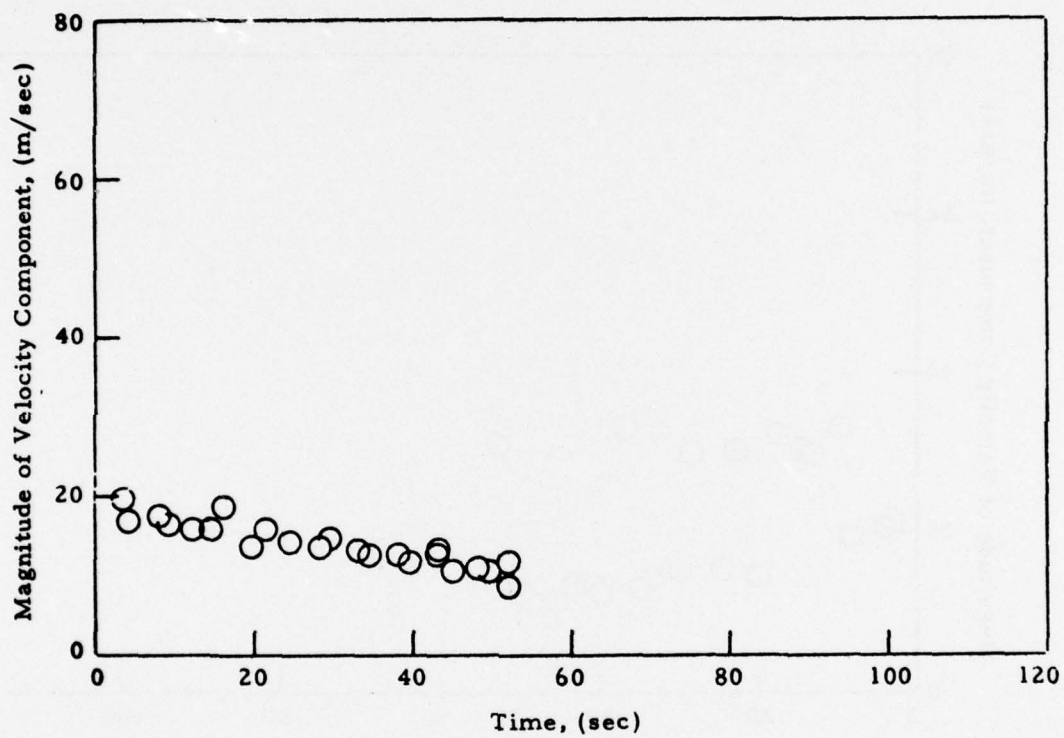


Fig. F-16 - $|V_{ms}|$ as a Function of Time for Rosamond B-747 Flyby 47
(from High-Speed Data)

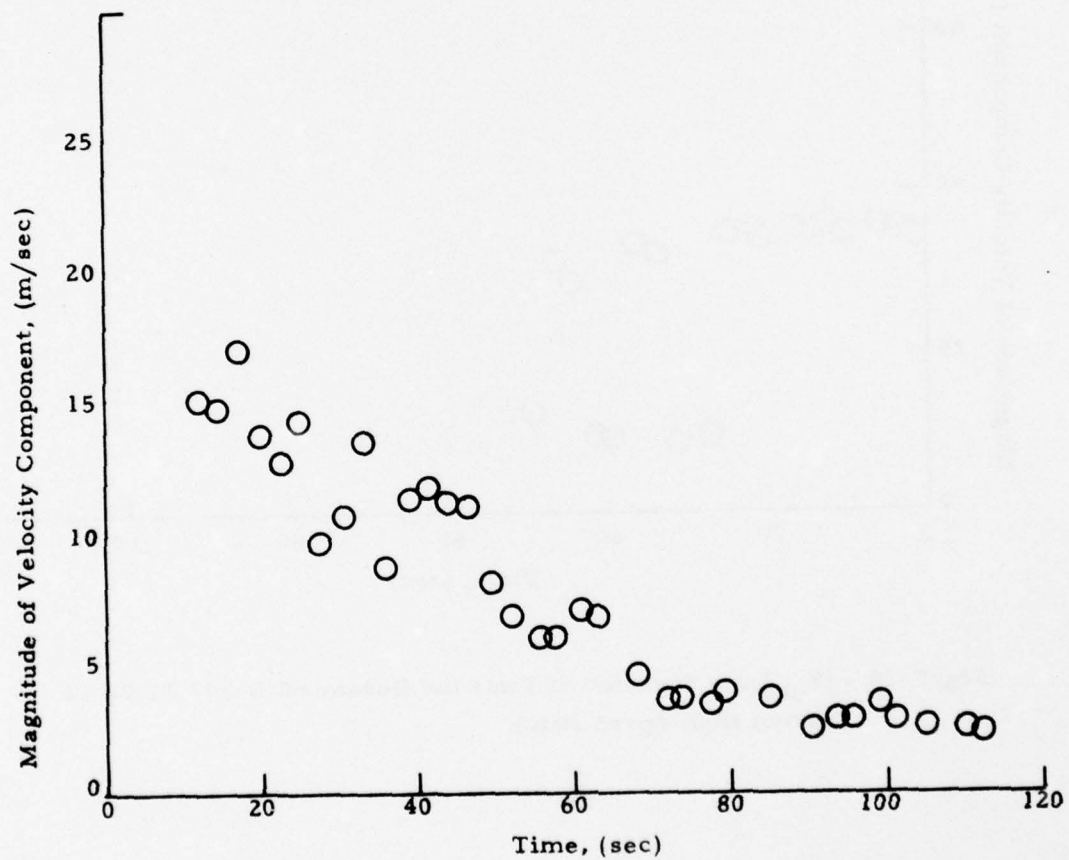


Fig. F-17 - $|V_{ms}|$ as a Function of Time for Rosamond B-747 Flyby 47
(from Low-Speed Data)

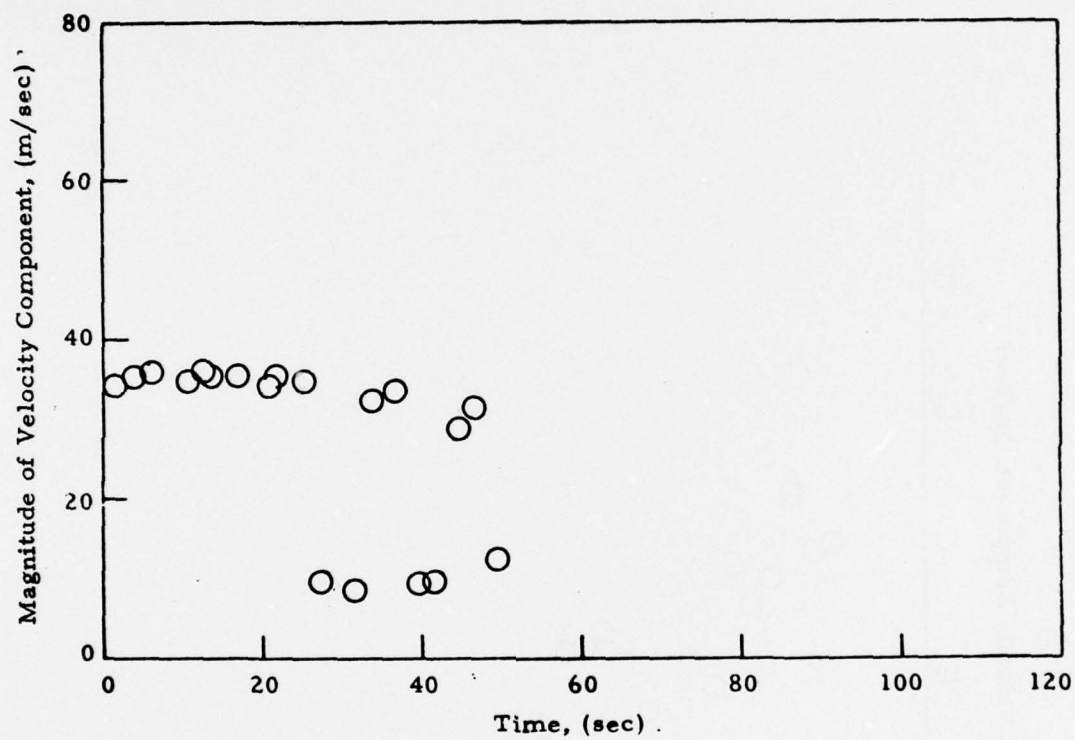


Fig. F-18 - $|V_{pk}|$ as a Function of Time for Rosamond B-747 Flyby 48
(from High-Speed Data)

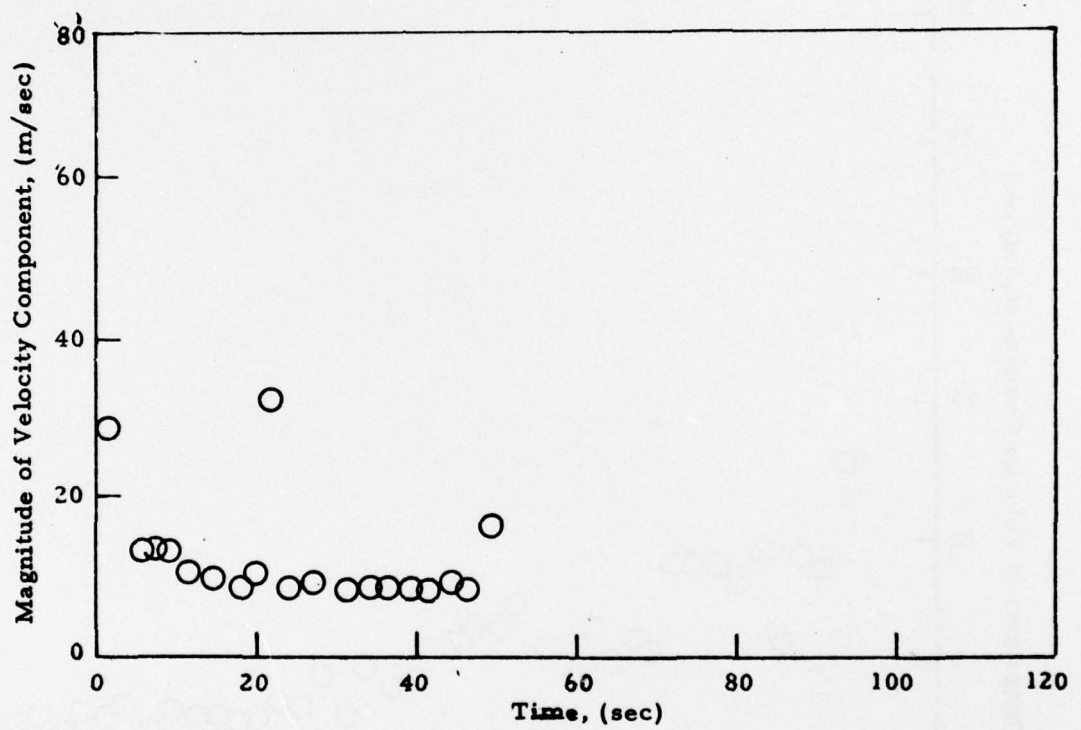


Fig. F-19 $-|V_{ms}|$ as a Function of Time for Rosamond B-747 Flyby 48
(from High-Speed Data)

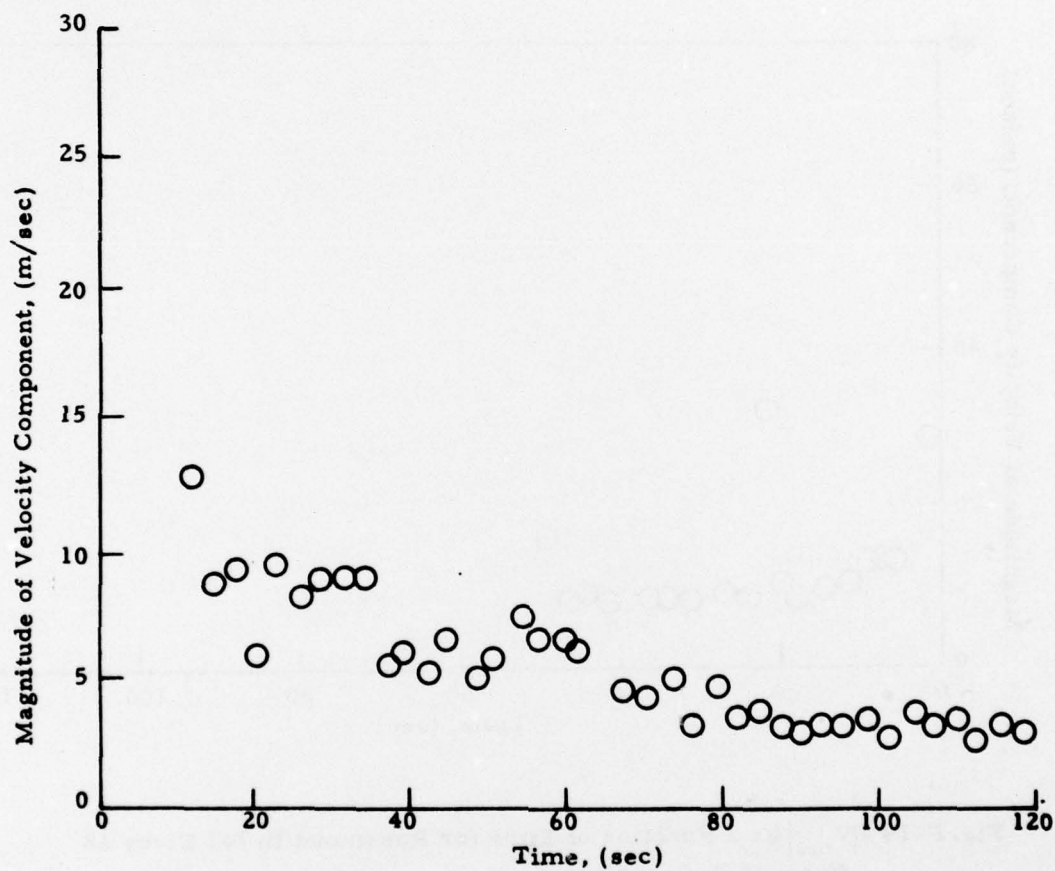


Fig. F-20- $|V_{ms}|$ as a Function of Time for Rosamond B-747 Flyby 48
(from Low-Speed Data)

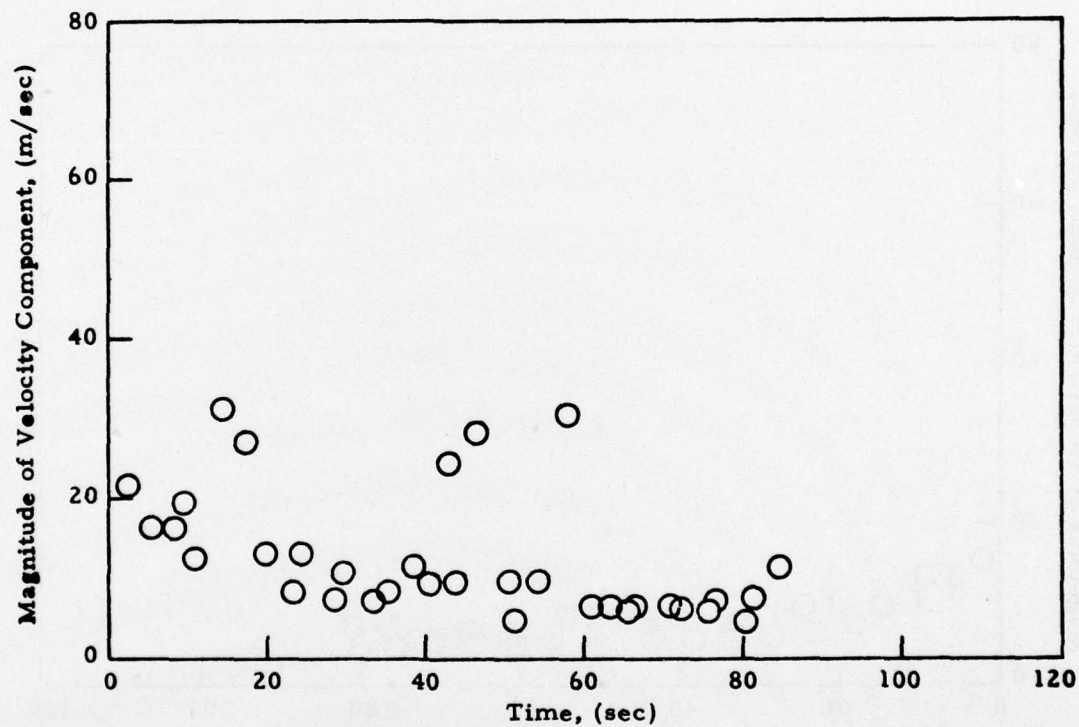


Fig. F-21 - $|V_{pk}|$ as a Function of Time for Rosamond B-747 Flyby 49
(from High-Speed Data)

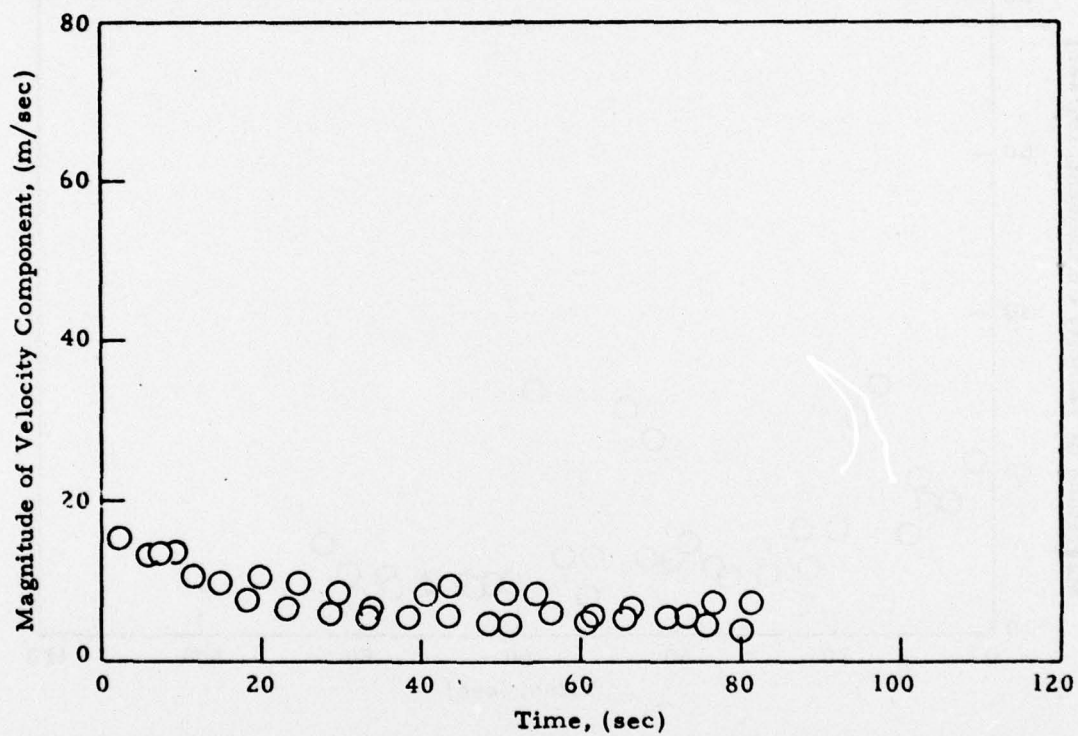


Fig. F-22 - $|V_{ms}|$ as a Function of Time for Rosamond B-747 Flyby 49
(from High-Speed Data)

Appendix G
TIME HISTORY OF VORTEX
CIRCULATION

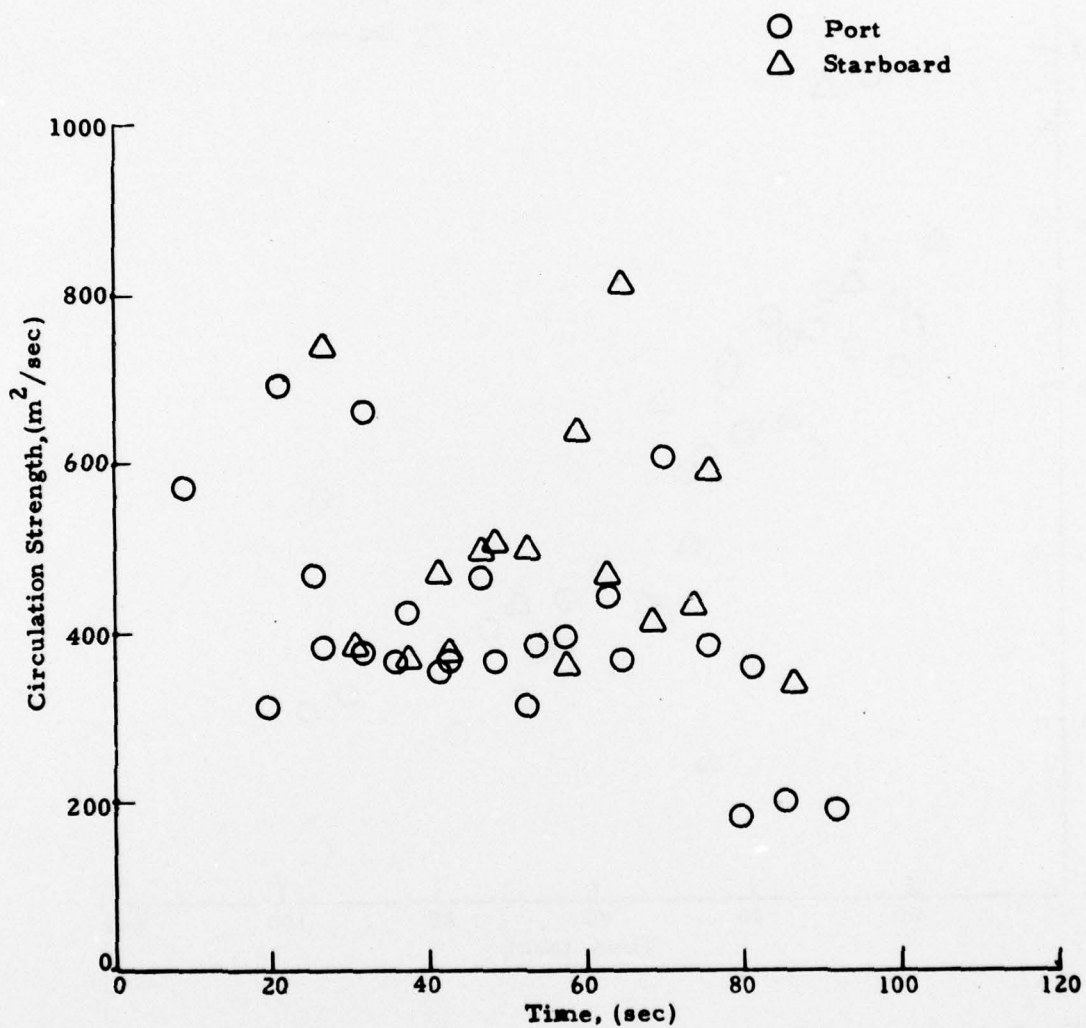


Fig. G-1 - Observed Circulation Time History for Rosamond B-747 Flyby 24

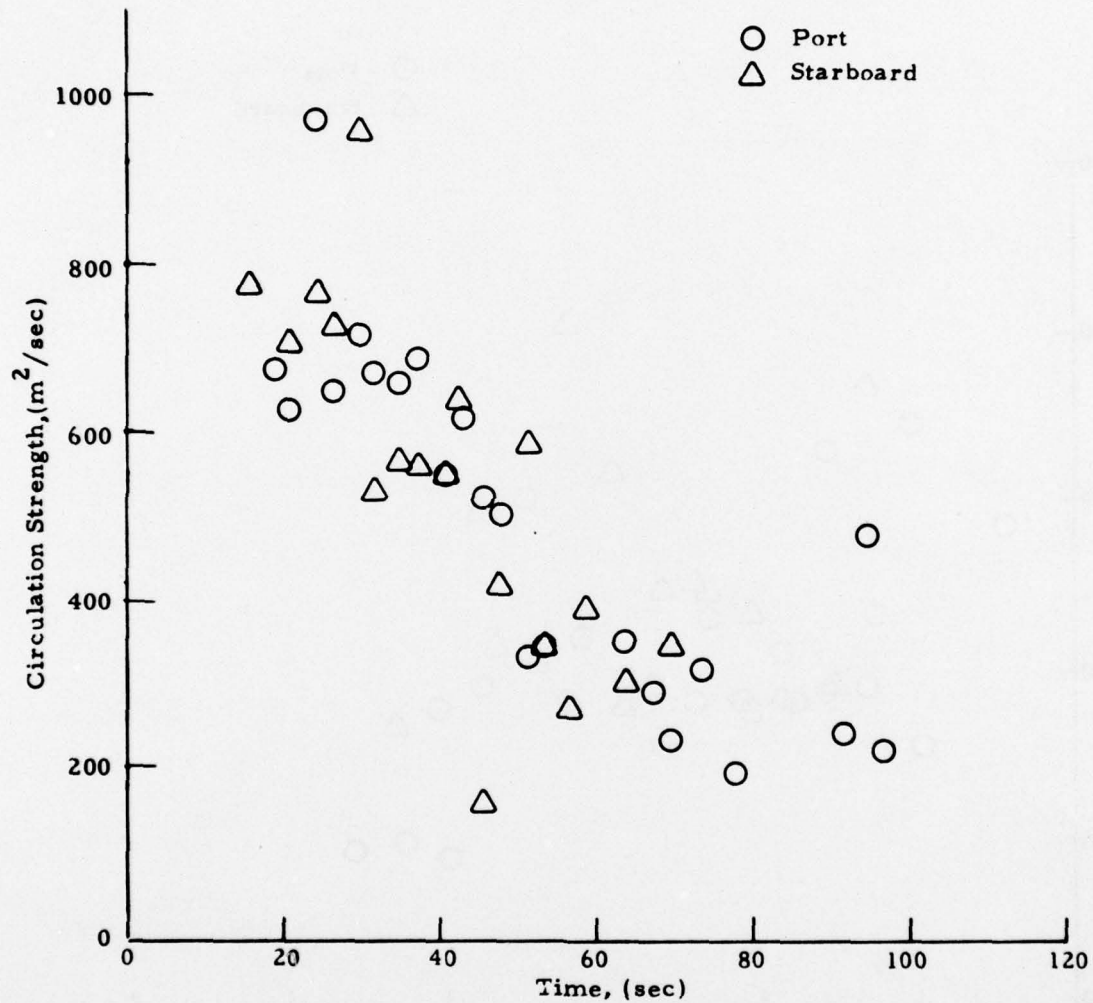


Fig.G-2 - Observed Circulation Time History for Rosamond B-747 Flyby 25

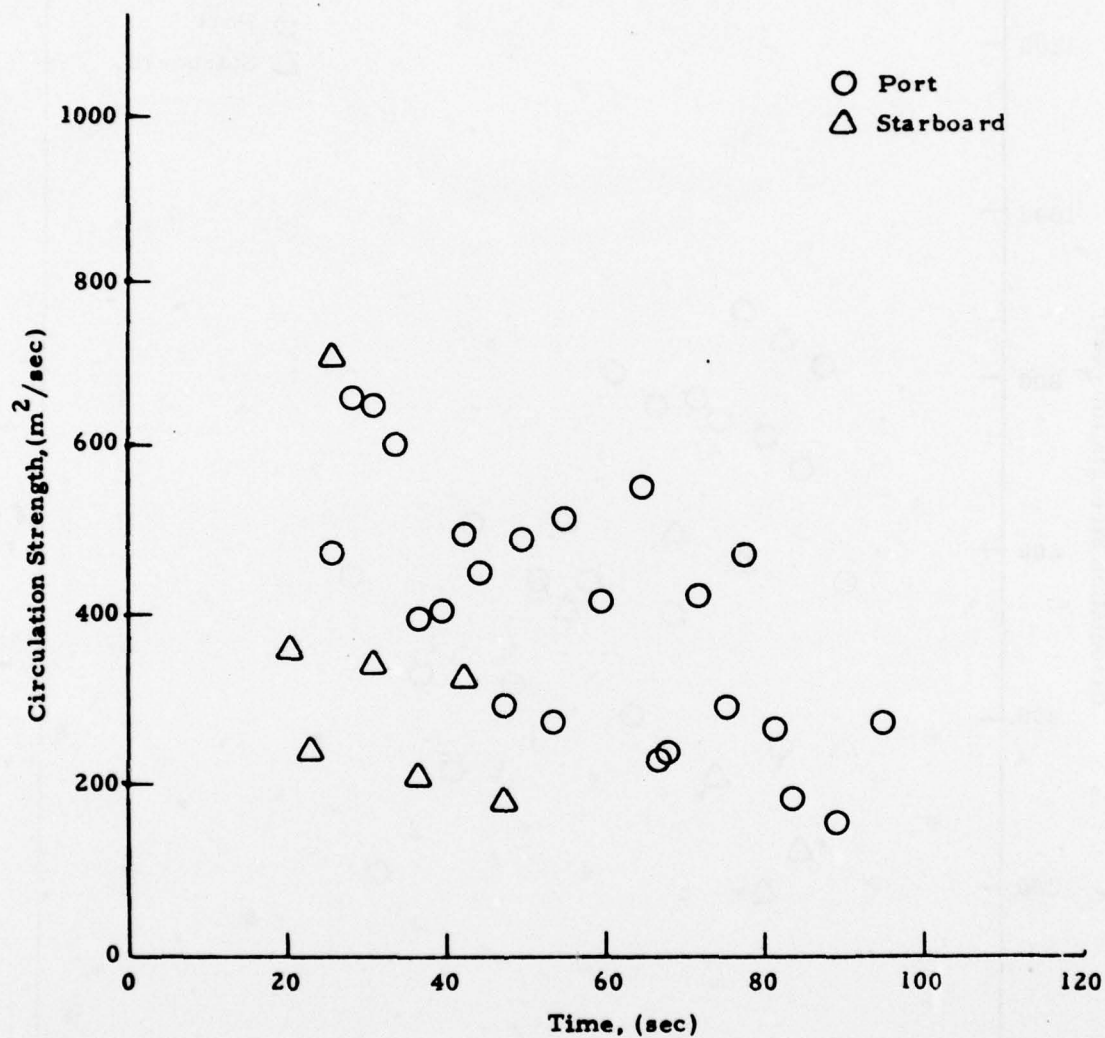


Fig.G-3 - Observed Circulation Time History for Rosamond B-747 Flyby 27

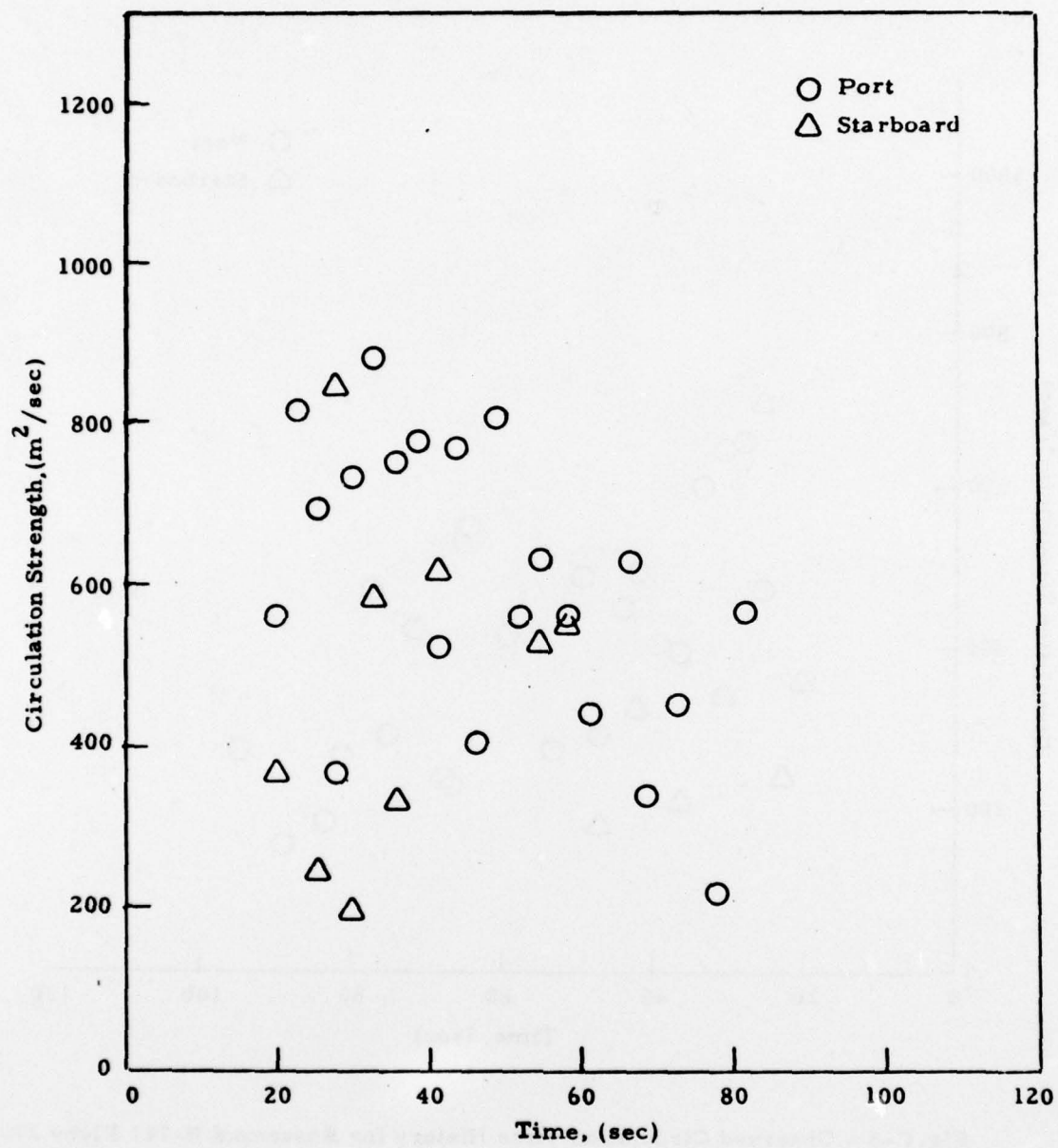


Fig.G-4 - Observed Circulation Time History for Rosamond B-747 Flyby 28

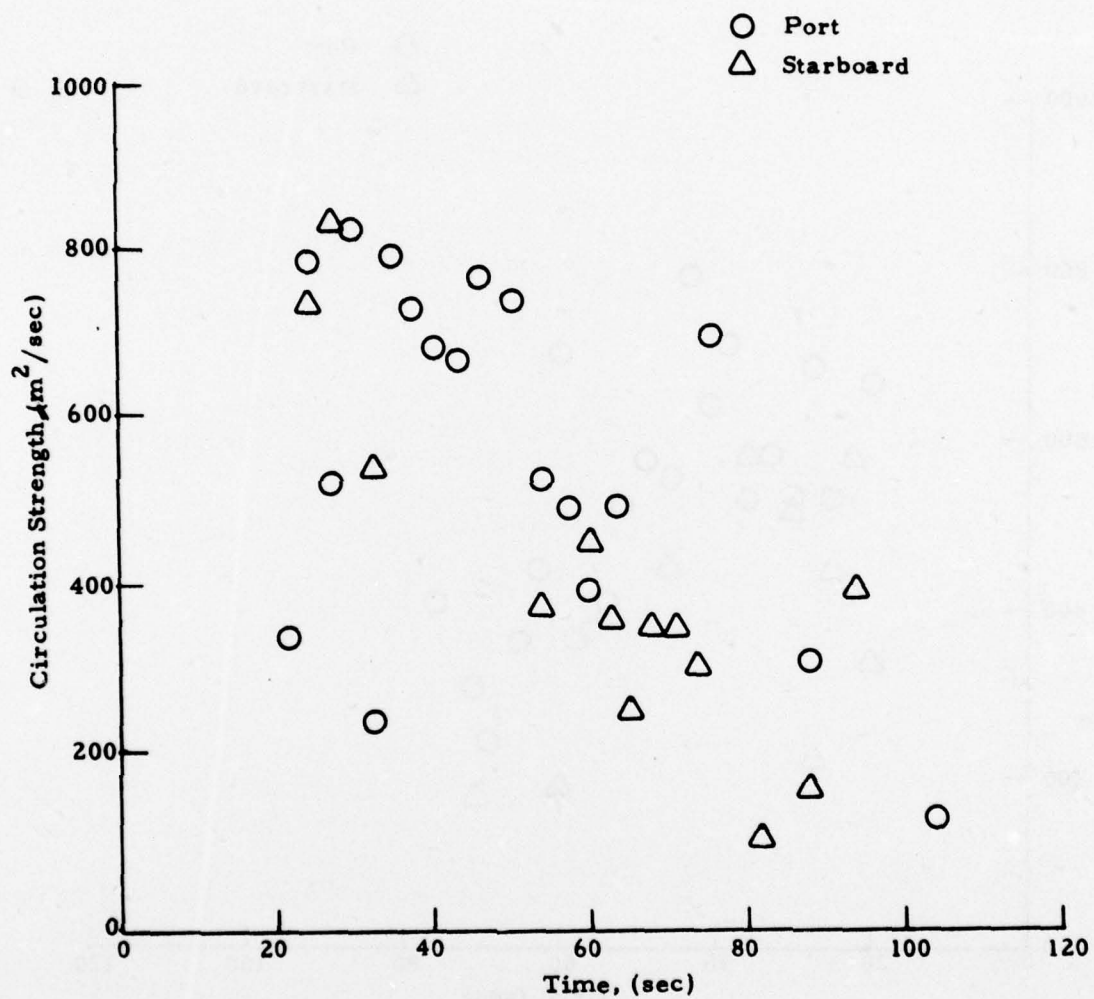


Fig. G-5 - Observed Circulation Time History for Rosamond B-747 Flyby 29

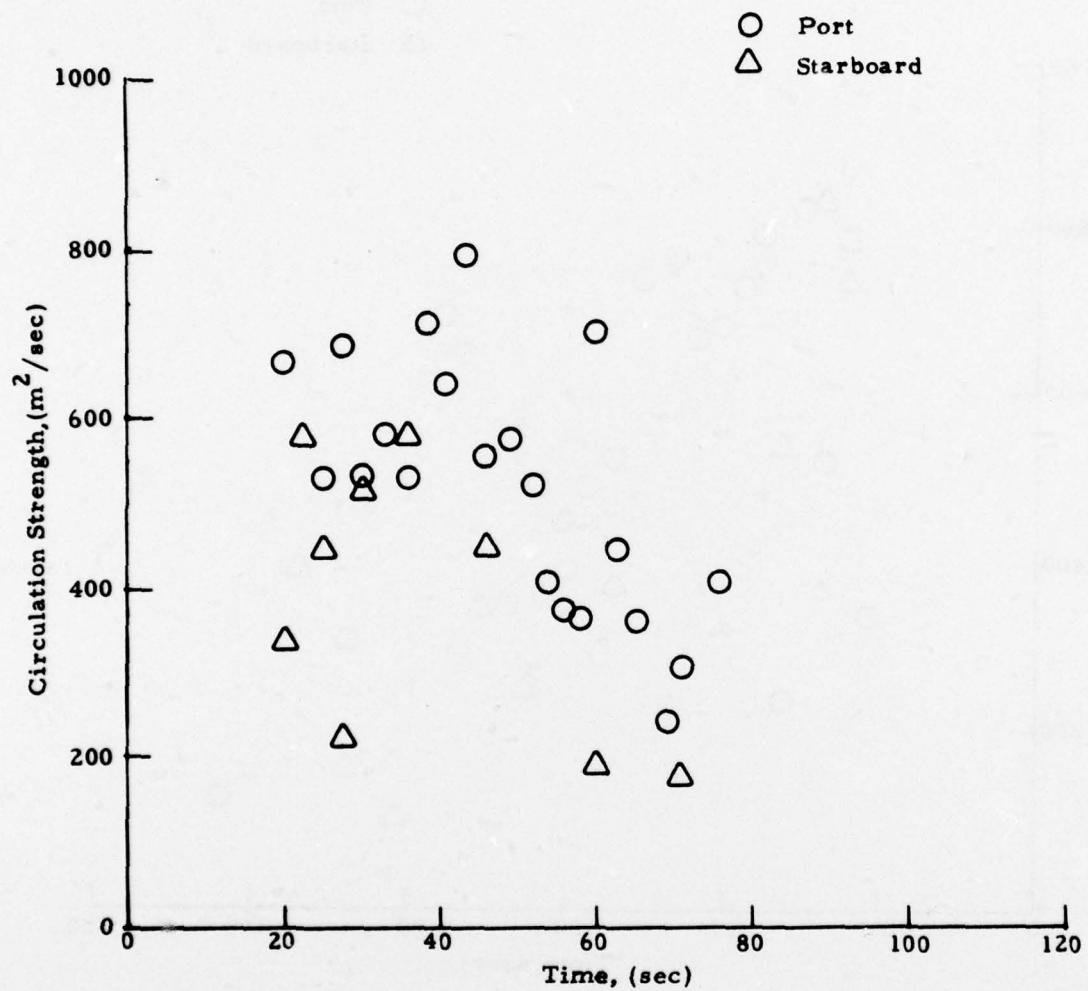


Fig.G-6 - Observed Circulation Time History for Rosamond B-747 Flyby 30

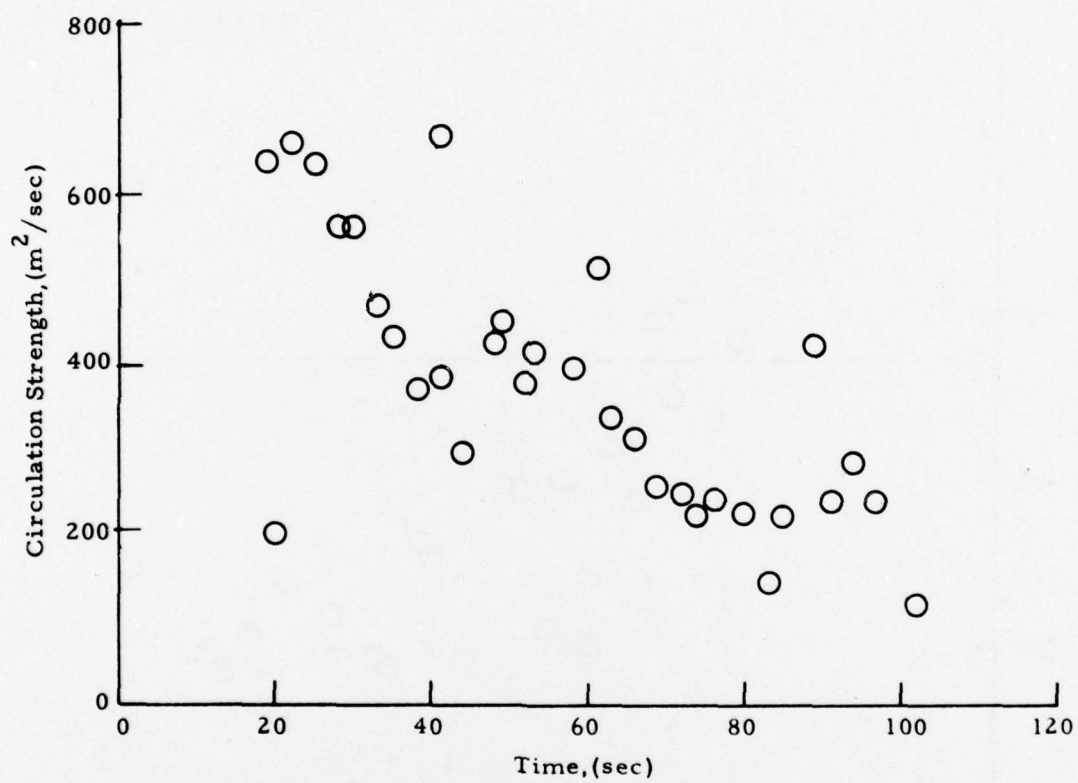


Fig.G-7 - Observed Circulation Time History for Rosamond B-747
Flyby 44, Starboard Vortex

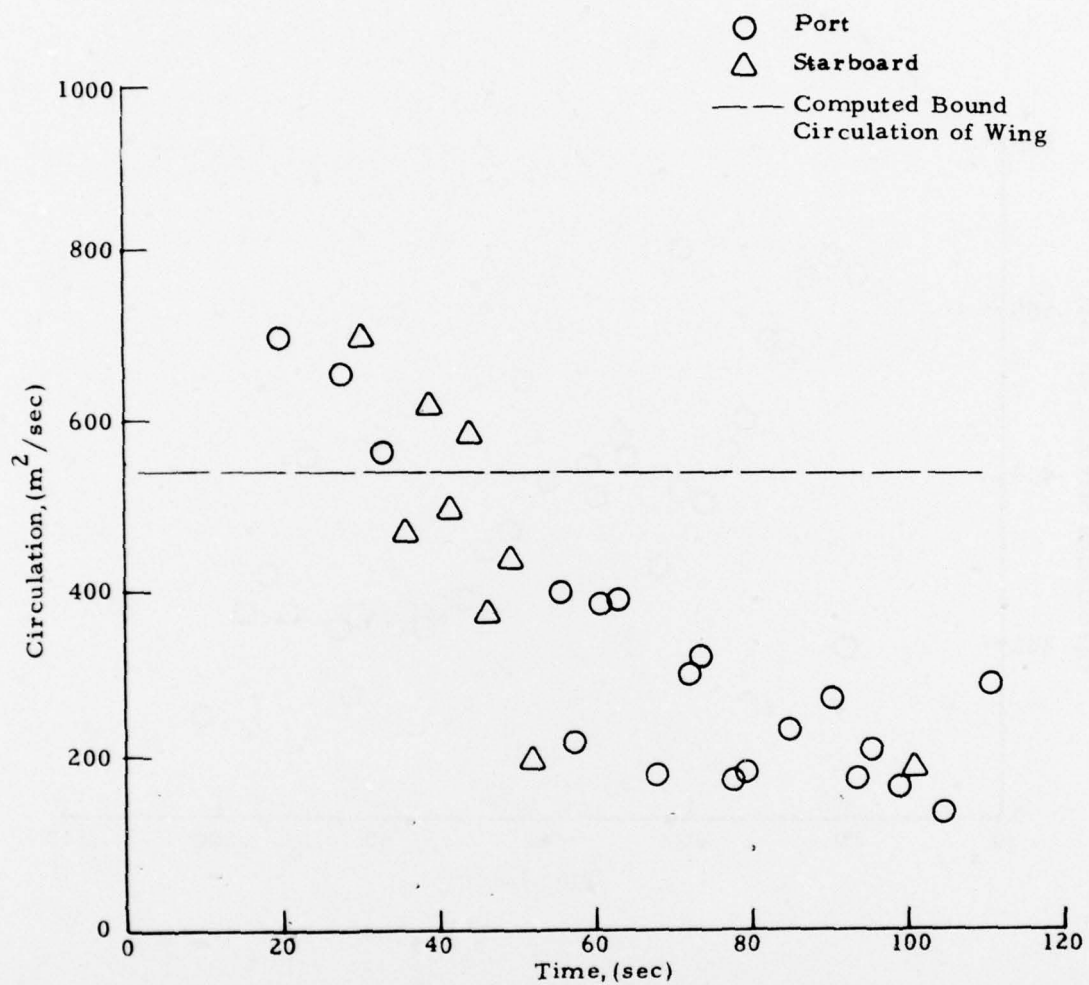


Fig.G-8 - Observed Circulation Time History for Rosamond B-747 Flyby 47

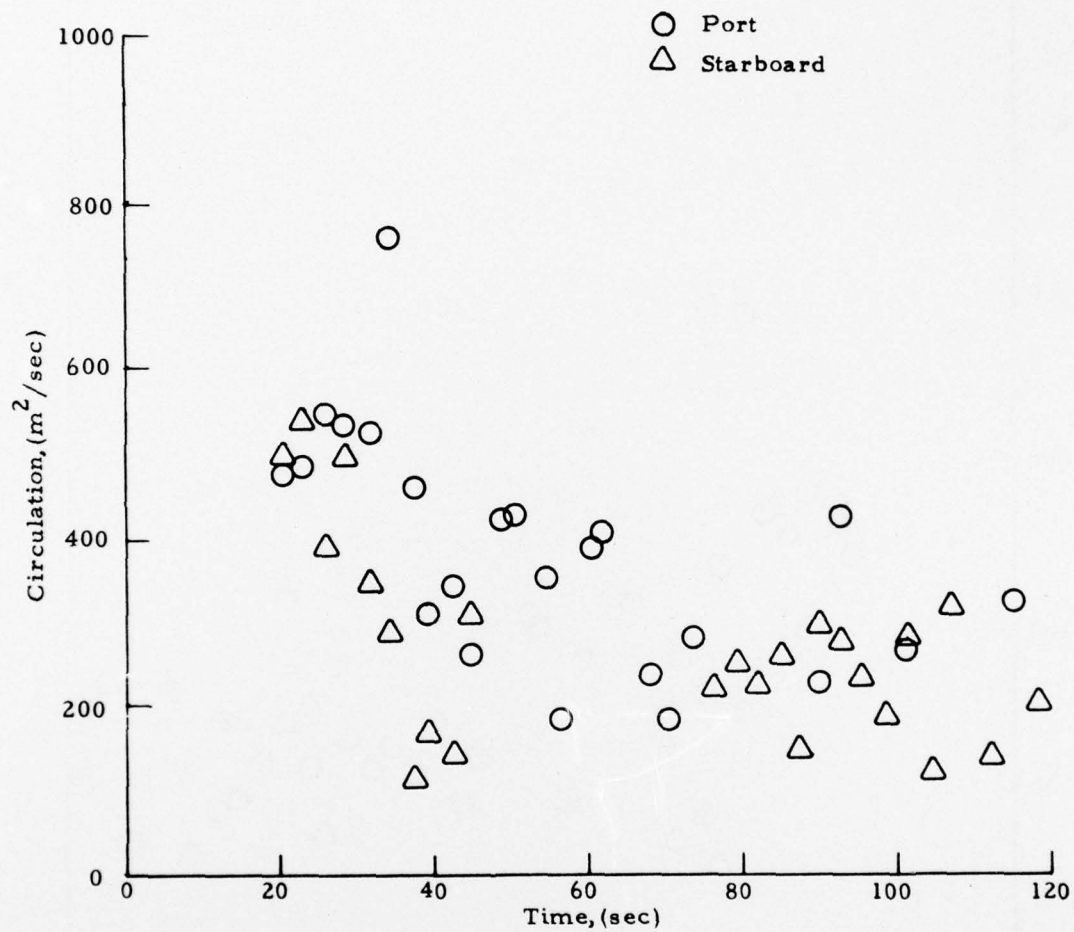


Fig. G-9 - Observed Circulation Time History for Rosamond B-747 Flyby 48

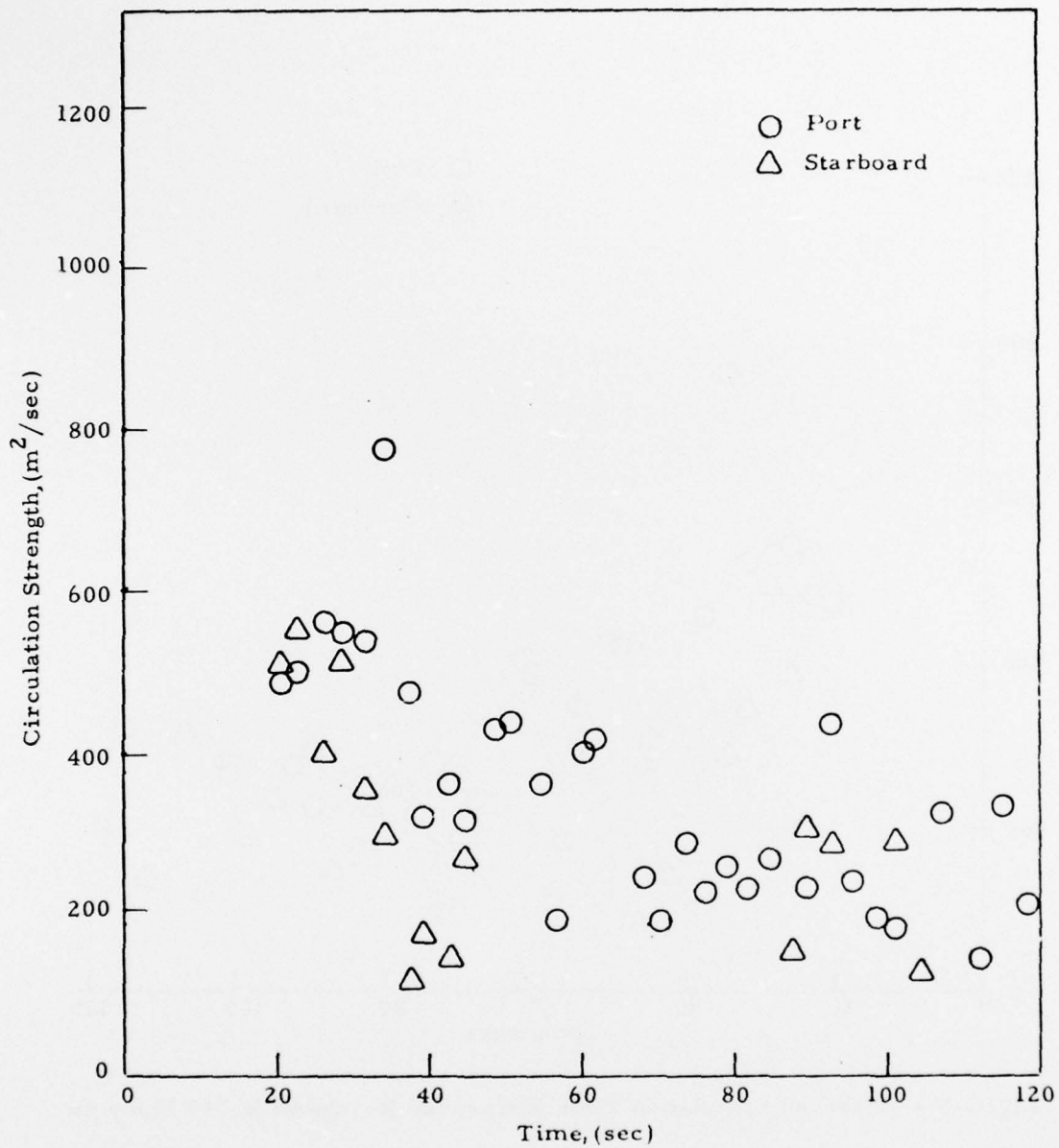


Fig. G-10 - Observed Circulation Time History for Rosamond B-747 Flyby 49

Appendix H
REPORT OF INVENTIONS

In accordance with the objectives of the contract, wake vortex and wind measurements were carried out at the Rosamond, California, test site with a scanning laser Doppler velocimeter system, and the LDV measurements were processed, reduced, and analyzed. The contract objectives were met, and no invention, discovery, or innovation was found.

U.S. GOVERNMENT PRINTING OFFICE: 1977-701-663/179